EXPERIMENTAL INVESTIGATION OF MECHANICAL BLOOD DAMAGE RELEVANT TO THE OPERATION OF CIRCULATORY-ASSIST DEVICES

by

Amanda Daly Sivek

B.S. Physics and B.A. Mathematics, Duquesne University, 2005

Submitted to the Graduate Faculty of

The Swanson School of Engineering in partial fulfillment

of the requirements for the degree of

Doctor of Philosophy

University of Pittsburgh

2015

UNIVERSITY OF PITTSBURGH

SWANSON SCHOOL OF ENGINEERING

This dissertation was presented

by

Amanda Daly Sivek

It was defended on

March 27, 2015

and approved by

James F. Antaki, Ph.D.,
Professor, Department of Biomedical Engineering and Computer Science, Carnegie Mellon University; Professor, Departments of Bioengineering and Surgery, University of Pittsburgh

Harvey S. Borovetz, Ph.D.,
Distinguished Professor and Former Chair, Department of Bioengineering; Robert L. Hardesty Professor, Department of Surgery; Professor, Department of Chemical and Petroleum Engineering

Richard R. Koepsel, Ph.D.,
Senior Research Scientist, Institute for Complex Engineered Systems, Carnegie Mellon University

Dissertation Director: Marina V. Kameneva, Ph.D., Research Professor, Departments of Bioengineering and Surgery

EXPERIMENTAL INVESTIGATION OF MECHANICAL BLOOD DAMAGE RELEVANT TO THE OPERATION OF CIRCULATORY-ASSIST DEVICES

Amanda Daly Sivek, PhD

University of Pittsburgh, 2015

Circulatory-assist devices (CAD) are commonly used in clinical practice for end stage cardiovascular disease patients as a bridge to transplant or as destination therapy. Despite decades of research, mechanical blood damage remains a problem in the clinical utilization of CAD, which results in a myriad of patient complications including device-induced erythrocyte lysis (hemolysis), bleeding and thrombosis. There is a clinical need to better understand the mechanisms of flow-induced blood damage to aid in the design and clinical utilization of CAD with enhanced biocompatibility as well as to determine specific factors responsible for blood damage and methods of their assessment.

The objectives were to study *in vitro* the mechanisms of flow-induced blood trauma and the parameters that affect *in vitro* hemolysis testing of CAD. The tested hypotheses were: 1) Mechanically induced polymer degradation in a high molecular weight polyethylene oxide (PEO) solution could predict the degree of shear-induced hemolysis within a CAD candidate without the use of animal or human blood; 2) Blood bank storage of packed red blood cells (RBC) could adversely affect RBC mechanical properties which may reduce the efficiency of RBC transfusion in CAD patients; 3) Cell-cell interactions and suspension viscosity are potential mechanisms of flow-induced hemolysis; and 4) The geometry of micro-gaps and crevices in

CAD blood flow paths could affect cell trafficking at supra-physiological shear stresses relevant to operating CAD.

We demonstrated that polymer mechanical degradation was highly correlated with hemolysis obtained due to circulation in the same CAD circuit as blood and ascertained valuable information on CAD performance predicting blood trauma without the need to use blood. We found that RBC deformability significantly decreased during blood bank storage which contributes to blood damage produced by CAD. Moreover, two additional mechanisms of flow-induced hemolysis relevant to operating CAD, cell-cell collisions and suspension viscosity, were elucidated. Finally, recirculating regions were observed in 100 μm wide rectangular and triangular crevices but not in wider crevices studied up to 500 μm, thus demonstrating the importance of the width of gaps and crevices in CAD blood flow paths for potential thrombogenesis.

This work provided information on mechanisms of flow-induced hemolysis and elucidated an important variable affecting thrombosis development in CAD blood flow paths at flow conditions relevant to *in vitro* and *in vivo* CAD operation. These results can contribute to the computational analysis, design and preclinical testing of next generation CAD.

TABLE OF CONTENTS

LIST OF TABLES

LIST OF FIGURES

NOMENCLATURE

ΔP	Pressure drop
η	Dynamic viscosity
ν	Kinematic viscosity
τ_{wall}	Wall shear stress
ANOVA	Analysis of Variance
BSA	Bovine serum albumin
CAD	Circulatory-assist device
CVD	Cardiovascular disease
d, D	Tube inner diameter
DPBS	Dulbecco's phosphate buffered saline without calcium or magnesium
DR	Drag reduction
DRP	Drag reducing polymer
FDA	Food and Drug Administration
freeHb	Free hemoglobin concentration
GRBC	Ghost RBC
Hb	Hemoglobin
Ht	Hematocrit
kDa	kilo Dalton

MW	Molecular weight
MFI	Mechanical fragility index
n, N	Sample size
NIH	Normalized Index of Hemolysis
PBS	Phosphate buffered saline
PDMS	Poly(dimethyl siloxane)
PEO	Poly(ethylene oxide)
plfHb	Plasma free hemoglobin concentration
PPP	Platelet-poor plasma
PRP	Platelet-rich plasma
PSFP	Platelet-sized fluorescent particles
Q	Flow rate
r	Tube radius
RBC	Red blood cell
Re	Reynolds number
RBC-A	RBC aggregability
RBC-D	RBC deformability
RBC-MF	RBC mechanical fragility
SD	Standard deviation
SEM	Standard error of the mean
tHb	Total hemoglobin concentration
VAD	Ventricular-assist device
VE	Viscoelasticity

PREFACE

For my husband Jeromy and daughter Elena

1.0 INTRODUCTION

Circulatory-assist devices (CAD) are commonly used in clinical practice for end stage cardiovascular disease patients as a bridge to heart transplant or as destination therapy. Pre-clinical CAD must demonstrate safety and efficacy prior to clinical approval by the FDA in the United States. Yet, mechanical (flow-induced) blood damage remains a significant complication in the development and clinical utilization of CAD, which results in a myriad of patient complications including stroke, pulmonary embolism, gastrointestinal bleeding, device-induced hemolysis and thrombosis.

Despite decades of research by numerous investigators the mechanisms of mechanical blood damage are not well understood. The generally accepted manifestation of mechanical blood damage is the amount of hemoglobin released into plasma, or hemolysis [1-5]. Other potential indicators of mechanical blood trauma include the activation of platelets [6-8], platelet aggregation [9-11], and changes in the mechanical properties of red blood cells (RBC) [12-15]. Newly developed or modified CAD require extensive *in vitro* testing in order to sufficiently demonstrate blood biocompatibility, a minimum trauma to RBC and other blood components, prior to conducting animal studies and ultimately translating the devices for clinical use.

Patients supported with CAD typically have prophylactic anticoagulation to offset the risk of thrombosis. Anticoagulation and anti-thrombotic protocols have been developed for CAD

patients, but bleeding and thromboembolic events often occur [16]. It is therefore imperative to better understand the mechanisms of flow-induced hemolysis and thrombosis to aid in the design and clinical utilization of CAD with enhanced blood compatibility. The objectives of this PhD study were to study *in vitro* the mechanisms of flow-induced blood trauma and the parameters that affect *in vitro* hemolysis testing of CAD. The specific aims in this thesis are listed as follows:

1) **To model flow-induced hemolysis using solutions of degradable polymers as a rheological substitute for blood**

   In vitro evaluation of pre-clinical CAD to damage blood cells has generally been performed using human or animal blood. Yet, the variability of RBC sensitivity to mechanical stress in different species, the preparation of blood including the adjustment of hematocrit to a standard value, the inconsistency of blood viscosity due to variability in plasma composition, the necessity to pool blood from different donors to obtain an adequate amount of blood for laboratory test systems and other issues related to work with blood (i.e. biohazard) remain problems of *in vitro* hemolysis testing. The use of a standard test fluid for the evaluation of potential hemolysis generated by CAD would be beneficial and obviate the need for blood. The objective of this specific aim was to investigate whether the mechanical degradation of a DRP in circulating solution can indicate/predict the degree of shear-induced hemolysis within a CAD candidate.

2) **To study adverse changes in rheological properties of donor RBC during blood bank storage that may cause hemolysis and impair microcirculation in CAD patients after blood transfusion**

Patients requiring transfusion of whole blood or packed RBC during surgery or the period of CAD implantation receive units from a blood bank that are stored for up to 42 days in an FDA-approved additive solution at 1-6°C. It is known that RBC-D decreases with storage time and thus the transfusion of less deformable stored RBC may lead to an increased blood viscosity, increased RBC-MF and the potential obstruction of capillaries in the microcirculation. The objective of this specific aim was to determine the effects of RBC storage time in the Blood Bank on RBC-MF and RBC-D; changes that may be harmful for CAD patients requiring RBC transfusion.

3) **To study flow-induced hemolysis as a function of shear stress and exposure time**

A mechanism of flow-induced hemolysis reported in the literature is the combination effects of shear stress and exposure time. The objective of this specific aim is to study the effects of shear stress and exposure time on mechanical hemolysis using *in vitro* flow systems with a CAD. The effect of varying blood exposure time to a constant shear stress on mechanical hemolysis was the study of Sub Aim 3.1. The objective of Sub Aim 3.2 was the examination of the effect of RBC-MF of the blood used for hemolysis testing of CAD on flow-induced hemolysis to discern whether RBC-MF can influence mechanical hemolysis in RBC exposed to the same shear stress and exposure times in an *in vitro* flow system with a CAD.

4) **To study potential mechanisms of flow-induced hemolysis and thrombosis**

Despite decades of research by numerous investigators, the mechanisms of flow-induced blood trauma are not well understood. The objective of Sub Aim 4.1 was to study the effects of cell-cell interactions and suspension media viscosity on flow-induced hemolysis using RBC and hemoglobin-depleted RBC ghosts (GRBC) suspended in

viscous media in a microtube flow system with a CAD. The objective of Sub Aim 4.2 was to examine the thrombogenicity of microscopic crevice flow by studying the trafficking of GRBC and platelet-sized fluorescent particles in a microchannel containing multiple crevices similar to the size of small gaps in some CAD at supra-physiological shear stresses. The microscopic examination of GRBC and PSFP pathlines may provide additional insight into the flow conditions and interaction of cells that promote thrombogenesis in the complex, microscopic geometries within CAD blood flow paths.

2.0 BACKGROUND

2.1 HEMORHEOLOGY

In the mammalian circulation, blood is pumped from the heart through arteries to deliver oxygen, hormones, electrolytes and heat to all cells, remove carbon dioxide and other waste products and then transports to the heart through venous return. Blood has an intrinsic mechanism for clotting to aid against the invasion of foreign materials in the body and also an extrinsic clotting mechanism to prevent considerable blood loss in the event of blood vessel penetration or rupture. The flow of blood is regulated to maintain adequate tissue perfusion in the normal circulation. Disturbances in blood flow can result in severe complications or exacerbate existing pathological conditions.

Blood is a suspension of erythrocytes (RBC), leukocytes (WBC) and thrombocytes (platelets) in plasma. The cellular elements in one microliter of normal human blood are 4-6 million RBC, 4,000-8,000 WBC and 200,000-500,000 platelets [17]. Erythrocytes have the shape of biconcave disks with a diameter of 7-8 μm and thickness of 2-2.5 μm [18]. WBC (lymphocytes, granulocytes, monocytes) are roughly spherical with a diameter of ~10–20 μm [19]. Platelets are discoid with a diameter of 2-3 μm and thickness of ~0.5 μm. Plasma consists of many proteins (albumin, fibrinogen, immunoglobulins, lipoproteins, etc.), ions, clotting factors and metabolites suspended in a salt solution [17].

RBC function in gas transport (oxygen delivery and carbon dioxide removal) from cells and constitute approximately 99% of blood corpuscles. RBC are filled with a viscous, Newtonian Hb solution [20] that is surrounded by a viscoelastic membrane consisting of an outer lipid bilayer and inner membrane cytoskeleton [21]. The normal Ht (volume fraction of RBC in whole blood) range is 45±5% for males and 41±5% for females [22]. RBC pronounced influence on hemorheology is due to their high concentration in whole blood.

The science of hemorheology comprises the flow properties of blood cells and plasma in macroscopic and microscopic dimensions [23]. Hemorheology is one of the oldest clinical sciences, but was not studied in great detail until the work of Fåhraeus in the early 20^{th} century. Knowledge of microcirculatory blood flow was expanded by the discovery of the Fåhraeus [24] and Fåhraeus-Lindqvist [25] effects. Moreover, Fåhraeus' studies of the suspension stability of blood in pregnancy [26] and several pathological conditions [27] found augmented red corpuscle sinking velocity, or RBC aggregability, compared to normal human blood.

Work by numerous investigators has shown that human blood is a non-Newtonian, shear-thinning [28-31], viscoelastic [32, 33], and thixotropic fluid [29, 34-36]. The shear-thinning nature of human blood was found to be dependent on RBC aggregability at stasis or low shear rates (below 80 s^{-1} [37]) and RBC deformability at medium to high shear rates [38-40]. As shear rate is increased, blood viscosity decreases until an asymptotic value is reached as modeled by the Casson equation [41].

2.2 HEMORHEOLOGY IN THE MICROCIRCULATION

The microcirculation is considered to comprise all blood vessels with less than ~300 μm diameter. A typical capillary has a 3-5 μm diameter, 350 μm length and pressure drop of ~25 mmHg [42]. In general, the vessels of the microcirculation have laminar, Stokes flow (Re<<1) [43, 44]. In microcirculatory blood flow, RBC, leukocytes and platelets interact differently than in larger blood vessels [45]. In 1921, Smith *et al.* reported that a non-uniform distribution of RBC in the microcirculation was possible [46] and soon confirmed by the *in vitro* work of Fåhraeus and Lindqvist. Fåhraeus found a reduction of Ht in capillary tubes below ~250 μm diameter due to augmented RBC velocity compared to the mean bulk flow velocity, i.e. the Fåhraeus effect [24]. Fåhraeus and Lindqvist studied the relative viscosity of blood (compared to water) in 40-500 μm diameter glass capillaries and discovered that in capillaries with ~300 μm diameter, blood viscosity progressively decreased with decreasing vessel diameter, i.e. the Fåhraeus-Lindqvist effect [25]. In capillaries less than 15 μm diameter, Dintenfass found an inverse Fåhraeus-Lindqvist effect in which relative blood viscosity increased with decreasing capillary diameter below ~14 μm [47]. Barbee and Cokelet studied RBC suspensions flowing in 29-221 μm glass capillaries and found that in capillary tubes with 59 μm or greater, the Ht of the RBC suspension flowing from the tube, when mixed, is equal to the feed Ht into the capillary [48].

In a novel *in vivo* study, Whittaker and Winton perfused the hind leg of a dog with blood of various Hts at several driving pressures and compared the flow rates with saline flow rates to examine the apparent viscosity of flowing blood [49]. Their results demonstrated a nearly constant blood viscosity at the pressure gradients and flow rates studied [49]. Further work by

Lipowsky *et al.* compared "*in vivo*" cat blood viscosity in 24–47 μm diameter vessels (calculated using the Hagen-Poiseuille equation) with viscometric data for the same blood at a 2000 s^{-1} shear rate and found very similar results over a range of Hts [50]. Thus, at high shear rates in the microcirculation *in vivo* and in viscometric methods *in vitro*, blood behaves approximately as a Newtonian fluid with an asymptotic value. Asymptotic viscosity occurs due to the effects of RBC deformation and flow-induced RBC organization [51].

The ability of RBC to deform when subjected to external forces is crucial to their role in tissue perfusion and gas transport. Normal mammalian erythrocytes are capable of deformation due to their low cytoplasmic viscosity, excess of surface membrane area in relation to cell volume, and viscoelastic membrane properties [52-54]. In the microcirculation, as RBC travel through vessels of decreasing diameter, the increase in external shear stresses compels them to undertake larger deformations. An erythrocyte can undergo innumerable large deformations that preserve the volume of the cell and surface area of the cell membrane without stretching or tearing the membrane [55]. As a result, normal, human RBC 7-8 μm in diameter are able to pass through capillaries as small as 3 μm without damaging the cell. Moreover, RBC circulating in the vascular system must frequently pass the wall of the splenic sinus where they squeeze through narrow (~2 μm) slits between endothelial cells numerous times during their lifespan. Any RBC that cannot pass are destroyed by the reticuloendothelial system and removed from the circulation [56].

The normal lifespan of human RBC is 100-120 days; thus the RBC in circulation comprise a spectrum of ages and deformabilities with the youngest cells being the most deformable and the oldest cells the least deformable [57, 58]. RBC-D may be reduced by

fluctuations in osmotic/oncotic pressure [53], contact with thermal stresses [59, 60], blood bank storage [61, 62] or prolonged exposure to non-physiological shear stresses in CADs [58, 63, 64].

2.3 DETERMINATION OF BLOOD OR RBC SUSPENSION VISCOSITY AND VISCOELASTICITY

Capillary viscometers were the first viscometer type used to measure the viscosity of blood and RBC suspensions [65]. For steady, laminar flow of a Newtonian, incompressible fluid in a rigid cylindrical tube, the Hagen-Poiseuille equation can be used to calculate the dynamic viscosity of the fluid:

$$\eta = \frac{\pi \Delta \mathrm{Pr}^4}{8QL} \tag{1}$$

where η is the dynamic viscosity, ΔP is the pressure drop in the capillary tube of length L, r is tube radius and Q is volumetric flow rate.

The Reynolds number (Re) is the ratio of inertial to viscous forces in a fluid flow and quantifies the type of flow conditions, whether laminar, transitional or turbulent. Laminar flow occurs for Re<2000, turbulent flow conditions for Re>4000 and transitional flow for 2000<Re<4000. The Re in a cylindrical tube is calculated as:

$$\mathrm{Re} = \frac{4R_H \vec{v}_{mean}}{\nu} = \frac{4Q}{\pi d \nu} \tag{2}$$

where R_H is the hydraulic radius and ν is kinematic viscosity.

Couette viscometers have been widely used to study the dynamic viscosity of Newtonian and Non-Newtonian fluids for decades [28, 31, 34]. In general, the rotational speed of an outer

cylinder (stationary inner cylinder) and the total torque exerted by a test fluid in the small gap between the inner and outer cylinders on the rotating outer cylinder is measured [66, 67]. The dynamic viscosity of a fluid in the small gap between a rotating outer cylinder and a stationary inner cylinder is calculated as:

$$\eta = \frac{T(R_o - R_I)}{2\pi\omega L R_o^{\ 3}} \tag{3}$$

where T is the measured torque on the outer cylinder, R_o is the radius of the outer cylinder, R_I is the radius of the inner cylinder, ω is the rotational speed of the outer cylinder, and L is the length of the outer cylinder.

The Re for determining laminar flow in Couette viscometers is calculated as:

$$\mathrm{Re} = \frac{R_o \omega \rho (R_O - R_I)}{\eta} \tag{4}$$

where ρ is fluid density.

Cone-and-plate viscometers are another common viscometer type used to measure the dynamic viscosity of Newtonian and Non-Newtonian fluids [68-71]. This viscometer consists of a rotating cone spindle at a small angle (<1°) with respect to a stationary flat plate. A test fluid is placed in the small gap between the rotating cone and the stationary plate. The cone is rotated at a range of rotational speeds and the torque on the cone produced by the test fluid is measured. The dynamic viscosity of a fluid in the small gap between a rotating cone and a stationary plate is calculated as:

$$\eta = \frac{3T \sin\theta}{2\pi\omega r^3} \tag{5}$$

where T is the measured torque on the cone, θ is the cone angle, ω is the rotational speed of the cone, and r is the radius of the cone.

The Re for determining laminar flow in cone-and-plate viscometers is calculated as:

$$\mathrm{Re} = \frac{\omega \rho r^2}{\eta} \tag{6}$$

In vivo, blood flow exhibits both elastic (energy storing) and viscous (energy dissipating) properties. *In vitro* measurements of blood or RBC suspension viscosity and elasticity depend on Ht, plasma viscosity, RBC-D, RBC-A, osmolality, pH, and temperature [32, 35, 51, 53, 54]. The measurement of fluid viscoelasticity can be performed under oscillatory flow at a standard frequency, e.g. of 2 Hz, in a rigid capillary tube [33]. For viscoelastic fluids undergoing oscillating flow of small amplitudes:

$$\gamma = \gamma_0 \sin(\omega t) \tag{7}$$

$$\tau = \tau_0 \cos(\omega t - \varphi) \tag{8}$$

where γ is shear strain, γ_0 is shear strain amplitude, τ is shear stress, τ_0 is shear stress amplitude, ω is radian frequency, Φ is viscoelastic phase angle between shear stress and shear rate and t is time [72]. Newtonian fluids lack elasticity and thus shear stress is in phase with shear rate ($\Phi=0$). For non-Newtonian viscoelastic fluids, shear stress and shear rate have a non-zero phase angle ($0<\Phi<90°$) that results in rheological behavior described as:

$$\eta^* = \eta' - i\eta'' \tag{9}$$

where η^* is the complex viscosity, η' is the viscosity, and η'' is the elasticity [32, 72].

2.4 CARDIOVASCULAR DISEASE AND CIRCULATORY-ASSIST DEVICES

Cardiovascular disease is the number one cause of death in the United States. Based on mortality data acquired from 2008, the American Heart Association reported that one out of every three Americans died of CVD, or approximately one death every 40 seconds [73]. Common CVD include congestive heart failure, atherosclerosis, hypertension, coronary artery disease, and myocardial infarction. Numerous morbidities can occur from CVD that significantly reduce the quality of life of patients, including stroke, pulmonary embolism, thromboembolism and multi-organ complications or failure.

Although medication may alleviate the degree of CVD in some patients, the use of mechanical circulatory support devices such as dialyzers, VAD and extracorporeal membrane oxygenation (ECMO) may be necessary for patients suffering from severe CVD. Each day, there are approximately 3,000 people in the United States on the waiting list for a heart transplant and only ~2,000 donor hearts are available annually [74]. Patients with end stage heart failure may require single or bi-ventricular VAD implantation as a bridge to transplant or as destination therapy (the patient will have the device for the remainder of their life) [75, 76]. The large patient population, lack of donor organs, long transplant wait times and use in destination therapy demonstrate the need for CAD with superior hemocompatibility to help improve the survival rate and quality of life for numerous patients that require mechanical circulatory support.

2.5 MECHANICAL BLOOD DAMAGE IN CIRCULATORY-ASSIST DEVICES

CAD have been in development since the 1950s and today there are numerous VAD with FDA approval for end stage heart failure, including the HeartMate II LVAS, HeartWare VAS, and Thoratec CentriMag. Yet, all of the approved CAD carry a risk of mechanical blood trauma and require prophylactic anticoagulation to reduce the risk of thrombosis. The problem of blood trauma in CAD and extracorporeal circulation was identified by investigators several decades ago, yet still remains one of the main problems associated with mechanical circulatory support. Studies by Kusserow [2] and Galletti [3, 77, 78] using extracorporeal perfusion in dogs first identified mechanical blood damage in CAD including hemolysis, leukocytosis, thrombocytopenia, post-perfusion anemia, and pump thrombus formation. Additional studies by Bernstein [4, 79-81], Kusserow [82], Sutera [15, 83] and Dormandy [84] demonstrated that RBC sublethal damage can occur in blood-contacting devices: morphological changes to RBC, increased RBC-MF and increased blood viscosity. More recent work by Baker *et al.* [85], Snyder *et al.* [86-88], and Woolley *et al.* [89] demonstrated platelet activation, platelet aggregation and leukocyte-platelet aggregate formation due to CAD exposure *in vivo*.

Newly developed or modified CAD undergo extensive *in vitro* testing to sufficiently demonstrate hemocompatibility, a minimum trauma to RBC and other blood components, to the FDA prior to conducting animal studies and translating the devices for clinical use. Yet, patients that require CAD implantation risk exacerbating the effects of preexisting diseases affecting the circulation due to mechanical blood trauma [56, 58, 90]. CAD design is an important parameter that affects mechanical blood damage and is largely still a trial-and-error process [91-95]. It is therefore necessary to elucidate the mechanisms governing flow-induced hemolysis and

thrombosis to aid in the design and clinical utilization of CAD with enhanced hemocompatibility.

2.6 FLOW-INDUCED HEMOLYSIS

Proposed mechanisms of flow-induced hemolysis reported in the literature include the effects of shear stress and exposure time [5, 96-98], accumulated sublethal RBC damage [3, 12, 78, 99, 100], cell-surface interactions [79, 101, 102], cell-cell interactions [98, 103] and turbulent flow conditions [83, 104-106].

A well supported mechanism of flow-induced hemolysis is the effect of shear stress and shear exposure time [5, 96, 97, 107]. Previous reports that studied hemolysis as a function of shear stress and exposure time primarily used concentric cylinder [67] or cone-and-plate viscometers [108] that exposed RBC to uniform shear conditions for certain shear exposure times [5, 97, 98]. Studies of variable shear stresses and exposure times have also been conducted in roller pumps [80], a capillary system [109] and other systems [110, 111]. Numerical predictions of blood damage are normally performed using power-law models of shear stress and shear exposure time such as those of Giersiepen *et al* [112] or Song *et al* [113, 114]:

$$D = A\tau^{\alpha}t^{\beta} \tag{10}$$

where D is damage, τ is shear stress, t is shear exposure time, and A, α and β are empirical coefficients.

Blackshear and colleagues investigated the effect of cell-wall interactions on mechanical hemolysis using stainless steel tubes and a turbulent flow jet [101, 102]. They reported that

hemolysis in tube flow appears to be related to wall interactions that are dependent upon shear [101]. Bacher and Williams reported similar findings in their study of flow through capillary tubes of different materials [109]. Their results demonstrated disparate amounts of hemolysis among the materials studied, which suggested that the tube surface affected the flow-induced hemolysis.

RBC have been shown to tank-tread and the relative velocity difference between colliding cells can alter the local shear rate on a cellular scale [115, 116]. Cell-cell interactions were first proposed as a potential mechanism for flow-induced hemolysis by Shapiro and Williams [103] and Sutera *et al* [83], but the authors did not study it. Leverett *et al* studied the effect of cell-cell collisions on mechanical hemolysis using 0.3-60% Ht human blood samples exposed to a 300 Pa shear stress in a Couette viscometer and concluded that the effect of cell-cell interaction was negligible on flow-induced hemolysis [98].

The type of flow (laminar, transitional or turbulent) is another parameter that affects flow-induced hemolysis *in vitro* and *in vivo*. In a pipe, laminar flow occurs when Re<2000 and turbulent flow conditions for Re>4000. Turbulent flow conditions have been shown to augment mechanical hemolysis in jet flow systems [102, 105], concentric cylinder viscometers [83, 104] and in an *in vitro* flow system with a CAD [106].

In the assisted circulation, RBC exposed to supra-physiological shear stresses can be damaged without membrane failure, which is demonstrated by a change in the mechanical properties of the cells. Although the damage does not result in immediate hemolysis, accumulated sublethal RBC damage in blood-contacting devices has been shown to augment mechanical hemolysis [3, 12, 13, 78, 99, 100]. Sublethal RBC damage is characterized by a

decrease in RBC-D and an increase in RBC-A, RBC-MF and RBC suspension or blood viscosity.

Numerous studies have demonstrated the adverse effects of *in vivo* and *in vitro* CAD exposure on the deformability of erythrocytes using micropipette aspiration [117], filtration [90], ektacytometry [118, 119], asymptotic blood viscosity [58, 63, 120, 121] and blood viscoelasticity measurements [122]. Decreased RBC-D may lead to shortening of erythrocyte lifespan [14], the obstruction of small capillaries [123] and an increase in blood viscosity [38], potentially leading to decreased capillary density, tissue ischemia, anemia, and organ failure [56]. Additional information on methods for determining RBC deformability is presented in **Appendix A**.

RBC-MF is a reliable hemorheological test for the evaluation of sublethal damage to RBC due to natural aging [124], blood bank storage [61], or exposure to mechanical stress in blood-contacting devices [12, 58, 63]. RBC-MF is assessed by measuring the freeHb produced after RBC are subjected to a standard mechanical stress for a controlled time [125, 126].

RBC aggregability (RBC-A) is generally assessed by measuring the erythrocyte sedimentation rate (ESR) in whole blood or suspensions at a normalized Ht in standard tubes for a standard time [22, 127, 128]. Another method for determining RBC-A is to shear RBC in suspension at a low shear rate in an aggregometer, stop flow after a controlled time and take images of RBC aggregate formation [129]. RBC-A is augmented in pathological conditions [27, 130, 131] and after CAD exposure *in vitro* and *in vivo* primarily due to elevated levels of fibrinogen [58, 63, 120, 132].

Viscometric methods have demonstrated augmented whole blood viscosity compared to normal human blood in patients after CAD exposure *in vivo* which is due to the reduction in RBC-D, increase in RBC-A and augmented plasma viscosity [90, 120, 133, 134]. In a

viscoelastometry study, Undar *et al.* reported an increase in blood viscoelasticity in pediatric patients after cardiopulmonary bypass [135].

2.7 THROMBOSIS IN ASSISTED CIRCULATION

Since Virchow's triad of blood, flow and surface were identified as potential factors for the development of thrombosis *in vivo* [136], numerous investigators have performed studies to elucidate the mechanisms of thrombosis. *In vivo*, the intrinsic coagulation system is activated by protein adsorption to foreign surfaces and ends with the activation of the common pathway and the formation of thrombin and fibrin (**Figure 2.1**).

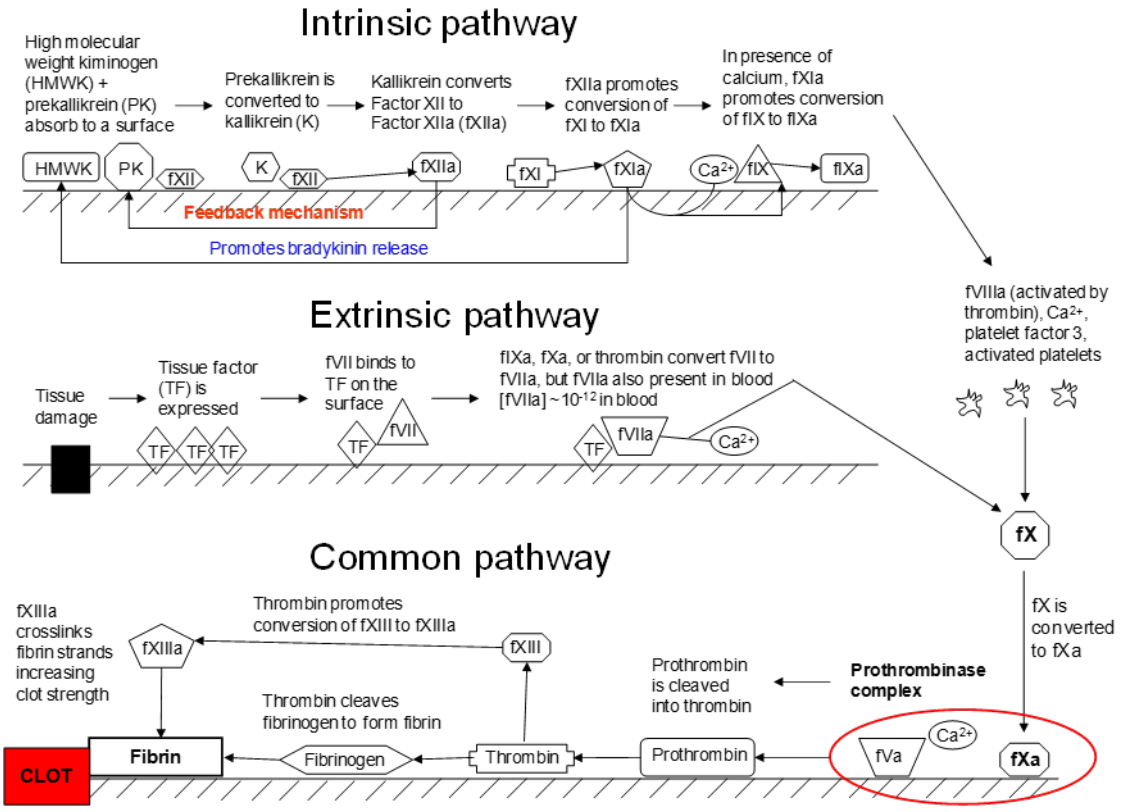

Figure 2.1. Intrinsic, extrinsic and common pathways of the coagulation cascade.

The mechanisms of thrombosis in the assisted circulation with a CAD are not well understood. Shear-induced damage to platelets can result in platelet adhesion [137-141], activation [6, 142-145], reversible or irreversible aggregation [9, 10, 146-148], and microparticle formation [149]. Moreover, the biochemical interactions between RBC, platelets and leukocytes in the assisted circulation with a CAD can contribute to thrombosis *in vivo* [87, 89].

Hellem first suggested that a humoral factor from RBC, Factor R, augmented platelet adhesion in a Ht dependent manner [150] and Gaarder *et al* confirmed that this factor was adenosine diphosphate (ADP) [151]. The work of Born [146, 147, 152] and Hellem and Odegaard [153] demonstrated that the addition of exogenous ADP to PRP or alternatively, the release of ADP from platelets or RBC can induce bulk platelet aggregation *in vitro*.

Reimers *et al.* [154] studied *in vitro* ADP release from RBC and platelet aggregation in a Couette viscometer (5 Pa shear stress for 5 minutes) using suspensions of RBC in PRP at different Hts. The authors found that ADP release from RBC increased with increasing Ht and resulted in augmented platelet aggregation [154]. In a complementary study, Alkhamis *et al.* [155] investigated ADP and Hb release from RBC, platelet aggregation and adhesion in a cone-and-plate viscometer (0-20 Pa shear stress) using whole blood, RBC in PPP and GRBC in PRP at the same Ht. The authors found that the release of Hb and ADP from RBC increased with increasing shear rate and that sheared whole blood produced the highest amount of ADP release, single platelet reduction, and platelet adhesion, followed by RBC in PPP and GRBC in PRP [155]. Hemoglobin alone can also cause platelet aggregation *in vitro* as reported by Wurzinger and colleagues who showed that the addition of stroma-free RBC lysate with Hb concentrations of 30 mg/dl and higher to PRP produced a significant increase in platelet aggregation in PRP exposed to a 40 s^{-1} shear rate for 12 minutes in a cone-and-plate viscometer [143, 156].

In the assisted circulation, there are regions within some CAD blood flow path that have microscopic crevices or steps that are a potential nidus for thrombosis development due to flow separation or flow stagnation [143, 157-160]. These CAD regions may be large enough for only a few cells to pass through concurrently, hence it is impossible to examine these regions macroscopically. The microscopic examination of cell trafficking within crevices similar to the size of small gaps in some CAD at supra-physiological shear stresses has not been previously reported in the literature.

3.0 POLYMER SOLUTION AS A TEST FLUID FOR *IN VITRO* EVALUATION OF POTENTIAL BLOOD DAMAGE IN CIRCULATORY-ASSIST DEVICES

Chapter 3 has been published in the ASAIO Journal [70].

3.1 INTRODUCTION

The problem of blood trauma in CAD and extracorporeal circulation was studied by prominent investigators such as Galletti [3, 77, 78], Kusserow [82, 99, 100], Bernstein [4, 79-81], Blackshear [5, 161], and Sutera [15, 83] decades ago, yet still remains one of the main problems associated with mechanical circulatory support. Newly developed or modified CAD require *in vitro* testing in order to sufficiently demonstrate hemocompatibility, a minimum trauma to RBC and other blood components, prior to conducting animal studies and ultimately translating the devices for clinical use. Sources of blood damage include non-physiological hemodynamics, cell contact with foreign surfaces, and chemical factors released from mechanically damaged blood cells or the vessel wall [56]. Potential indicators of mechanical blood trauma include hemolysis, activation of platelets and leukocytes, and sub-lethal trauma to RBC. The generally accepted manifestation of mechanical blood damage is the amount of Hb released into plasma, or hemolysis [1, 3, 15, 79, 100].

Assessment of hemolysis has been performed using animal blood from different species in mock circulation systems with the tested blood pump [91, 162-166]. The variations in testing conditions, sensitivity to mechanical stress of RBC from different species and dependence of RBC-MF on storage time make the comparison of hemolysis test results quite difficult [58, 61, 163, 167-170]. A standard test fluid for the evaluation of potential blood damage within blood pumps would be beneficial for comparison of different pre-clinical CAD.

Previous test solutions proposed for the evaluation of hemolytic characteristics of CAD include suspensions of polyurethane microcapsule filled with leuco dye [171]. According to the authors, microcapsule suspensions were proposed due to their non-biological nature and ability to simulate the static mechanical properties of RBC [171]. Yet, this method has several disadvantages, such as the difficult preparation of microcapsule suspensions and the broad size distribution (from ~70 to ~200 μm) of polyurethane capsules with the largest concentration of capsules at 100 μm. Consequently, these suspensions cannot simulate the hemodynamics in CAD.

Polyacrylamide (PAA) solutions with molecular weight (MW) 10^7 Da at 300 ppm concentration were also proposed as a potential test fluid for evaluation of CAD due to their comparable rheological behavior as that of blood and the shear-induced degradation of PAA molecules over time [172, 173]. The authors characterized the shear-induced degradation of PAA via measurement of viscosity over a wide range of shear rates in a shearing device [172, 173]. The authors observed changes in low shear viscosity of PAA solution without significant changes in viscosity at high shear rates, which may be related to disentanglement and disaggregation of the polymer molecules, not to their physical degradation [172, 173]. Since the authors did not test PAA solutions in a flow system with a CAD, it is not clear how relevant their

method of testing the potential damage to PAA molecules during a very short exposure time in a shearing device is for *in vitro* hemolysis testing of rotary blood pumps. The authors did not discuss how to apply their method for this purpose nor did they prove whether a damage index based on changes of low shear viscosity would be informative for *in vitro* testing of CAD.

For this study, a DRP solution of ~4000 kDa MW PEO at a concentration of 1 mg/ml in a turbulent flow circulating system is proposed as a potential blood substitute for the *in vitro* assessment of potential mechanical blood damage in a tested CAD. Previous studies of PEO performed in the Kameneva Laboratory using a Viscotek Triple Detector Array gel permeation chromatography (GPC) system (Viscotek, Houston, TX) found that the average MW of this polymer was $4.4x10^6 \pm 0.2x10^6$ Da and the polydispersity index was 1.7 ± 0.4 [174]. Turbulent flow conditions (Re greater than 4000) must be attained in order to observe DRP drag reduction [175]. A PEO test fluid for *in vitro* testing of CAD has many advantages; PEO is a non-toxic, water-soluble, readily available DRP that is known to be the most effective drag reducer and also the most fragile compared to other DRPs [176-179]. Finally, the relatively fast mechanical degradation of PEO solutions over a 1-2 hour test time is advantageous for *in vitro* testing of CAD [70].

3.2 MATERIALS AND METHODS

A stock PEO solution of 2500 ppm concentration was prepared from Polyox WSR-301 (Dow Chemical, Midland, MI) by slowly dissolving the polymer powder in saline over several hours to avoid molecular degradation during the preparation procedure. Prior to testing, the stock solution

was diluted with saline to 1000 ppm and gently mixed for 2 hours. A fresh stock solution was prepared 1-2 days prior to each test.

Porcine blood was collected in plastic containers with 10% acid-citrate-dextrose anticoagulant (ACD; Gambro BCT, Lakewood, CO) from a local abattoir. Blood was filtered in 40 μm pore size filters (Pall Biomedical, SQ49S, Fajardo, PR) to remove white blood cells and platelet aggregates. Gentamicin (0.25 g/L; American Pharmaceutical Partners, Schaumburg, IL) was added to prevent bacterial growth. Blood Ht was measured using microhematocrit centrifugation (IEC MB Centrifuge, International Equipment Company, Needham Heights, MA) at 2,000×g for four minutes. Hematocrit was adjusted to a standard value of 30.0 ± 1.0% using autologous plasma. All blood testing was completed within three days of blood collection.

A Wells-Brookfield Cone/Plate viscometer (Model LVDV-IIIUCP, Middleboro, MA) with CPE-40 cone (cone radius = 2.4 cm, cone angle = 0.8º, sample volume = 0.5 ml) was used to measure viscosity of PEO solutions and blood samples. The viscosity of tested fluids was measured over a range of shear rates (40 to 400 s^{-1}) at a temperature of 25°C. A circulating water bath (Neslab RTE7, Thermo Fisher Scientific, Waltham, MA) was used to maintain constant temperature.

The turbulent flow circulating system used in this study is shown schematically in **Figure 3.1**. The system consisted of a centrifugal pump, either the Bio-Pump® BPX-80 (Medtronic, Inc., Minneapolis, MN) or CentriMag® (Thoratec Corporation), a glass tube (0.44 cm ID, 91.5 cm length), and a one liter open fluid reservoir. All parts of the flow system were interconnected with 3⁄8 inch ID Tygon® tubing (Cole-Parmer, Vernon Hills, IL). The fluid reservoir (1000 ml glass beaker) was immersed in a water bath to maintain constant temperature. A flow probe (8CB9, Transonic Systems Inc., Ithaca, NY) and pressure transducer (PCB Piezotronics, Inc.,

Depew, NY) were used to record flow rate and pressure. Wall shear stress (τ_{wall}) was maintained constant in the glass tube during each test and was calculated according to **Equation 11**. τ_{wall} was approximately 50 Pa for all tests.

$$\tau_{wall} = \frac{\Delta \mathrm{Pr}}{2L} \tag{11}$$

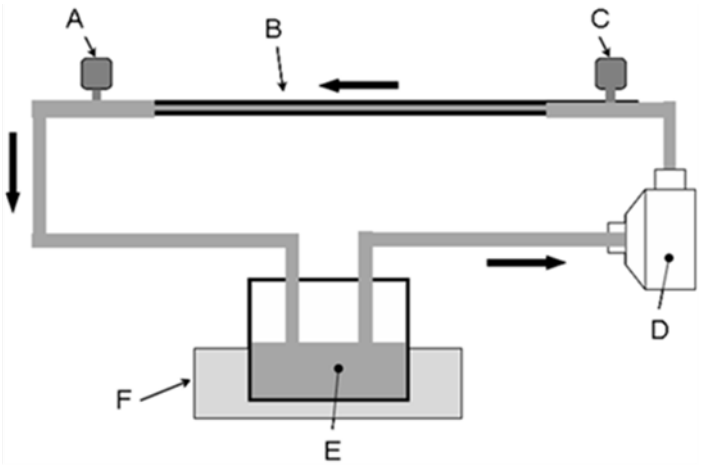

Figure 3.1. Schematic of the flow system used for studies of DRP mechanical degradation and shear-induced hemolysis in the centrifugal pumps studied.

[A] flow probe, [B] glass tube (0.44 cm ID, 91.5 cm length), [C] pressure transducer, [D] centrifugal pump (Bio-Pump® BPX-80 or CentriMag®), [E] open reservoir, [F] water bath.

1 L of 1000 ppm PEO solution was driven through the flow system for 120 minutes. The pressure gradient across the glass tube was maintained constant at 300 mmHg and flow rates were recorded. Since polymer drag reduction occurs only at turbulent flow conditions, the presence of turbulence in the system was verified by calculation of Re (**Equation 2**).

Mechanical degradation of DRP is defined as the loss of effectiveness in a polymer drag-reducing ability that is not regained once mechanical stress is removed [180]. In our study, PEO degradation was evaluated via reduction in drag-reducing efficiency and polymer solution

viscosity. Four experiments were performed (n=2 for each pump) and small samples (2 ml) of PEO solution were collected from the reservoir at 0, 3, 15, 30, 60 and 120 minutes to measure viscosity. DR was calculated as a percentage:

$$DR = \frac{Q_{DRP} - Q_{saline}}{Q_{saline}} \times 100 \tag{12}$$

where Q_{DRP} is the flow rate of the DRP solution and Q_{saline} is the flow rate of saline at the same pressure.

Mechanical degradation of PEO solution was quantified using the DRP mechanical degradation index (PDI) defined as:

$$PDI = \frac{DR_0 - DR_{120}}{\int Qdt} \tag{13}$$

where DR_0 is the original drag reduction of the PEO solution and DR_{120} is the drag reduction of the PEO solution after 120 minutes of testing.

For each centrifugal pump, hemolysis tests (n=4) were performed using the same flow circuit and conditions as in DRP degradation studies to directly compare the mechanical degradation of PEO with hemolysis generated by the pumps during 120 minute studies. Temperature in the flow system was maintained at 23 ± 2.0°C. Blood samples were obtained every 30 minutes from the reservoir for measurement of plfHb. Briefly, sample tubes were centrifuged for 15 minutes at 2200×g to obtain plasma. Plasma was transferred to microcentrifuge tubes and centrifuged at 20,800×g for 20 minutes in a microcentrifuge (Eppendorf 5417R, Eppendorf North America). Plasma was then transferred to disposable semi-micro cuvettes (Thermo Fisher Scientific, Waltham, MA). PlfHb was assessed for each sample using a spectrophotometer (Spectronic GENESYS 5, Thermo Fisher Scientific Inc., Waltham,

MA) at 540 nm wavelength. The spectrophotometer was calibrated to zero using a water blank. A standard curve of bovine Hb concentrations vs. absorbance values was used to calculate plfHb. The plfHb value used for subsequent blood damage quantification was the difference between the plfHb concentration in the 120 minute sample and the baseline sample.

Blood damage was characterized by the NIH [181]:

$$NIH = \frac{\Delta freeHb \times V \times \frac{(100 - Ht)}{100}}{Q \times T} \times 100 \qquad (14)$$

where ΔfreeHb is freeHb released during the test period T and V is blood volume of the circuit.

Statistical analysis was performed using two-tailed Student's *t*-tests for paired observations to determine the statistical significance of the difference in mean drag reduction, DRP degradation index (PDI), plfHb and NIH for the two flow systems. Linear regression analysis was performed to determine the correlation between the PDI and NIH for the Bio-Pump® and CentriMag® flow systems. Statistical significance was defined at $p<0.05$. Additional information regarding statistical analysis is presented in **Appendix B**.

3.3 RESULTS

Figure 3.2 shows the similar rheological behavior of 1000 ppm PEO solutions (n=4) and 30% Ht porcine samples (n=4) at a temperature of 25°C. To ensure comparable flow fields within the centrifugal pumps studied, H-Q testing was performed on the Bio-Pump® and CentriMag® flow systems using water as a test fluid. H-Q behavior was very similar in both systems (**Figure 3.3**).

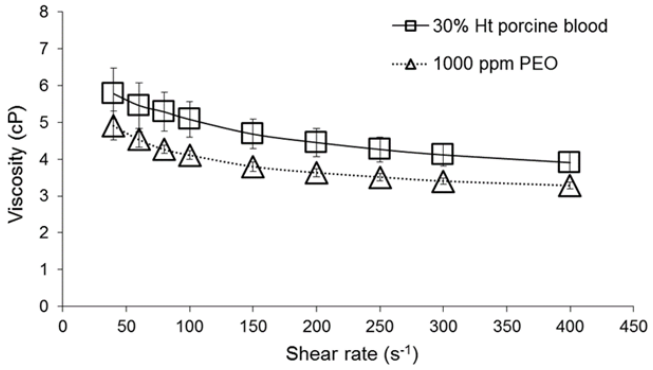

Figure 3.2. Viscosity of 30% hematocrit porcine blood and 1000 ppm PEO solution measured at 25°C. Values are shown as mean±SD.

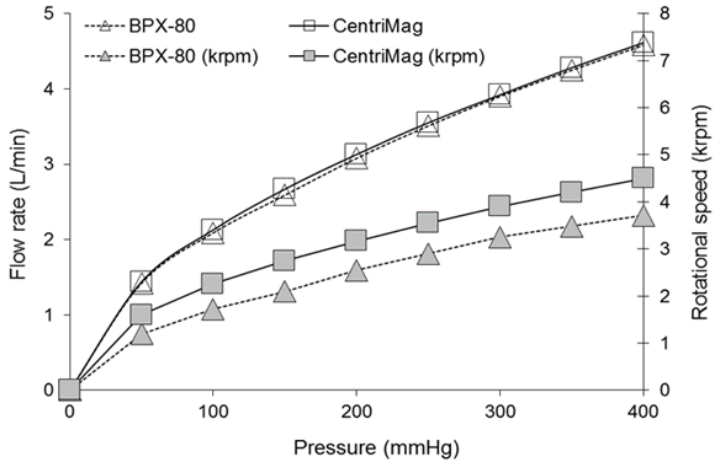

Figure 3.3. Flow-pressure characteristics of the flow system and rotational speed of the Bio-Pump® and CentriMag® centrifugal pumps.

Reynolds numbers in the glass tube ranged from 7000 to 11000 in the DRP experiments characterizing a fully-developed turbulent flow in the tube. Flow rate of the PEO solution in the flow system at the beginning of each study was 5.0 L/min. After two hours, flow rate in both the Bio-Pump® and CentriMag® flow systems decreased to 4.05 ± 0.01 and 4.17 ± 0.03 L/min respectively. The decrease in flow rate represented the decrease in PEO drag-reducing ability, hence indicating polymer mechanical degradation (**Figure 3.4**). Calculated drag reduction of the

PEO solution declined during 120 minute tests in the two flow systems (**Figure 3.5**). Analysis revealed a statistically significant difference ($p = 0.005$) between the mean DR calculated for the two flow systems.

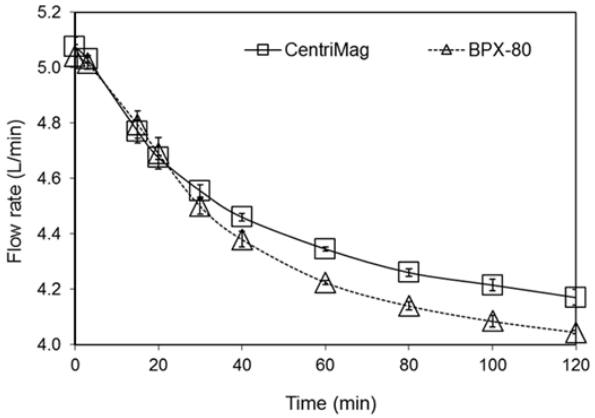

Figure 3.4. Changes in PEO solution flow rate in Bio-Pump® and CentriMag® flow systems. Values are shown as mean±SD.

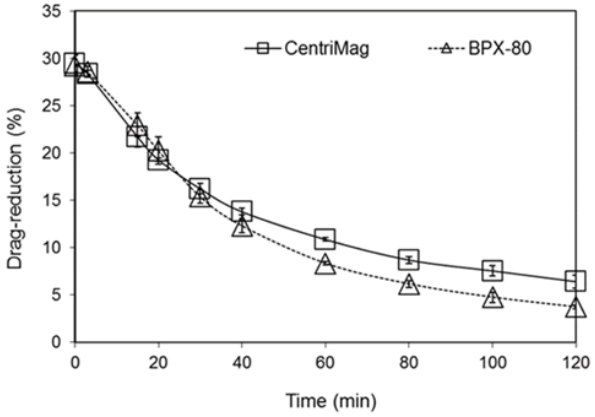

Figure 3.5. Changes in PEO solution drag reduction in Bio-Pump® and CentriMag® flow systems. Values are shown as mean±SD.

A direct measurement of PEO mechanical degradation was attained by evaluating the changes in PEO MW and solution viscosity during degradation tests. **Figure 3.6** shows the extrapolation of MW vs. viscosity values obtained for several commercial PEO with known MW

to determine PEO MW during tests. At 120 minutes, PEO MW was calculated as 868 kDa and 1,410 kDa in the Bio-Pump® and CentriMag® flow systems, respectively (**Figure 3.7**). Statistical analysis revealed a significant difference ($p = 0.01$) between the MW calculated for the two flow systems. Viscosity of PEO solution (150 s^{-1} shear rate, 25°C temperature) decreased in both flow systems during tests. At baseline, PEO solution viscosity was 3.80 ± 0.12 cP in each flow system and decreased to 1.79 ± 0.05 cP and 2.19 ± 0.08 cP after 120 minutes in the Bio-Pump® and CentriMag® flow systems, respectively (**Figure 3.8**).

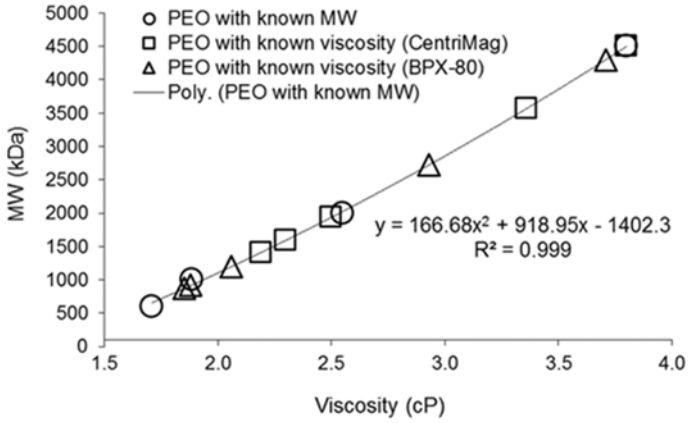

Figure 3.6. 1000 ppm PEO MW calculated using PEO solution viscosities measured during flow tests and measured for 1000 ppm PEO preparations with known MW.

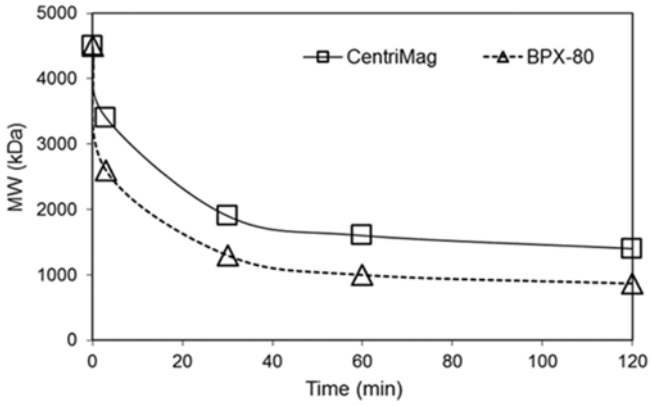

Figure 3.7. Changes in molecular weight of PEO solution in Bio-Pump® and CentriMag® flow systems.

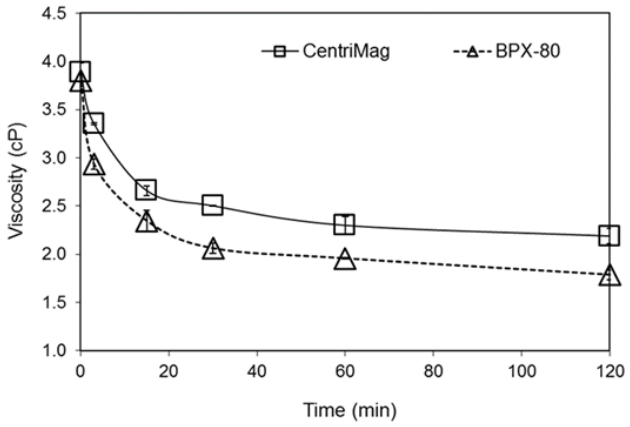

Figure 3.8. Changes in asymptotic viscosity of PEO solution in Bio-Pump® and CentriMag® flow systems. Values are shown as mean±SD.

Mean PDI of the Bio-Pump® and CentriMag® flow systems at 120 minutes was calculated as 0.049 ± 0.001 %/L and 0.041 ± 0.002 %/L, respectively. Statistical analysis revealed a significant difference (p=0.03) between the mean PDI calculated for the two flow systems.

Change in plfHb from baseline to end of study was 29.8% higher in the Bio-Pump® than the CentriMag® flow system (**Figure 3.9**). Mean plfHb values were statistically significantly different (p = 0.048) in the two flow systems. Mean NIH of the CentriMag® and Bio-Pump® flow systems at 120 minutes was calculated as 0.005 ± 0.003 g/100L and 0.018 ± 0.003 g/100L, respectively. Analysis revealed a significant difference (p=0.006) between the mean NIH calculated for the two flow systems.

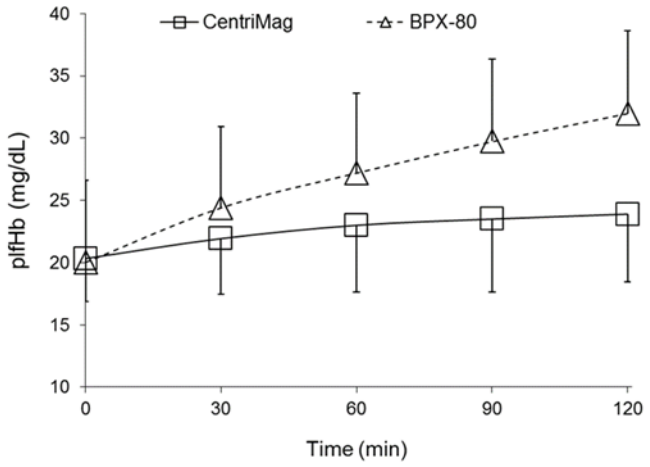

Figure 3.9. Changes in plasma free hemoglobin concentration of 30% Ht porcine blood in Bio-Pump® and CentriMag® flow systems. Values are shown as mean+SD.

Linear regression of the PDI and the NIH at 120 minute time points for the CentriMag® and Bio-Pump® flow systems is shown in **Figure 3.10**. The coefficient of determination for this analysis is 0.991.

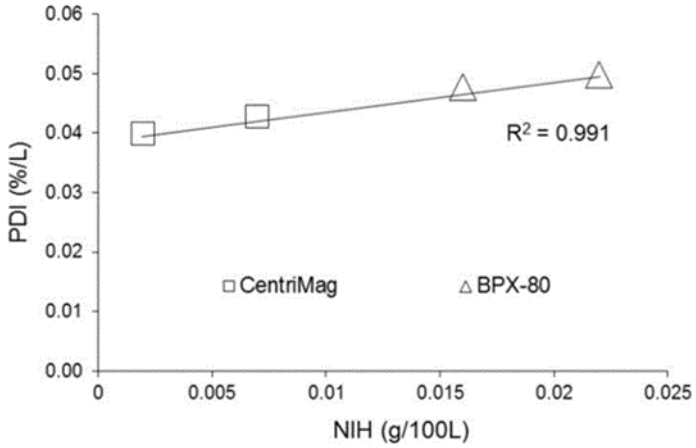

Figure 3.10. Linear regression of the DRP degradation index and normalized index of hemolysis at 120 minutes of testing for the Bio-Pump® and CentriMag® flow systems.

3.4 DISCUSSION

Development of mechanical circulatory support devices requires extensive *in vitro* testing prior to conducting animal studies and the ultimate realization of clinical use. Due to the variations in testing conditions, different sensitivity to mechanical stress of RBC from various species, and dependence of RBC-MF on storage time, the comparison of results of different blood pump tests is difficult. I proposed to use a solution of water-soluble DRP with rheological properties and shear stress sensitivity similar to that of blood as a substitute for human or animal blood in the *in vitro* assessment of potential mechanical blood damage in CAD.

A PEO solution was investigated to determine whether the loss of PEO drag-reducing ability due to the mechanical degradation of the polymer can indicate the degree of shear-induced blood damage within two clinically-used CAD. DRP mechanical degradation was determined empirically via recording a decrease in fluid flow rate at a constant pressure gradient and by calculation of drag reduction after 120 minutes of circulation in the two flow systems (**Figure 3.4** and **Figure 3.5**). In addition, PEO mechanical degradation was confirmed by reduction in PEO molecular weight and solution viscosity (**Figure 3.7** and **Figure 3.8**). PEO solution viscosity, MW, and drag-reducing ability exhibited a larger decrease in the Bio-Pump® system than in the CentriMag® flow system, signifying that the Bio-Pump® exerted greater mechanical stress on PEO molecules.

The novel PDI, based upon the change in PEO drag reduction per passing volume, was significantly higher in the Bio-Pump® than the CentriMag® flow system at 120 minutes of testing. Hemolysis testing revealed that mean plfHb concentration and NIH in the Bio-Pump® flow system were also significantly higher than corresponding values for the CentriMag® flow

system, thereby confirming a higher degree of mechanical stress in the Bio-Pump® than the CentriMag®. The PDI was compared to the NIH typically used to characterize blood damage in *in vitro* hemolysis tests and compare various CAD. The two indices were found to be highly correlated with a coefficient of determination of 0.991 (**Figure 3.10**).

With improvements in biocompatibility of novel CAD, *in vitro* hemolysis testing becomes more challenging due to the reduction in mechanical blood damage produced by the devices. Thus, hemolysis testing of novel CAD would require prolonged test times to detect blood damage with the likelihood for test artifacts. The results of this study showed that the mechanical degradation of DRP can predict the potential mechanical hemolysis produced in CAD. The PDI may be used as a sensitive indicator of hemolysis produced in the pumps without the use of blood and with a faster response to mechanical stress. PEO solutions may provide simple standard test fluids for the *in vitro* evaluation of potential blood trauma produced in CAD.

3.5 CONCLUSIONS

This chapter summarizes the investigation to determine whether the mechanical degradation of a DRP solution resulting in the loss of drag-reducing ability can indicate the degree of shear-induced blood damage within blood pumps. Results demonstrated that DRP mechanical degradation in a turbulent flow system with an incorporated blood pump may provide useful information on the device performance predicting potential hemolysis produced by a CAD without the use of blood. A simple, reliable method for the characterization of DRP mechanical degradation was realized via recording the decrease in DRP solution flow rate at a constant

pressure and measurements of polymer solution viscosity in samples collected from the flow system during testing. A novel PDI was found to be highly correlated to the NIH in these studies. Moreover, the use of a PEO solution as a test fluid for the *in vitro* testing of CAD and calculation of the PDI yields an innovative, useful substitute to blood and a similar damage index as the NIH traditionally used for evaluation and comparison of CAD.

4.0 BLOOD BANK STORAGE EFFECT ON THE RHEOLOGICAL PROPERTIES OF MALE AND FEMALE DONOR ERYTHROCYTES

Chapter 4 has been published in the journal Clinical Hemorheology and Microcirculation [62].

4.1 INTRODUCTION

It has been long known that RBC-D decreases during blood bank storage of donor RBC [182]. The various changes that occur to RBC during storage in blood banks are known as the storage lesion [183] and include decreased intracellular concentrations of adenosine triphosphate (ATP) [182] and 2,3-diphosphoglycerate (2,3-DPG) [184], increased freeHb and microparticle formation [185]. Currently, allogeneic RBC units can be transfused within 42 days when preserved in an FDA approved additive solution and stored at 1-6°C. One unit of RBC contains approximately 200 ml RBC, 100 ml additive solution and approximately 50 ml donor plasma. AS-5 is a commonly used additive solution for packed RBC storage and consists of saline, mannitol, adenine, and dextrose [186].

Previous investigators examined the changes in RBC-D of whole blood or RBC suspensions during prolonged laboratory storage (up to 42 days) at ~4°C using filtration [184], viscometry [187], a cell flow properties analyzer [188], an oscillatory flow chamber [189] and

ektacytometry [187]. Another sensitive assessment of RBC-D was proposed and implemented through the measurement of RBC suspension or whole blood viscoelasticity [32, 190]. Human blood and RBC suspensions were proven to be viscoelastic fluids that exhibit both viscous (energy-dissipative) and elastic (energy-storing) characteristics when exposed to shear deformation [32, 190]. The measurement of fluid viscoelasticity can be performed under oscillatory flow at a standard frequency, e.g. of 2 Hz, in a rigid capillary tube [33]. Additional information on the measurement of whole blood or RBC suspension viscoelasticity is presented in **Section 2.3**.

Human blood or RBC suspensions under flow require a finite time for microstructural changes to occur and the rate of change is dependent on the time for the fluid to reach equilibrium upon a change in flow conditions [191]. Hence, flowing human blood or RBC suspensions possess a non-zero relaxation time, which defines the time dependency of how elastic structures return to their original shape after the cessation of flow [72]. Increased RBC suspension relaxation times are a result of decreased RBC deformability and increased RBC-A [72, 191]. Relaxation time can be calculated as [72, 191]:

$$\lambda = \frac{\eta''}{\omega \eta'} \tag{15}$$

where variables are defined in **Section 2.3**.

Previous studies of the effect of prolonged laboratory storage at ~4°C on blood or RBC suspension viscoelasticity were conducted with donor RBC units prepared in a laboratory. Farges *et al.* examined the changes in RBC membrane viscoelasticity of stored RBC in SAG-M (sodium chloride, adenine, glucose, mannitol) solution during 42 days of storage using an oscillatory flow chamber with 0.03% Ht samples [189]. Riquelme *et al.* studied whole blood and

RBC from three donors stored in CPDA (trisodium citrate, citric acid, sodium dihydrogen phosphate, dextrose and adenine) solution for 28 days using a cone-and-plate viscometer and homemade ektacytometer [187]. Although a general decrease in RBC-D as storage time increased was reported in both studies, neither study investigated the effects of prolonged storage on donor RBC at blood bank preparation and storage conditions.

Recent studies of the effect of prolonged blood bank storage at ~4°C on RBC membrane deformability were conducted with AS-3 [192] and SAG-M [193] preserved leukoreduced RBC units using a laser-assisted optical rotational cell analyzer (LORCA). Bennett-Guerrero *et al.* reported significant decreases in RBC membrane deformability (elongation indices measured at 3 Pa and 30 Pa shear stresses) during 42 days of storage in AS-3 solution [192] while Henkelman *et al.* reported significant decreases in RBC membrane deformability (elongation indices measured at 50 Pa shear stress) during 49 days of storage in SAG-M solution [193]. Although both studies examined single RBC membrane deformability during blood bank storage, neither assessed changes in cell deformability of a bulk RBC suspension. In this study, the potential effects of donor gender and storage period on RBC suspension viscoelasticity and relaxation time using leukoreduced RBC preserved in AS-5 solution tested at 7, 28 and 49 days of storage at ~ 4ºC in a blood bank were investigated.

4.2 MATERIALS AND METHODS

AS-5 preserved, prestorage leukoreduced RBC units were provided by the regional FDA licensed Blood Bank (Central Blood Bank, Pittsburgh, PA). A total of 24 packed RBC units

(three units from each of the ABO groups) were obtained from both male (n=12) and female donors (age<50 years, n=12) and stored between 1-6°C in a blood bank refrigerator for seven weeks. Approximately 60 ml of RBC were aseptically removed from each unit and transferred into a sterile container. The original Ht of each sample was measured using microhematocrit centrifugation with an average Ht of 58.8±2.6%. Each sample was then diluted to a 40±1% Ht using DPBS in 50 ml conical tubes at the end of storage weeks 1, 4, and 7. The storage times were chosen to maintain a three week interval between measurements.

Viscoelasticity of male (n=12) and female (n=12) RBC suspensions was measured using a Vilastic-3 Viscoelasticity Analyzer (Vilastic Instruments Inc., Austin, TX) with a stainless steel capillary measurement tube (0.512 mm inner radius, 6.18 cm length). The RBC suspensions were exposed to oscillating flow at a fixed frequency of 2 Hz at linearly increasing shear rates ranging from 25 to 250 s^{-1} with increments of 25 s^{-1}. Prior to recording results at each shear rate, the RBC suspensions were permitted to equilibrate to the higher shear rate for five seconds. A circulating water bath (Neslab RTE7, Thermo Fisher Scientific, Waltham, MA) was used to maintain a temperature of 25.0±0.1ºC for all measurements. Relaxation time of the stored RBC suspensions was calculated by the Vilastic software utilizing the measured RBC suspension viscosity and elasticity at each shear rate according to **Equation 15** with a frequency of 2 Hz.

Statistical analysis was performed using ANOVA to analyze the effect of storage time on the viscosity, elasticity and relaxation time of RBC suspensions measured at shear rates of 25 s^{-1} and 100 s^{-1}. Post-hoc testing was conducted using the Tukey method. Independent two-way *t*-tests were performed to compare male and female RBC suspension viscosity, elasticity and relaxation time measured at 25-250 s^{-1} shear rates at equivalent storage times. Correlations between the changes in the RBC-MFI measured for the same RBC suspensions prepared from

the same male and female donor units and reported in [61] and the changes in RBC rheological parameters reported in this study were calculated using bivariate correlation analysis. Statistical significance was defined at $p<0.05$. Additional information regarding statistical analysis is presented in **Appendix C**.

4.3 RESULTS

Figures 4.1 and 4.2 show male and female RBC suspension viscosity measured at shear rates of 25 s^{-1} and 100 s^{-1} at each storage time. Male RBC suspension viscosity demonstrated significant increases from Week 1 to Week 4 and from Week 1 to Week 7 of blood bank storage (**Figure 4.1**), while female RBC suspension viscosity significantly increased during each storage time period (**Figure 4.2**).

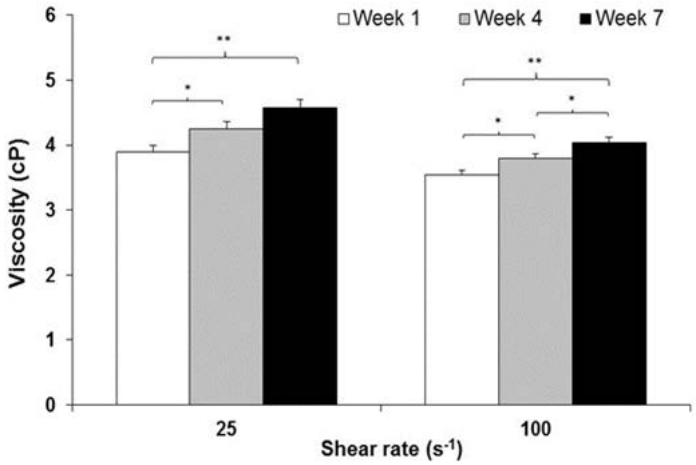

Figure 4.1. Viscosity of male 40% hematocrit RBC suspensions measured at 25 s^{-1} and 100 s^{-1} shear rates at Weeks 1, 4 and 7 of storage. Values are shown as mean±SEM. * indicates $p<0.05$ and ** indicates $p<0.001$.

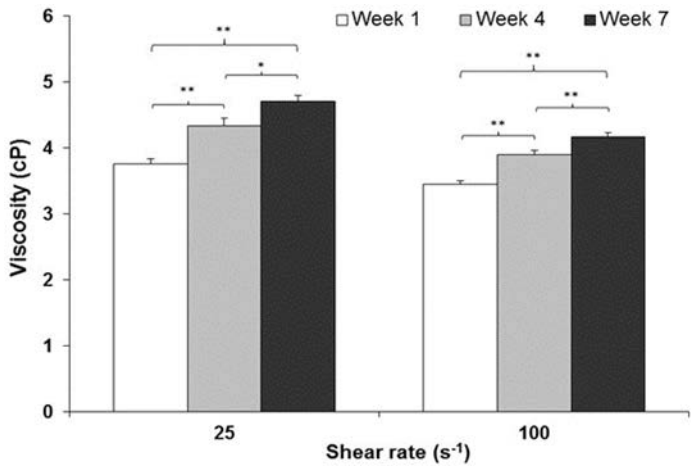

Figure 4.2. Viscosity of female 40% hematocrit RBC suspensions measured at 25 s^{-1} and 100 s^{-1} shear rates at Weeks 1, 4 and 7 of storage. Values are shown as mean±SEM. * indicates $p<0.05$ and ** indicates $p<0.001$.

Similarly, **Figures 4.3 and 4.4** show male and female RBC suspension elasticity, respectively, measured at shear rates of 25 s^{-1} and 100 s^{-1} at each storage time. Male RBC suspension elasticity demonstrated significant increases from Week 1 to Week 4 and from Week 1 to Week 7 of blood bank storage (**Figure 4.3**), while female RBC suspension elasticity significantly increased during each storage time period (**Figure 4.4**).

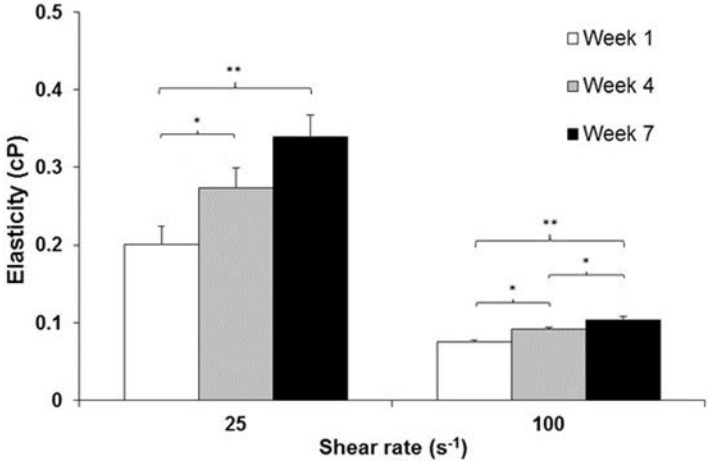

Figure 4.3. Elasticity of male 40% hematocrit RBC suspensions measured at 25 s^{-1} and 100 s^{-1} shear rates at Weeks 1, 4 and 7 of storage. Values are shown as mean±SEM. * indicates $p<0.05$ and ** indicates $p<0.001$.

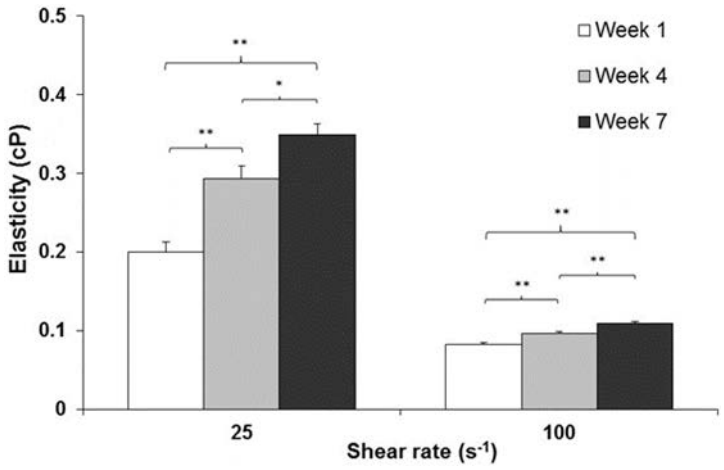

Figure 4.4. Elasticity of female 40% hematocrit RBC suspensions measured at 25 s^{-1} and 100 s^{-1} shear rates at Weeks 1, 4 and 7 of storage. Values are shown as mean±SEM. * indicates $p<0.05$ and ** indicates $p<0.001$.

Figures 4.5 and 4.6 show male and female RBC suspension relaxation time calculated at 25 s^{-1} and 100 s^{-1} shear rates at each storage time. Male RBC suspension relaxation time demonstrated significant increases from Week 1 to Week 4 and from Week 1 to Week 7 of blood bank storage (**Figure 4.5**), while female RBC suspension relaxation time significantly increased during each storage time period (**Figure 4.6**).

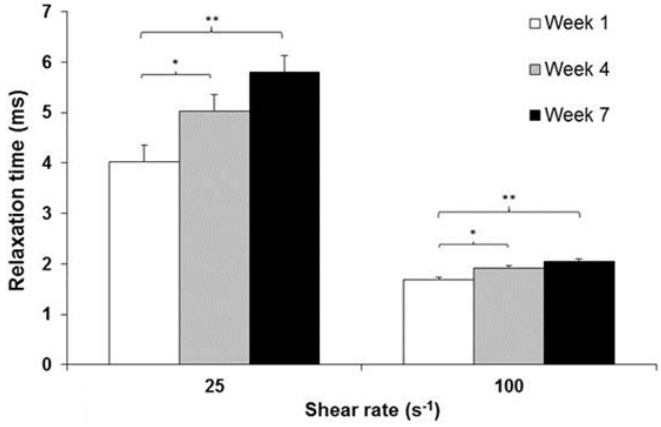

Figure 4.5. Relaxation time of male 40% hematocrit suspensions calculated at 25 s^{-1} and 100 s^{-1} shear rates at Weeks 1, 4 and 7 of storage. Values are shown as mean±SEM. * indicates $p<0.05$ and ** indicates $p<0.001$.

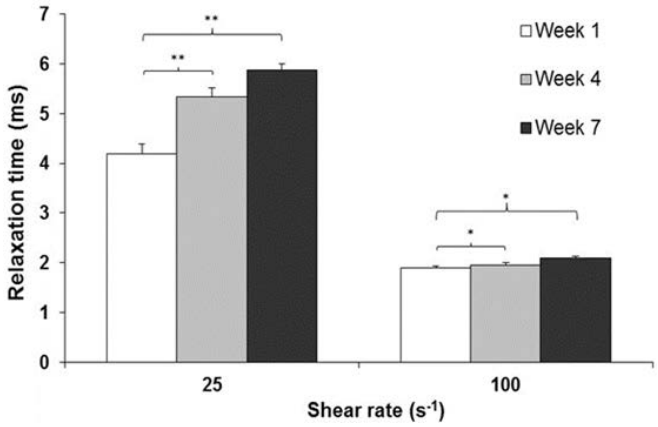

Figure 4.6. Relaxation time of female 40% hematocrit suspensions calculated at 25 s^{-1} and 100 s^{-1} shear rates at Weeks 1, 4 and 7 of storage. Values are shown as mean±SEM. * indicates $p<0.05$ and ** indicates $p<0.001$.

RBC suspension elasticity, viscosity and relaxation time measured at shear rates of 25 - 250 s^{-1} were not statistically significantly different ($p>0.05$) between males and females at any storage time point. **Table 4.1** shows the correlations between the changes in RBC-MFI reported in [61] and RBC suspension VE and relaxation time measured in this study using the same RBC suspensions prepared from the same 12 male and 12 female RBC units during seven weeks of blood bank storage. The correlations between RBC-MFI and RBC suspension VE and relaxation time are highly significant and suggest that both parameters, RBC-D and RBC-MFI, are indicative of changes in sublethal RBC damage during blood bank storage.

Table 4.1. Correlation between changes from Week 1 to Week 7 of storage in RBC mechanical fragility index reported in [61] and RBC suspension elasticity, viscosity, and relaxation time measured at a 100 s^{-1} shear rate reported herein.

	MFI vs. Elasticity		**MFI vs. Viscosity**		**MFI vs. Relaxation time**	
	Pearson correlation coefficient, r	*p*-value	Pearson correlation coefficient, r	*p*-value	Pearson correlation coefficient, r	*p*-value
Male (n=12)	0.44	<0.01	0.29	>0.05	0.49	<0.01
Female (n=12)	0.76	<0.01	0.68	<0.01	0.50	<0.01

4.4 DISCUSSION

It has been long known that laboratory storage of RBC at 4ºC results in a decrease in RBC-D as the length of storage increases. Yet, there are no reported studies of the effects of prolonged blood bank storage of donor RBC preserved in AS-5 solution on packed RBC VE and relaxation time. In this chapter, we investigated the effect of storage time on male and female RBC-D and relaxation time derived from the measurement of bulk RBC suspension VE.

Male and female RBC suspension VE and relaxation time significantly increased during seven weeks of blood bank storage. These results demonstrate that RBC-D of the male and female RBC decreased during the blood bank storage period, which was evident at 28 days and continued to decrease as the storage time increased to 49 days. There were no statistically significant differences between male and female RBC suspension viscosity, elasticity and relaxation time at any storage time.

RBC suspension relaxation time is a calculated parameter that is an indicator of RBC rigidity. Thurston and Henderson found that the relaxation time of hardened human RBC had

longer relaxation times than normal RBC [191]. Chmiel *et al.* found that RBC relaxation time of human blood increased in several pathological conditions, including cardiovascular disease, stroke and peripheral vascular disease compared to normal human blood [72]. These results corroborate the results presented herein that the increase in male and female RBC suspension relaxation time during blood bank storage is due to the progressively decreased deformability of stored male and female RBC during the seven week period. The decrease in RBC-D during blood bank storage may reduce capillary flow and tissue perfusion in transfused patients and accelerate RBC post-transfusion removal from the vascular system.

The storage related changes in RBC-MF measured in the same set of male and female RBC units as those used in this study and reported in [61] were compared to the changes in RBC suspension viscosity, elasticity and relaxation time presented in this report. Bivariate correlations of storage related changes in the RBC-MFI and viscoelastic parameters demonstrated significant correlations for the male and female donor groups. This suggests that the assessment of RBC-D can be used in conjunction with the RBC-MF test [126] to provide a comprehensive evaluation of the extent of sublethal RBC damage in a variety of conditions, including blood bank storage.

Recent publications report numerous incidences of adverse clinical outcomes associated with the transfusion of older blood bank RBC units, but it is highly debated whether there is a significant relationship between storage-induced RBC changes (i.e. decreased RBC-D, increased RBC-MF, etc.) and the outcome in transfused patients [194-198]. Results of our study support the need for large, randomized, controlled trials that elucidate the clinical impact of transfusing patients with brief storage versus prolonged storage blood bank RBC [197].

4.5 CONCLUSIONS

This chapter summarizes the investigation of the effects of donor gender and blood bank storage time on bulk RBC-D (RBC suspension VE and relaxation time) of leukoreduced RBC stored in AS-5 solution at 4ºC. Both male and female RBC suspensions demonstrated significant increases (p<0.05) in viscosity, elasticity and relaxation time over seven weeks of blood bank storage, which signifies a decrease in donor RBC-D. No statistically significant differences in RBC-D or relaxation time were observed between male and female RBC at any storage time point. The clinical significance of the changes in donor RBC-D and relaxation time during blood bank storage warrant further investigation.

5.0 EXPERIMENTAL INVESTIGATION OF FLOW-INDUCED HEMOLYSIS AS A FUNCTION OF SHEAR STRESS AND EXPOSURE TIME

5.1 EFFECT OF VARYING EXPOSURE TIME TO A CONSTANT SHEAR STRESS ON FLOW-INDUCED HEMOLYSIS

5.1.1 Introduction

A well supported mechanism of flow-induced hemolysis reported in the literature is the effect of shear stress and exposure time (t_{exp}) [5, 96, 97, 107]. Previous reports that studied hemolysis as a function of shear stress and exposure time primarily used concentric cylinder viscometers [67] that exposed RBC to uniform shear conditions for certain exposure times [5, 97, 98]. Studies of variable shear stresses and exposure times have also been conducted in roller pumps [80], a capillary system [109] and other systems [110, 111].

For testing *in vitro* blood damage produced by a CAD, the ASTM recommends using 500 ml or 1 L of human or animal blood in a large flow circuit [199]. Currently, there are no ASTM recommendations for hemolysis testing of pediatric CAD. The testing of CAD designed for these small patients should be performed using a circulating volume similar to the blood volume of these children, approximately 150-350 ml [77]. However, *in vitro* hemolysis testing in small volume flow systems may affect the resulting blood damage due to increased RBC total exposure

time (T_{exp}) in the CAD [200]. This may cause cumulative sublethal damage during testing and lead to elevated hemolysis not accounted for by the NIH, but a study of this effect has not been reported. The objective of this study was to examine the effect of varying blood T_{exp} at a constant shear stress on the resulting mechanical hemolysis and calculated NIH.

5.1.2 Materials and Methods

Bovine blood was collected from donor or abattoir animals, filtered and Ht was measured and adjusted to 30±1% using autologous plasma. THb was measured for blood samples at T=0 of testing using a hemoximeter (OSM3, Radiometer Inc.). The centrifugal pump flow system used in this study was modified from Kameneva *et al.* [106] and consisted of a blood bag (Qosina Inc.), microtube, CentriMag® or PediMag® centrifugal pump (Thoratec Corporation), flow probe (Transonic Systems Inc.), thermistor (Cole-Parmer Instrument Company), three pressure transducers (PCB Piezotronics, Inc.) and Tygon tubing.

Blood volumes of 60 ml (n=6), 125 ml (n=8), 250 ml (n=6) and 500 ml (n=6) were tested in the flow systems at similar τ_{wall} ~150-190 Pa in the microtubes. Hemolysis tests were performed in the CentriMag® system with a microtube (1.4 mm ID, 140 mm length) and blood volumes of 250 ml (n=6) and 500 ml (n=6). The flow rate was ~0.8 L/min which corresponded to τ_{wall} ~150 Pa and Re in the tube ~3000-3400. The PediMag® flow system had a microtube (1 mm ID, 70 mm length) and tests were performed with blood volumes of 60 ml (n=6) and 125 ml (n=12). The flow rate in these tests were ~0.30 L/min which corresponded to τ_{wall} ~190 Pa and Re~1600-2000 in the microtube. All tests were performed for one hour and blood samples were

withdrawn from the loop at 0 and 60 minutes of testing for measurement of freeHb and calculation of NIH. Exposure time in the microtubes were calculated as:

$$t_{\exp} = \frac{V}{Q} = \frac{\pi r^2 L}{Q} \tag{16}$$

where V is the volume of the tube, L is tube length, r is tube radius, and Q is flow rate.

The number of passes through the system was calculated as:

$$N = \frac{QT}{V} \tag{17}$$

where Q is flow rate, T is test time and V is circulating blood volume.

Total exposure time (T_{exp}) was calculated as:

$$T_{\exp} = Nt_{\exp} \tag{18}$$

For each blood volume, T_{exp} was between ~1.6-3.3 s.

Blood damage was further characterized by an Index of Hemolysis (IH):

$$IH = \frac{\Delta freeHb}{tHb} \tag{19}$$

where ΔfreeHb is the change in freeHb from baseline after testing and tHb is the total hemoglobin concentration in the RBC suspension.

Statistical analysis was performed using ANOVA to determine the statistical significance of the difference in freeHb generation and the calculated NIH among the 60 ml, 125 ml, 250 ml and 500 ml blood volumes tested in the centrifugal pump flow systems. Post-hoc testing was conducted using either the Tukey or Games-Howell methods contingent upon the results of homogeneity of variances tests. Multiple regression analysis was performed using the power model to determine the empirical coefficients (A, α and β) for the IH (ΔfreeHb/tHb) in the

centrifugal pump flow systems. Statistical significance was defined at $p<0.05$. Additional information regarding statistical analysis is presented in **Appendix D**.

5.1.3 Results

Figure 5.1 shows freeHb measured for the 60 ml, 125 ml, 250 ml and 500 ml blood volumes at 1.6-3.3 s total exposure times in the glass capillaries of the CentriMag® or PediMag® flow systems. All blood volumes studied had a similar rate of increase in freeHb at comparable total exposure times in the microtubes of the centrifugal pump flow systems, but the change in freeHb from baseline (ΔfreeHb) for the 250 ml blood volume was statistically significantly different from the 500 ml blood volume (p=0.045) tested at the same 150 Pa τ_{wall} in the glass capillary of the CentriMag® flow system.

Figure 5.2 shows the NIH calculated for each blood volume at 60 minutes of testing, which corresponds to RBC T_{exp} of 1.6-3.3 s. The NIH calculated for the 60 ml blood volume was statistically significantly different from all other blood volumes studied (**Figure 5.2**). Moreover, the NIH calculated for the 125 ml blood volume was significantly different than the 500 ml blood volume (p=0.04).

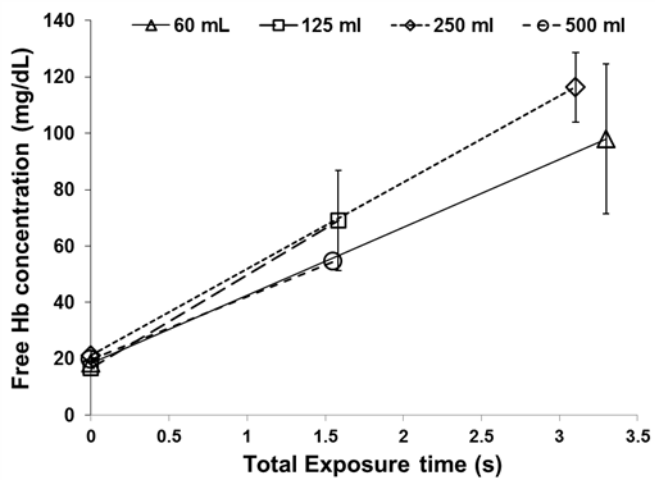

Figure 5.1. Free hemoglobin concentration in 60 ml, 125 ml, 250 ml and 500 ml 30% hematocrit bovine blood volumes at various total exposure times in centrifugal pump flow systems. Values are shown as mean±SEM.

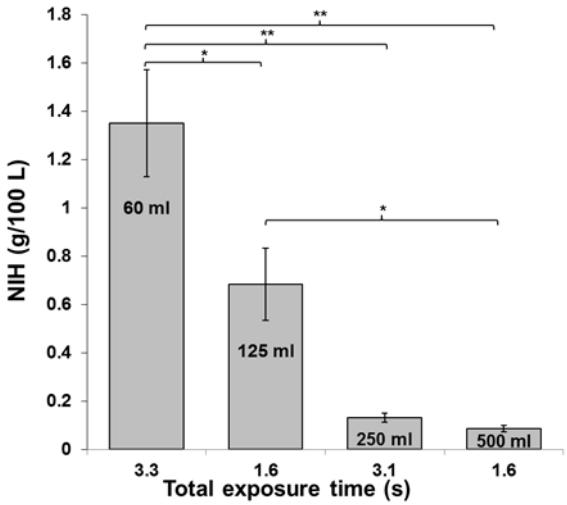

Figure 5.2. Normalized index of hemolysis calculated for 60 ml, 125 ml, 250 ml and 500 ml 30% hematocrit bovine blood volumes at various total exposure times in centrifugal pump flow systems.

Values are shown as mean±SEM. * indicates $p<0.05$ and ** indicates $p<0.001$.

Multiple regression analysis of the IH (ΔfreeHb/tHb) of the centrifugal pump hemolysis results was performed using the power model and compared to published results in the literature

[112-114]. The empirical coefficients A, α and β, of the power law model (**Equation 10)** of IH in mechanical heart valves [112] and centrifugal pumps [113, 114] are shown in **Table 5.1**.

Table 5.1. Power law empirical coefficients obtained from multiple regression of mechanical hemolysis in three reported studies.

Author	**Index of Hemolysis**	**A**	**α**	**β**	**Primary source of blood damage**
Giersiepen *et al.* (1990)	ΔHb/Hb	0.0000362	2.416	0.758	Mechanical heart valves
Song *et al.* (2003 & 2004)	ΔHb/Hb	0.0000018	1.991	0.765	Centrifugal pump
Sivek (current work)	ΔHb/Hb	0.0000482	1.748	0.514	Centrifugal pumps

5.1.4 Discussion

It is well known that shear stress and exposure time contribute toward mechanical hemolysis *in vitro* [5, 96, 97, 107]. Yet, a dearth of literature regarding the effect of *in vitro* CAD testing using small volume (< 500 ml) systems on mechanical hemolysis and the NIH exists. The objective of this study was to examine the effect of varying blood T_{exp} at constant shear stresses in centrifugal pump flow systems.

In centrifugal pump flow systems with glass capillaries, testing of 60 ml, 125 ml, 250 ml and 500 ml 30% Ht bovine blood volumes for 60 minutes demonstrated similar rates of increase in freeHb at comparable total exposure times in the microtubes (**Figure 5.1**). The ΔfreeHb between the 250 ml and 500 ml blood volumes were significantly different (p=0.045). The tests occurred at the same 150 Pa wall shear stress in the glass capillary, but had T_{exp} of 1.6 s (500 ml) and 3.1 s (250 ml). The NIH calculated for the 60 ml blood volume was significantly different from all other blood volumes studied (**Figure 5.2**). The NIH between the 125 ml and 500 ml

blood volumes were significantly different (p=0.039). Although the 30% Ht blood volumes were tested at approximately the same 1.6 s T_{exp} in the capillary flow system, the 125 ml volume (190 Pa) was exposed to a ~40 Pa higher wall shear stress in the glass capillaries than the 500 ml blood volume (150 Pa).

Numerical predictions of blood damage are commonly performed using power-law models such as those of Giersiepen *et al.* [112] and Song *et al.* [113, 114]. To compare the hemolysis results from the centrifugal pump studies with these reports, multiple regression analysis was performed using the power model to determine the empirical coefficients (A, α and β) of the IH. The empirical coefficients A, α and β were 0.0000482, 1.748 and 0.514, respectively. The coefficients in this study were similar to the empirical coefficients in published reports (**Table 5.1**) and thus, the predicted blood damage in the centrifugal pump flow system is comparable to results in the literature [112-114].

For hemolysis testing of pediatric CAD, a circulating blood volume similar to the blood volume of these children, approximately 150-350 ml [77], should be used in the test circuit. This study examined *in vitro* hemolysis in 60-500 ml volume flow systems to elucidate whether blood damage and the calculated NIH was augmented by increased RBC T_{exp} in CAD in small volume test circuits. The results from the centrifugal pump flow system tests identify a range of blood volumes suitable for *in vitro* hemolysis testing of pediatric CAD as $150ml \leq V < 500$ ml.

5.1.5 Conclusions

This section summarizes the investigation of the effects of shear stress and RBC total exposure time in centrifugal pump flow systems using blood volumes ranging from 60-500 ml. *In vitro*

hemolysis testing in centrifugal pump flow systems demonstrated the statistically significant effect of RBC T_{exp} on flow-induced hemolysis (ΔfreeHb, NIH and ΔfreeHb/tHb). Multiple regression analysis using the power model demonstrated similar blood damage (ΔfreeHb/tHb) in the centrifugal pump flow systems as predicted in published reports. The hemolysis results from the centrifugal pump flow systems indicate that a suitable blood volume range for conducting *in vitro* hemolysis testing of pediatric CAD is 150ml≤V<500 ml.

5.2 EFFECT OF RED BLOOD CELL MECHANICAL FRAGILITY ON FLOW-INDUCED HEMOLYSIS

5.2.1 Introduction

Sublethal RBC damage was first described by Galletti [3, 78] for partial extracorporeal circulation experiments and is characterized by a decrease in RBC-D and an increase in RBC-A, RBC-MF and RBC suspension or blood viscosity [117, 134]. RBC-MF is defined qualitatively as the erythrocytes susceptibility to damage due to mechanical forces encountered *in vivo* or *in vitro*.

The relationship of mechanical hemolysis and RBC-MF *in vitro* was examined by several investigators using different apparatus. Rous and Turner studied the species difference in RBC-MF of human, dog, rabbit and sheep RBC by shaking tubes of RBC in salt solution [167]. Shen *et al.* used two wheels with slots for tubes containing blood and glass beads that rotated at specific RPM to assess RBC-MF [125]. Fok and Schubothe used a rotating platform with slots

for Erlenmeyer flasks containing quartz beads and blood [201, 202] and a Fleisch hemoresistometer [12, 13, 203] has been used to investigate RBC-MF under various conditions.

Gu *et al.* performed a comparison study of six methods for assessing RBC-MF: a hemoresistometer, Couette viscometer, spinning disk, capillary tube (driven by a syringe pump), a stainless steel bead test with a rocker platform [126] and a glass bead test with a rocker platform [204]. Gu *et al.* also compared the results of the different RBC-MF tests with the hemolysis produced by a Bio-Pump® (BP-80, Medtronic Inc.) tested in a flow circuit at a 5 L/min flow rate, 100 mmHg pressure head and a 4 hour test time. They reported that the stainless steel bead test with a rocker platform described in Kameneva *et al.* [126] was the most practical RBC-MF test and had a high correlation with *in vitro* hemolysis produced by the Bio-Pump® [204]. The standard RBC-MF test [126] has proven to be a reliable hemorheological test for the evaluation of sublethal damage to RBC due to storage, natural aging, and exposure to mechanical stress [58, 61, 124].

RBC-MF has often been overlooked in hemolysis testing of CAD although this parameter may have a potential influence on the resulting mechanical hemolysis. There is currently a dearth of literature regarding the relationship between the blood quality as assessed by the measurement of RBC-MF and the mechanical hemolysis produced by a CAD in a flow circuit. The objective of this study was to examine the effect of RBC-MF of the blood used for hemolysis testing of CAD on flow-induced hemolysis to discern whether RBC-MF can influence mechanical hemolysis of RBC exposed to the same shear stress and exposure times in an *in vitro* flow system with a CAD.

5.2.2 Materials and Methods

Bovine blood was purchased from Lampire Biological Laboratories, filtered and RBC were washed thrice in PBS. Ht of the washed RBC was measured and adjusted to 30±1% using autologous plasma or DPBS. The flow system used in this study was modified from Kameneva *et al.* [106] and consisted of a compliance chamber (R-38, Medtronic Inc), plastic nozzle (2.5 mm ID, 6 mm length), PediMag® centrifugal pump (Thoratec Corporation), flow probe (Transonic Systems Inc.), thermistor (Cole-Parmer Instrument Company), two pressure transducers (Cole-Parmer Instrument Company) and Tygon tubing. 65 ml (n=13) or 200 ml (n=4) of RBC suspension was circulated through the flow system for 120 minutes at a constant rate of 2 L/min corresponding to a Re~5000, τ_{wall} in the capillary~250 Pa, and T_{exp} in the tube ~1-3.5 s. Samples were withdrawn from the loop at 0, 60 and 120 minutes of testing for measurement of freeHb and calculation of the NIH according to **Equation 14**.

RBC-MF was assessed in the same RBC suspension filled in the flow loop for hemolysis testing using the standard RBC-MF test [61, 126]. Six 7 ml no-additive vacutainers (BD) were opened and in three tubes five 1/8” stainless steel ball bearings (BBs, Small Parts, Inc.) were added. The remaining three tubes without BBs served as a no-rocked control and two control samples. The no-rocked control was used to verify the freeHb measured in the control samples and not used in analysis.

Three milliliters of RBC suspension was added to each tube and the control BB tubes were rocked on a platform rocker at 18 cycles per minute and a rocking angle of ±17° for one hour. After one hour, freeHb was measured for all samples and a RBC mechanical fragility index (RBC-MFI) was calculated as:

$$RBC - MFI = \frac{(\Delta fHb_{exper} - \Delta fHb_{control})}{(tHb - \Delta fHb_{control})} x\,100 \quad (20)$$

where ΔfHb_{exper} is the freeHb in samples with BBs, $\Delta fHb_{control}$ is the freeHb in control samples and tHb is the total hemoglobin concentration of the RBC suspension used for test.

Bivariate correlations were performed to determine the Pearson correlation coefficients and statistical significance of the RBC-MFI, the change in freeHb from baseline (ΔfreeHb) and the NIH obtained from 17 RBC-MF and hemolysis tests.

5.2.3 Results

Table 5.2 shows the correlations for the RBC-MFI, ΔfreeHb and NIH obtained from RBC-MF and hemolysis tests (n=17). A large, significant correlation between RBC-MFI and the ΔfreeHb from hemolysis testing in the PediMag® flow system was observed. The Pearson correlation coefficient for this analysis was 0.95 ($p<0.01$). A moderate but statistically significant correlation between the RBC-MFI and NIH data was found (**Figure 5.3**). The Pearson correlation coefficient for this analysis was 0.83 ($p<0.01$).

Table 5.2. Correlations between the RBC mechanical fragility index obtained from RBC mechanical fragility tests and the normalized index of hemolysis and change in free hemoglobin concentration from baseline in hemolysis tests in a PediMag® flow system.

Correlations

		MFI	NIH	delta_freeHb
MFI	Pearson Correlation	1	.828**	.950**
	Sig. (2-tailed)		.000	.000
	N	17	17	17
NIH	Pearson Correlation	.828**	1	.876**
	Sig. (2-tailed)	.000		.000
	N	17	17	17
delta_freeHb	Pearson Correlation	.950**	.876**	1
	Sig. (2-tailed)	.000	.000	
	N	17	17	17

**. Correlation is significant at the 0.01 level (2-tailed).

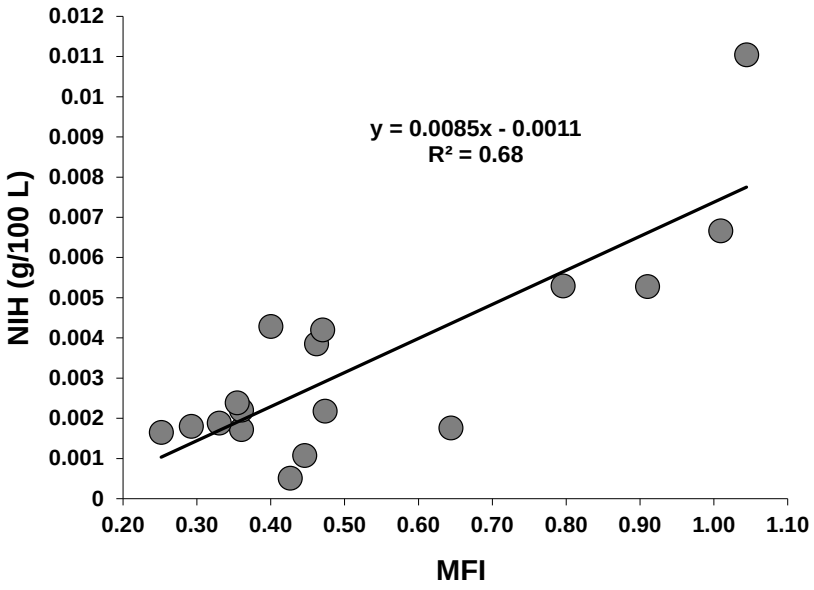

Figure 5.3. Correlation between the normalized index of hemolysis calculated for *in vitro* tests in a PediMag® flow system and the RBC mechanical fragility index.

5.2.4 Discussion

There is currently a dearth of knowledge regarding the relationship between the blood quality as assessed by RBC-MF and flow-induced hemolysis produced by a CAD in a flow system. The objective of this study was to examine the effect of RBC-MF of the blood used for CAD hemolysis testing on mechanical hemolysis to discern whether RBC-MF can influence flow-induced hemolysis of RBC exposed to the same shear stress and T_{exp} in an *in vitro* flow system with a CAD.

Seventeen experiments with the standard RBC-MF test [126] and an *in vitro* PediMag® flow system were conducted using the same 30% Ht bovine RBC suspensions. The results demonstrated a large, statistically significant correlation between the ΔfreeHb from the hemolysis tests and RBC-MF ($r=0.95$, $p<0.01$). Moreover, RBC-MF is correlated ($r=0.83$, $p<0.01$) with the NIH and can be used in conjunction with *in vitro* hemolysis testing of CAD to ensure the quality of blood used for tests.

5.2.5 Conclusions

This section summarizes the investigation of the relationship between RBC mechanical fragility and flow-induced hemolysis produced by a CAD in a flow system. RBC-MF was found to be correlated with the change in freeHb during hemolysis testing ($r=0.95$, $p<0.01$) and the NIH ($r=0.83$, $p<0.01$). The standard RBC-MF test [126] can aid in the analysis of hemolysis testing of blood pumps by providing important information on the susceptibility of the blood used for testing to flow-induced trauma.

6.0 EFFECTS OF CELL-CELL INTERACTIONS AND SUSPENSION MEDIA VISCOSITY ON FLOW-INDUCED HEMOLYSIS

6.1 INTRODUCTION

Cell-cell interactions were first proposed as a potential mechanism for flow-induced hemolysis by Shapiro and Williams [103] and Sutera *et al.* [83], but the authors did not study it. Leverett *et al.* studied the effect of cell-cell collisions on mechanical hemolysis using a Couette viscometer [98]. The authors exposed 0.3-60% Ht human blood samples to a 300 Pa shear stress for 120 seconds. They reported ~10% hemolysis at each Ht and thus concluded that the effect of cell-cell interaction was negligible on mechanical hemolysis [98]. However, the authors do not report whether they used blood of multiple donors or a single donor nor do they state the sample size of this study [98]. Furthermore, the Couette viscometer used by Leverett *et al.* operated at shear rates up to ~180,000 s^{-1} for the low Ht blood samples and produced a linear increasing temperature up to 20ºC during the 120 second exposure time [98]. Thus, the hemolysis of the low Ht samples in the Couette viscometer used by Leverett *et al.* was augmented by the rapid temperature increase to a greater degree than the higher Ht blood samples during the two minute exposure time. Therefore, cell-cell interactions are a potential mechanism of hemolysis that warrants further study.

The relationship between the macroscopic flow conditions and blood damage on the cellular level are not well understood. A study of the effect of cell-cell interactions on mechanical hemolysis should be performed with RBC suspensions with both normal and very little Hb concentration to examine the release of Hb independent of cell concentration. For this purpose, Hb-depleted resealed RBC ghosts (GRBC) are used. The preparation of resealed GRBC [205] with similar rheological properties as RBC has been reported [71, 206, 207]. GRBC were shown to behave similarly to RBC in maintaining a normal platelet interaction with subendothelium under conditions of moderate shear rate [1000 s^{-1}] and constant Ht [40%] in an *ex vivo* perfusion chamber [208].

The objective of this study was to examine the effect of cell-cell interactions and suspension viscosity on flow-induced hemolysis in a microtube flow system with flow conditions and exposure times relevant to those in operating CAD. The effects of RBC/GRBC concentration and the suspension medium on hemolysis were directly examined to determine a potential proportional difference in hemolysis between suspensions. The use herein of RBC, GRBC, and dextran additive allows for independent control of bulk Ht, viscosity, tHb, shear stress and total exposure time (T_{exp}).

6.2 MATERIALS AND METHODS

Donor bovine blood was collected via venipuncture in K_3-EDTA anticoagulant purchased from Lampire Biological Laboratories and shipped overnight to the laboratory. Blood was filtered and RBC were washed thrice in PBS. Gentamicin (0.25 g/L; American Pharmaceutical Partners,

Schaumburg, IL) was added to prevent bacterial growth. RBC suspension Ht was measured using microhematocrit centrifugation (IEC MB Centrifuge, International Equipment Company) at 2,000×g for three minutes. RBC were used within four days of blood collection.

GRBC were prepared (n=8) according to the "two-day" resealed GRBC protocol described in Jamiolkowski *et al.* [71]. Briefly, an 80 ml of washed RBC resuspended at 50% Ht in PBS was added to 720 ml of hemolysis buffer (MgSO4 4.0 mM; glacial acetic acid 3.8 mM; pH 4-5) at a temperature of 0°C. After five minute incubation, 5X PBS (0.3 ml/ml) and Tris buffer (2μL/mL) were added to refill lysed RBC and increase the pH. Cell suspensions were incubated overnight at 0°C for approximately 16 hours. Suspensions were then incubated in a water bath at 37°C for 60 minutes to reseal GRBC membranes. The GRBC suspension was centrifuged (30 minutes, 27,000×g) and the supernatant was discarded. The pellet of GRBC concentrate was washed thrice with PBS containing 1% BSA (30 minutes, 27,000×g). Gentamicin (0.25 g/L; American Pharmaceutical Partners, Schaumburg, IL) was added to the packed GRBC to prevent bacterial growth. Ht of the packed GRBC and all GRBC/RBC suspensions was measured using microhematocrit centrifugation (30 minutes, 2,000×g). GRBC were used within five days of preparation.

Suspensions of 40% RBC in PBS (n=12), 10% RBC and 30% GRBC in PBS (n=6), 20% RBC and 20% GRBC in PBS (n=6), and the viscosity-matched controls for the GRBC/RBC suspensions, 20% RBC in 7% Dextran 40 (n=6) and 10% RBC in 7% Dextran 40 (n=6) were prepared and used on the same day as hemolysis testing. Dextran 40 solution was chosen to increase the viscosity of the 10% and 20% Ht RBC suspensions to closely match the viscosity of the corresponding RBC/GRBC suspensions. A pilot study found that 7% Dextran 40 in PBS was a suitable concentration for the suspension medium to achieve the desired suspension viscosities

(**Figure 6.1**). Polyvinylpyrrolidone (PVP) solution in PBS was also investigated as a cell suspension medium but was too dense for the accurate measurement of freeHb in hemolysis tests.

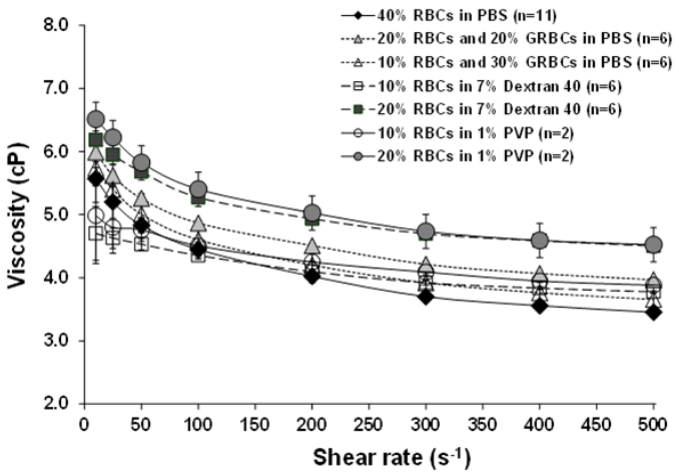

Figure 6.1. Viscosity of RBC and GRBC suspended in phosphate buffered saline and viscosity controls of 10% and 20% RBC suspended in Dextran 40 and polyvinylpyrrolidone measured at 10-500 s^{-1} shear rates. Values are shown as mean±SD.

The flow system used for this study consisted of a compliance chamber (R-38, Medtronic Inc.), glass microtube (1.4 mm D, 140 mm length), PediMag® centrifugal pump (Thoratec Corporation), flow probe (Transonic Inc.), thermistor (Cole-Parmer Instrument Company), two pressure transducers (PCB Piezotronics, Inc.) and ¼" D Tygon tubing (**Figure 6.2**). Flow was assessed by calculation of Re (**Equation 2**). Wall shear stress (τ_{wall}), number of passes (N), exposure time (t_{exp}) and total exposure time (T_{exp}) in the glass microtube were calculated according to **Equations 11, 16, 18** and **17** respectively.

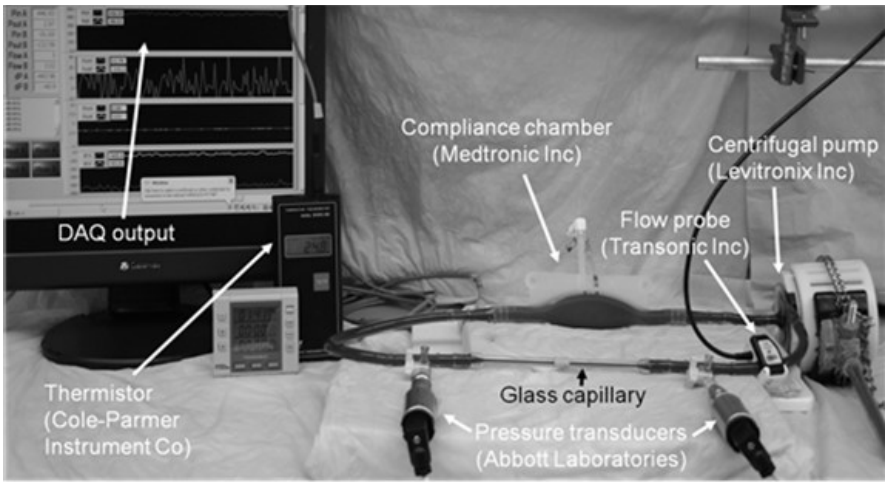

Figure 6.2. Capillary flow system filled with RBC and GRBC suspended in phosphate buffered saline.

70 ml of each suspension was circulated in the flow system for 2 hours at 0.80 LPM flow rate corresponding to a ~5300 pump RPM, Re~3500-4200, τ_{wall}~150 Pa, and T_{exp}~24 sec. Flow-induced damage to RBC and GRBC was assessed through the measurement of freeHb in samples withdrawn from the loop at T=0, 60 and 120 minutes of testing. Briefly, sample tubes were centrifuged for 15 minutes at 2200×g. Supernatant was transferred to microcentrifuge tubes and centrifuged at 21,800×g for 20 minutes in a microcentrifuge. Supernatant was then transferred into spectrophotometer cuvettes for measurement of freeHb at a 540 nm wavelength.

THb was measured for all suspensions at T=0 and 120 minutes of testing using a hemoximeter (OSM3, Radiometer Inc.). Blood damage was characterized by the Index of Hemolysis (**Equation 19**). Cell mechanical fragility was assessed in the same RBC/GRBC suspensions filled in the flow loop for hemolysis testing using the standard RBC-MF test [61, 126] described in **Section 5.2.2**.

A Wells-Brookfield Cone/Plate viscometer (Model LVDV-IIIUCP, Middleboro, MA) with CPE-40 cone (cone radius= 2.4 cm, cone angle=0.8°, sample volume=0.5 mL) was used to

measure viscosity of RBC/GRBC suspensions at T=0 and 120 minutes of testing. The viscosity of tested suspensions was measured over a range of shear rates (25–500 s^{-1}) at a temperature of 25°C. A circulating water bath (Neslab RTE7, Thermo Fisher Scientific, Waltham, MA) was used to maintain constant temperature.

Statistical analysis was performed using ANOVA with the Games-Howell post-hoc method to analyze the change in freeHb from baseline after 120 minutes of testing (ΔfreeHb), MFI and IH among the five RBC/GRBC suspensions. Additional information regarding statistical analysis is presented in **Appendix E**.

6.3 RESULTS

Figure 6.3 and **Figure 6.4** show the viscosity of all tested suspensions measured at a 25ºC temperature and 50 and 500 s^{-1} shear rates, respectively. The 40% RBC in PBS, 20% RBC in 7% Dextran 40 and 10% RBC in 7% Dextran 40 suspensions did not change from baseline and were similar to the baseline measurements of the GRBC suspensions. The suspensions containing GRBC demonstrated a reduction in viscosity during the test period due to a ~3-4% decrease in GRBC concentration.

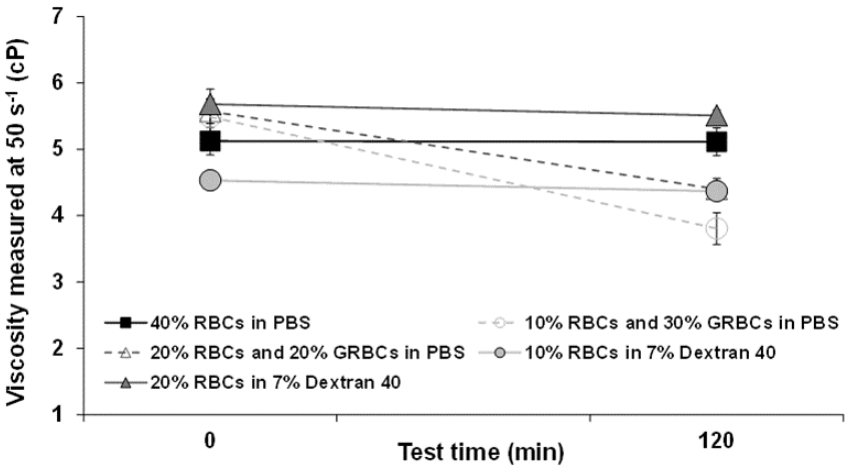

Figure 6.3. Viscosity of cell suspensions measured at a 50 s^{-1} shear rate at baseline and after 120 minutes of testing in a capillary flow system.

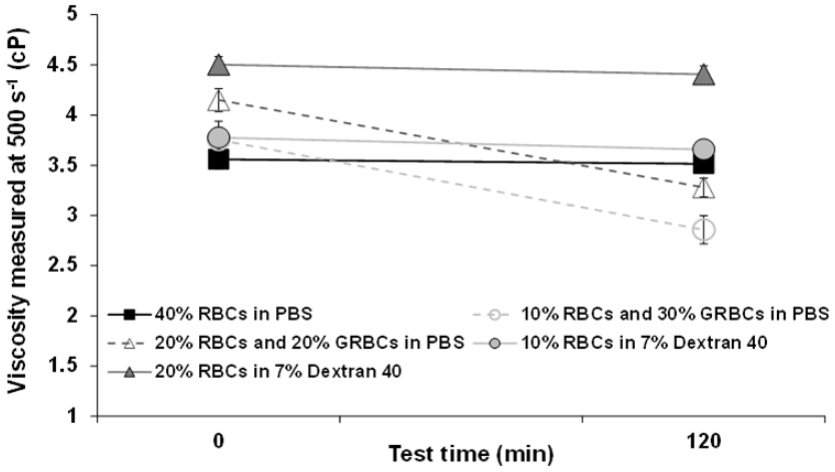

Figure 6.4. Viscosity of cell suspensions measured at a 500 s^{-1} shear rate at baseline and after 120 minutes of testing in a capillary flow system.

The freeHb measurements and the change in freeHb from baseline (ΔfreeHb) of GRBC and RBC suspended in PBS and RBC suspended in 7% Dextran 40 after 120 minutes of testing in the glass capillary flow system are shown in **Figure 6.5** and **Figure 6.6**. For the 120 minutes samples, the ΔfreeHb was 55 mg/dl, 75 mg/dl and 131 mg/dl for the 30% GRBC and 10% RBC suspension, 20% GRBC and 20% RBC suspension and 40% RBC suspension, respectively.

Figure 6.6 shows the ΔfreeHb of the 40% RBC in PBS suspension was significantly different from all tested suspensions ($p<0.01$). Moreover, the ΔfreeHb of the 30% GRBC and 10% RBC in PBS and 20% GRBC and 20% RBC in PBS suspensions were significantly different from their viscosity matched controls, 10% RBC in 7% Dextran 40 ($p<0.002$) and 20% RBC in 7% Dextran 40 ($p<0.02$), respectively.

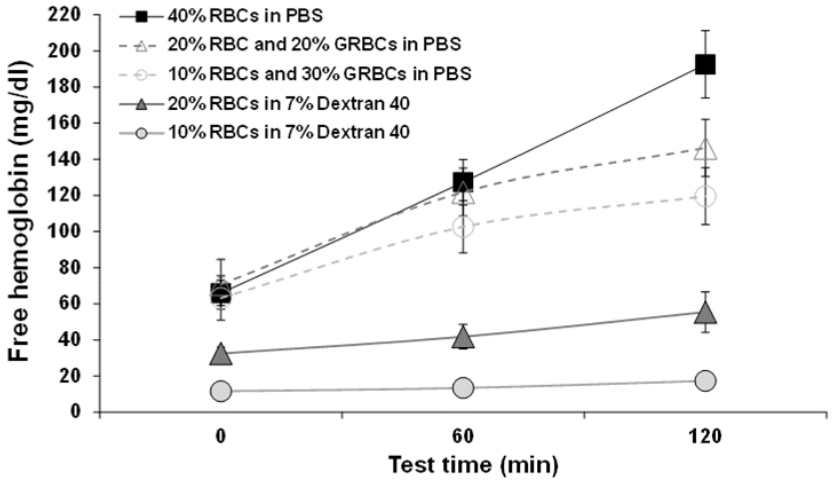

Figure 6.5. Free hemoglobin concentration in the 40% RBC in PBS, 10% RBC and 30% GRBC in PBS, 20% RBC and 20% GRBC in PBS, 10% RBC in 7% Dextran 40 and 20% RBC in 7% Dextran 40 suspensions during 120 minutes of testing in the capillary flow system. Values are shown as mean±SEM.

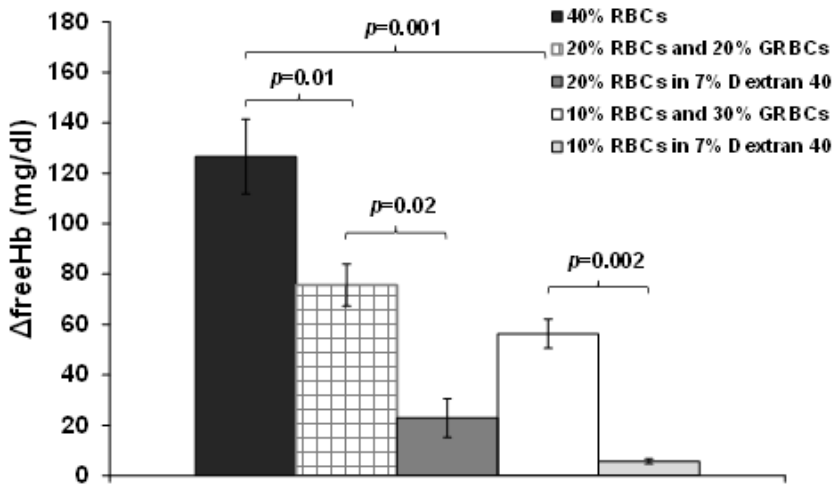

Figure 6.6. Change in free hemoglobin concentration from baseline in the 40% RBC in PBS, 10% RBC and 30% GRBC in PBS, 20% RBC and 20% GRBC in PBS, 10% RBC in 7% Dextran 40 and 20% RBC in 7% Dextran 40 suspensions after 120 minutes of testing in the capillary flow system. Values are shown as mean±SEM.

Figure 6.7 shows the Index of Hemolysis calculated for each tested suspension. The IH was similar for all suspensions with 40% cell concentration and statistically significantly lower for the 20% RBC and 10% RBC suspensions in 7% Dextran 40 ($p<0.02$). **Figure 6.8** shows the cell mechanical fragility index calculated for each tested suspension. Similarly to the IH results, the MFI for all suspensions with 40% cell concentration was similar and statistically significantly lower for the 20% RBC and 10% RBC suspensions in 7% Dextran 40 ($p<0.003$).

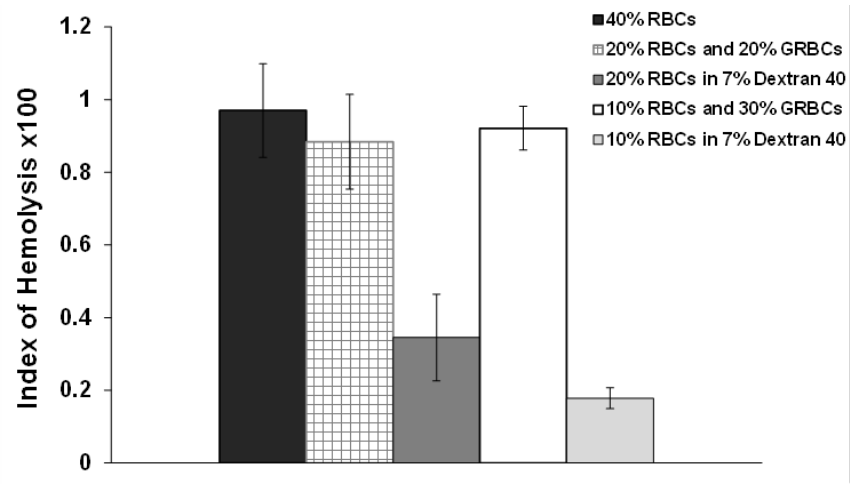

Figure 6.7. Index of Hemolysis calculated for the 40% RBC in PBS, 10% RBC and 30% GRBC in PBS, 20% RBC and 20% GRBC in PBS, 10% RBC in 7% Dextran 40 and 20% RBC in 7% Dextran 40 suspensions after 120 minutes of testing in the capillary flow system. Values are shown as mean±SEM.

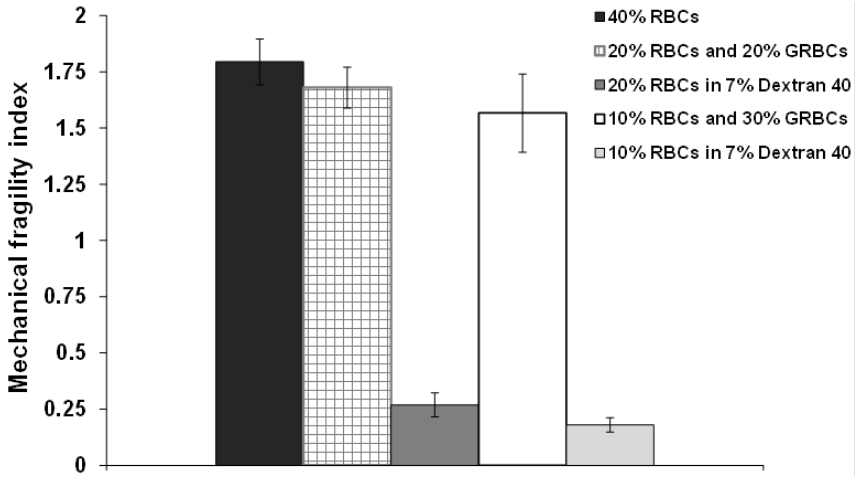

Figure 6.8. Mechanical fragility index calculated for the 40% RBC in PBS, 10% RBC and 30% GRBC in PBS, 20% RBC and 20% GRBC in PBS, 10% RBC in 7% Dextran 40 and 20% RBC in 7% Dextran 40 suspensions after 120 minutes of testing in the capillary flow system. Values are shown as mean±SEM.

6.4 DISCUSSION

The proposed mechanisms of flow-induced hemolysis reported in the literature include the effects of shear stress and exposure time [5, 96-98], accumulated sublethal RBC damage [3, 12, 78, 99, 100], cell-wall interactions [79, 101, 102], cell-cell interactions [98, 103] and turbulent flow conditions [83, 104-106]. This *in vitro* study examined the effects of cell-cell interactions and suspension viscosity on flow-induced hemolysis.

The viscosity of RBC suspensions did not change from baseline and were similar to the baseline measurements of the GRBC suspensions (**Figure 6.3** and **Figure 6.4**). The viscosity of the RBC/GRBC suspensions measured at 120 minutes decreased from baseline due to a ~3-4% decrease in GRBC concentration during testing.

The ΔfreeHb after 120 minutes of testing is nearly proportional to the amount of RBC in cell suspensions (**Figure 6.6**). Statistical analysis of the ΔfreeHb in the 40% RBC in PBS suspensions demonstrated significant differences from the ΔfreeHb of the 20% RBC and 20% GRBC in PBS and 10% RBC and 30% GRBC in PBS suspensions ($p=0.01$ and $p=0.001$, respectively). The 20% RBC and 20% GRBC in PBS suspension was significantly greater than the viscosity-matched control, 20% RBC in 7% Dextran 40 ($p=0.02$). Similarly, the 10% RBC and 30% GRBC in PBS suspension was significantly greater than its viscosity matched control, 10% RBC in 7% Dextran 40 ($p=0.002$). These results demonstrate a greater effect of cell-cell collisions on flow-induced hemolysis than suspension viscosity.

The calculated IH normalized the ΔfreeHb by the tHb of the tested suspension. The IH was not significantly different among the suspensions with 40% cell concentration. However, the IH of the 20% RBC in 7% Dextran 40 and 10% RBC in 7% Dextran 40 were significantly lower

than the IH of the 40% cell concentration suspensions ($p<0.02$). Similarly, the calculated MFI for 40% cell concentration suspensions were not significantly different. Yet, the MFI of the 10% RBC and 20% RBC suspensions in 7% Dextran 40 were significantly lower than the MFI of the 40% cell concentration suspensions ($p<0.003$). The IH and MFI results demonstrate a greater effect of cell-cell interaction on flow-induced hemolysis than the suspension viscosity.

At physiological hematocrits, RBC continuously collide with other RBC in the circulation, resulting in the displacement of nearby cells. Goldsmith and colleagues studied RBC collisions in a microtube flow system and found that a collision between two RBC results in the displacement of both RBC trajectories in a direction normal to the flow direction [209]. The mechanism of cell-cell interactions on flow-induced hemolysis is likely the result of a local velocity gradient between colliding cells when cells traveling along adjacent streamlines are brought into close proximity and interact [210].

6.5 CONCLUSIONS

This chapter summarizes the investigation of the effects of cell-cell interactions and suspension viscosity on flow-induced hemolysis in a capillary flow system. The increase in freeHb from baseline for RBC and GRBC suspensions was nearly proportional to the amount of RBC in suspension. Moreover, the hemolysis in the RBC and GRBC suspensions was found to be significantly higher than that in their viscosity-matched controls (RBC in viscous media). The results demonstrate a greater contribution of cell-cell interactions to flow-induced hemolysis than that of the suspension bulk viscosity.

7.0 TRAFFICKING OF ERYTHROCYTE GHOSTS AND PLATELET-SIZED PARTICLES IN A MICROFLUIDIC SYSTEM UNDER FLOW CONDITIONS THAT MAY PROMOTE THROMBOSIS IN ASSISTED BLOOD CIRCULATION

7.1 INTRODUCTION

In microcirculatory blood flow, RBC and platelets interact differently than in larger blood vessels [45]. In 1921, Smith *et al.* reported that a non-uniform distribution of RBC in the microcirculation was possible [46] and soon confirmed by the studies of Fåhraeus [24] and Fåhraeus and Lindqvist [25] in vessels with less than 300 μm diameter. In capillaries less than 14 μm diameter, Dintenfass found an inverse Fåhraeus-Lindqvist effect in which relative viscosity increased with decreasing capillary diameter due to approaching the scale of single RBC [47]. Goldsmith *et al.* [211, 212], Turitto and Baumgartner [213], Eckstein *et al.* [214, 215], and Aarts *et al.* [216-218] demonstrated the non-uniform distribution of RBC and platelets in the microcirculation.

Goldsmith studied the flow of suspensions of 44% RBC ghosts (GRBC) and platelet-sized particles in a ~80 μm straight tube and reported the platelet-sized particles have increased radial motion and collisions with the wall compared to GRBC [219, 220]. Eckstein and colleagues and Aarts *et al.* examined flow of whole blood, GRBC and PRP in straight channels and reported an elevated platelet concentration near the tube wall [214, 218, 221]. Goldsmith

reported that after flow through *in vitro* models of bifurcations and constrictions that produced flow separation and recirculating regions, platelet thrombus can occur [159]. Moreover, the flow of platelets in recirculation zones (deadwaters), regions with local supra-physiological shear rates and stagnation points have been shown to contribute toward thrombosis *in vitro* [143].

The transport of platelets toward the vessel wall by RBC in the microcirculation is one important cause for the development of thrombosis. RBC size [216], RBC deformability [217, 222], Ht [223] and shear rate [137, 223] were shown to augment platelet adhesion to artery subendothelium in the *ex vivo* perfusion system developed by Baumgartner [224, 225]. Aarts *et al.* showed that GRBC expel platelets toward the vessel wall in the microcirculation in a similar manner as normal RBC [218]. Sakariassen *et al.* [226] used an *in vitro* endothelial cell covered perfusion system and Bozzo *et al.* [208] used an *ex vivo* perfusion chamber to show that GRBC behaved similarly to normal RBC in maintaining a normal platelet interaction with subendothelium under conditions of moderate shear rate [1000 s^{-1}] and constant Ht [40%].

In the assisted blood circulation, RBC and platelets are exposed to non-physiological forces and surfaces that may promote hemolysis and thrombosis. Channel geometries previously used to study particle/cell distributions under physiological or supra-physiological shear stresses include straight channels (τ_{wall}~0.15-30 Pa) [214, 221], sudden expansions [159, 227] and rounded and square T-junctions [228, 229]. Platelet margination was first reported by Goldsmith in sudden expansion channels using GRBC and particles [159]. Zhao recently extended these studies to consider elevated shear stresses, representative of that found in assisted circulation. Her studies were conducted in a 100 μm height straight channel (τ_{wall}~40-200 Pa) [230] and a 100 μm:200 μm height backward step microchannel (τ_{wall}~20-100 Pa) [231] using suspensions of bovine RBC and 2 μm diameter platelet-sized fluorescent particles (PSFP).

The objective of this study was to examine the trafficking of GRBC and PSFP in more complicated geometries, specifically a microchannel containing multiple crevices similar to the size of small gaps in some VAD under flow conditions that may cause thrombosis in the assisted blood circulation. The microscopic examination of GRBC and PSFP pathlines in these channels may provide additional insight into the flow conditions and interaction of cells that lead to the development of thrombosis in the microcirculation and small crevices similar to those within some CAD.

7.2 MATERIALS AND METHODS

A microchannel containing multiple crevices was made in SolidWorks 2013 by Professor Antaki (**Figure 7.1**). Microchannel fabrication was performed using polydimethylsiloxane (PDMS) with a mask of the novel channel designs. Individual PDMS channels and coverslips (Fisherfinest Premium Cover Glasses, Fisher Scientific Inc.) were treated with no-residue tape before sealing the channels to coverslips using corona treatment. The sealed channels were incubated overnight at 60°C. After cooling, polyethylene capillary (PE-60, 0.76 mm ID, Braintree Scientific Inc.) was treated with no-residue tape and inserted into the inlet (8 cm length) and outlet (11 cm length) of the microchannel to be tested. Additional information regarding microchannel fabrication is presented in **Appendix F**.

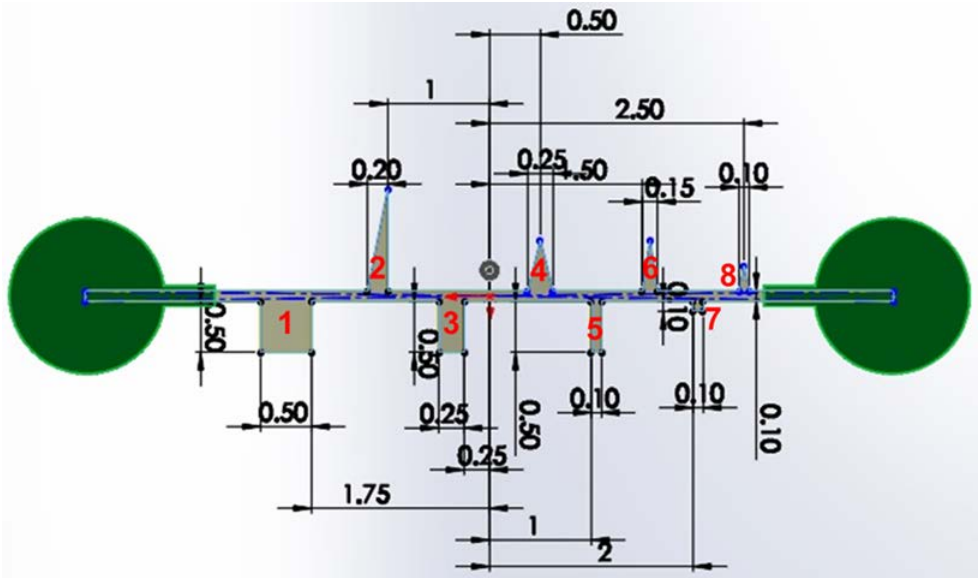

Figure 7.1. Multiple crevice microchannel used to study the trafficking of erythrocyte ghosts and platelet-sized fluorescent particles under flow conditions that may promote thrombosis in the assisted blood circulation. Channel height was 75 µm. Units are shown in millimeters.

The red numbers designate the crevice numbering convention.

Human O- RBC units were purchased from Valley Biomedical Inc. RBC were sterilely extracted from the unit and washed thrice in PBS. GRBC were prepared according to the method described in **Section 6.2**. Platelet-sized fluorescent polystyrene particles (2 µm mean diameter, light excitation peak=542 nm, emission peak=612 nm; R0200, Duke Scientific Corporation, Palo Alto, CA) were well mixed prior to pipetting into GRBC suspensions. Suspensions of 20% GRBC and ~1,000,000 PSFP/µl in 30% Dextran 40 solution (n=6) and 40% GRBC and ~1,000,000 PSFP/µl in 20% Dextran 40 solution (n=6) were prepared and the viscosity of all tested suspensions was measured using a Wells-Brookfield Cone/Plate viscometer (LVDV-IIIUCP, Middleboro, MA) at shear rates of 10-100 s^{-1} and a 25°C temperature. The viscosity of all tested suspensions was ~20 cP at a 100 s^{-1} shear rate (**Figure 7.2**).

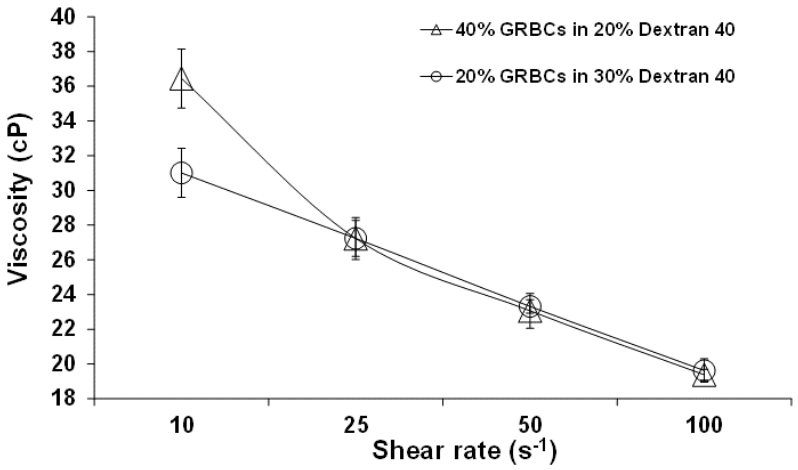

Figure 7.2. Viscosity of GRBC suspensions in Dextran 40 measured at 10-100 s^{-1} shear rates in a cone-and-plate viscometer at a 25°C temperature. Values are shown as mean±SEM.

The microfluidic system used in this study consisted of a syringe pump (PHD2000, Harvard Apparatus), 200 µl pipet tip (fluid inlet), small cap over the inlet (prevent debris from entering the channel), an outlet pressure transducer (Abbott Laboratories), 5 ml syringe, and a crevice microchannel on the stage of a microscope (**Figure 7.3**). All microchannels were rinsed twice with sterile filtered PBS and incubated with sterile filtered 1% BSA for 30 minutes prior to testing to passivate all cell-contacting surfaces. Test suspensions were examined at controlled withdrawal flow rates of 5 and 25 µl/min corresponding to Re~0.03-0.3 and wall shear stresses of 30-200 Pa in the main branch of the crevice microchannels.

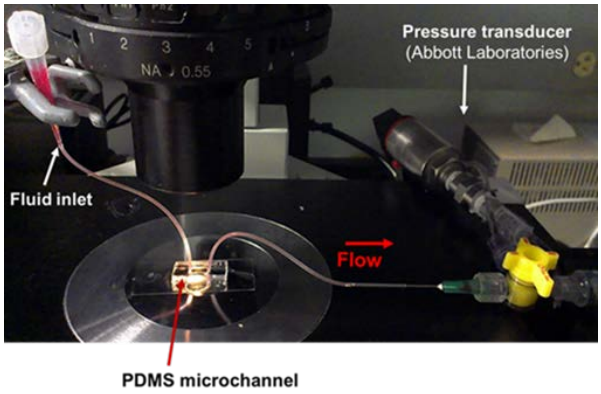

Figure 7.3. Microchannel flow system filled with GRBC suspension on the stage of an inverted microscope.

Microchannel testing was performed using suspensions of 20% GRBC and ~1,000,000 PSFP/µl in 30% Dextran 40 (n=6) and 40% GRBC and ~1,000,000 PSFP/µl in 20% Dextran 40 (n=6). Suspensions were visualized in crevice microchannels using an inverted fluorescent microscope (IX70, Olympus Inc., Melville, NY) with a 20X objective (LCPlanFL, working distance=7.55mm, numerical aperture=0.40; Olympus Inc.) and a 103W HBO short arc mercury lamp light source (OSRAM GmbH, Munich, Germany) to examine PSFP trafficking. A 40X objective (PlanFL, phase contrast, working distance=6.5–8.3 mm, numerical aperture=0.55, maximum coverslip thicknesses=2.6 mm; Olympus Inc.) and a halogen backlight were used for Brightfield visualization of GRBC trafficking in crevices. The channel height visualized for all experiments was 38±5 µm.

A high speed camera (FastCam SA4, Photron USA Inc.) attached to the side port of the microscope was used to capture magnified images of GRBC (40X Brightfield visualization) and PSFP (20X fluorescent visualization). A personal computer with Photron FASTCAM Viewer software was used to record video (2000-8500 images) of flowing GRBC (125 frames per second, 1 s exposure time) and PSFP (60 frames per second, 1 s exposure time) in Crevices 1-8 at each flow rate. Analysis software (PFA, Photron USA Inc.) was used to obtain 10-40 GRBC

and 25-75 PSFP pathlines in the videos of each crevice at both flow rates and GRBC suspensions. Particle counts were obtained by processing 50 images (Analyze Particles, ImageJ, NIH) in stepwise increments of 25-100 images for the 2000-8500 total images for each Crevice 1-8 at both flow rates and GRBC suspensions.

Statistical analysis was performed using ANOVA to analyze the difference in mean PSFP counts in Crevices 1-8 at flow rates of 0, 5 and 25 µl/min. Post-hoc testing was conducted using either the Tukey or Games-Howell methods contingent upon the results of homogeneity of variances tests. Two-tailed Student's *t*-tests for independent observations was performed to determine the statistical significance of the difference in mean PSFP counts in Crevices 1-8 for the two GRBC concentrations. Statistical significance was defined at $p<0.05$.

7.3 RESULTS

7.3.1 Trafficking of platelet-sized particles and GRBC in a 500 µm wide and 500 µm long square crevice (Crevice 1)

Figure 7.4 shows images of 20% GRBC and ~1,000,000 PSFP/µl in 30% Dextran 40 and 40% GRBC and ~1,000,000 PSFP/µl in 20% Dextran 40 flowing through Crevice 1 at 5 and 25 µl/min. A representative analysis of PSFP trafficking for the 20% GRBC suspension is shown at both flow rates in **Figure 7.5.** Pathlines of PSFP in Crevice 1 for the 20% GRBC suspension at 5 and 25 µl/min flow rates are shown in **Figure 7.6** and **Figure 7.7**, respectively. Platelet-sized particle trafficking in Crevice 1 for the 20% GRBC suspension had apex distances less than 400

μm for 90% of PSFP studied at 5 μl/min (**Figure 7.6**) and 47% of PSFP examined at 25 μl/min (**Figure 7.7**).

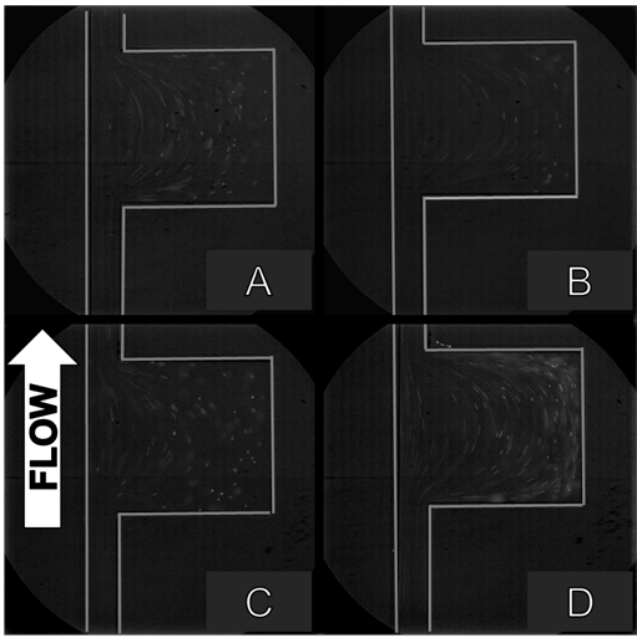

Figure 7.4. Representative fluorescent images of suspensions of 20% GRBC and ~1,000,000 PSFP/μl in 30% Dextran 40 and 40% GRBC and ~1,000,000 PSFP/μl in 20% Dextran 40 examined in Crevice 1 at 5 and 25 μl/min flow rates. Channel height was 75 μm.

[A] 20% GRBC suspension at 5 μl/min, [B] 20% GRBC suspension at 25 μl/min, [C] 40% GRBC suspension at 5 μl/min, [D] 40% GRBC suspension at 25 μl/min. 20x magnification. Field of view in A-D is 1000 μm by 1000 μm.

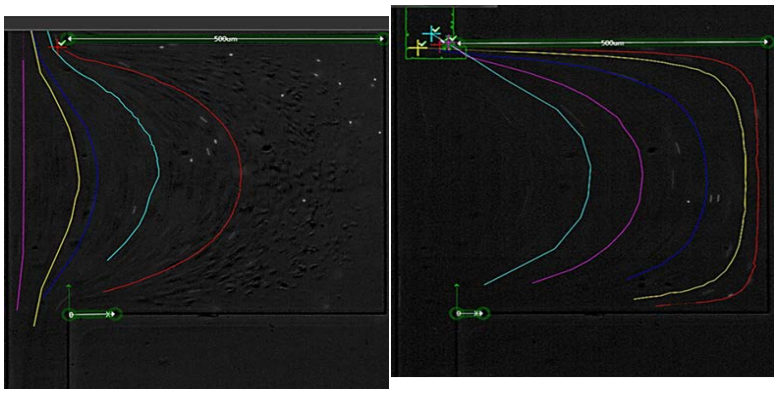

Figure 7.5. Trafficking of five platelet-sized particles in 20% GRBC suspension at 5 µl/min [left] and 25 µl/min [right] flow rates in Crevice 1. 20x magnification. Dimension shown with horizontal green line is 500 µm. Origin defined at channel entrance.

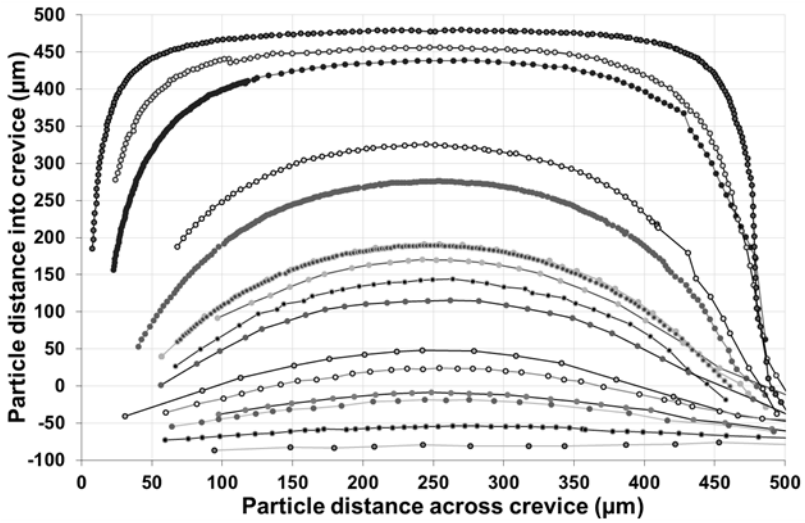

Figure 7.6. Pathlines of platelet-sized particles in 20% GRBC suspension at a 5 µl/min flow rate in Crevice 1.

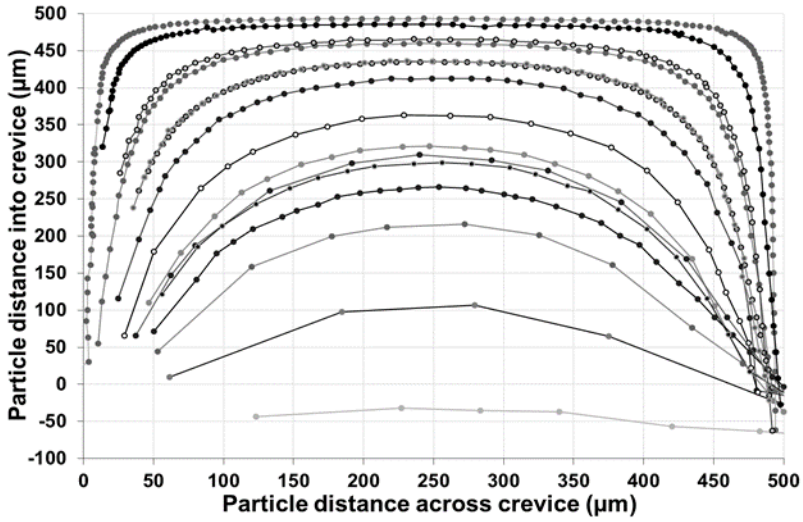

Figure 7.7. Pathlines of platelet-sized particles in 20% GRBC suspension at a 25 µl/min flow rate in Crevice 1.

Figure 7.8 shows a representative analysis of PSFP trafficking in Crevice 1 for the 40% GRBC suspension examined at 5 and 25 µl/min**.** PSFP pathlines for the 40% GRBC suspension at 5 and 25 µl/min flow rates are shown in **Figure 7.9** and **Figure 7.10**, respectively. Platelet-sized particle trafficking in Crevice 1 for the 40% GRBC suspension had apex distances less than 400 µm for 61% of the PSFP studied at 5 µl/min (**Figure 7.9**) and 50% of PSFP examined at 25 µl/min (**Figure 7.10**).

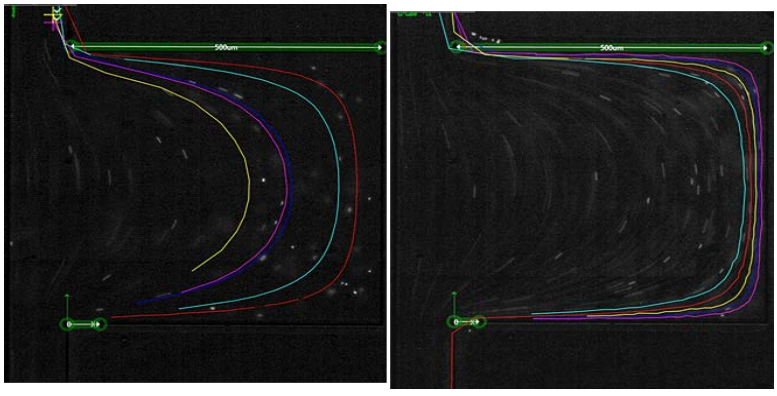

Figure 7.8. Trafficking of five platelet-sized particles in 40% GRBC suspension at 5 µl/min [left] and 25 µl/min [right] flow rates in Crevice 1. 20x magnification. Dimension shown with horizontal green line is 500 µm. Origin defined at channel entrance.

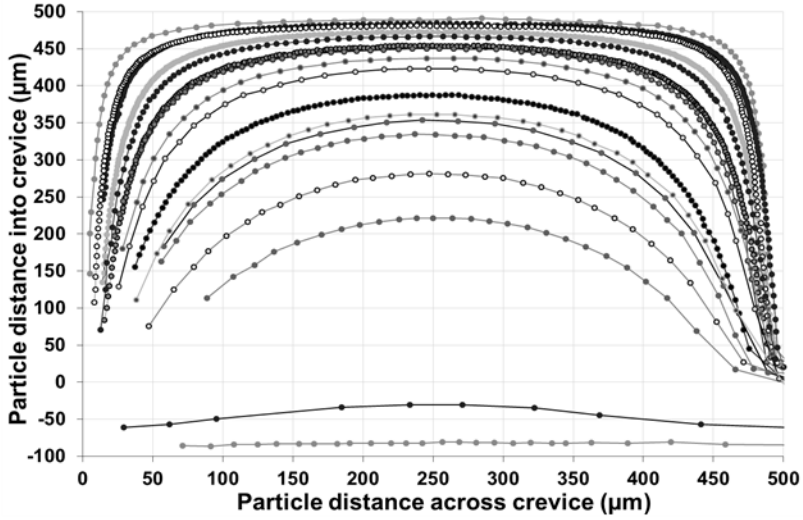

Figure 7.9. Pathlines of platelet-sized particles in 40% GRBC suspension at a 5 µl/min flow rate in Crevice 1.

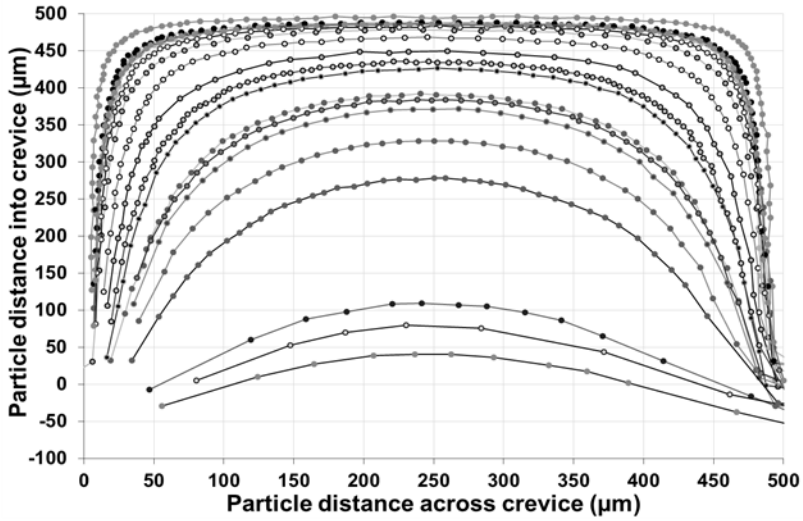

Figure 7.10. Pathlines of platelet-sized particles in 40% GRBC suspension at a 25 µl/min flow rate in Crevice 1.

Figure 7.11 shows a representative analysis of GRBC trafficking in Crevice 1 for the 40% GRBC suspension examined at 5 and 25 µl/min. GRBC pathlines for the 20% GRBC suspension at 5 and 25 µl/min flow rates are shown in **Figure 7.12** and **Figure 7.13**, respectively. GRBC trafficking in Crevice 1 for the 20% GRBC suspension had apex distances less than 400 µm for 65% of GRBC studied at 5 µl/min (**Figure 7.12**) and 45% of GRBC

examined at 25 µl/min (**Figure 7.13**). GRBC pathlines for the 40% GRBC suspension in Crevice 1 were not analyzed due to the inability to accurately track GRBC at a 5 µl/min flow rate.

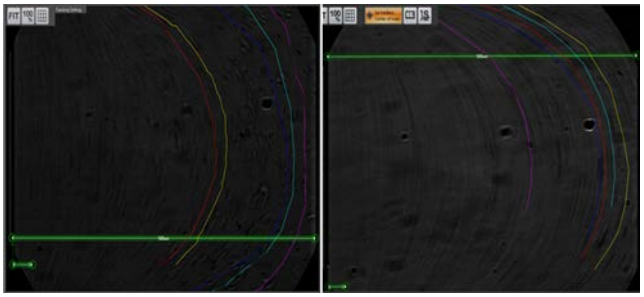

Figure 7.11. Trafficking of five GRBC in 20% GRBC suspension at 5 µl/min [left] and 25 µl/min [right] flow rates in Crevice 1. 40x magnification. Dimension shown with horizontal green line is 500 µm. Origin defined at channel entrance.

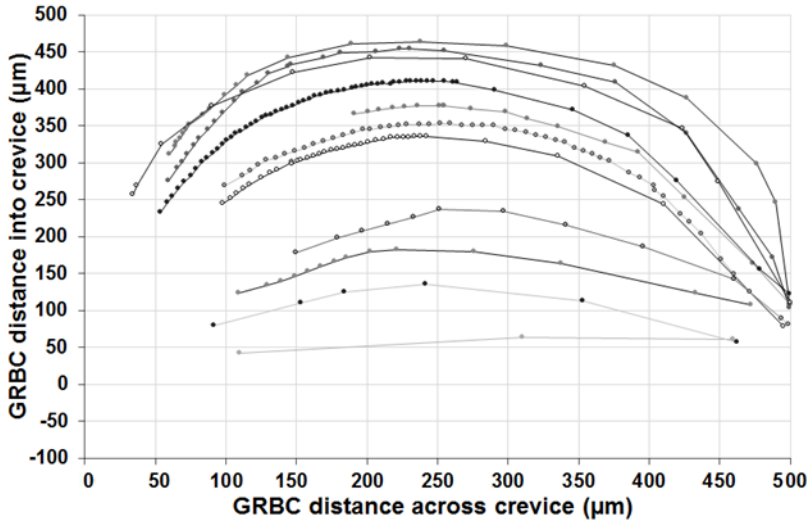

Figure 7.12. Pathlines of GRBC in 20% GRBC suspension at a 5 µl/min flow rate in Crevice 1.

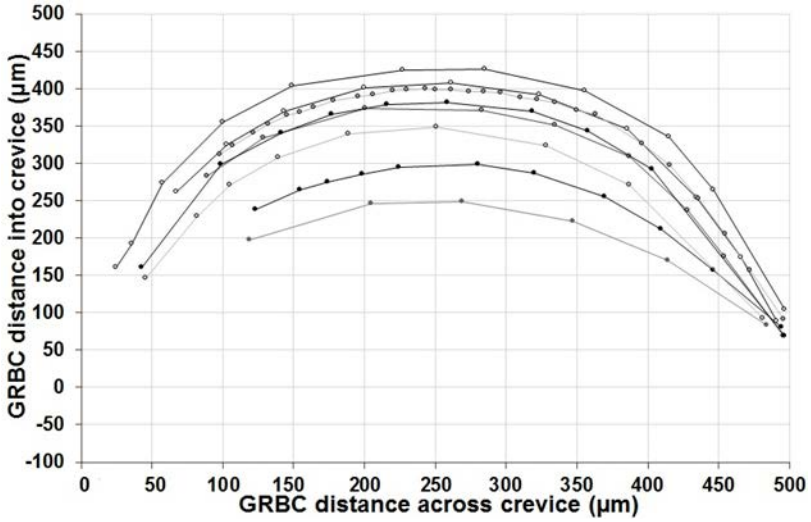

Figure 7.13. Pathlines of GRBC in 20% GRBC suspension at a 25 µl/min flow rate in Crevice 1.

7.3.2 Trafficking of platelet-sized particles and GRBC in a 200 µm height and 1000 µm base triangular crevice (Crevice 2)

Figure 7.14 shows images of 20% GRBC and ~1,000,000 PSFP/µl in 30% Dextran 40 and 40% GRBC and ~1,000,000 PSFP/µl in 20% Dextran 40 flowing through Crevice 2 at 5 and 25 µl/min. A representative analysis of PSFP trafficking for the 20% GRBC suspension is shown at both flow rates in **Figure 7.15**. Pathlines of PSFP in Crevice 2 for the 20% GRBC suspension at 5 and 25 µl/min flow rates are shown in **Figure 7.16** and **Figure 7.17**, respectively. Platelet-sized particle trafficking in Crevice 2 for the 20% GRBC suspension had apex distances less than 200 µm for 80% of PSFP studied at 5 µl/min (**Figure 7.16**) and 87% of PSFP examined 25 µl/min (**Figure 7.17**).

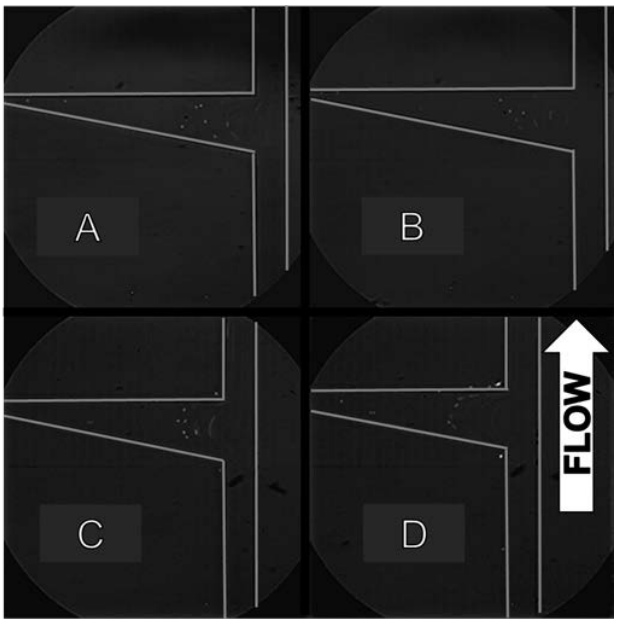

Figure 7.14. Representative fluorescent images of suspensions of 20% GRBC and ~1,000,000 PSFP/µl in 30% Dextran 40 and 40% GRBC and ~1,000,000 PSFP/µl in 20% Dextran 40 examined in Crevice 2 at 5 and 25 µl/min flow rates. Channel height was 75 µm.

[A] 20% GRBC suspension at 5 µl/min, [B] 20% GRBC suspension at 25 µl/min, [C] 40% GRBC suspension at 5 µl/min, [D] 40% GRBC suspension at 25 µl/min. 20x magnification. Field of view in A-D is 1000 µm by 1000 µm.

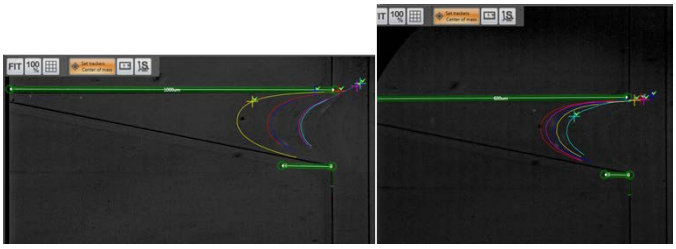

Figure 7.15. Trafficking of five platelet-sized particles in 20% GRBC suspension at 5 µl/min [left] and 25 µl/min [right] flow rates in Crevice 2. 20x magnification. Dimension shown with horizontal green line is 1000 µm. Origin defined at channel entrance.

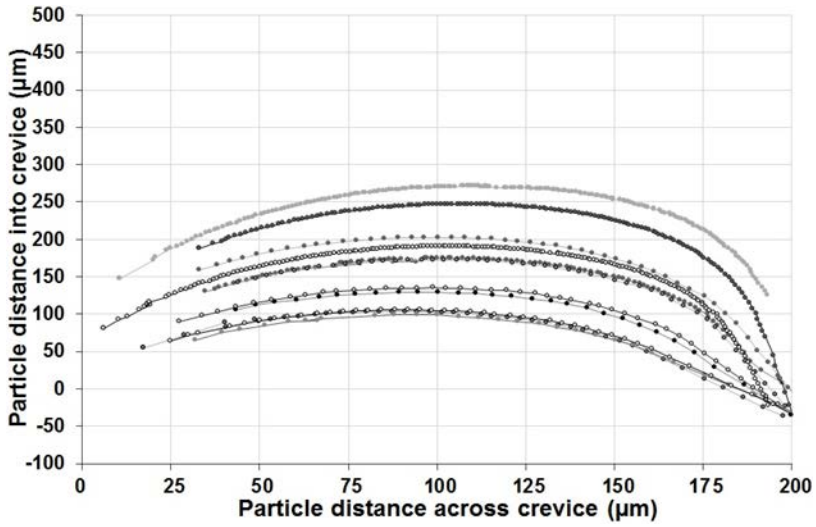

Figure 7.16. Pathlines of platelet-sized particles in 20% GRBC suspension at a 5 µl/min flow rate in Crevice 2.

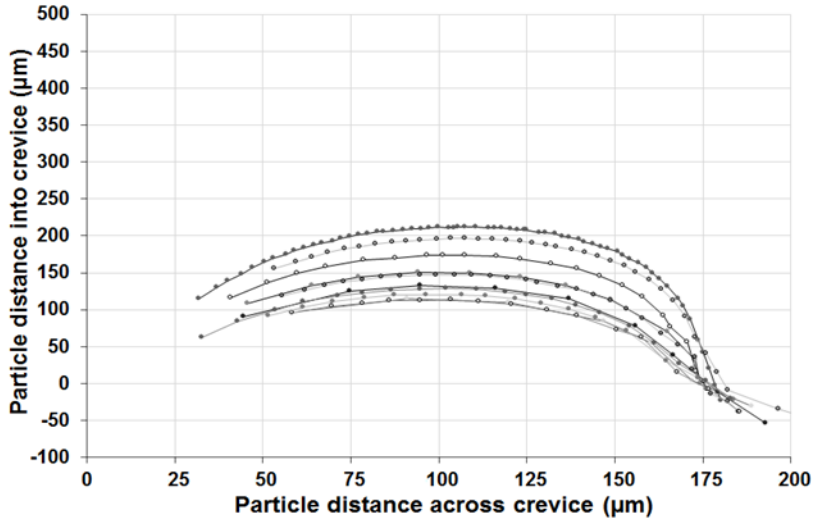

Figure 7.17. Pathlines of platelet-sized particles in 20% GRBC suspension at a 25 µl/min flow rate in Crevice 2.

Figure 7.18 shows a representative analysis of PSFP trafficking in Crevice 2 for the 40% GRBC suspension examined at both flow rates. PSFP pathlines for the 40% GRBC suspension at 5 and 25 µl/min flow rates are shown in **Figure 7.19** and **Figure 7.20**, respectively. Platelet-sized particle trafficking in Crevice 2 for the 40% GRBC suspension had apex distances less than

200 µm for all PSFP studied at 5 µl/min (**Figure 7.19**) and 46% of PSFP examined 25 µl/min (**Figure 7.20**).

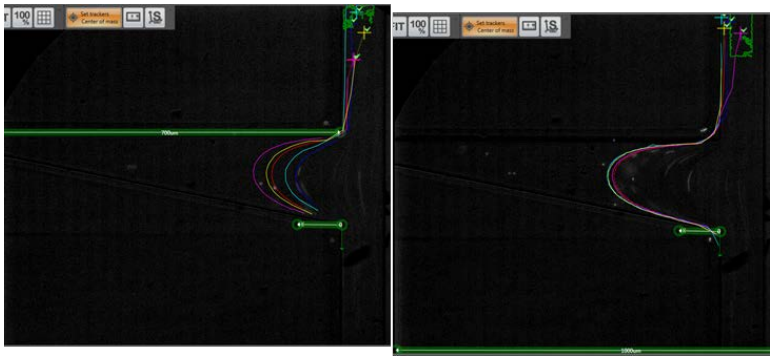

Figure 7.18. Trafficking of five platelet-sized particles in 40% GRBC suspension at 5 µl/min [left] and 25 µl/min [right] flow rates in Crevice 2. 20x magnification. Dimension shown with horizontal green line is 1000 µm. Origin defined at channel entrance.

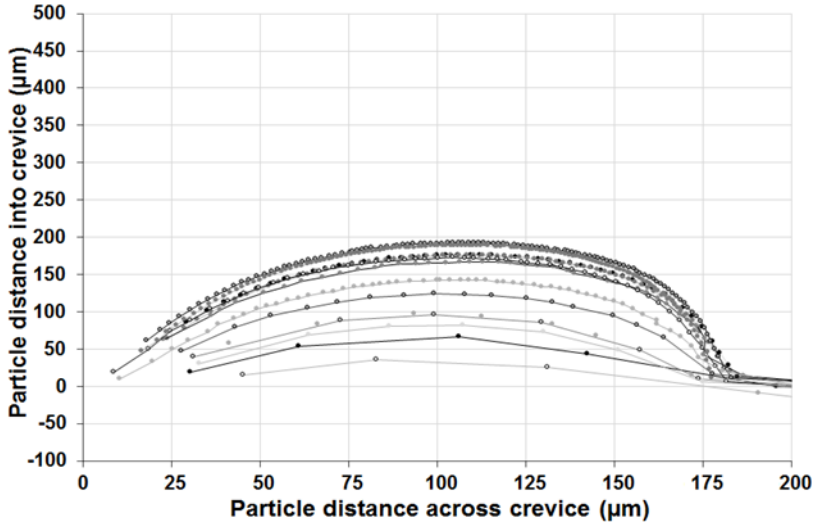

Figure 7.19. Pathlines of platelet-sized particles in 40% GRBC suspension at a 5 µl/min flow rate in Crevice 2.

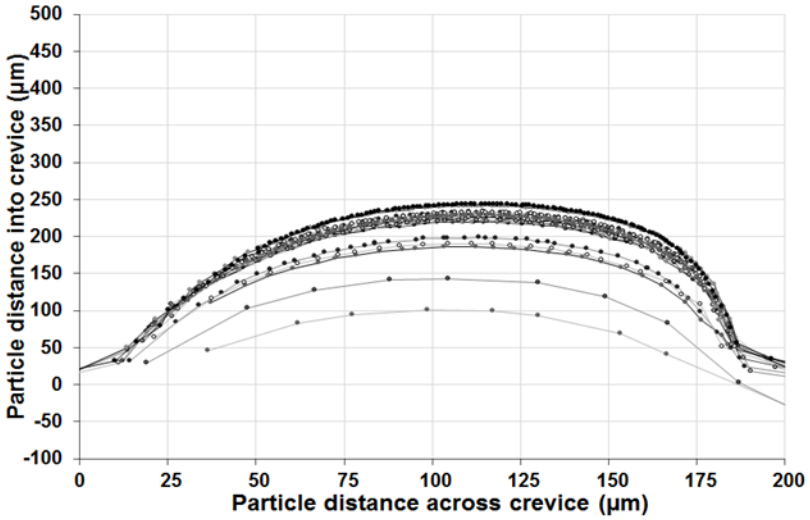

Figure 7.20. Pathlines of platelet-sized particles in 40% GRBC suspension at a 25 µl/min flow rate in Crevice 2.

Figure 7.21 shows a representative analysis of GRBC trafficking in Crevice 2 for the 20% GRBC suspension examined at 5 and 25 µl/min**.** GRBC pathlines for the 20% GRBC suspension at 5 and 25 µl/min flow rates are shown in **Figure 7.22** and **Figure 7.23**, respectively. GRBC trafficking in Crevice 2 for the 20% GRBC suspension had apex distances less than 200 µm at a 5 µl/min flow rate (**Figure 7.22**) and 96% of GRBC pathlines with less than 200 µm apices at a 25 µl/min flow rate (**Figure 7.23**).

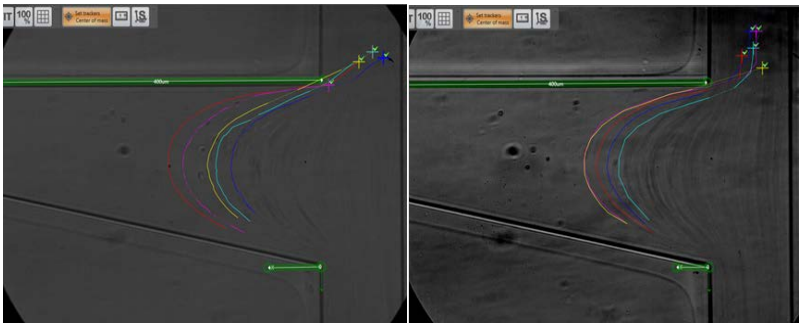

Figure 7.21. Trafficking of five GRBC in 20% GRBC suspension at 5 µl/min [left] and 25 µl/min [right] flow rates in Crevice 2. 40x magnification. Dimension shown with horizontal green line is 400 µm. Origin defined at channel entrance.

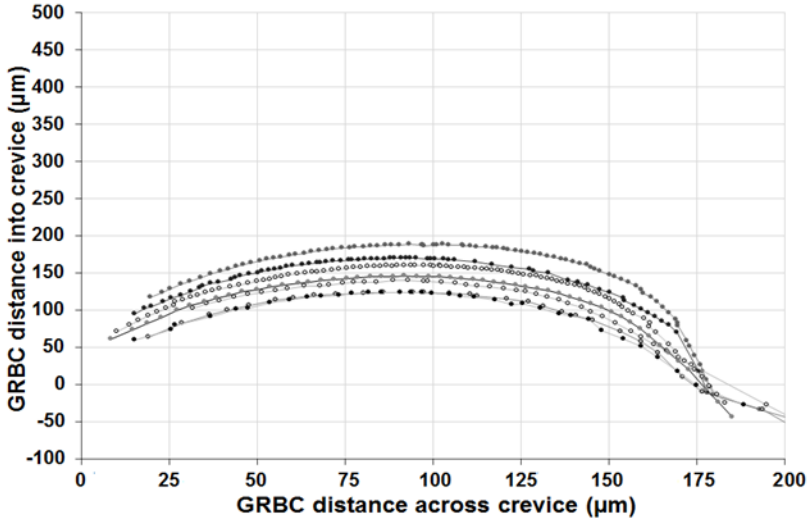

Figure 7.22. Pathlines of GRBC in 20% GRBC suspension at a 5 µl/min flow rate in Crevice 2.

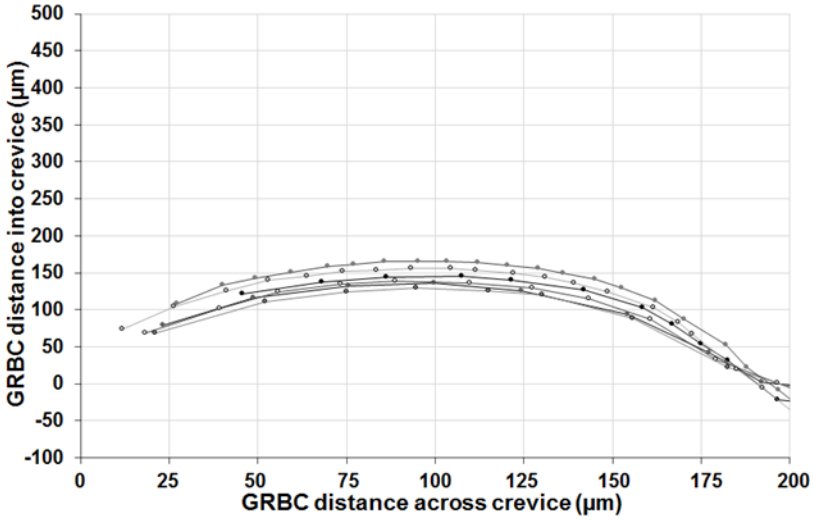

Figure 7.23. Pathlines of GRBC in 20% GRBC suspension at a 25 µl/min flow rate in Crevice 2.

Figure 7.24 shows a representative analysis of GRBC trafficking in Crevice 2 for the 40% GRBC suspension examined at 5 and 25 µl/min**.** GRBC pathlines for the 40% GRBC suspension at 5 and 25 µl/min flow rates are shown in **Figure 7.25** and **Figure 7.26**, respectively. GRBC trafficking in Crevice 2 for the 40% GRBC suspension had apex distances

less than 200 µm for 70% of GRBC studied at 5 µl/min (**Figure 7.25**) and 50% of GRBC examined at 25 µl/min (**Figure 7.26**).

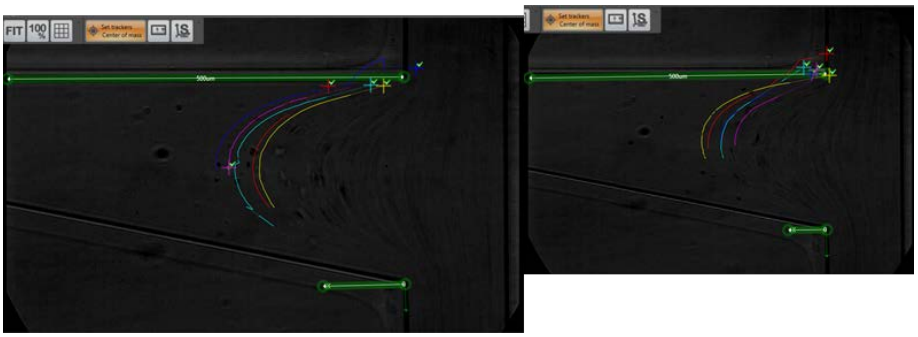

Figure 7.24. Trafficking of five GRBC in 40% GRBC suspension at 5 µl/min [left] and 25 µl/min [right] flow rates in Crevice 2. 40x magnification. Dimension shown with horizontal green line is 400 µm. Origin defined at channel entrance.

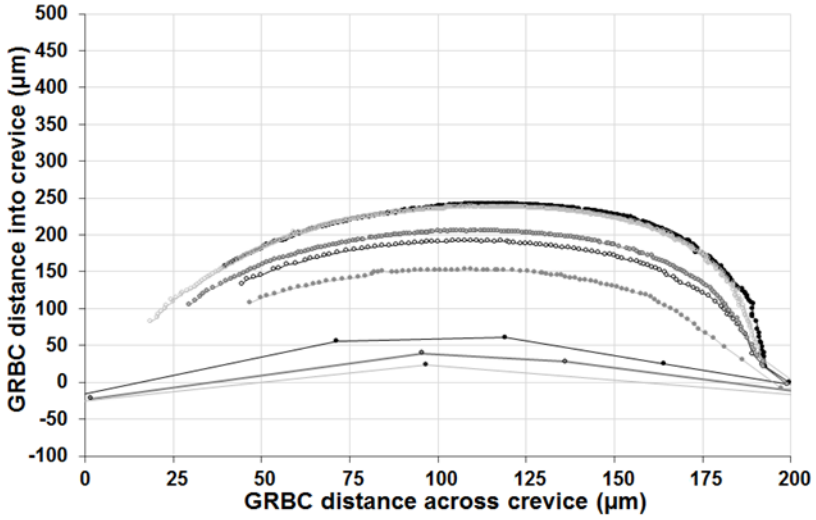

Figure 7.25. Pathlines of GRBC in 40% GRBC suspension at a 5 µl/min flow rate in Crevice 2.

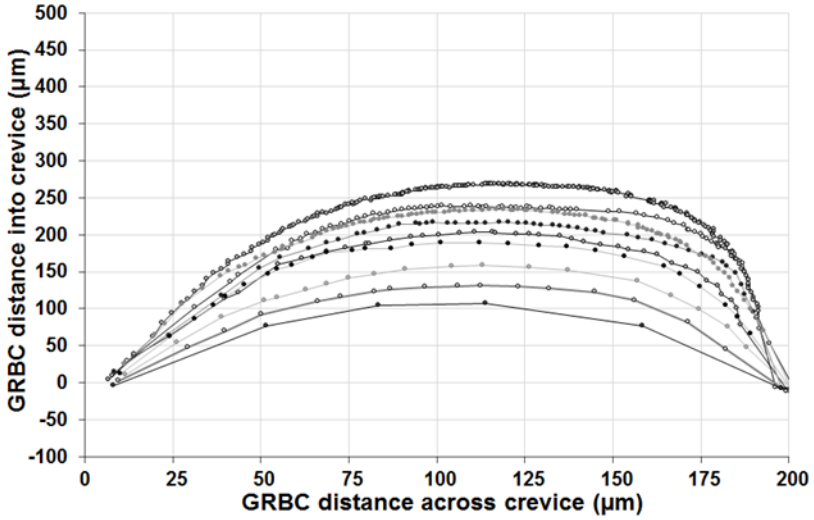

Figure 7.26. Pathlines of GRBC in 40% GRBC suspension at a 25 µl/min flow rate in Crevice 2.

7.3.3 Trafficking of platelet-sized particles and GRBC in a 250 µm wide and 500 µm long rectangular crevice (Crevice 3)

Figure 7.27 shows images of 20% GRBC and ~1,000,000 PSFP/µl in 30% Dextran 40 and 40% GRBC and ~1,000,000 PSFP/µl in 20% Dextran 40 flowing through Crevice 3 at 5 and 25 µl/min. A representative analysis of PSFP trafficking for the 20% GRBC suspension is shown at both flow rates in **Figure 7.28**. Pathlines of PSFP in Crevice 3 for the 20% GRBC suspension at 5 and 25 µl/min flow rates are shown in **Figure 7.29** and **Figure 7.30**, respectively. Platelet-sized particle trafficking in Crevice 3 for the 20% GRBC suspension had apex distances less than 400 µm for 97% of PSFP studied at 5 µl/min (**Figure 7.29**) and 76% of PSFP examined at 25 µl/min (**Figure 7.30**).

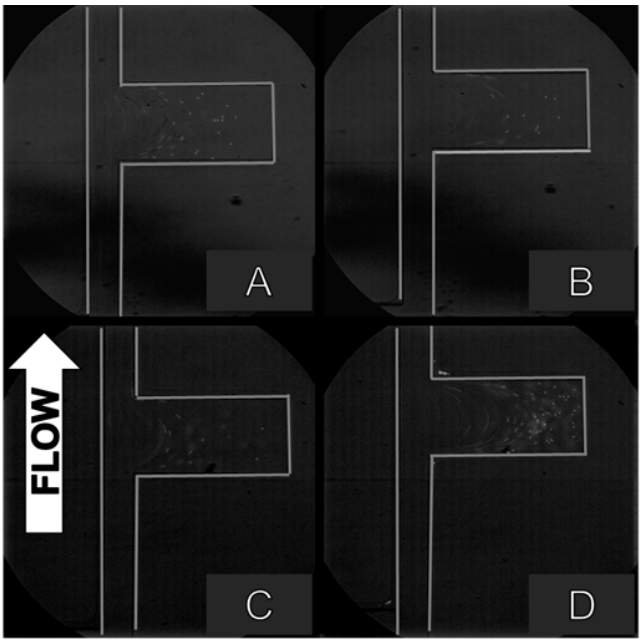

Figure 7.27. Representative fluorescent images of suspensions of 20% GRBC and ~1,000,000 PSFP/µl in 30% Dextran 40 and 40% GRBC and ~1,000,000 PSFP/µl in 20% Dextran 40 examined in Crevice 3 at 5 and 25 µl/min flow rates. Channel height was 75 µm.

[A] 20% GRBC suspension at 5 µl/min, [B] 20% GRBC suspension at 25 µl/min, [C] 40% GRBC suspension at 5 µl/min, [D] 40% GRBC suspension at 25 µl/min. 20x magnification. Field of view in A-D is 1000 µm by 1000 µm.

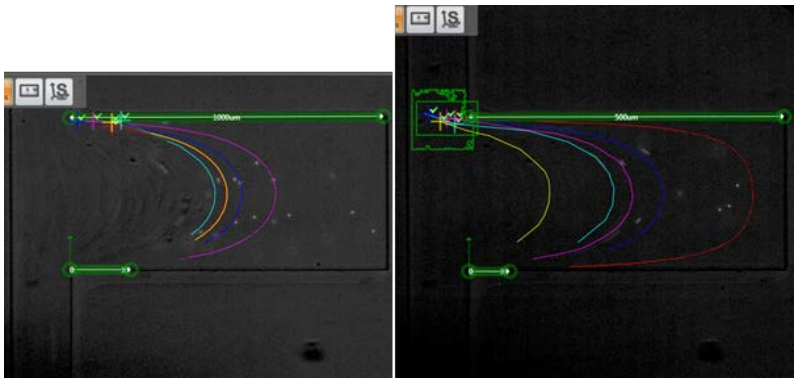

Figure 7.28. Trafficking of five platelet-sized particles in 20% GRBC suspension at 5 µl/min [left] and 25 µl/min [right] flow rates in Crevice 3. 20x magnification. Dimension shown with horizontal green line is 500 µm. Origin defined at channel entrance.

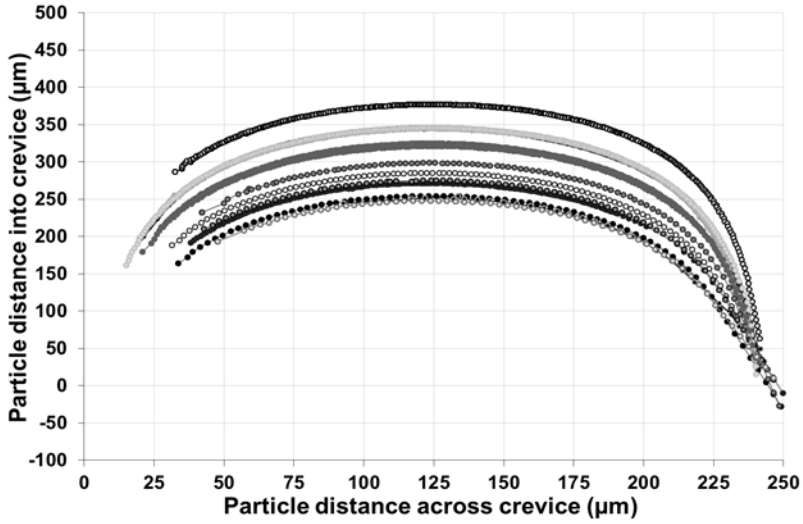

Figure 7.29. Pathlines of platelet-sized particles in 20% GRBC suspension at a 5 µl/min flow rate in Crevice 3.

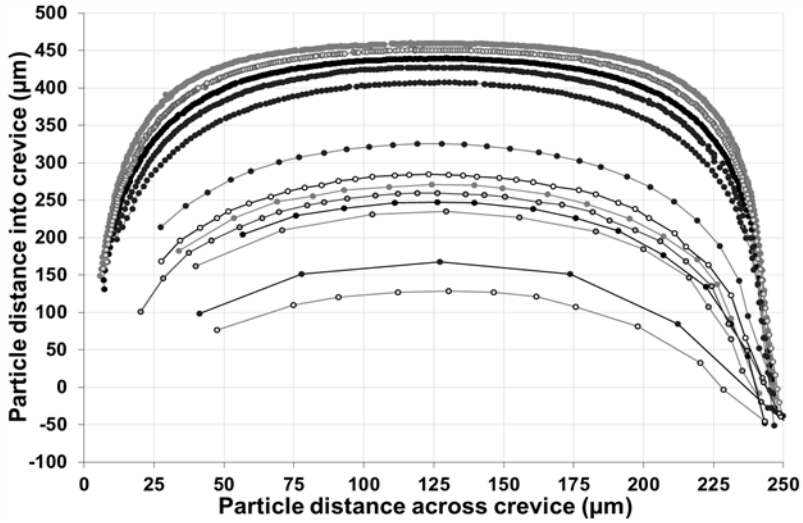

Figure 7.30. Pathlines of platelet-sized particles in 20% GRBC suspension at a 25 µl/min flow rate in Crevice 3.

Figure 7.31 shows a representative analysis of PSFP trafficking in Crevice 3 for the 40% GRBC suspension examined at 5 and 25 µl/min**.** PSFP pathlines for the 40% GRBC suspension at 5 and 25 µl/min flow rates are shown in **Figure 7.32** and **Figure 7.33**, respectively. Platelet-sized particle trafficking in Crevice 3 for the 40% GRBC suspension had apex distances less than

400 µm for 93% of PSFP studied at 5 µl/min (**Figure 7.32**) and 48% of PSFP examined at 25 µl/min (**Figure 7.33**).

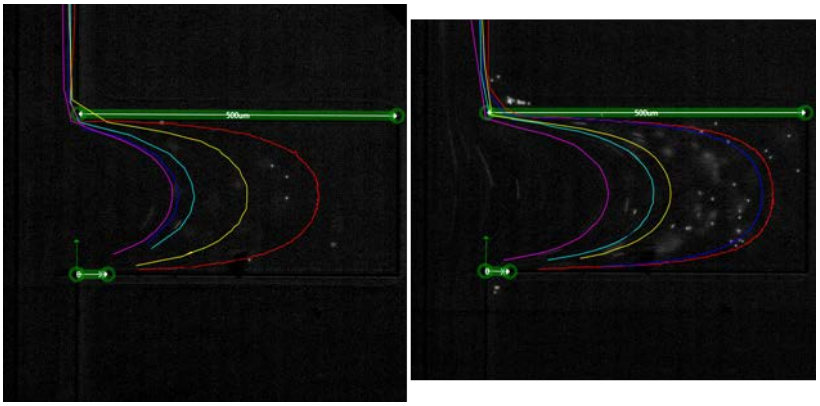

Figure 7.31. Trafficking of five platelet-sized particles in 40% GRBC suspension at 5 µl/min [left] and 25 µl/min [right] flow rates in Crevice 3. 20x magnification. Dimension shown with horizontal green line is 500 µm. Origin defined at channel entrance.

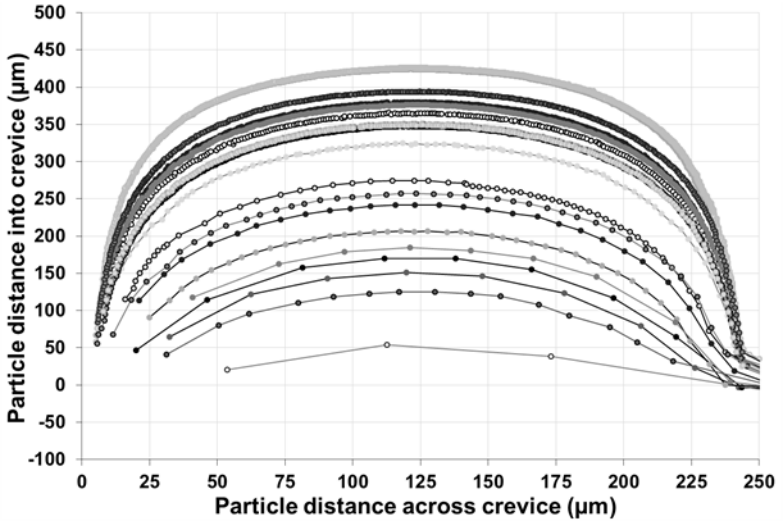

Figure 7.32. Pathlines of platelet-sized particles in 40% GRBC suspension at a 5 µl/min flow rate in Crevice 3.

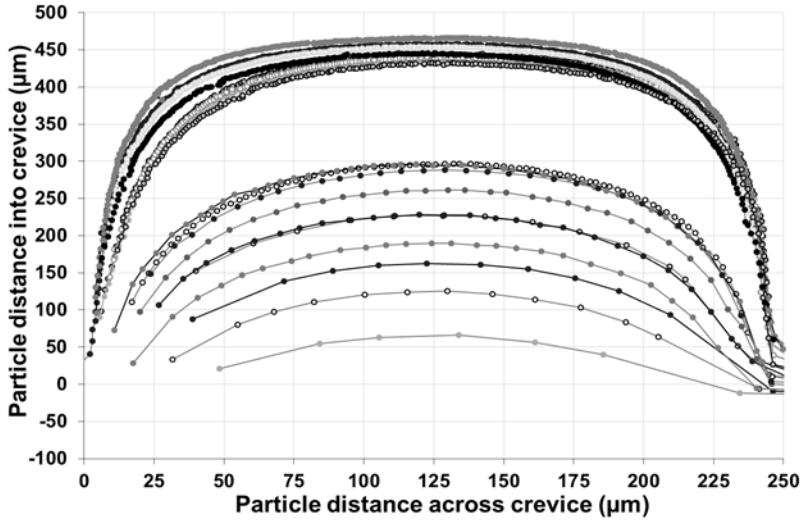

Figure 7.33. Pathlines of platelet-sized particles in 40% GRBC suspension at a 25 µl/min flow rate in Crevice 3.

Figure 7.34 shows a representative analysis of GRBC trafficking in Crevice 3 for the 20% GRBC suspension examined at 5 and 25 µl/min**.** GRBC pathlines for the 20% GRBC suspension at 5 and 25 µl/min flow rates are shown in **Figure 7.35** and **Figure 7.36**, respectively. GRBC trafficking in Crevice 3 for the 20% GRBC suspension had apex distances less than 300 µm for 96% of GRBC studied at 5 µl/min (**Figure 7.35**) and 72% of GRBC examined at 25 µl/min (**Figure 7.36**).

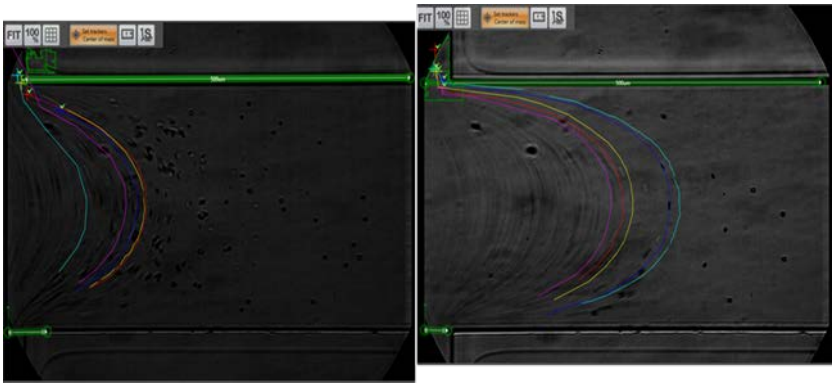

Figure 7.34. Trafficking of five GRBC in 20% GRBC suspension at 5 µl/min [left] and 25 µl/min [right] flow rates in Crevice 3. 40x magnification. Dimension shown with horizontal green line is 500 µm. Origin defined at channel entrance.

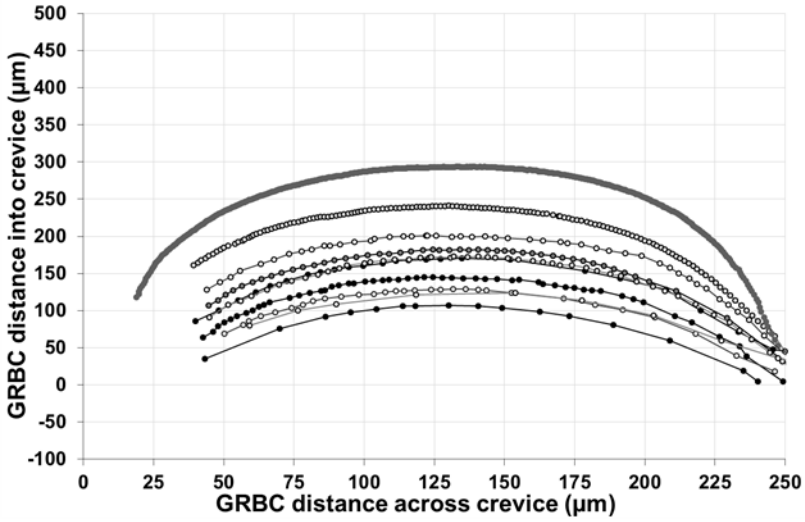

Figure 7.35. Pathlines of GRBC in 20% GRBC suspension at a 5 µl/min flow rate in Crevice 3.

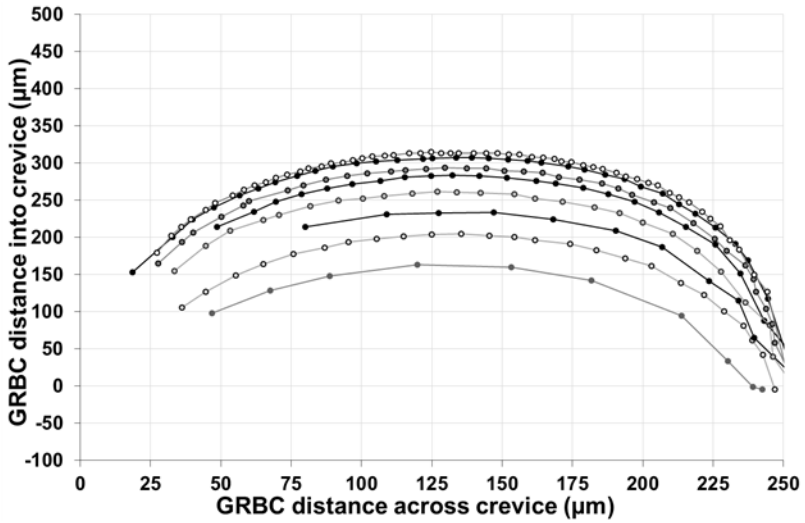

Figure 7.36. Pathlines of GRBC in 20% GRBC suspension at a 25 µl/min flow rate in Crevice 3.

Figure 7.37 shows a representative analysis of GRBC trafficking in Crevice 3 for the 40% GRBC suspension examined at 5 and 25 µl/min**.** GRBC pathlines for the 40% GRBC suspension at 5 and 25 µl/min flow rates are shown in **Figure 7.38** and **Figure 7.39**, respectively. GRBC trafficking in Crevice 3 for the 40% GRBC suspension had apex distances

less than 300 µm for 70% of GRBC studied at 5 and 25 µl/min flow rates (**Figure 7.38** and **Figure 7.39**).

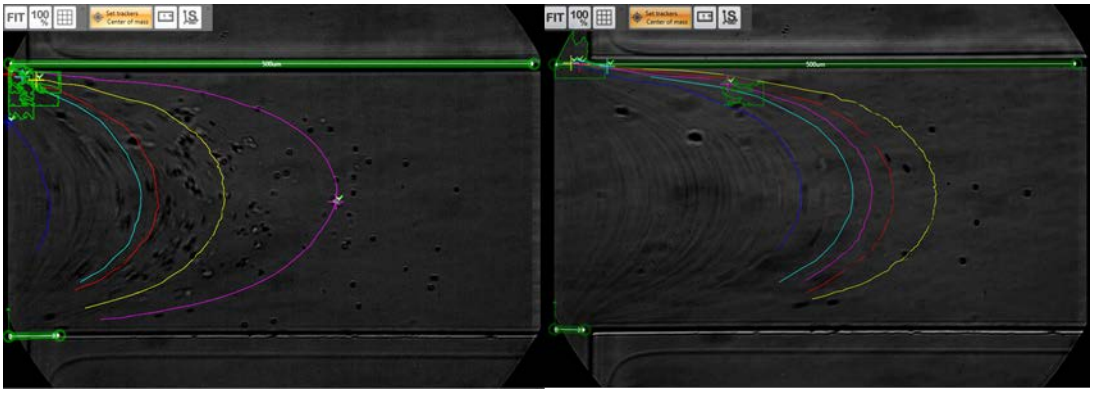

Figure 7.37. Trafficking of five GRBC in 40% GRBC suspension at 5 µl/min [left] and 25 µl/min [right] flow rates in Crevice 3. 40x magnification. Dimension shown with horizontal green line is 500 µm. Origin defined at channel entrance.

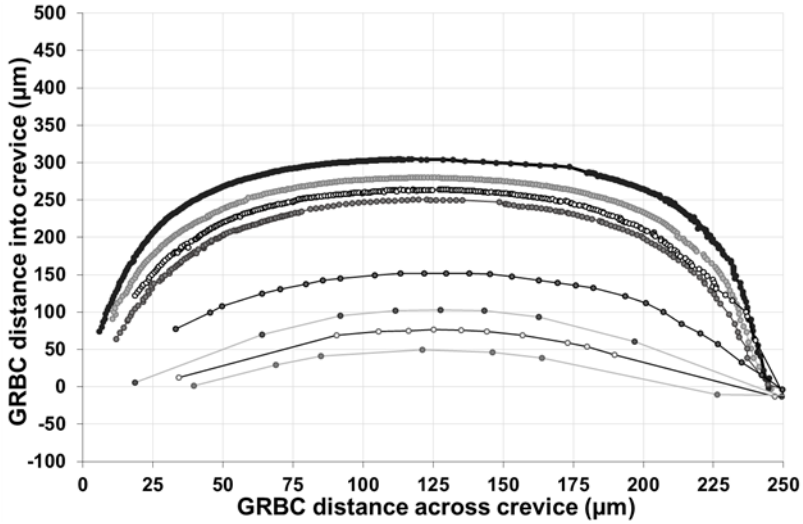

Figure 7.38. Pathlines of GRBC in 40% GRBC suspension at a 5 µl/min flow rate in Crevice 3.

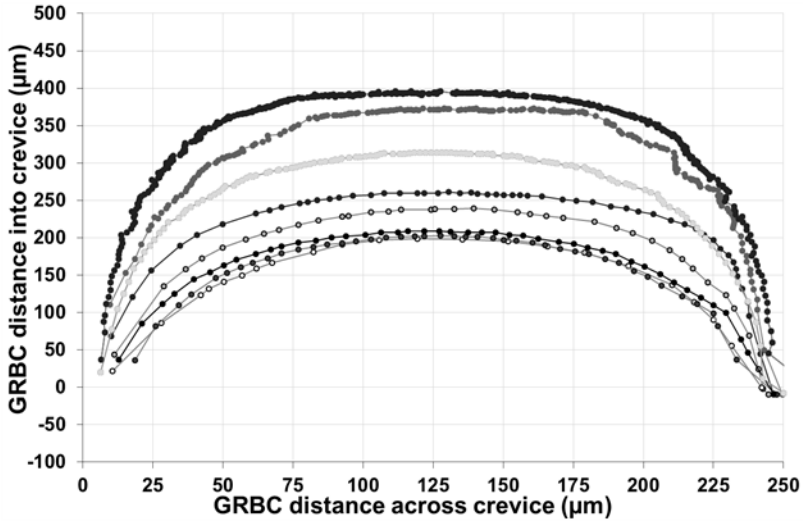

Figure 7.39. Pathlines of GRBC in 40% GRBC suspension at a 25 µl/min flow rate in Crevice 3.

7.3.4 Trafficking of platelet-sized particles and GRBC in a 250 µm height and 500 µm base triangular crevice (Crevice 4)

Figure 7.40 shows images of 20% GRBC and ~1,000,000 PSFP/µl in 30% Dextran 40 and 40% GRBC and ~1,000,000 PSFP/µl in 20% Dextran 40 flowing through Crevice 4 at 5 and 25 µl/min. A representative analysis of PSFP trafficking for the 20% GRBC suspension examined at 5 and 25 µl/min is shown in **Figure 7.41**. Pathlines of PSFP in Crevice 4 for the 20% GRBC suspension at 5 and 25 µl/min flow rates are shown in **Figure 7.42** and **Figure 7.43**, respectively. Platelet-sized particle trafficking in Crevice 4 for the 20% GRBC suspension had apex distances less than 200 µm for 75% of PSFP studied at 5 µl/min (**Figure 7.42**) and 27% of PSFP examined at 25 µl/min (**Figure 7.43**).

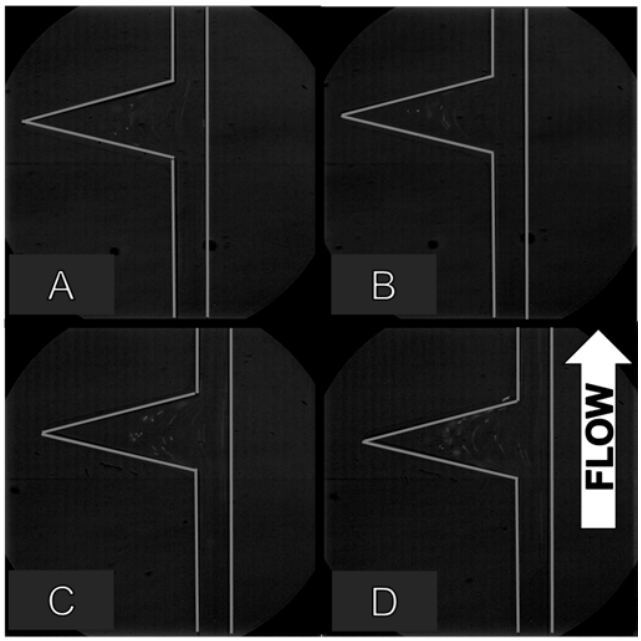

Figure 7.40. Representative fluorescent images of suspensions of 20% GRBC and ~1,000,000 PSFP/µl in 30% Dextran 40 and 40% GRBC and ~1,000,000 PSFP/µl in 20% Dextran 40 examined in Crevice 4 at 5 and 25 µl/min flow rates. Channel height was 75 µm.

[A] 20% GRBC suspension at 5 µl/min, [B] 20% GRBC suspension at 25 µl/min, [C] 40% GRBC suspension at 5 µl/min, [D] 40% GRBC suspension at 25 µl/min. 20x magnification. Field of view in A-D is 1000 µm by 1000 µm.

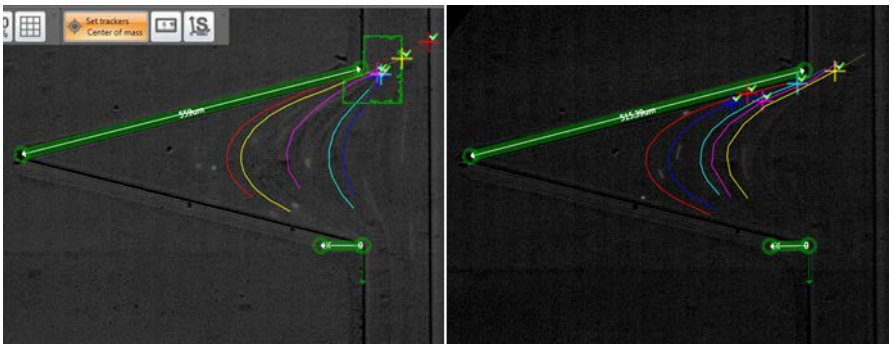

Figure 7.41. Trafficking of five platelet-sized particles in 20% GRBC suspension at 5 µl/min [left] and 25 µl/min [right] flow rates in Crevice 4. 20x magnification. Dimension shown with green line is 515.4 µm. Origin defined at channel entrance.

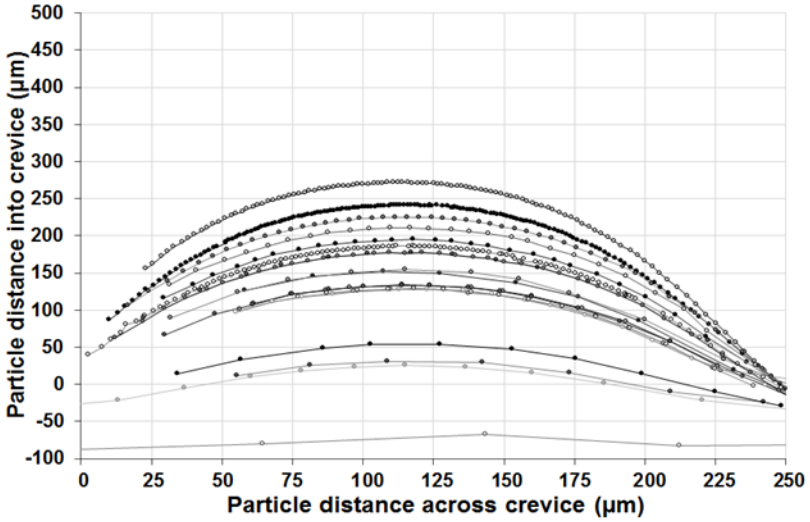

Figure 7.42. Pathlines of platelet-sized particles in 20% GRBC suspension at a 5 µl/min flow rate in Crevice 4.

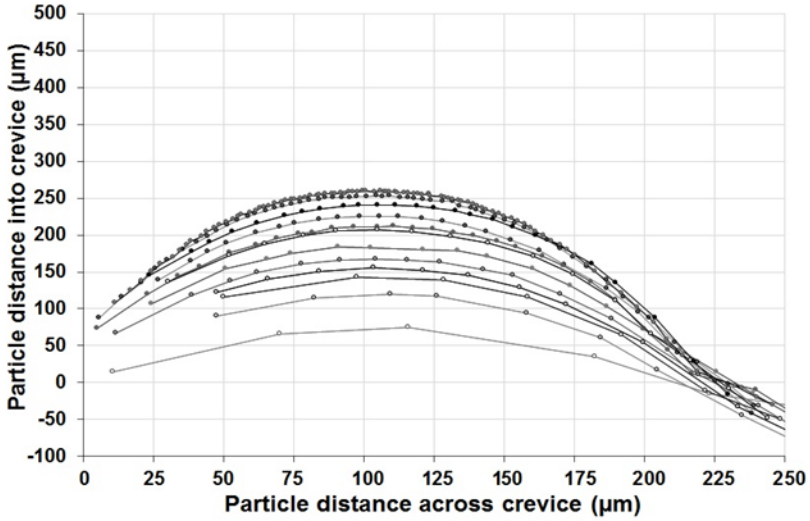

Figure 7.43. Pathlines of platelet-sized particles in 20% GRBC suspension at a 25 µl/min flow rate in Crevice 4.

Figure 7.44 shows a representative analysis of PSFP trafficking in Crevice 4 for the 40% GRBC suspension examined at 5 and 25 µl/min**.** Pathlines of PSFP for the 40% GRBC suspension at 5 and 25 µl/min flow rates are shown in **Figure 7.45** and **Figure 7.46**, respectively. Platelet-sized particle trafficking in Crevice 4 for the 40% GRBC suspension had

apex distances less than 200 µm for 68% of PSFP studied at 5 µl/min (**Figure 7.45**) and 48% of PSFP examined at 25 µl/min (**Figure 7.46**).

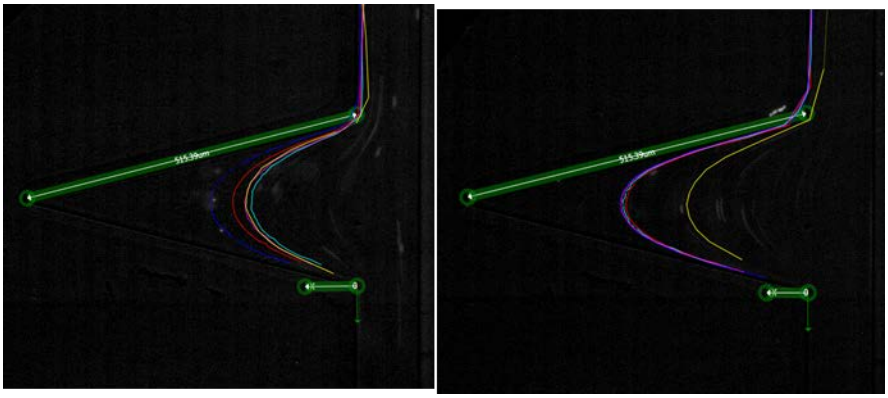

Figure 7.44. Trafficking of five platelet-sized particles in 40% GRBC suspension at 5 µl/min [left] and 25 µl/min [right] flow rates in Crevice 4. 20x magnification. Dimension shown with green line is 515.4 µm. Origin defined at channel entrance.

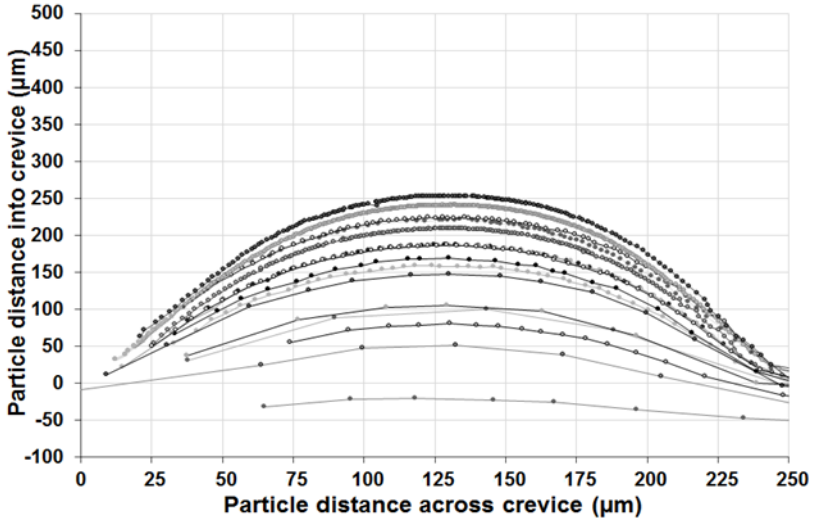

Figure 7.45. Pathlines of platelet-sized particles in 40% GRBC suspension at a 5 µl/min flow rate in Crevice 4.

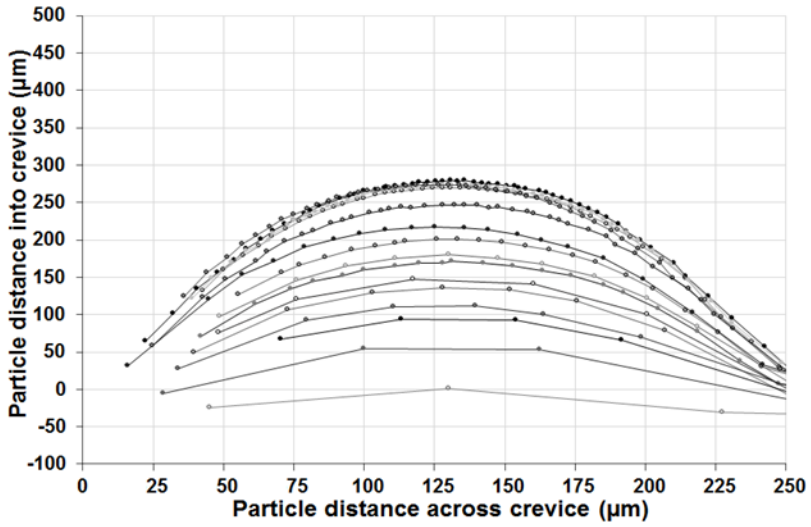

Figure 7.46. Pathlines of platelet-sized particles in 40% GRBC suspension at a 25 µl/min flow rate in Crevice 4.

Figure 7.47 shows a representative analysis of GRBC trafficking in Crevice 4 for the 20% GRBC suspension examined at 5 and 25 µl/min**.** Pathlines of GRBC for the 20% GRBC suspension at 5 and 25 µl/min flow rates are shown in **Figure 7.48** and **Figure 7.49**, respectively. GRBC trafficking in Crevice 4 for the 20% GRBC suspension had apex distances less than 200 µm for all GRBC studied at 5 µl/min (**Figure 7.48**) and 72% of GRBC examined at 25 µl/min (**Figure 7.49**).

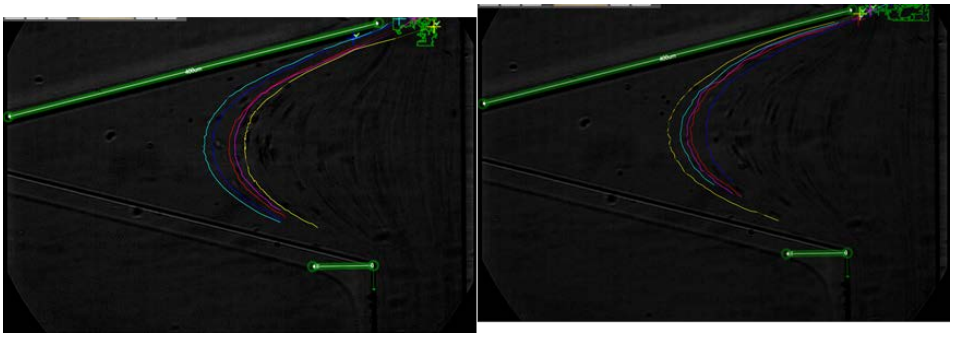

Figure 7.47. Trafficking of five GRBC in 20% GRBC suspension at 5 µl/min [left] and 25 µl/min [right] flow rates in Crevice 4. 40x magnification. Dimension shown with green line is 371.7 µm. Origin defined at channel entrance.

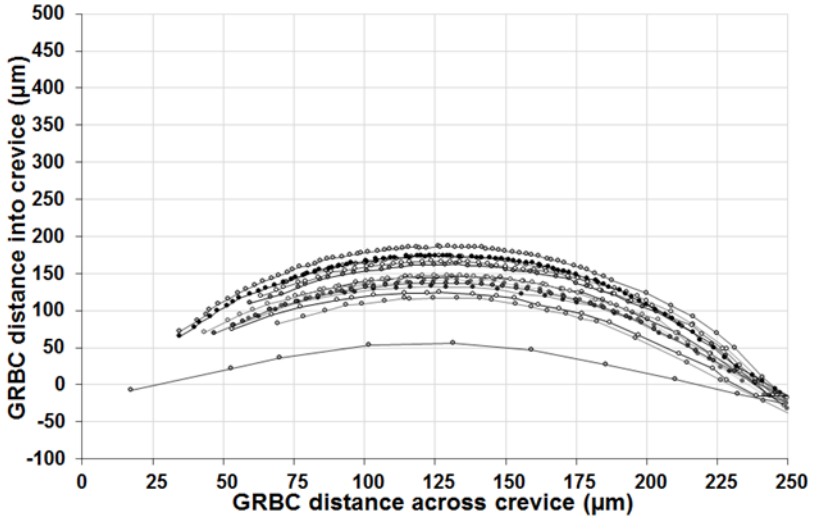

Figure 7.48. Pathlines of GRBC in 20% GRBC suspension at a 5 µl/min flow rate in Crevice 4.

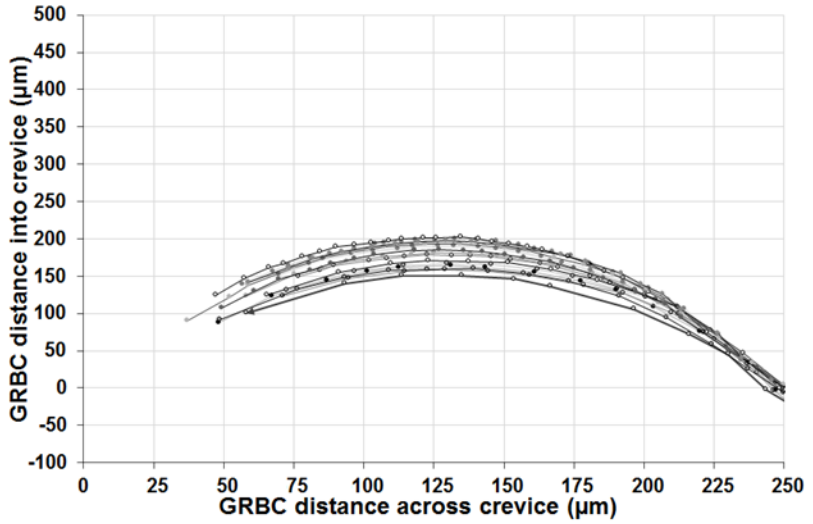

Figure 7.49. Pathlines of GRBC in 20% GRBC suspension at a 25 µl/min flow rate in Crevice 4.

Figure 7.50 shows a representative analysis of GRBC trafficking in Crevice 4 for the 40% GRBC suspension examined at 5 and 25 µl/min**.** Pathlines of GRBC for the 40% GRBC suspension at 5 and 25 µl/min flow rates are shown in **Figure 7.51** and **Figure 7.52**, respectively. GRBC trafficking in Crevice 4 for the 40% GRBC suspension had apex distances

less than 200 µm for 70% of GRBC studied at 5 µl/min (**Figure 7.51**) and 10% of GRBC examined at 25 µl/min (**Figure 7.52**).

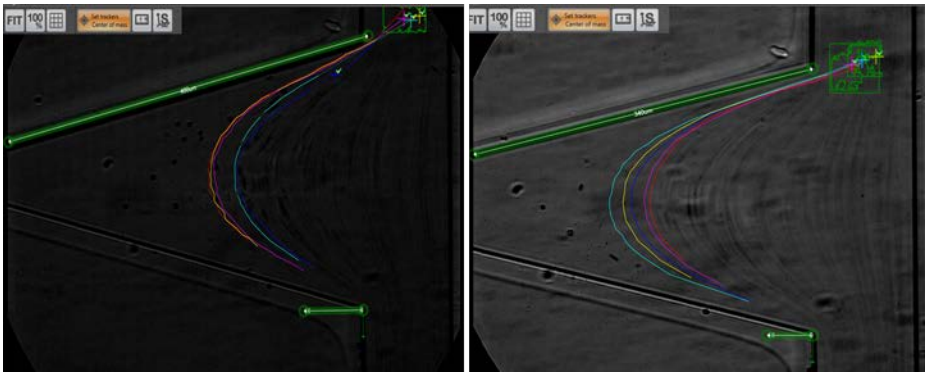

Figure 7.50. Trafficking of five GRBC in 40% GRBC suspension at 5 µl/min [left] and 25 µl/min [right] flow rates in Crevice 4. 40x magnification. Dimension shown with green line is 371.7 µm. Origin defined at channel entrance.

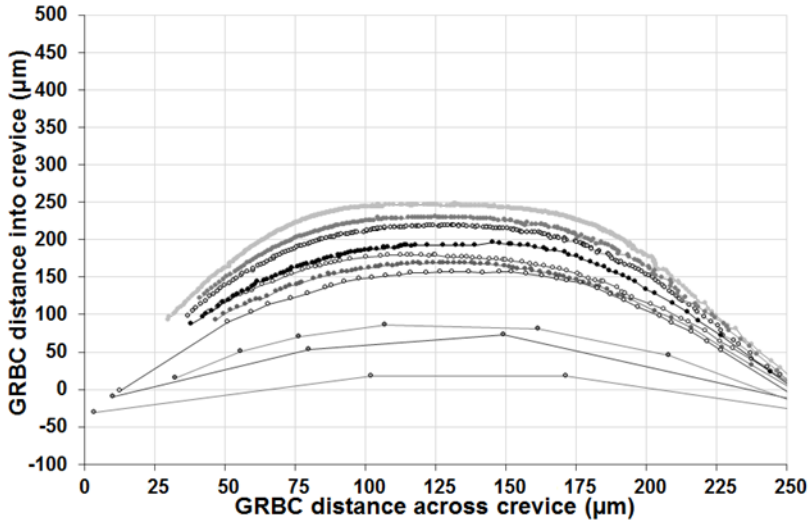

Figure 7.51. Pathlines of GRBC in 40% GRBC suspension at a 5 µl/min flow rate in Crevice 4.

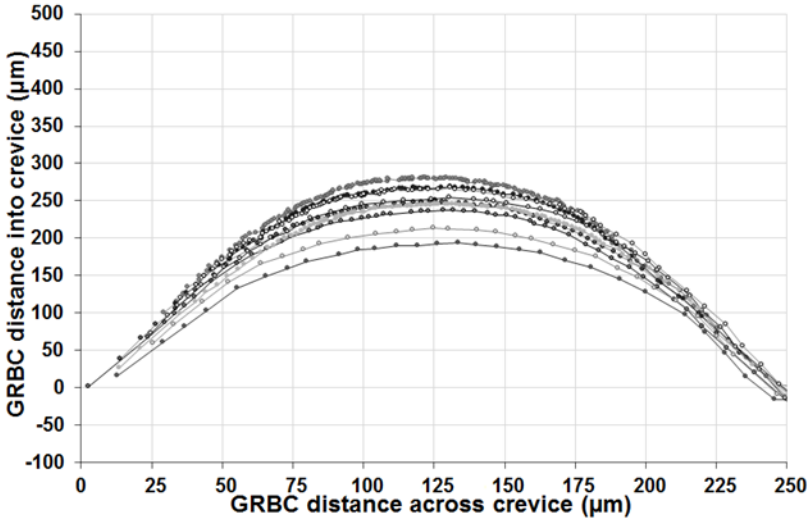

Figure 7.52. Pathlines of GRBC in 40% GRBC suspension at a 25 µl/min flow rate in Crevice 4.

7.3.5 Trafficking of platelet-sized particles and GRBC in a 100 µm wide and 500 µm long rectangular crevice (Crevice 5)

Figure 7.53 shows images of 20% GRBC and ~1,000,000 PSFP/µl in 30% Dextran 40 and 40% GRBC and ~1,000,000 PSFP/µl in 20% Dextran 40 flowing through Crevice 5 at 5 and 25 µl/min. A representative analysis of PSFP trafficking for the 20% GRBC suspension is shown at both flow rates in **Figure 7.54**. PSFP pathlines in Crevice 5 for the 20% GRBC suspension examined at 5 and 25 µl/min are shown in **Figure 7.55** and **Figure 7.56**, respectively. PSFP trafficking in Crevice 5 for 20% GRBC suspension studied at 5 and 25 µl/min identified a recirculating region beginning between 75-80 µm. Three PSFP pathlines that had greater than 75 µm apex distance recirculated 1-6 times before PSFP adhesion to the crevice wall near the outlet (**Figure 7.55** and **Figure 7.56**). Trafficking of non-recirculating PSFP in Crevice 5 for the 20%

GRBC suspension had apex distances less than 60 µm for 93% of PSFP studied at 5 µl/min (**Figure 7.55**) and 42% of PSFP examined at 25 µl/min (**Figure 7.56**).

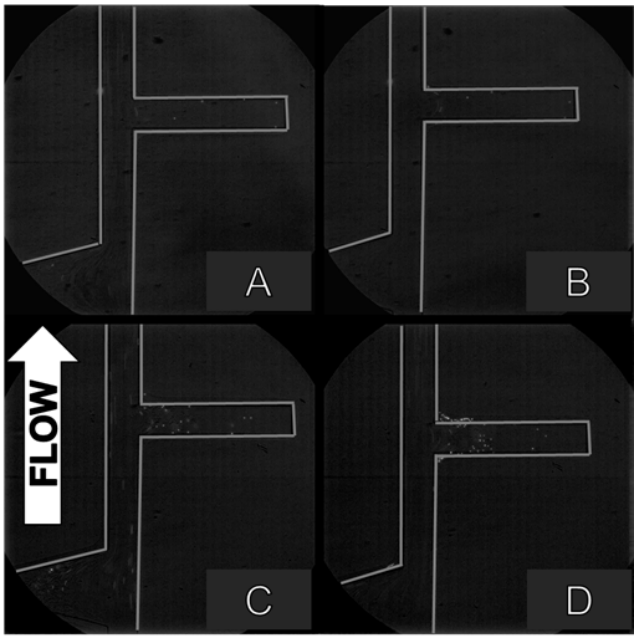

Figure 7.53. Representative fluorescent images of suspensions of 20% GRBC and ~1,000,000 PSFP/µl in 30% Dextran 40 and 40% GRBC and ~1,000,000 PSFP/µl in 20% Dextran 40 examined in Crevice 5 at 5 and 25 µl/min flow rates. Channel height was 75 µm.

[A] 20% GRBC suspension at 5 µl/min, [B] 20% GRBC suspension at 25 µl/min, [C] 40% GRBC suspension at 5 µl/min, [D] 40% GRBC suspension at 25 µl/min. 20x magnification. Field of view in A-D is 1000 µm by 1000 µm.

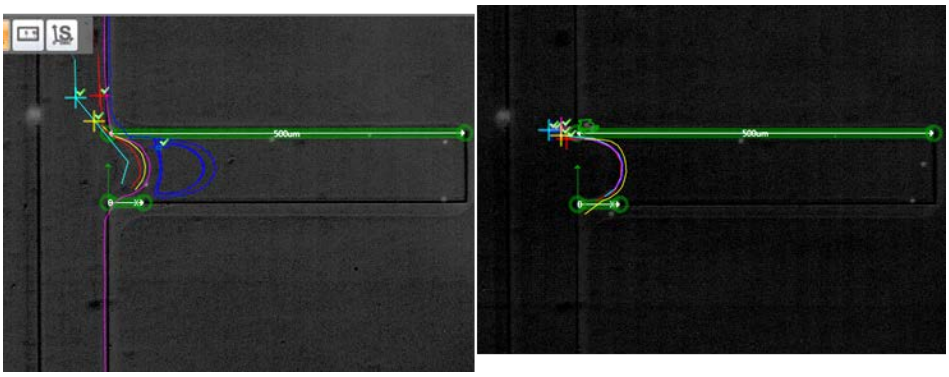

Figure 7.54. Trafficking of five platelet-sized particles in 20% GRBC suspension at 5 µl/min [left] and 25 µl/min [right] flow rates in Crevice 5. 20x magnification. Dimension shown with horizontal green line is 500 µm. Origin defined at channel entrance.

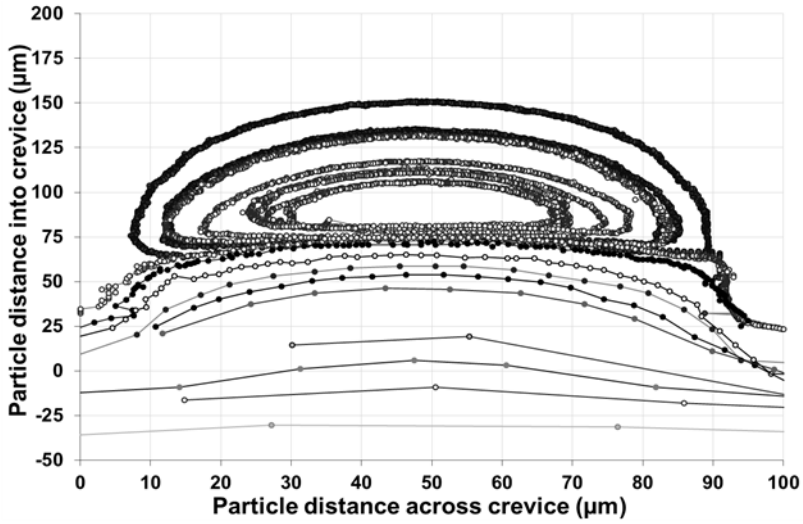

Figure 7.55. Pathlines of platelet-sized particles in 20% GRBC suspension at a 5 µl/min flow rate in Crevice 5.

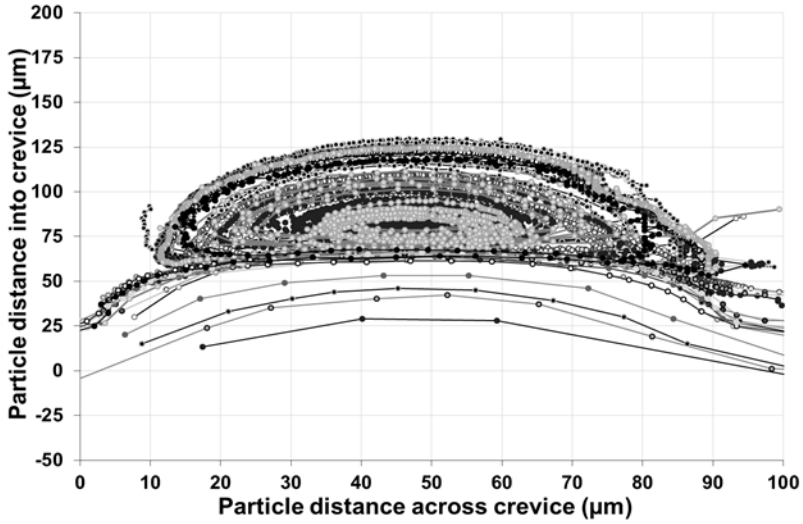

Figure 7.56. Pathlines of platelet-sized particles in 20% GRBC suspension at a 25 µl/min flow rate in Crevice 5.

Figure 7.57 shows a representative analysis of PSFP trafficking in Crevice 5 for the 40% GRBC suspension examined at 5 and 25 µl/min. Platelet-sized particle pathlines for the 40% GRBC suspension at 5 and 25 µl/min flow rates are shown in **Figure 7.58** and **Figure 7.59**, respectively. PSFP trafficking in Crevice 5 for the 40% GRBC suspension at 5 and 25 µl/min confirmed the presence of a recirculating region in Crevice 5 beginning between 75-80 µm. Recirculation of PSFP in Crevice 5 for the 40% GRBC suspension occurred for 44% of PSFP studied at 5 µl/min and 52% of PSFP examined at 25 µl/min before PSFP exit or adhesion to the crevice wall near the outlet (**Figure 7.58** and **Figure 7.59**). Trafficking of non-recirculating PSFP in Crevice 5 for the 40% GRBC suspension had apex distances less than 60 µm for 93% of PSFP studied at 5 µl/min (**Figure 7.58**) and 58% of PSFP examined at 25 µl/min (**Figure 7.59**).

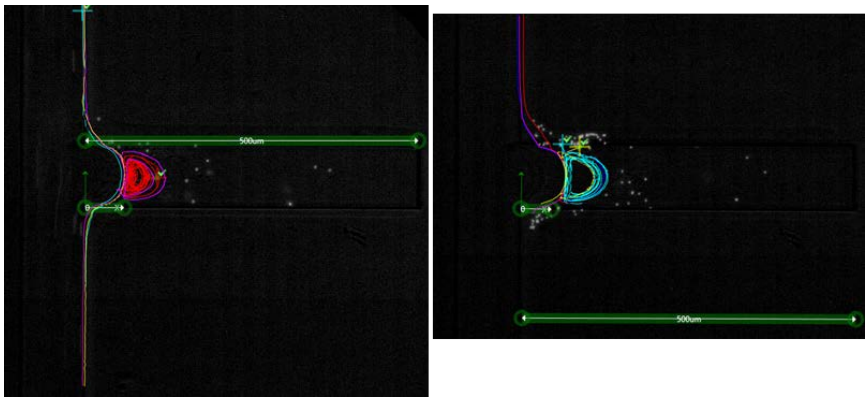

Figure 7.57. Trafficking of five platelet-sized particles in 40% GRBC suspension at 5 µl/min [left] and 25 µl/min [right] flow rates in Crevice 5. 20x magnification. Dimension shown with horizontal green line is 500 µm. Origin defined at channel entrance.

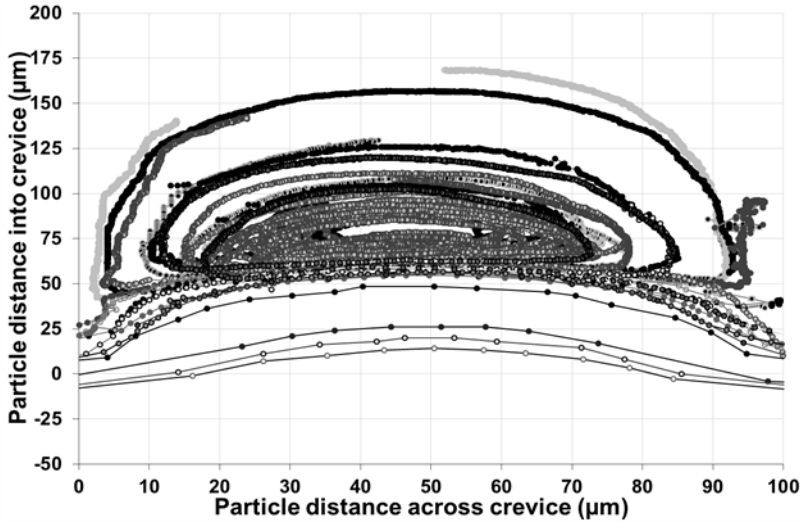

Figure 7.58. Pathlines of platelet-sized particles in 40% GRBC suspension at a 5 µl/min flow rate in Crevice 5.

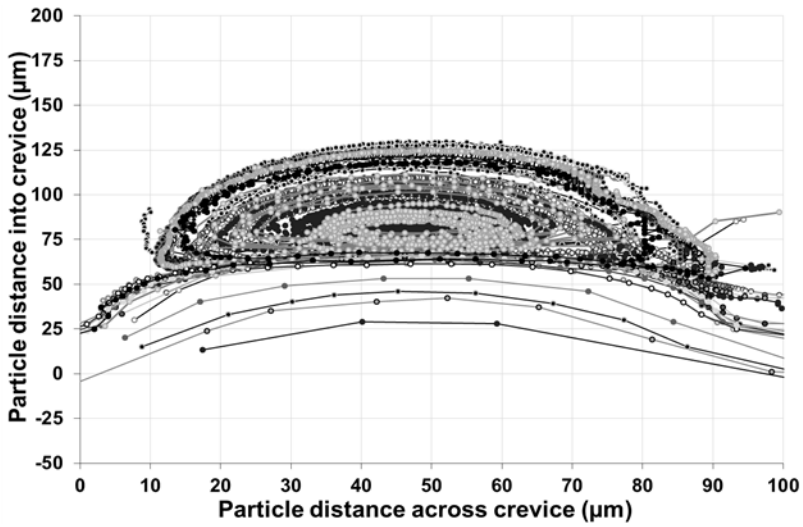

Figure 7.59. Pathlines of platelet-sized particles in 40% GRBC suspension at a 25 µl/min flow rate in Crevice 5.

Figure 7.60 shows a representative analysis of GRBC trafficking in Crevice 5 for the 20% GRBC suspension examined at 5 and 25 µl/min**.** Pathlines of GRBC for the 20% GRBC suspension at 5 and 25 µl/min flow rates are shown in **Figure 7.61** and **Figure 7.62**, respectively. GRBC trafficking in Crevice 5 for 20% GRBC suspension at 5 and 25 µl/min flow rates had apex distances less than 60 µm (**Figure 7.61** and **Figure 7.62**). GRBC pathlines in Crevice 5 for the 20% GRBC suspension did not recirculate at either flow rate.

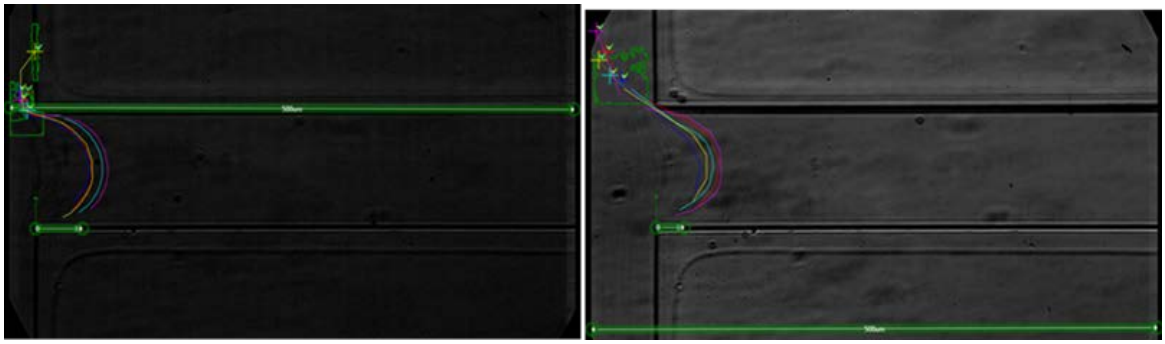

Figure 7.60. Trafficking of five GRBC in 20% GRBC suspension at 5 µl/min [left] and 25 µl/min [right] flow rates in Crevice 5. 40x magnification. Dimension shown with horizontal green line is 500 µm. Origin defined at channel entrance.

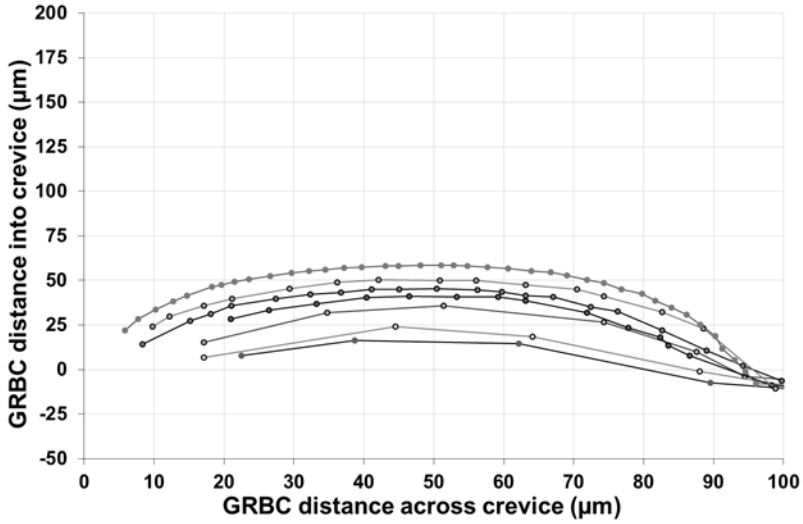

Figure 7.61. Pathlines of GRBC in 20% GRBC suspension at a 5 µl/min flow rate in Crevice 5.

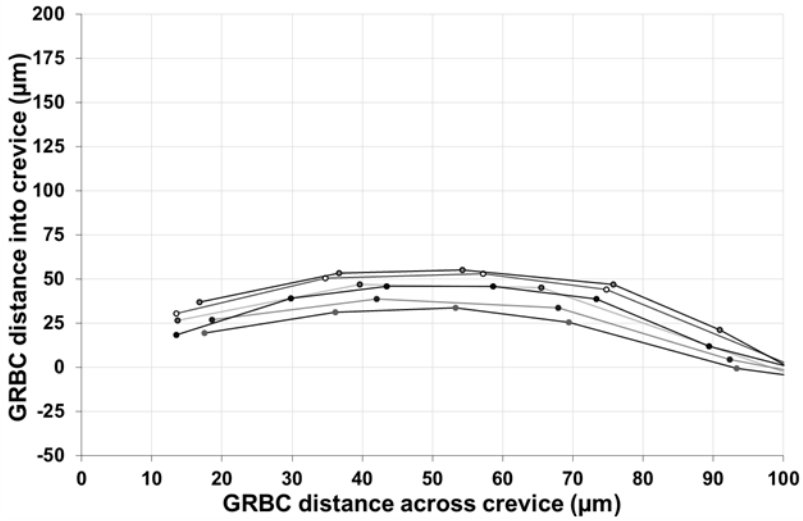

Figure 7.62. Pathlines of GRBC in 20% GRBC suspension at a 25 µl/min flow rate in Crevice 5.

Figure 7.63 shows a representative analysis of GRBC trafficking in Crevice 5 for the 40% GRBC suspension examined at 5 and 25 µl/min**.** Pathlines of GRBC for the 40% GRBC suspension at 5 and 25 µl/min flow rates are shown in **Figure 7.64** and **Figure 7.65**, respectively. GRBC trafficking in Crevice 5 for the 40% GRBC suspension had apex distances less than 60 µm for all GRBC studied at 5 µl/min (**Figure 7.64**) and 60% of GRBC examined at

25 µl/min (**Figure 7.65**). GRBC pathlines in Crevice 5 for the 40% GRBC suspension did not recirculate at either flow rate.

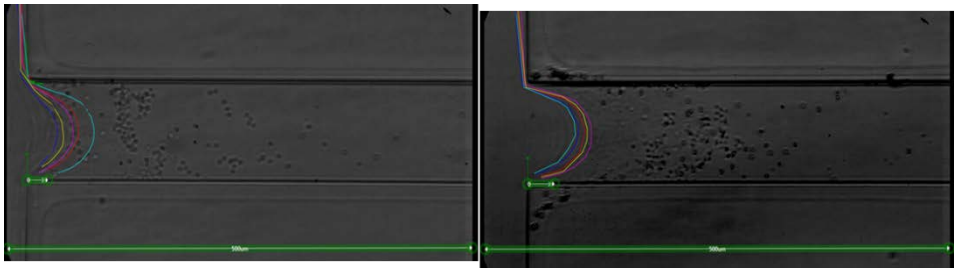

Figure 7.63. Trafficking of five GRBC in 40% GRBC suspension at 5 µl/min [left] and 25 µl/min [right] flow rates in Crevice 5. 40x magnification. Dimension shown with horizontal green line is 500 µm. Origin defined at channel entrance.

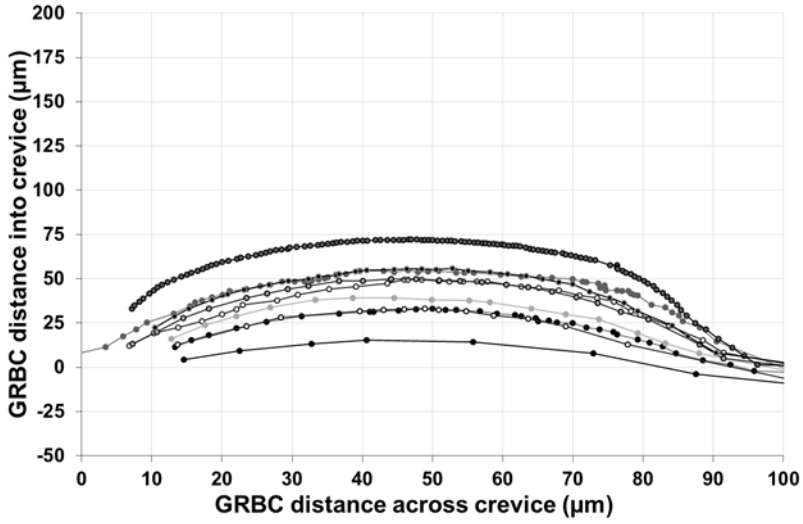

Figure 7.64. Pathlines of GRBC in 40% GRBC suspension at a 5 µl/min flow rate in Crevice 5.

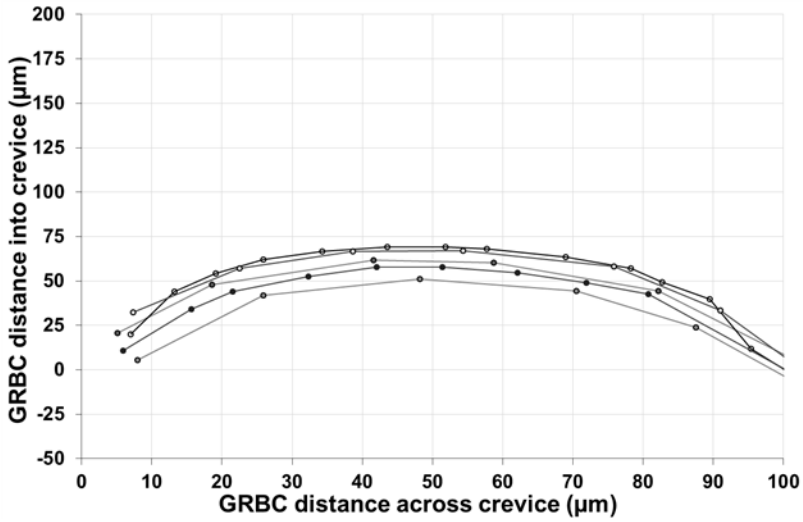

Figure 7.65. Pathlines of GRBC in 40% GRBC suspension at a 25 µl/min flow rate in Crevice 5.

7.3.6 Trafficking of platelet-sized particles and GRBC in a 150 µm height and 500 µm base triangular crevice (Crevice 6)

Figure 7.66 shows images of 20% GRBC and ~1,000,000 PSFP/µl in 30% Dextran 40 and 40% GRBC and ~1,000,000 PSFP/µl in 20% Dextran 40 flowing through Crevice 6 at 5 and 25 µl/min. A representative analysis of PSFP trafficking for the 20% GRBC suspension is shown at both flow rates in **Figure 7.67**. PSFP pathlines in Crevice 6 for the 20% GRBC suspension examined at 5 and 25 µl/min are shown in **Figure 7.68** and **Figure 7.69**, respectively. PSFP trafficking in Crevice 6 for the 20% GRBC suspension had apex distances less than 150 µm for all PSFP studied at 5 µl/min (**Figure 7.68**) and 76% of PSFP examined at 25 µl/min (**Figure 7.69**).

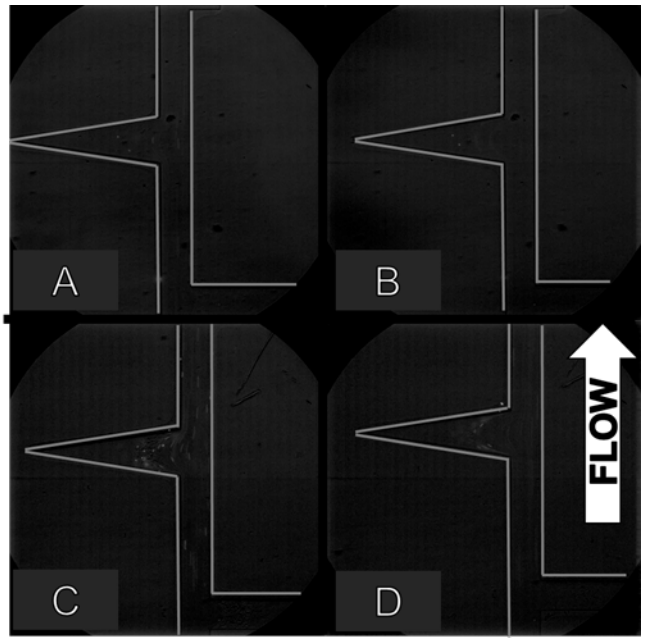

Figure 7.66. Representative fluorescent images of suspensions of 20% GRBC and ~1,000,000 PSFP/µl in 30% Dextran 40 and 40% GRBC and ~1,000,000 PSFP/µl in 20% Dextran 40 examined in Crevice 6 at 5 and 25 µl/min flow rates. Channel height was 75 µm.

[A] 20% GRBC suspension at 5 µl/min, [B] 20% GRBC suspension at 25 µl/min, [C] 40% GRBC suspension at 5 µl/min, [D] 40% GRBC suspension at 25 µl/min. 20x magnification. Field of view in A-D is 1000 µm by 1000 µm.

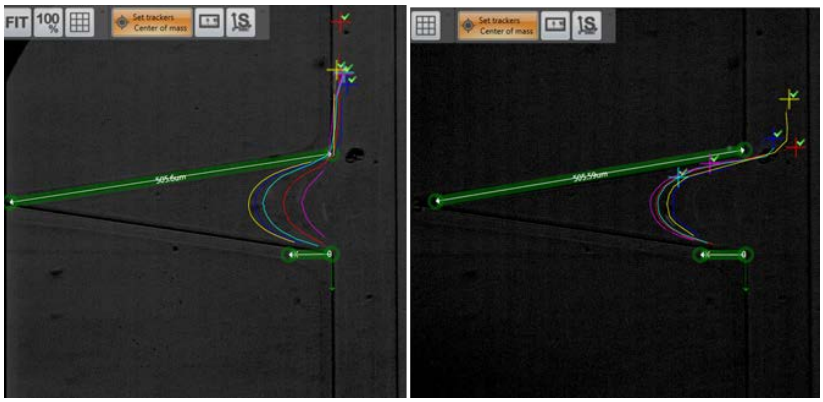

Figure 7.67. Trafficking of five platelet-sized particles in 20% GRBC suspension at 5 µl/min [left] and 25 µl/min [right] flow rates in Crevice 6. 20x magnification. Dimension shown with green line is 505.6 µm. Origin defined at channel entrance.

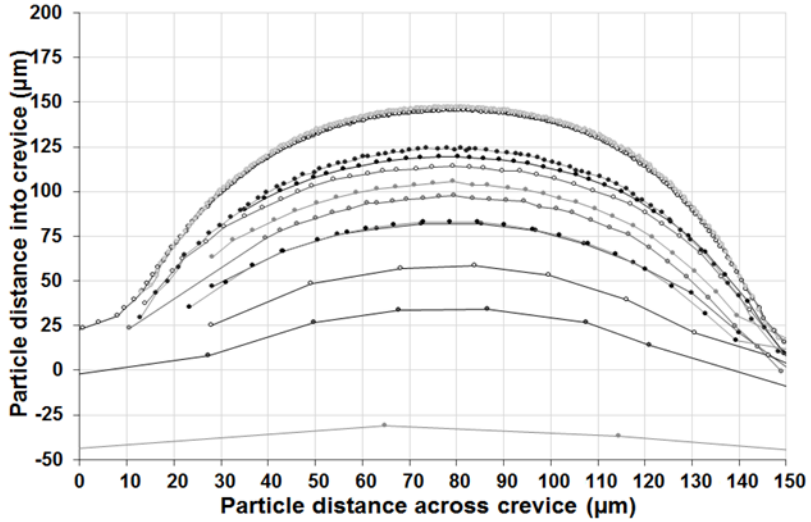

Figure 7.68. Pathlines of platelet-sized particles in 20% GRBC suspension at a 5 µl/min flow rate in Crevice 6.

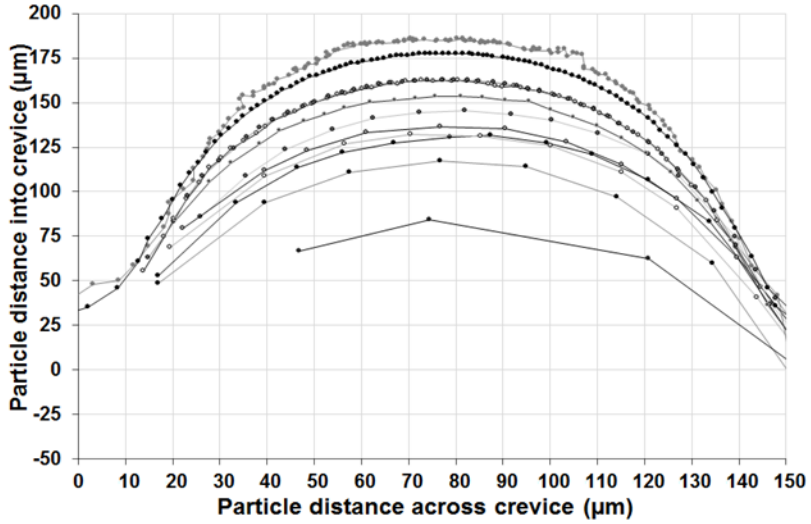

Figure 7.69. Pathlines of platelet-sized particles in 20% GRBC suspension at a 25 µl/min flow rate in Crevice 6.

Figure 7.70 shows a representative analysis of PSFP trafficking in Crevice 6 for the 40% GRBC suspension examined at 5 and 25 µl/min**.** Platelet-sized particle pathlines for the 40% GRBC suspension at 5 and 25 µl/min flow rates are shown in **Figure 7.71** and **Figure 7.72**, respectively. PSFP trafficking in Crevice 6 for the 40% GRBC suspension had apex distances

less than 150 µm for 64% of PSFP studied at both 5 and 25 µl/min (**Figure 7.71** and **Figure 7.72**).

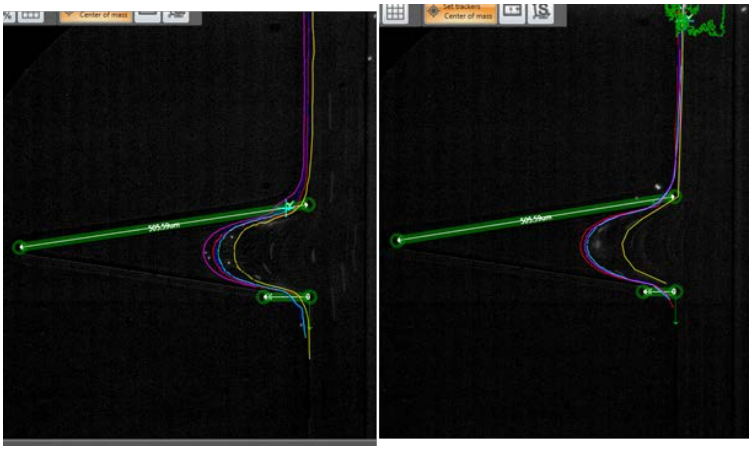

Figure 7.70. Trafficking of five platelet-sized particles in 40% GRBC suspension at 5 µl/min [left] and 25 µl/min [right] flow rates in Crevice 6. 20x magnification. Dimension shown with green line is 505.6 µm. Origin defined at channel entrance.

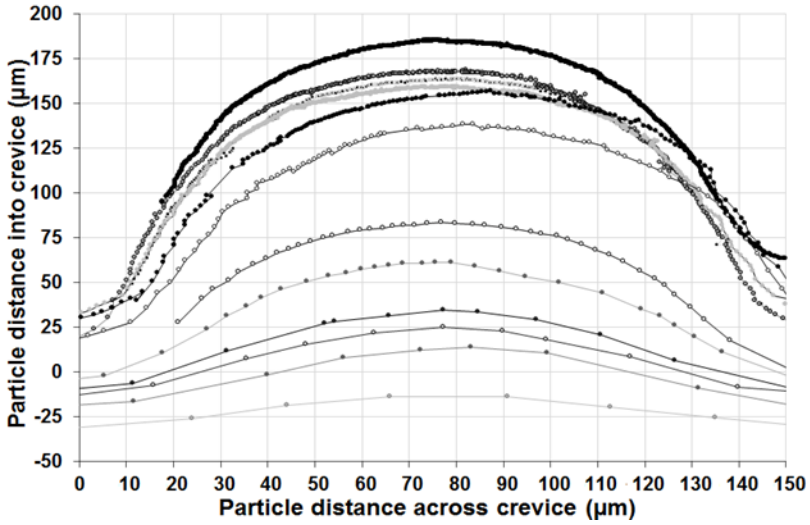

Figure 7.71. Pathlines of platelet-sized particles in 40% GRBC suspension at a 5 µl/min flow rate in Crevice 6.

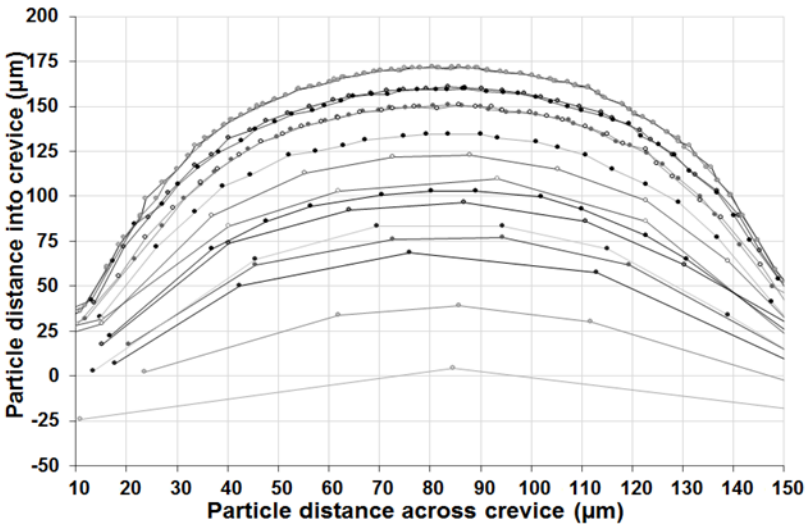

Figure 7.72. Pathlines of platelet-sized particles in 40% GRBC suspension at a 25 µl/min flow rate in Crevice 6.

Figure 7.73 shows a representative analysis of GRBC trafficking in Crevice 6 for the 20% GRBC suspension examined at 5 and 25 µl/min**.** Pathlines of GRBC for the 20% GRBC suspension at 5 and 25 µl/min flow rates are shown in **Figure 7.74** and **Figure 7.75**, respectively. GRBC trafficking in Crevice 6 for the 20% GRBC suspension had apex distances less than 100 µm for 88% of GRBC studied at both 5 and 25 µl/min flow rates (**Figure 7.74** and **Figure 7.75**).

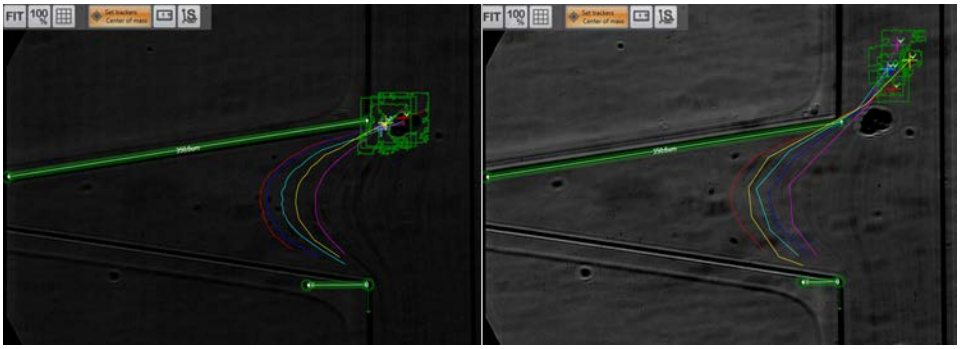

Figure 7.73. Trafficking of five GRBC in 20% GRBC suspension at 5 µl/min [left] and 25 µl/min [right] flow rates in Crevice 6. 40x magnification. Dimension shown with green line is 357.9 µm. Origin defined at channel entrance.

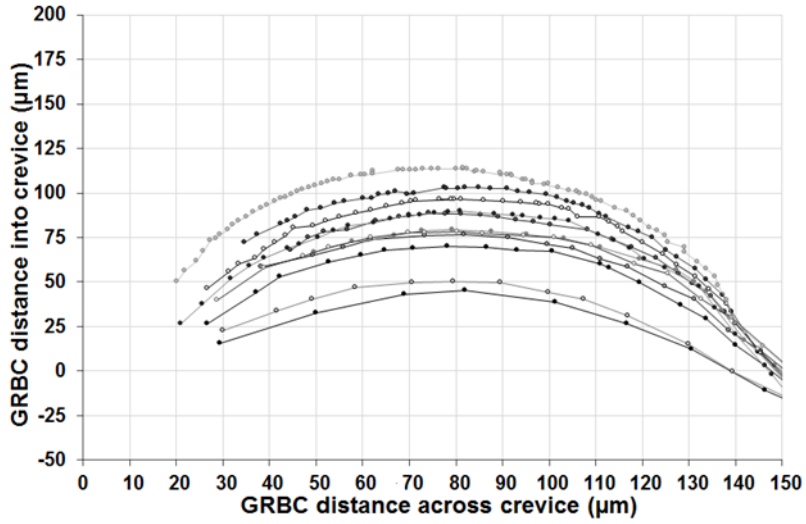

Figure 7.74. Pathlines of GRBC in 20% GRBC suspension at a 5 µl/min flow rate in Crevice 6.

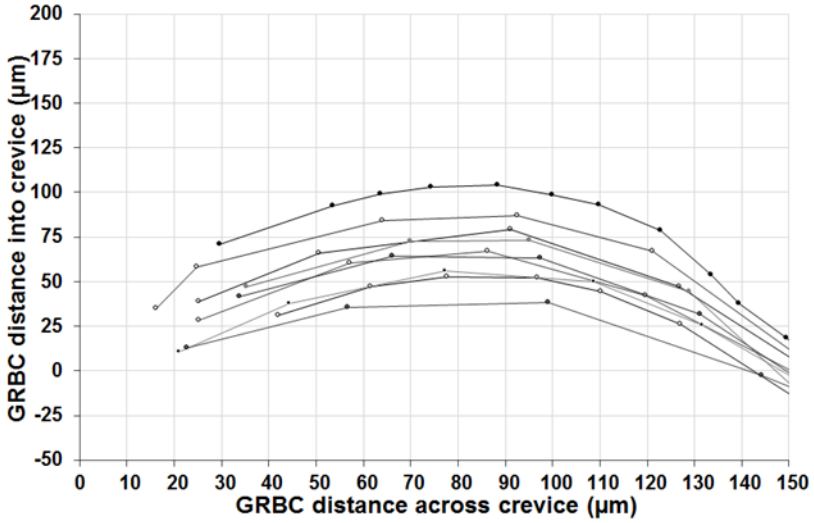

Figure 7.75. Pathlines of GRBC in 20% GRBC suspension at a 25 µl/min flow rate in Crevice 6.

Figure 7.76 shows a representative analysis of GRBC trafficking in Crevice 6 for the 40% GRBC suspension examined at 5 and 25 µl/min**.** Pathlines of GRBC for the 40% GRBC suspension at 5 and 25 µl/min flow rates are shown in **Figure 7.77** and **Figure 7.78**, respectively. GRBC trafficking in Crevice 6 for the 40% GRBC suspension had apex distances

less than 100 µm for 90% of GRBC studied at 5 µl/min (**Figure 7.77**) and 30% of GRBC examined at 25 µl/min (**Figure 7.78**).

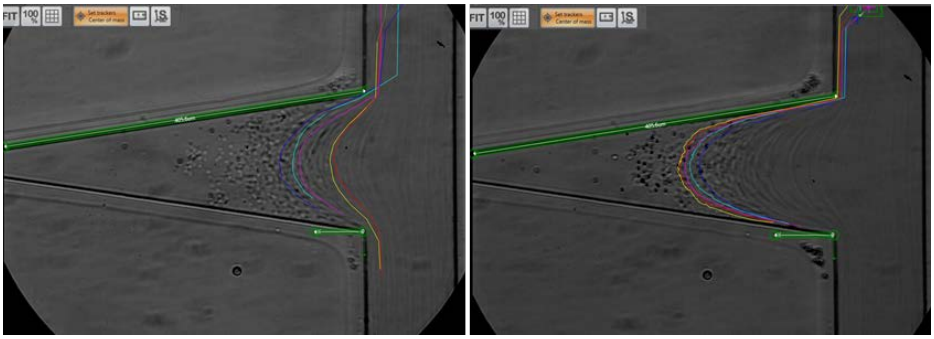

Figure 7.76. Trafficking of five GRBC in 40% GRBC suspension at 5 µl/min [left] and 25 µl/min [right] flow rates in Crevice 6. Dimension shown with green line is 382.4 µm. Origin defined at channel entrance.

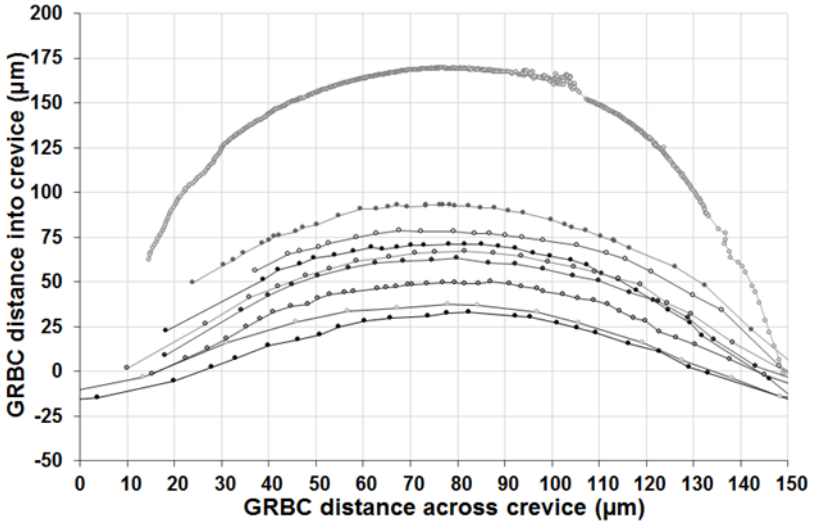

Figure 7.77. Pathlines of GRBC in 40% GRBC suspension at a 5 µl/min flow rate in Crevice 6.

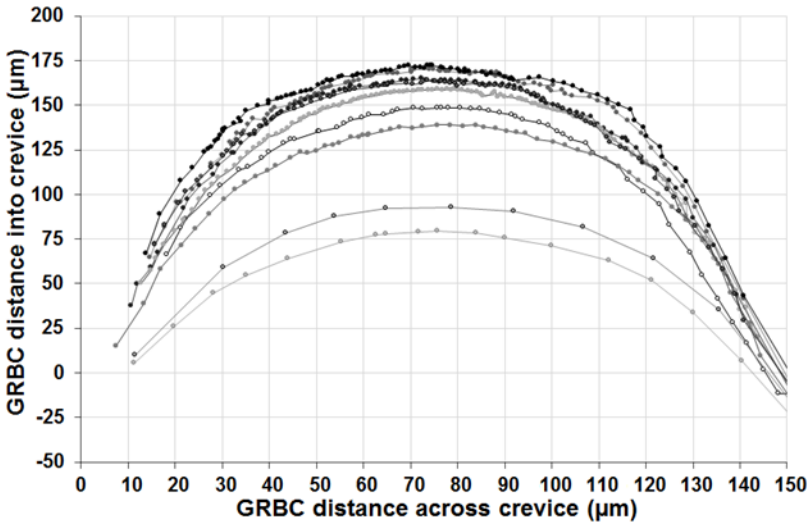

Figure 7.78. Pathlines of GRBC in 40% GRBC suspension at a 25 µl/min flow rate in Crevice 6.

7.3.7 Trafficking of platelet-sized particles and GRBC in a 100 µm wide and 100 µm long square crevice (Crevice 7)

Figure 7.79 shows images of 20% GRBC and ~1,000,000 PSFP/µl in 30% Dextran 40 and 40% GRBC and ~1,000,000 PSFP/µl in 20% Dextran 40 flowing through Crevice 7 at 5 and 25 µl/min. A representative analysis of PSFP trafficking in Crevice 7 for the 20% GRBC suspension examined at 5 and 25 µl/min is shown in **Figure 7.80**. Pathlines of PSFP for the 20% GRBC suspension at 5 and 25 µl/min flow rates are shown in **Figure 7.81** and **Figure 7.82**, respectively. Platelet-sized particle trafficking for the 20% GRBC suspension had apex distances less than 60 µm for 68% of PSFP studied at 5 µl/min (**Figure 7.81**) and 50% of PSFP examined at 25 µl/min (**Figure 7.82**). PSFP pathlines in Crevice 7 for the 20% GRBC suspension did not recirculate at either flow rate.

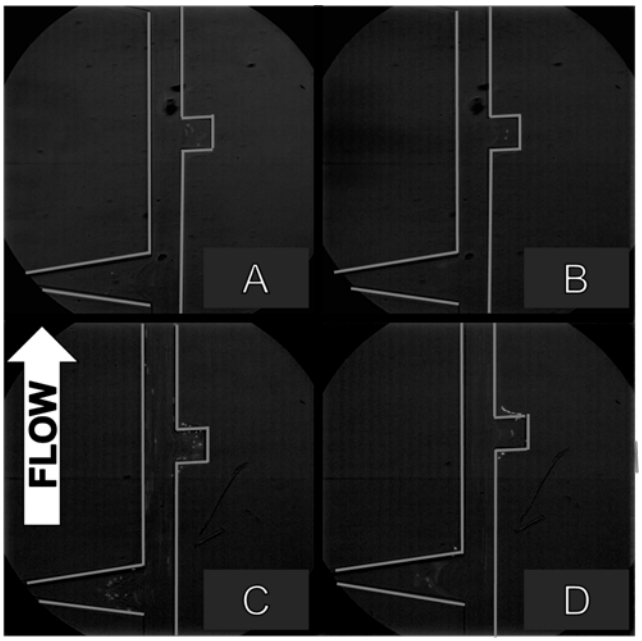

Figure 7.79. Representative fluorescent images of suspensions of 20% GRBC and ~1,000,000 PSFP/µl in 30% Dextran 40 and 40% GRBC and ~1,000,000 PSFP/µl in 20% Dextran 40 examined in Crevice 7 at 5 and 25 µl/min flow rates. Channel height was 75 µm.

[A] 20% GRBC suspension at 5 µl/min, [B] 20% GRBC suspension at 25 µl/min, [C] 40% GRBC suspension at 5 µl/min, [D] 40% GRBC suspension at 25 µl/min. 20x magnification. Field of view in A-D is 1000 µm by 1000 µm.

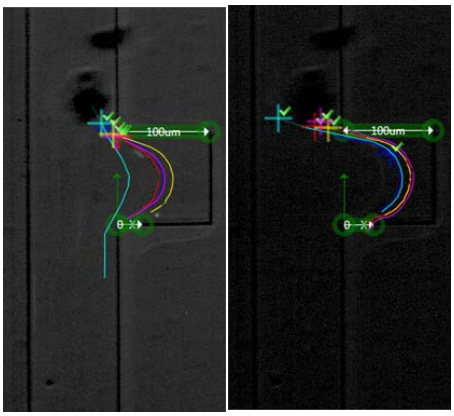

Figure 7.80. Trafficking of five platelet-sized particles in 20% GRBC suspension at 5 µl/min [left] and 25 µl/min [right] flow rates in Crevice 7. 20x magnification. Dimension shown with horizontal green line is 100 µm. Origin defined at channel entrance.

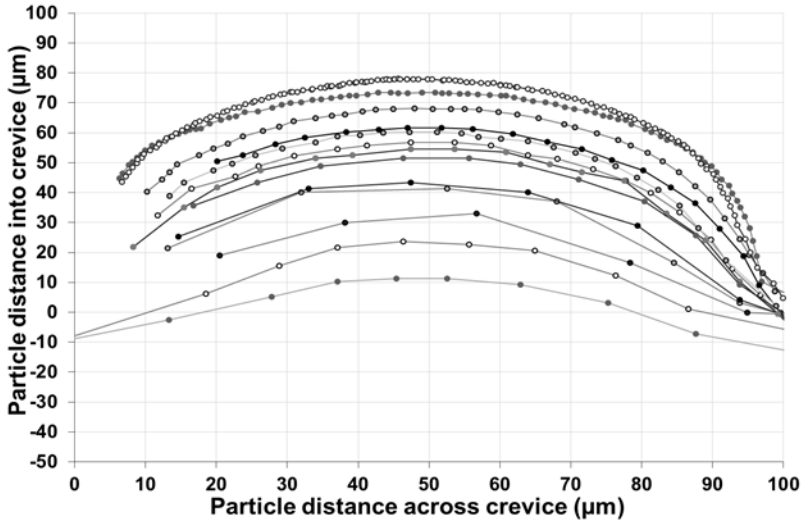

Figure 7.81. Pathlines of platelet-sized particles in 20% GRBC suspension at a 5 µl/min flow rate in Crevice 7.

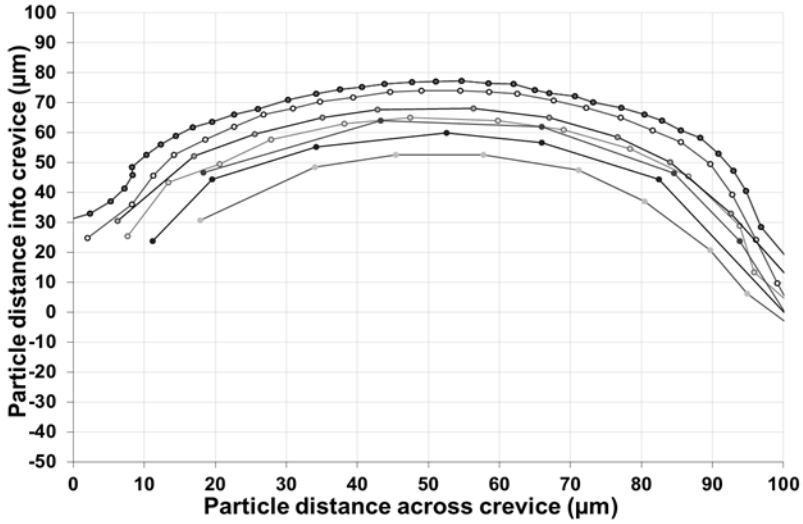

Figure 7.82. Pathlines of platelet-sized particles in 20% GRBC suspension at a 25 µl/min flow rate in Crevice 7.

Figure 7.83 shows a representative analysis of PSFP trafficking in Crevice 7 for the 40% GRBC suspension examined at 5 and 25 µl/min. Pathlines of PSFP for the 40% GRBC suspension at 5 and 25 µl/min flow rates are shown in **Figure 7.84** and **Figure 7.85**, respectively. Platelet-sized particle trafficking in Crevice 7 for the 40% GRBC suspension at 5 and 25 µl/min flow rates identified a recirculating region beginning between 78-85 µm. Seven

PSFP pathlines that had greater than 78 µm apex distance recirculated 2-10 times before PSFP adhesion to the crevice wall near the outlet (**Figure 7.84** and **Figure 7.85**). Trafficking of non-recirculating PSFP in Crevice 7 for the 40% GRBC suspension had apex distances less than 60 µm for 43% of PSFP studied at 5 µl/min (**Figure 7.84**) and 44% of PSFP examined at 25 µl/min (**Figure 7.85**).

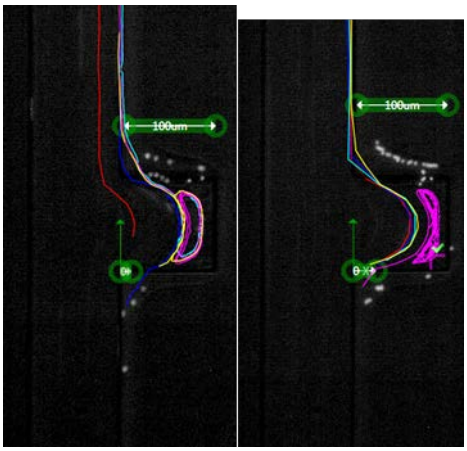

Figure 7.83. Trafficking of five platelet-sized particles in 40% GRBC suspension at 5 µl/min [left] and 25 µl/min [right] flow rates in Crevice 7. 20x magnification. Dimension shown with horizontal green line is 100 µm. Origin defined at channel entrance.

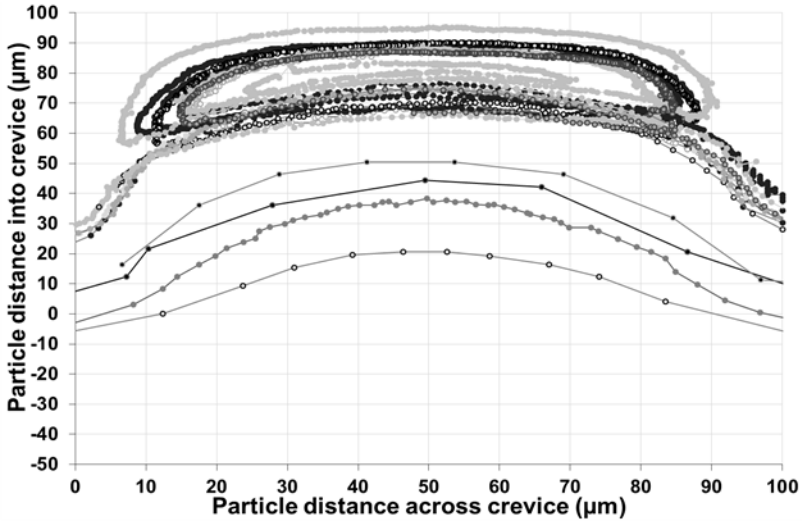

Figure 7.84. Pathlines of platelet-sized particles in 40% GRBC suspension at a 5 µl/min flow rate in Crevice 7.

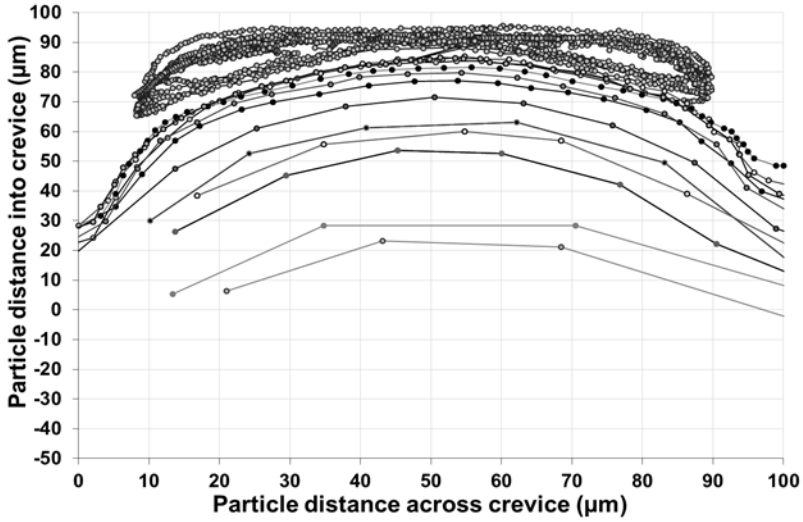

Figure 7.85. Pathlines of platelet-sized particles in 40% GRBC suspension at a 25 µl/min flow rate in Crevice 7.

Figure 7.86 shows a representative analysis of GRBC trafficking in Crevice 7 for the 20% GRBC suspension examined at 5 and 25 µl/min. Pathlines of GRBC for the 20% GRBC suspension at 5 and 25 µl/min flow rates are shown in **Figure 7.87** and **Figure 7.88**, respectively. GRBC trafficking in Crevice 7 for the 20% GRBC suspension had apex distances less than 60 µm for all GRBC studied at 5 µl/min (**Figure 7.87**) and 84% of GRBC examined at 25 µl/min (**Figure 7.88**); GRBC pathlines did not recirculate at either flow rate.

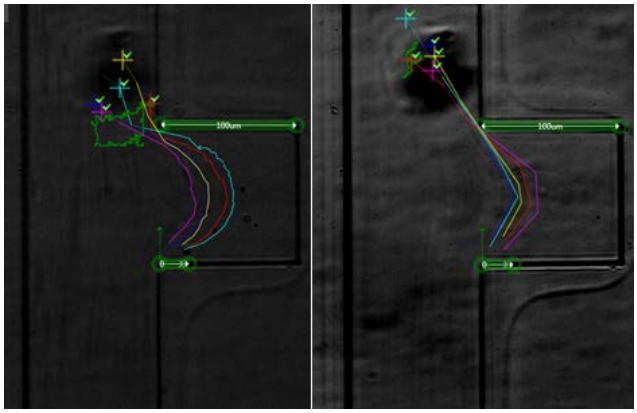

Figure 7.86. Trafficking of five GRBC in 20% GRBC suspension at 5 µl/min [left] and 25 µl/min [right] flow rates in Crevice 7. 40x magnification. Dimension shown with horizontal green line is 100 µm. Origin defined at channel entrance.

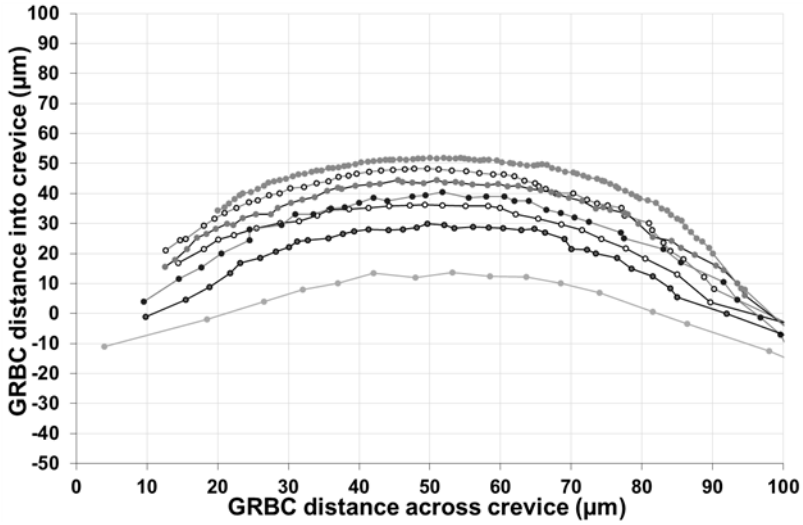

Figure 7.87. Pathlines of GRBC in 20% GRBC suspension at a 5 µl/min flow rate in Crevice 7.

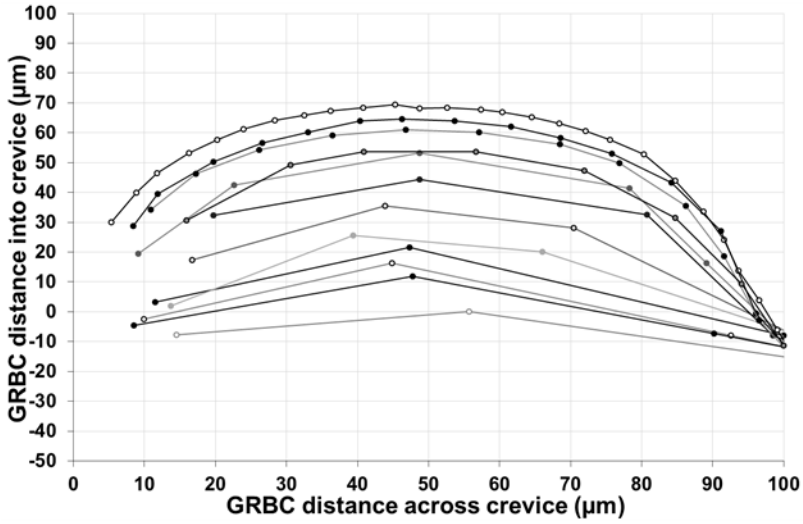

Figure 7.88. Pathlines of GRBC in 20% GRBC suspension at a 25 µl/min flow rate in Crevice 7.

Figure 7.89 shows a representative analysis of GRBC trafficking in Crevice 7 for the 40% GRBC suspension examined at 5 and 25 µl/min. Pathlines of GRBC for the 40% GRBC suspension at 5 and 25 µl/min flow rates are shown in **Figure 7.90** and **Figure 7.91**, respectively. GRBC trafficking in Crevice 7 for the 40% GRBC suspension had apex distances less than 60 µm for 60% of GRBC studied at 5 µl/min (**Figure 7.90**) and 20% of GRBC examined at 25 µl/min (**Figure 7.91**); GRBC pathlines did not recirculate at either flow rate.

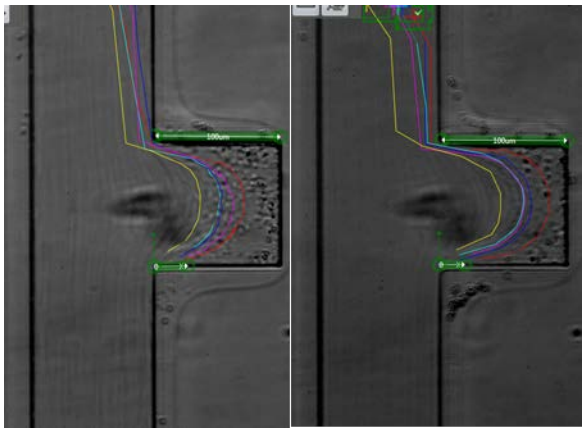

Figure 7.89. Trafficking of five GRBC in 40% GRBC suspension at 5 µl/min [left] and 25 µl/min [right] flow rates in Crevice 7. 40x magnification. Dimension shown with horizontal green line is 100 µm. Origin defined at channel entrance.

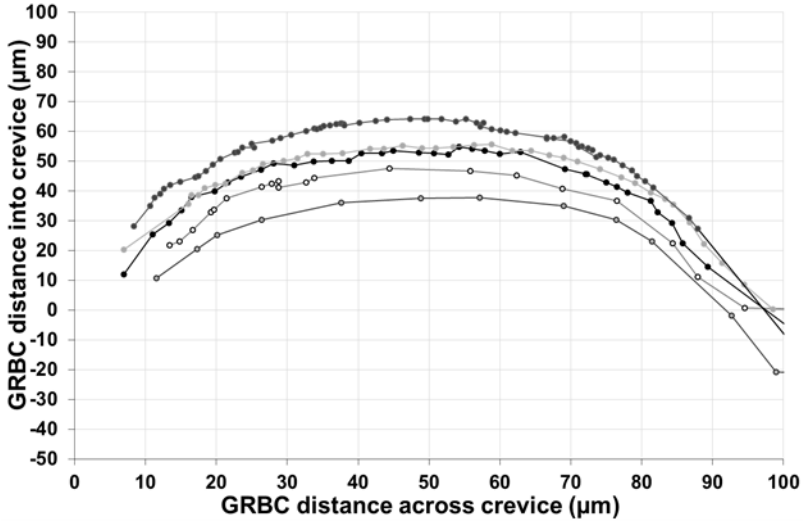

Figure 7.90. Pathlines of GRBC in 40% GRBC suspension at a 5 µl/min flow rate in Crevice 7.

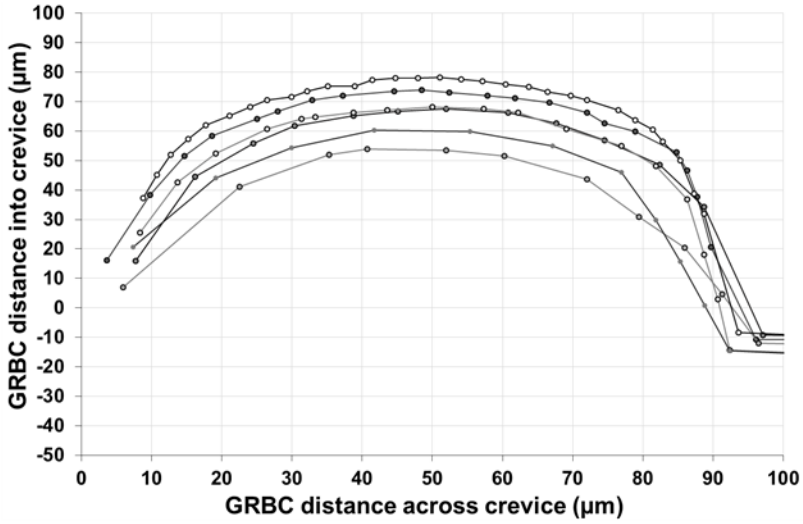

Figure 7.91. Pathlines of GRBC in 40% GRBC suspension at a 25 µl/min flow rate in Crevice 7.

7.3.8 Trafficking of platelet-sized particles and GRBC in a 100 µm height and 250 µm base triangular crevice (Crevice 8)

Figure 7.92 shows images of 20% GRBC and ~1,000,000 PSFP/µl in 30% Dextran 40 and 40% GRBC and ~1,000,000 PSFP/µl in 20% Dextran 40 flowing through Crevice 8 at 5 and 25 µl/min. A representative analysis of PSFP trafficking for the 20% GRBC suspension is shown at both flow rates in **Figure 7.93**. PSFP pathlines in Crevice 8 for the 20% GRBC suspension examined at 5 and 25 µl/min are shown in **Figure 7.94** and **Figure 7.95**, respectively. Platelet-sized particle trafficking in Crevice 8 for the 20% GRBC suspension had apex distances less than 60 µm for 85% of PSFP studied at 5 µl/min (**Figure 7.94**) and 64% of PSFP examined at 25 µl/min (**Figure 7.95**).

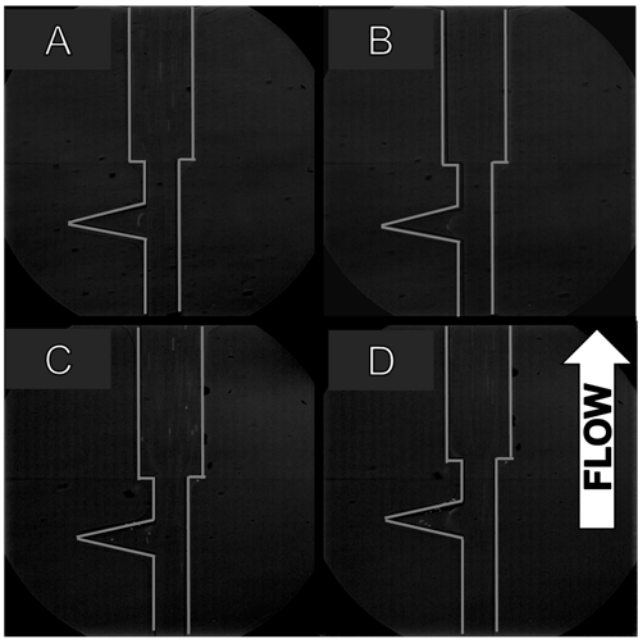

Figure 7.92. Representative fluorescent images of suspensions of 20% GRBC and ~1,000,000 PSFP/µl in 30% Dextran 40 and 40% GRBC and ~1,000,000 PSFP/µl in 20% Dextran 40 examined in Crevice 8 at 5 and 25 µl/min flow rates. Channel height was 75 µm.

[A] 20% GRBC suspension at 5 µl/min, [B] 20% GRBC suspension at 25 µl/min, [C] 40% GRBC suspension at 5 µl/min, [D] 40% GRBC suspension at 25 µl/min. 20x magnification. Field of view in A-D is 1000 µm by 1000 µm.

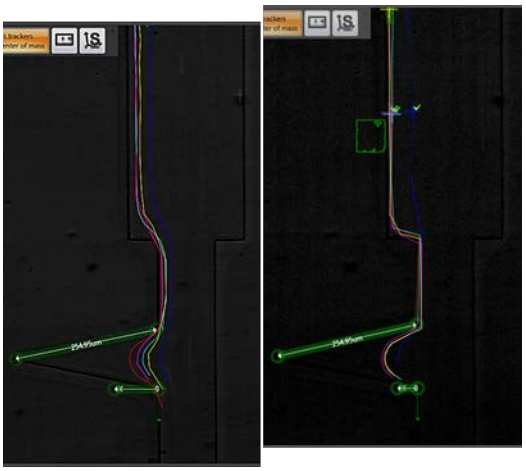

Figure 7.93. Trafficking of five platelet-sized particles in 20% GRBC suspension at 5 µl/min [left] and 25 µl/min [right] flow rates in Crevice 8. 20x magnification. Dimension shown with green line is 254.95 µm. Origin defined at channel entrance.

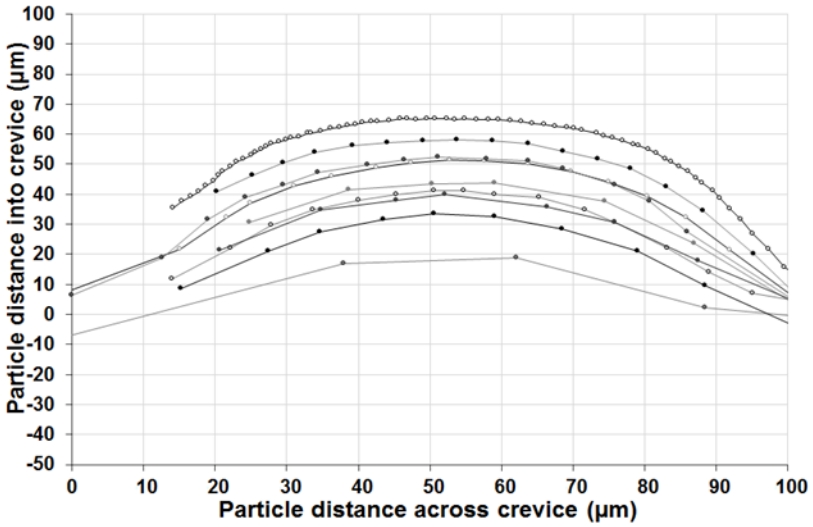

Figure 7.94. Pathlines of platelet-sized particles in 20% GRBC suspension at a 5 µl/min flow rate in Crevice 8.

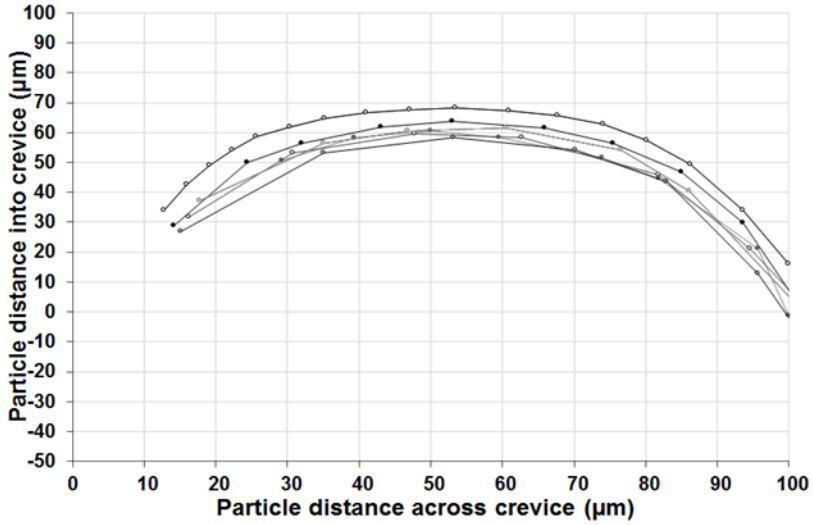

Figure 7.95. Pathlines of platelet-sized particles in 20% GRBC suspension at a 25 µl/min flow rate in Crevice 8.

Figure 7.96 shows a representative analysis of PSFP trafficking in Crevice 8 for the 40% GRBC suspension examined at 5 and 25 µl/min. Pathlines of PSFP for the 40% GRBC suspension at 5 and 25 µl/min flow rates are shown in **Figure 7.97** and **Figure 7.98**, respectively. Platelet-sized particle trafficking in Crevice 8 for the 40% GRBC suspension had

apex distances less than 60 µm for 92% of PSFP studied at 5 µl/min (**Figure 7.97**) and 60% of PSFP examined at 25 µl/min (**Figure 7.98**).

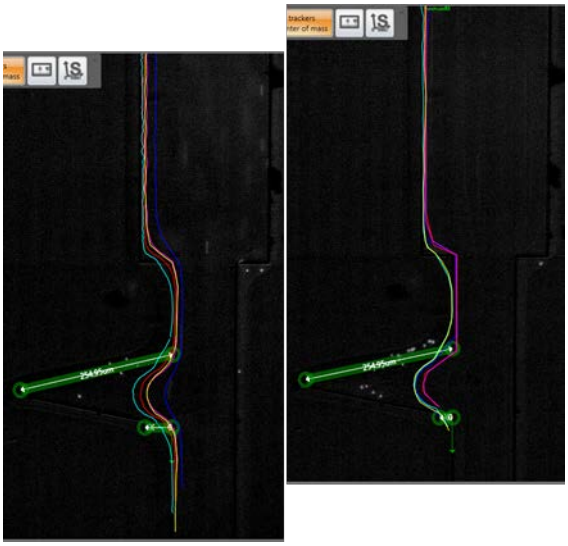

Figure 7.96. Trafficking of five platelet-sized particles in 40% GRBC suspension at 5 µl/min [left] and 25 µl/min [right] flow rates in Crevice 8. 20x magnification. Dimension shown with green line is 254.95 µm. Origin defined at channel entrance.

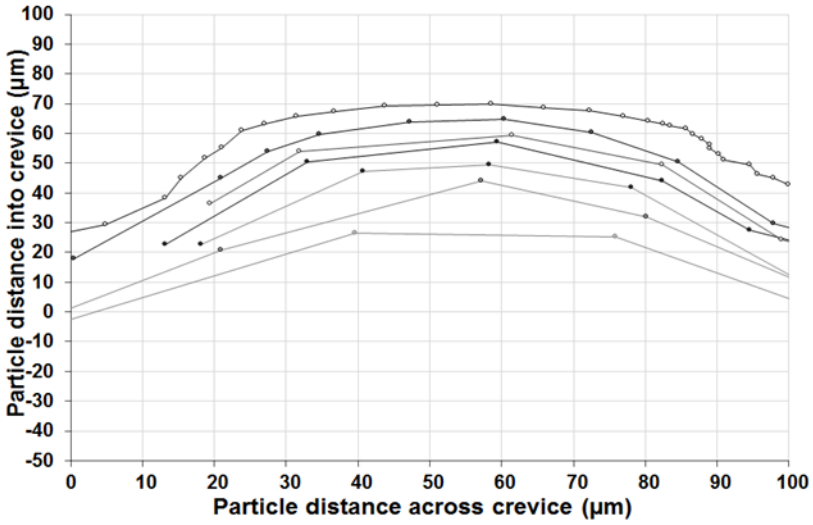

Figure 7.97. Pathlines of platelet-sized particles in 40% GRBC suspension at a 5 µl/min flow rate in Crevice 8.

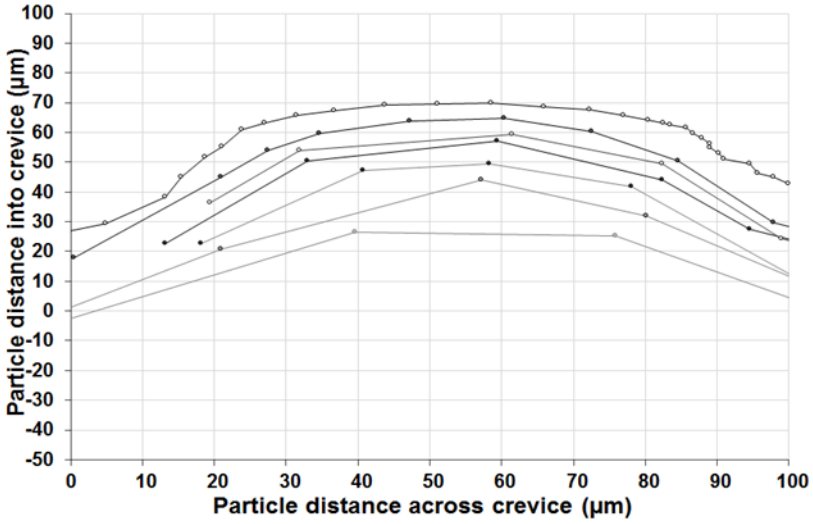

Figure 7.98. Pathlines of platelet-sized particles in 40% GRBC suspension at a 25 µl/min flow rate in Crevice 8.

Figure 7.99 shows a representative analysis of GRBC trafficking in Crevice 8 for the 20% GRBC suspension examined at 5 and 25 µl/min. Pathlines of GRBC for the 20% GRBC suspension at 5 and 25 µl/min flow rates are shown in **Figure 7.100** and **Figure 7.101**, respectively. GRBC trafficking in Crevice 8 for the 20% GRBC suspension had apex distances less than 60 µm for all GRBC studied at 5 µl/min (**Figure 7.100**) and 96% of GRBC examined at 25 µl/min (**Figure 7.101**).

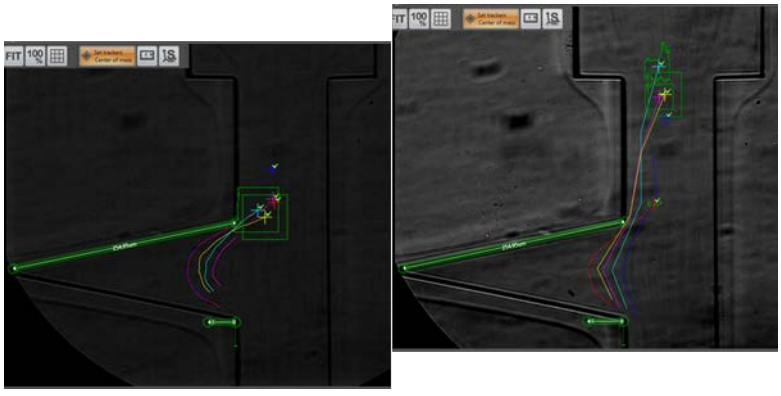

Figure 7.99. Trafficking of five GRBC in 20% GRBC suspension at 5 µl/min [left] and 25 µl/min [right] flow rates in Crevice 8. 40x magnification. Dimension shown with green line is 254.95 µm. Origin defined at channel entrance.

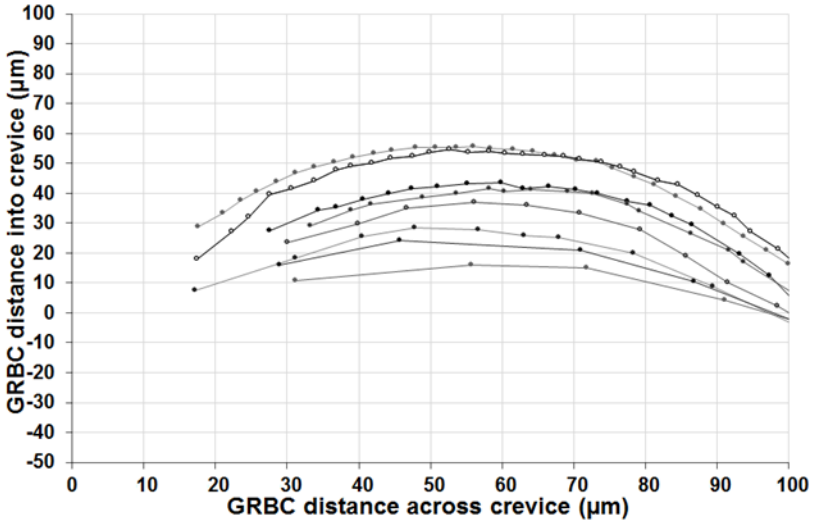

Figure 7.100. Pathlines of GRBC in 20% GRBC suspension at a 5 µl/min flow rate in Crevice 8.

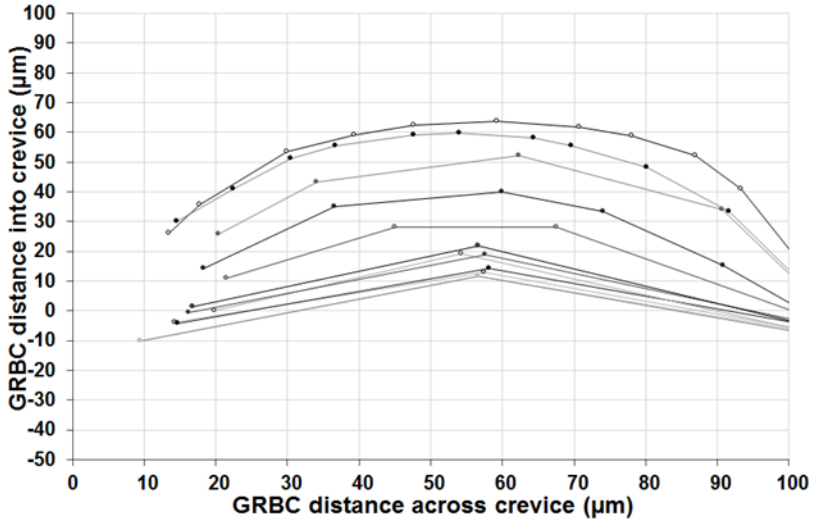

Figure 7.101. GRBC pathlines in 20% GRBC suspension at a 25 µl/min flow rate in Crevice 8.

Figure 7.102 shows a representative analysis of GRBC trafficking in Crevice 8 for the 40% GRBC suspension examined at 5 and 25 µl/min. Pathlines of GRBC for the 40% GRBC suspension at 5 and 25 µl/min flow rates are shown in **Figure 7.103** and **Figure 7.104**, respectively. GRBC trafficking in Crevice 8 for 40% GRBC suspension studied at 5 µl/min identified a recirculating region beginning between 75-80 µm. Two GRBC pathlines that had

greater than 75 µm apex distance recirculated 1-3 times before GRBC crevice exit (**Figure 7.103**). Trafficking of non-recirculating GRBC in Crevice 8 for the 40% GRBC suspension had apex distances less than 60 µm for 70% of GRBC studied at 5 µl/min (**Figure 7.103**) and 50% of GRBC examined at 25 µl/min (**Figure 7.104**).

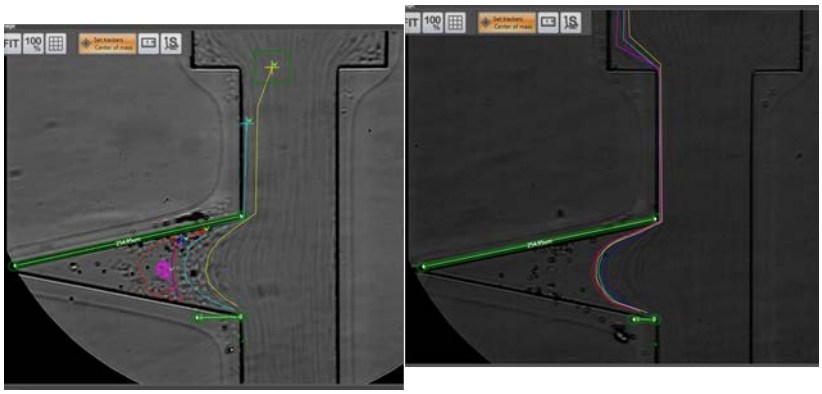

Figure 7.102. Trafficking of five GRBC in 40% GRBC suspension at 5 µl/min [left] and 25 µl/min [right] flow rates in Crevice 8. 40x magnification. Dimension shown with green line is 254.95 µm. Origin defined at channel entrance.

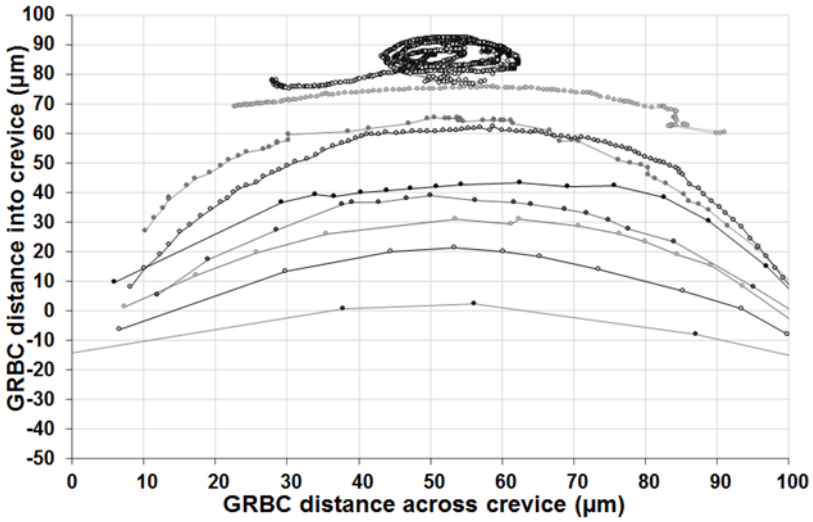

Figure 7.103. GRBC pathlines in 40% GRBC suspension at a 5 µl/min flow rate in Crevice 8.

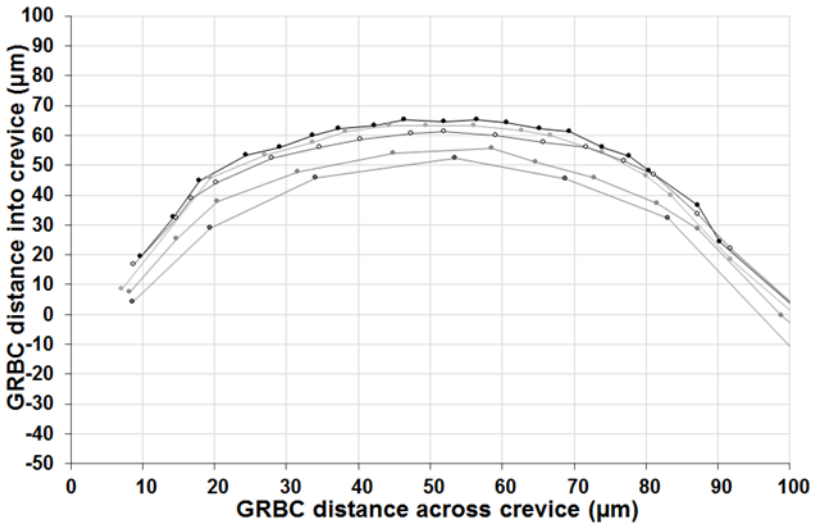

Figure 7.104. GRBC pathlines in 40% GRBC suspension at a 25 µl/min flow rate in Crevice 8.

7.3.9 Platelet-sized particle counts in the crevice microchannel

PSFP counts in Crevices 1-8 for the 20% GRBC and 40% GRBC suspensions examined at 0, 5 and 25 µl/min are shown in **Table 7.1**. Statistical analysis revealed a significant difference ($p<0.05$) between the mean PSFP counts in Crevices 1-8 at 0, 5 and 25 µl/min flow rates for both GRBC concentrations, with one exception of the PSFP count in Crevice 2 for the 20% GRBC suspension between 5 and 25 µl/min flow rates ($p=0.25$).

Table 7.1 shows that platelet-sized particle counts in Crevices 3-7 for the 20% GRBC suspension significantly increased when flow rate increased from 0 to 5 µl/min ($p<0.001$) and 5 µl/min to 25 µl/min ($p<0.005$). In Crevice 2, PSFP count for the 20% GRBC suspension significantly increased from 0 to 5 µl/min ($p<0.001$) and 0 to 25 µl/min ($p=0.02$). In Crevices 1 and 8, PSFP counts for the 20% GRBC suspension significantly decreased when flow rate increased from 0 to 5 µl/min and 5 µl/min to 25 µl/min ($p<0.001$).

Platelet-sized particle counts in Crevices 1, 2, 4, 5, 7 and 8 for the 40% GRBC suspension significantly increased when flow rate increased from 0 to 5 µl/min and 5 µl/min to 25 µl/min ($p<0.001$) (**Table 7.1**). In Crevices 3 and 6, PSFP counts for the 40% RBC suspension significantly increased from 0 to 5 µl/min ($p<0.001$) and significantly decreased when flow rate increased from 5 µl/min to 25 µl/min ($p<0.001$).

Analysis of the PSFP counts in Crevices 1-8 at flow rates of 0, 5 and 25 µl/min revealed significant differences between the PSFP counts of the 20% and 40% GRBC suspensions in the eight crevices at each flow rate ($p<0.001$), except for the PSFP counts of the 20% and 40% GRBC suspensions examined in Crevice 4 at zero flow ($p=0.49$) and 5 µl/min ($p=0.11$), Crevice 6 at 25 µl/min ($p=0.09$) and Crevice 8 at zero flow ($p=0.19$).

Table 7.1. Platelet-sized particle counts in the crevice microchannel for suspensions of 20% GRBC and ~1,000,000 PSFP/µl in 30% Dextran 40 and 40% GRBC and ~1,000,000 PSFP/µl in 20% Dextran 40 tested at 0, 5 and 25 µl/min flow rates.

	GRBC concentration	Flow rate (µl/min)	Mean PSFP count	SD PSFP count	N	0 vs. 5 µl/min *p* value	0 vs. 25 µl/min *p*-value	5 vs. 25 µl/min *p*-value
Crevice 1	20%	0	270	26	50	$p<0.001$	$p<0.001$	$p<0.001$
		5	167	28	53			
		25	138	29	53			
	40%	0	177	17	50	$p<0.001$	$p<0.001$	$p<0.001$
		5	244	44	50			
		25	433	53	50			
Crevice 2	20%	0	25	5	50	$p<0.001$	$p=0.02$	$p=0.25$
		5	38	19	49			
		25	33	17	50			
	40%	0	65	13	55	$p<0.001$	$p<0.001$	$p<0.001$
		5	103	9	50			
		25	138	24	50			
Crevice 3	20%	0	35	6	50	$p<0.001$	$p<0.001$	$p<0.001$
		5	87	19	50			
		25	132	21	50			
	40%	0	291	39	50	$p<0.001$	$p<0.001$	$p<0.001$
		5	352	32	50			
		25	191	17	51			
Crevice 4	20%	0	30	8	50	$p<0.001$	$p<0.001$	$p<0.001$
		5	45	7	50			
		25	61	11	51			
	40%	0	31	11	52	$p<0.001$	$p<0.001$	$p<0.001$
		5	43	6	46			
		25	66	8	50			
Crevice 5	20%	0	17	3	50	$p<0.001$	$p<0.001$	$p<0.001$
		5	32	13	51			
		25	71	11	50			
	40%	0	53	17	50	$p<0.001$	$p<0.001$	$p<0.001$
		5	81	9	50			
		25	107	7	51			
Crevice 6	20%	0	12	3	50	$p<0.001$	$p<0.001$	$p=0.003$
		5	27	4	50			
		25	37	21	50			
	40%	0	29	10	52	$p<0.001$	$p<0.001$	$p<0.001$
		5	70	8	50			
		25	43	7	50			
Crevice 7	20%	0	5	2	50	$p<0.001$	$p<0.001$	$p<0.001$
		5	7	2	50			
		25	21	9	54			
	40%	0	17	4	50	$p<0.001$	$p<0.001$	$p<0.001$
		5	38	4	53			
		25	42	5	51			
Crevice 8	20%	0	12	7	50	$p<0.001$	$p<0.001$	$p<0.001$
		5	6	2	50			
		25	3	1	50			
	40%	0	11	2	50	$p<0.001$	$p<0.001$	$p<0.001$
		5	17	4	50			
		25	27	3	51			

7.3.10 Comparison of platelet-sized particle and GRBC trafficking in the crevice microchannel

Platelet-sized particle and GRBC trafficking in Crevices 1-8 for the 20% and 40% GRBC suspensions were compared by computing the percent increase in PSFP and GRBC pathline apices from 5 to 25 µl/min. An apex distance threshold for the comparison of PSFP and GRBC trafficking in each crevice was established prior to calculation of the percent increase of PSFP and GRBC apex distance from 5 to 25 µl/min for both GRBC suspensions (**Table 7.2**).

Table 7.2. Percent increase of platelet-sized particle and GRBC apex distance in the crevice microchannel for a five-fold flow rate increase of suspensions of 20% GRBC and ~1,000,000 PSFP/µl in 30% Dextran 40 and 40% GRBC and ~1,000,000 PSFP/µl in 20% Dextran 40.

	GRBC concentration	Apex distances into crevice (µm)	Percent increase in PSFP apices 5 to 25 µl/min	Percent increase in GRBC apices 5 to 25 µl/min
Crevice 1	20%	>400	43	20
	40%		11	-
Crevice 2	20%	>200	-22	4
	40%		54	20
Crevice 3	20%	>400	21	-
	40%		45	2
Crevice 4	20%	>200	48	28
	40%		20	60
Crevice 5	20%	>60	51	-
	40%		35	40
Crevice 5	20%	>75	-1	-
	40%		8	-
Crevice 6	20%	>150	24	-
	40%		-	40
Crevice 7	20%	>60	18	16
	40%		-1	40
Crevice 7	20%	>78	-	-
	40%		-2	-
Crevice 8	20%	>60	21	4
	40%		32	20
Crevice 8	20%	>75	-	-
	40%		-	-10

Platelet-sized particle and GRBC trafficking in Crevices 1-8 for the 20% versus 40% GRBC suspensions were compared by computing the percent increase in PSFP and GRBC pathline apices at 5 and 25 µl/min flow rates. An apex distance threshold for the comparison of PSFP and GRBC trafficking for 20% versus 40% GRBC suspensions in each crevice was established prior to calculation of the percent increase of PSFP and GRBC apex distance examined at 5 and 25 µl/min flow rates (**Table 7.3**).

Table 7.3. Percent increase of platelet-sized particle and GRBC apex distance in the crevice microchannel for 20% GRBC and ~1,000,000 PSFP/µl in 30% Dextran 40 versus 40% GRBC and ~1,000,000 PSFP/µl in 20% Dextran 40 suspensions tested at 5 and 25 µl/min flow rates.

	Flow rate (µl/min)	Apex distances into crevice (µm)	Percent increase in PSFP apices 20% GRBC to 40% GRBC suspensions	Percent increase in GRBC apices 20% GRBC to 40% GRBC suspensions
Crevice 1	5	>400	29	-
	25		-3	-
Crevice 2	5	>200	-35	30
	25		41	46
Crevice 3	5	>400	4	10
	25		28	12
Crevice 4	5	>200	7	30
	25		-21	62
Crevice 5	5	>60	-	-
	25		-16	40
Crevice 5	5	>75	39	-
	25		48	-
Crevice 6	5	>150	36	10
	25		12	50
Crevice 7	5	>60	25	40
	25		7	64
Crevice 7	5	>78	22	-
	25		20	-
Crevice 8	5	>60	-7	30
	25		4	46
Crevice 8	5	>75	-	10
	25		-	-

7.4 DISCUSSION

Microscopic crevices or steps are unavoidable features within CAD blood flow path that are potentially thrombogenic areas due to flow separation, recirculation zones (deadwaters) and flow stagnation [143, 157-160, 232]. The objective of this study was to examine the thrombogenicity of microscopic crevice flow by studying the trafficking of erythrocyte ghosts and platelet-sized particles in a microchannel containing multiple crevices similar to the size of small gaps in some CAD at supra-physiological shear stresses.

The results of this study showed that platelet-sized particle concentration inside the crevices was augmented by flow rate and GRBC trafficking. Platelet-sized particle counts in Crevices 1-8 were significantly different between 5 and 25 µl/min flow rates for both GRBC concentrations ($p<0.05$), except for the 20% GRBC suspension counts in Crevice 2 ($p=0.25$). The effect of GRBC concentration on platelet-sized particle concentration in the crevices demonstrated significant differences between PSFP counts in Crevices 1-8 at 5 and 25 µl/min flow rates for both GRBC suspensions ($p<0.001$), except for the PSFP counts of 20% and 40% GRBC suspensions in Crevice 4 at 5 µl/min ($p=0.11$) and Crevice 6 at 25 µl/min ($p=0.09$).

Trafficking of platelet-sized particles in rectangular and triangular crevices with 500 µm or less length demonstrated augmented apex distances for 20% GRBC suspension when flow rate increased from 5 µl/min to 25 µl/min. For the 40% GRBC suspension, PSFP trafficking in all crevices demonstrated greater PSFP apex distances or negligible changes in PSFP pathline apices when flow rate increased from 5 µl/min to 25 µl/min.

Overall, platelet-sized particle trafficking in the crevices was augmented by GRBC concentration. A comparison of PSFP trafficking in eight crevices for the 20% and 40% GRBC

suspensions examined at 25 µl/min demonstrated a negligible change in PSFP apex distances in Crevice 1, augmented PSFP apex distances in Crevices 2, 3, 5-8 and a decrease in PSFP pathline apices in Crevice 4 for 40% GRBC suspensions.

Flow rate had much less influence on GRBC trafficking in the crevices compared to GRBC concentration. Trafficking of GRBC in the crevice microchannel for 20% GRBC suspension demonstrated negligible changes in GRBC pathlines (Crevices 2, 3, 5, 6 and 8) or augmented GRBC apex distances (Crevices 1, 4 and 7) when flow rate increased from 5 µl/min to 25 µl/min. For the 40% GRBC suspension, negligible changes in GRBC apex distance were observed in Crevices 1 and 3, increased GRBC pathline apices were found in Crevices 2 and 4-8, and a decrease in GRBC apex distance in Crevice 8 above 75 µm occurred when flow rate increased from 5 µl/min to 25 µl/min. GRBC trafficking in Crevices 2-8 for the 20% and 40% GRBC suspensions examined at 25 µl/min demonstrated augmented GRBC apex distances in all crevices studied.

An important finding of this study was the occurrence of flow separation in 100 µm wide crevices. A separated flow is a region in which streamlines form closed areas and fluid elements follow closed paths until diffusion occurs [232]. Flow recirculation is known to contribute to thrombogenesis as shown in *in vitro* studies of bifurcations, bends and expansions [157, 159, 233]. Recirculation regions were observed in a 100 µm wide and 500 µm long rectangular crevice (Crevice 5), a 100 µm square crevice (Crevice 7) and a 100 µm height triangular crevice (Crevice 8) starting at approximately 75-85 µm in the crevices. Trafficking of PSFP and GRBC in Crevices 5 and 8 with greater than 75 µm apex distance had recirculating pathlines while in Crevice 7, PSFP with greater than 78 µm apex distance had recirculating pathlines. Platelet-sized

particle and GRBC pathlines with less than 75 μm apex distance in the 100 μm width crevices did not recirculate.

The novel result of this study is the discovery of the effect of crevice width on thrombosis development at supra-physiological shear stresses relevant to the operation of CADs. Flow separation occurred for GRBC suspensions studied in 100 μm wide rectangular and triangular crevices but not in wider crevices studied up to 500 μm. Crevices 5, 7 and 8 are each 100 μm wide and have rectangular, square, and triangular geometries. Although Crevices 1, 3 and 5 have the same crevice length, recirculation regions were not observed in Crevices 1 or 3 that have larger entrance widths. The presence of recirculation regions in 100 μm wide crevices in this study demonstrated that the width of gaps and crevices in CAD blood flow paths is an important parameter for thrombogenesis at supra-physiological shear stresses encountered during *in vitro* and *in vivo* CAD operation.

7.5 CONCLUSIONS

This chapter summarizes the microscopic visualization and analysis of the trafficking of erythrocyte ghosts and platelet-sized particles in a custom-fabricated microchannel containing multiple crevices similar to the size of small gaps within CAD at supra-physiological shear stresses. The results of this study showed that platelet-sized particle concentration and PSFP trafficking inside the crevices were augmented by flow rate and GRBC concentration; flow rate had much less influence on GRBC trafficking in the crevices compared to GRBC concentration. A novel finding was the importance of the width of gaps and crevices in CAD blood flow paths

for thrombosis development at supra-physiological shear stresses encountered during *in vitro* and *in vivo* CAD operation. Recirculation regions were observed in 100 μm wide rectangular and triangular crevices but not in wider crevices studied up to 500 μm. The width of gaps and crevices in the blood flow path of CAD is an important variable to include in the modeling of thrombosis in the assisted circulation and warrants further study *in vitro*.

8.0 SUMMARY

8.1 CONCLUSIONS

The goals of this dissertation were to study *in vitro* the mechanisms of flow-induced blood trauma and the parameters that affect *in vitro* hemolysis testing of circulatory-assist devices. The specific aims of this study were as follows: to model flow-induced hemolysis using solutions of degradable polymers as a rheological substitute for blood, to study adverse changes in the rheological properties of donor RBC during blood bank storage, to study flow-induced hemolysis as a function of shear stress and exposure time, and to study potential mechanisms of flow-induced hemolysis and thrombosis.

A drag-reducing polymer solution of ~4000 kDa MW polyethylene oxide at a concentration of 1 mg/ml in a turbulent flow circulating system was shown to be a novel blood substitute for the *in vitro* assessment of potential mechanical blood damage in a tested CAD. DRP mechanical degradation was successfully characterized by recording the decrease in DRP solution flow rate at a constant pressure and measurements of polymer solution viscosity in samples collected from the flow system during testing. A novel polymer degradation index was found to be highly correlated to the normalized index of hemolysis in these studies. Hence, the use of a PEO solution as a test fluid for the *in vitro* testing of CAD and calculation of the PDI

yields an innovative, useful substitute to blood and a similar damage index as the NIH traditionally used for evaluation and comparison of CAD.

The effects of donor gender and storage time on bulk RBC deformability (RBC suspension viscoelasticity and relaxation time) of leukoreduced RBC stored in AS-5 solution at 4ºC in a blood bank were successfully demonstrated. Both male and female RBC suspensions showed significant increases in viscosity, elasticity and relaxation time over seven weeks of blood bank storage, which signifies a decrease in donor RBC deformability. No significant differences in RBC deformability were observed between male and female RBC at any storage time point. The clinical significance of the changes in donor RBC deformability during blood bank storage warrant further study to elucidate the impact of transfusion of brief storage versus prolonged storage blood bank RBC on patient morbidity and mortality.

In vitro flow systems were used to further elucidate the effects of shear stress, exposure time and RBC mechanical fragility on flow-induced hemolysis at flow conditions relevant to CAD operation. *In vitro* hemolysis testing in a centrifugal pump flow system demonstrated the statistically significant effect of RBC total exposure time on mechanical hemolysis. Multiple regression using the power model demonstrated similar blood damage in two centrifugal pump flow systems as in published reports. Notably, this study identified a blood volume range for conducting *in vitro* hemolysis testing of pediatric CAD as $150ml \leq V < 500$ ml. The RBC mechanical fragility index was found to be largely correlated with the results of *in vitro* hemolysis testing and thus demonstrated that the standard RBC mechanical fragility test can aid in the analysis of hemolysis testing of CAD by providing important information on the susceptibility of the blood used for testing to flow-induced trauma.

A capillary flow system with a clinically used centrifugal CAD was used to discern the effects of cell-cell interactions and suspension viscosity on flow-induced hemolysis. Novel results showed that the increase in freeHb from baseline for RBC and GRBC suspensions was nearly proportional to the amount of RBC in suspension. Notably, the hemolysis in the RBC and GRBC suspensions was found to be significantly higher than that in their viscosity-matched controls (RBC in viscous media). Hence, cell-cell interactions is a greater contributor to mechanical hemolysis than bulk viscosity.

In vitro microfluidic experiments and image analysis of the trafficking of GRBC and platelet-sized particles in a custom-fabricated microchannel containing multiple crevices similar to the size of small gaps within CAD at supra-physiological shear stresses revealed a significant finding. Flow separation occurred in 100 μm wide rectangular and triangular crevices but not in wider crevices studied up to 500 μm. Thus, this study demonstrated that the width of gaps and crevices in CAD blood flow paths are an important parameter for thrombogenesis at supra-physiological shear stresses encountered during *in vitro* and *in vivo* CAD operation.

This dissertation provided additional information on the mechanisms of flow-induced hemolysis and elucidated that the width of gaps and crevices in the blood flow path of CAD is an important parameter affecting the development of thrombosis at supra-physiological shear stresses in the assisted circulation.

8.2 STUDY LIMITATIONS

Although the completed dissertation work provided additional information on mechanisms of flow-induced hemolysis and revealed an important parameter affecting thrombogenesis in some CAD blood flow paths, there were several limitations in this study. The work of Specific Aim 1 was performed under turbulent flow conditions in order to ascertain the effectiveness of a DRP solution as a potential test fluid for *in vitro* testing of pre-clinical CAD by assessing the changes in PEO drag-reducing ability during testing. Turbulent stresses are known to augment mechanical hemolysis [105, 106, 234, 235] and in this study, wall shear stress was approximately 50 Pa in the capillary tube for DRP and hemolysis tests. Kameneva *et al.* reported that hemolysis levels were not significantly augmented from laminar flow conditions in a capillary flow system tested at a 100 Pa wall shear stress [106]. Hence, it is unlikely that turbulent stresses significantly augmented the resulting hemolysis in this study. An additional limitation in the work of Specific Aim 1 was that DRP mechanical degradation occurring in the capillary tube and centrifugal pumps, respectively, was not examined.

A limitation in the study of Specific Aim 2 was the preparation of donor RBC suspensions in PBS rather than autologous donor plasma. RBC deformability is reduced in suspensions of PBS compared to plasma [63]. Due to the unavailability of donor plasma, it was necessary to use PBS as the suspension medium for donor RBC in this study. The work of Specific Aim 3 was performed under laminar, transitional and turbulent flow conditions in the capillary flow systems used for *in vitro* hemolysis tests. The results of the study of exposure time of blood to a constant shear stress was likely not significantly affected by the transitional flow conditions for the 250 ml and 500 ml blood volumes tested at 150 Pa wall shear stresses as

demonstrated by Kameneva *et al.* [106]. However, the comparison of RBC-MFI and the resulting *in vitro* hemolysis in a capillary flow system with a CAD may have been affected by the augmented hemolysis produced at a wall shear stress of ~250 Pa and Reynolds number of ~5000 in the studied capillary.

The first study of Specific Aim 4 to elucidate the effects of cell-cell interactions and suspension viscosity on flow-induced hemolysis was performed using RBC and GRBC suspensions in a 70 ml volume capillary flow system. Tests were performed at wall shear stresses of ~150 Pa under transitional flow conditions in a capillary, but the resulting hemolysis was likely not significantly increased by the non-laminar flow conditions in the capillary as demonstrated by Kameneva *et al.* [106]. Although the low circulating volume may have augmented hemolysis in this study as shown by the results of Specific Aim 3, this study was a comparative study of the flow-induced hemolysis among RBC and GRBC suspensions and their viscosity-matched controls (RBC in viscous media).

The study of GRBC and platelet-sized particle trafficking in a multiple crevice microchannel at flow conditions relevant to CAD operation had several limitations. The supra-physiological concentration of 1,000,000 PSFP/µl was chosen to visualize PSFP trafficking in both GRBC suspensions in the microfluidic system. Platelet-sized spherical particles were used in this study as a substitute for discoid human platelets, but the shape of the platelet-sized particles could have affected their trafficking in the studied crevices. A pilot study of cell trafficking in PDMS channels was performed using fixed, fluorescently-dyed human platelets prior to conducting this work. The results of that study revealed that fixed platelets were reactive to PDMS and adhered to the channel surfaces. Thus, platelet-sized spherical particles were used to investigate the fluid dynamic effect on thrombogenesis in small gaps and crevices in VAD

independent of the effects of surface and other biochemical factors. An additional limitation is that this study was performed under steady flow conditions, whereas blood flow in continuous-flow CAD and the microcirculation exhibits some pulsatility.

A major limitation of the final study of Specific Aim 4 was particle trafficking and adhesion at the walls of the inlets and outlets of some crevices in the seal between the PDMS channel and glass coverslip. Adhered particles could disrupt the pathlines of flowing particles, which was an unintended outcome of this study. An additional limitation of this work was the direction of flow in the crevice microchannel. Crevices 1-8 were examined microscopically at 5 and 25 µl/min flow rates entering the channel into Crevice 1. There is a possibility that flow into the largest crevice first could affect the trafficking of PSFP and GRBC in the smaller crevices further down the channel. Furthermore, the study of platelet-sized particle and GRBC trafficking in eight crevices within a 5 mm long channel may not be representative of the crevices and gaps in many CAD blood flow paths.

8.3 FUTURE STUDIES

This dissertation provided additional information on mechanisms of flow-induced hemolysis and parameters that affect *in vitro* hemolysis testing of CAD through the design and use of *in vitro* flow systems with several clinical CAD. Moreover, microfluidic studies in a novel multiple crevice channel at flow conditions relevant to CAD operation revealed an important variable affecting thrombogenesis in CAD blood flow paths. This work provides a basis for several future

studies to further elucidate mechanisms of flow-induced hemolysis and parameters affecting thrombosis development in the assisted circulation.

A supplementary study of the effect of cell-cell interactions on flow-induced hemolysis should be conducted in a microfluidic system to discern GRBC streamlines in suspensions of 10%, 20% and 40% GRBC in high viscosity Dextran 40 solutions with similar viscosities. A nozzle microchannel with similar geometry as the FDA benchmark nozzle model [236] was previously fabricated in PDMS and would be useful for this study. Hence, the proposed mechanism of cell-cell interactions as the consequence of a local velocity gradient between colliding cells when cells traveling along adjacent streamlines interact could be examined microscopically.

The microfluidic studies in an eight crevice channel at supra-physiological shear stresses revealed an important variable affecting thrombosis development in some CAD blood flow paths. To further investigate the effect of crevice width on thrombogenesis at flow conditions relevant to CAD operation, the study of individual crevices with various geometries (rectangular, triangular, etc.) and widths (~20-150 μm) is recommended. A microfluidic system similar to the one used by Jamiolkowski *et al*. [71] could be modified to study individual crevices, or several crevice microchannels fabricated in PDMS could be used for this study. The results of this work could elucidate the effect of crevice width on the development of thrombosis at supra-physiological shear stresses in some CAD and possibly identify a range of crevice widths in which recirculation regions occur.

Supplementary microfluidic studies to the investigation of the effect of crevice width on thrombogenesis in some CAD blood flow paths are investigations of the effects of GRBC deformability, pulsatile flow and use of fluorescently-labeled platelets in test suspensions studied

in the crevice widths and geometries of most interest. Suspensions of GRBC and fluorescently-dyed platelets or PSFP should be examined in crevices with the same shape and width to directly compare platelet and PSFP trafficking and adhesion in the crevices. Ektacytometric studies of GRBC and glutaraldehyde-treated GRBC [104] would quantify cell elongation indices and the trafficking of PSFP or fluorescently-dyed platelets in suspensions of GRBC and glutaraldehyde-treated GRBC could be assessed in the crevices. Finally, the effect of pulsatile flow on the trafficking of GRBC and platelet-sized particles or platelets in the crevice microchannels could be performed by programming a syringe pump to infuse and refill test suspension at specific time intervals. This study would allow a direct comparison of cell trafficking and adhesion at steady flow and pulsatile flow conditions in crevice widths and geometries that affect the development of thrombosis at supra-physiological shear stresses within some CAD blood flow paths.

APPENDIX A

METHODS FOR THE ASSESSMENT OF ERYTHROCYTE DEFORMABILITY

The deformation of erythrocytes in the microcirculation was first observed by van Leeuwenhoek [237] and studied *in vitro* by Goldsmith in Poiseuille and Couette flow [238, 239]. Chien *et al.* studied the effect of RBC-D on blood viscosity using normal and acetaldehyde hardened human and canine RBC [38]. At the same 45% Ht, rigid dog RBC suspended in saline exhibited Newtonian fluid behavior with a higher viscosity than normal dog RBC suspended in saline with Non-Newtonian properties at the same shear rates [38]. Further work by Chien *et al.* [240-242], Sutera *et al.* [57, 243] and Kameneva *et al.* [124, 170] have shown that RBC-D affects the Non-Newtonian behavior of human blood and that changes in RBC-D can impact the preponderance of patient morbidities due to augmented blood viscosity. There are several methods for the assessment of RBC membrane deformability (micropipette aspiration and ektacytometry) and bulk RBC suspension deformability (filtration and viscoelastometry).

A.1 MICROPIPETTE ASPIRATION

Micropipette aspiration of an entire RBC or part of its membrane has been used as a technique for measuring cellular membrane deformability since the original studies of Mitchison and Swann in 1954 [244]. In this method, a negative pressure is applied to partially or completely aspirate a single RBC into a glass micropipette with diameter ranging from less than 1 μm to 5 μm [54, 60]. Quantification is based on the amount of negative pressure needed to aspirate either a part or the entire RBC: aspiration of a portion of the RBC membrane yields the shear elastic modulus of the membrane, while complete aspiration ascertains RBC membrane deformability [245, 246]. Micropipette aspiration is an established technique that has been used to quantify RBC membrane deformability in malaria [247], sickle-cell anemia [248-250], and assisted circulation [117].

Determination of the viscoelastic behavior of individual erythrocytes and quantification of RBC membrane deformability of a single cell are advantages of the micropipette method. However, a high degree of technical skill is required to use this method and reproducibility of micropipette fabrication can be problematic [246]. Due to the study of individual cells, the method is time consuming and limited in that only a small numbers of cells can be studied.

A.2 FILTRATION

Filtration is a technique for determining bulk erythrocyte deformability developed by Reid *et al.* [251] that involves the filtering of RBC suspensions through 3-5 μm polycarbonate membranes

by a constant negative pressure of -20 cm H_2O. Quantification of the process is achieved either by the time required for passage of a certain volume of RBC suspension (transit time) or by the pressure-flow relationship [251]. Filtration is an established technique that has been used to study bulk RBC-D in diabetes [252, 253], pregnancy [254], neonates [255, 256], sickle-cell anemia [257], acute anemia [258], cardiopulmonary bypass [259], sepsis [260] and cold storage [261, 262].

Problems with filtration technique can develop if whole blood is used. Factors present within whole blood, including leukocytes and platelet microaggregates, may impair RBC filtration by causing pore blockage [54, 60, 246]. Thus, it is necessary to thoroughly wash RBC and prepare RBC suspensions at a standard Ht prior to filtration tests so that an accurate measure of RBC filterability can be achieved [54, 60]. A further problem with this method is the lack of calibration standards due to variations in the filters used, leading to poor reproducibility of results [54, 60, 246].

A.3 EKTACYTOMETRY (ELLIPSOMETRY)

Ektacytometry is a conventional technique for assessment of RBC membrane deformability that subjects RBC suspended in a highly viscous medium to a defined, continuous shear flow in a slit rheometer, counter-rotating cone-and-plate, plate-and-plate, or Couette system [263-266]. In this method, shear-deformed RBC appear as ellipsoids that can be analyzed using imaging ellipse-fit software [e.g. Image J (NIH)]. An elongation index (EI) of erythrocyte membrane deformability is calculated according to **Equation 21**.

Quantification of the deformability of numerous erythrocyte membranes yields a RBC membrane deformability distribution for a given sample [264, 267]. Rheoscopy provides data for individual erythrocytes, and as such allows for a more precise quantification at the individual cell level. For example, direct visualization of individual malaria-infected RBC in sheared suspension in a rheoscope allowed Cranston [268] to extend the earlier viscometric studies of Miller [269] to relate the extent of modification of RBC mechanical properties to different life cycle stages of the malaria parasite.

RBC suspensions sheared within flow chambers of laser diffraction ektacytometers are traversed with a laser beam that is diffracted by the RBC present in the volume [263, 265]. Laser diffraction ektacytometry methods have been used to study RBC membrane deformability in various pathological situations associated with impaired microcirculatory flow, including diabetes, malaria, elliptocytosis, and sickle-cell anemia [270, 271].

The Laser-Assisted Optical Rotational Cell Analyzer (LORCA) device incorporates a Couette shearing system in which RBC membrane deformability is assessed in the gap between the inner cylinder (bob) and outer cylinder (cup). This device uses minute blood or RBC volumes ($\leq$ 25 μL) and is advantageous for the rapid assessment of membrane deformability of several hundred RBC [272]. Yet, these techniques are not used clinically due to the need for considerable human interaction: suspending RBC in a highly viscous medium at a prescribed concentration, loading/cleaning the device, and image analysis.

A.4 VISCOELASTOMETRY

Blood and RBC suspension viscoelastometry is a sensitive, established technique for assessing bulk erythrocyte deformability that approximates blood flow in longer vessels of the circulation [32, 51]. In viscometric (viscosity and viscoelastometry) techniques, decreased erythrocyte deformability is observed by an increase in blood viscosity and elasticity without changes in Ht, plasma viscosity or temperature. Elasticity is a direct measure of erythrocyte deformability as it relates the amount of energy storage due to the elastic deformation of RBC [273].

APPENDIX B

CHAPTER 3 STATISTICAL ANALYSIS

Dependent *t*-tests are reliable and robust statistical tests when two assumptions are followed (p. 287 of [274]):

1) Data are measured on at least an interval scale
2) Data is approximately normally distributed

Table B. 1 shows the descriptive statistics for the normalized index of hemolysis of 30% Ht porcine blood in the CentriMag® and Bio-Pump® flow systems. **Table B. 2** shows the descriptive statistics for the drag reduction of 1000 ppm PEO solution calculated at 120 minutes of testing in the CentriMag® and Bio-Pump® flow systems.

Table B. 1. Descriptive statistics for the normalized index of hemolysis of 30% Ht porcine blood calculated at 120 minutes of testing in the CentriMag and BPX-80 flow systems.

Statistics

NIH

CentriMag	N	Valid	3
		Missing	0
	Mean		.00567
	Std. Error of Mean		.001856
	Std. Deviation		.003215
	Variance		.000
	Range		.006
	Minimum		.002
	Maximum		.008
BPX-80	N	Valid	3
		Missing	0
	Mean		.01867
	Std. Error of Mean		.001764
	Std. Deviation		.003055
	Variance		.000
	Range		.006
	Minimum		.016
	Maximum		.022
.	N	Valid	0
		Missing	73

Table B. 2. Descriptive statistics for the drag reduction of 1000 ppm PEO solution calculated at 120 minutes of testing in the CentriMag and BPX-80 flow systems.

Statistics

DR

CentriMag	N	Valid	2
		Missing	1
	Mean		22.3000
	Std. Error of Mean		.40000
	Std. Deviation		.56569
	Variance		.320
	Range		.80
	Minimum		21.90
	Maximum		22.70
BPX-80	N	Valid	2
		Missing	1
	Mean		25.5250
	Std. Error of Mean		.62500
	Std. Deviation		.88388
	Variance		.781
	Range		1.25
	Minimum		24.90
	Maximum		26.15
.	N	Valid	0
		Missing	73

Table B. 3 shows the descriptive statistics for the polymer degradation index of 1000 ppm PEO solution calculated at 120 minutes of testing in the CentriMag® and Bio-Pump® flow systems.

Table B. 3. Descriptive statistics for the polymer degradation index of 1000 ppm PEO solution calculated at 120 minutes of testing in the CentriMag and BPX-80 flow systems.

Statistics

PDI

CentriMag	N	Valid	2
		Missing	1
	Mean		.04135
	Std. Error of Mean		.000150
	Std. Deviation		.000212
	Variance		.000
	Range		.000
	Minimum		.041
	Maximum		.042
BPX-80	N	Valid	2
		Missing	1
	Mean		.04880
	Std. Error of Mean		.001000
	Std. Deviation		.001414
	Variance		.000
	Range		.002
	Minimum		.048
	Maximum		.050
.	N	Valid	0
		Missing	73

APPENDIX C

CHAPTER 4 STATISTICAL ANALYSIS

Independent *t*-tests and ANOVA are reliable and robust statistical tests when four assumptions are followed (p. 324 of [274]):

1) Observations are independent
2) Dependent variable is measured on at least an interval scale
3) Data is approximately normally distributed
4) Variances in each experimental condition are fairly similar

Table C.1 and **Table C.2** show the descriptive statistics and Homogeneity of Variances Test, respectively, for male (n=12) and female (n=12) RBC suspension viscosity measured at a 25 s^{-1} shear rate at Week 1, 4 and 7 of blood bank storage. **Table C.3** and **Table C.4** show the descriptive statistics and Homogeneity of Variances Test, respectively, for male (n=12) and female (n=12) RBC suspension viscosity measured at a 100 s^{-1} shear rate at Week 1, 4 and 7 of blood bank storage.

Table C. 1. Descriptive statistics for male and female RBC suspension viscosity measured at a 25 s^{-1} shear rate at Week 1, 4 and 7 of storage.

Descriptive Statistics

Dependent Variable: Viscosity_at_SR_25

Sex	Storage_time	Mean	Std. Deviation	N
Male	Week 1	4.00167	.377075	12
	Week 4	4.39692	.437330	12
	Week 7	4.63292	.465988	12
	Total	4.34383	.492749	36
Female	Week 1	3.83174	.379860	12
	Week 4	4.36950	.423400	12
	Week 7	4.70675	.336749	12
	Total	4.30266	.520462	36

Table C. 2. Levene's Test for Homogeneity of Variances for male and female RBC suspension viscosity measured at a 25 s^{-1} shear rate at Week 1, 4 and 7 of storage.

Levene's Test of Equality of Error Variances[a]

Dependent Variable: Viscosity_at_SR_25

Sex	F	df1	df2	Sig.
Male	.340	2	33	.714
Female	.196	2	33	.823

Tests the null hypothesis that the error variance of the dependent variable is equal across groups.

Table C. 3. Descriptive statistics for male and female RBC suspension viscosity measured at a 100 s^{-1} shear rate at Week 1, 4 and 7 of storage.

Descriptive Statistics

Dependent Variable: Viscosity_at_SR_100

Sex	Storage_time	Mean	Std. Deviation	N
Male	Week 1	3.63875	.232626	12
	Week 4	3.92808	.256499	12
	Week 7	4.09000	.278273	12
	Total	3.88561	.312821	36
Female	Week 1	3.51950	.261177	12
	Week 4	3.92300	.261813	12
	Week 7	4.16475	.218136	12
	Total	3.86908	.361670	36

Table C. 4. Levene's Test for Homogeneity of Variances for male and female RBC suspension viscosity measured at a 100 s^{-1} shear rate at Week 1, 4 and 7 of storage.

Levene's Test of Equality of Error Variances[a]

Dependent Variable: Viscosity_at_SR_100

Sex	F	df1	df2	Sig.
Male	.172	2	33	.843
Female	.182	2	33	.835

Tests the null hypothesis that the error variance of the dependent variable is equal across groups.

Table C.5 and **Table C.6** show the descriptive statistics and Homogeneity of Variances Test, respectively, for male (n=12) and female (n=12) RBC suspension elasticity measured at a 25 s^{-1} shear rate at Week 1, 4 and 7 of blood bank storage.

Table C. 5. Descriptive statistics for male and female RBC suspension elasticity measured at a 25 s^{-1} shear rate at Week 1, 4 and 7 of storage.

Descriptive Statistics

Dependent Variable: Elasticity_at_SR_25

Sex	Storage_time	Mean	Std. Deviation	N
Male	Week 1	.207150	.0820669	12
	Week 4	.284733	.0934068	12
	Week 7	.342317	.1036343	12
	Total	.278067	.1067198	36
Female	Week 1	.203983	.0561120	12
	Week 4	.295242	.0606583	12
	Week 7	.348158	.0484446	12
	Total	.282461	.0808141	36

Table C. 6. Levene's Test for Homogeneity of Variances for male and female RBC suspension elasticity measured at a 25 s^{-1} shear rate at Week 1, 4 and 7 of storage.

Levene's Test of Equality of Error Variances[a]

Dependent Variable: Elasticity_at_SR_25

Sex	F	df1	df2	Sig.
Male	.670	2	33	.519
Female	.061	2	33	.941

Tests the null hypothesis that the error variance of the dependent variable is equal across groups.

Table C.7 and **Table C.8** show the descriptive statistics and Homogeneity of Variances Test, respectively, for male (n=12) and female (n=12) RBC suspension elasticity measured at a 100 s^{-1} shear rate at Week 1, 4 and 7 of blood bank storage.

Table C. 7. Descriptive statistics for male and female RBC suspension elasticity measured at a 100 s^{-1} shear rate at Week 1, 4 and 7 of storage.

Descriptive Statistics

Dependent Variable: Elasticity_at_SR_100

Sex	Storage_time	Mean	Std. Deviation	N
Male	Week 1	.077167	.0076983	12
	Week 4	.094208	.0105640	12
	Week 7	.104717	.0145642	12
	Total	.092031	.0159034	36
Female	Week 1	.083658	.0059724	12
	Week 4	.096383	.0067616	12
	Week 7	.109183	.0087347	12
	Total	.096408	.0126984	36

Table C. 8. Levene's Test for Homogeneity of Variances for male and female RBC suspension elasticity measured at a 100 s^{-1} shear rate at Week 1, 4 and 7 of storage.

Levene's Test of Equality of Error Variances[a]

Dependent Variable: Elasticity_at_SR_100

Sex	F	df1	df2	Sig.
Male	.841	2	33	.440
Female	3.158	2	33	.056

Tests the null hypothesis that the error variance of the dependent variable is equal across groups.

APPENDIX D

CHAPTER 5 STATISTICAL ANALYSIS

Table D. 1 and **Table D. 2** show the descriptive statistics and Homogeneity of Variances Test, respectively, for the normalized index of hemolysis calculated for the 30% hematocrit bovine blood volumes after 60 minutes of testing in the centrifugal pump flow systems.

Table D. 1. Descriptive statistics for the normalized index of hemolysis calculated for the 60 ml, 125 ml, 250 ml and 500 ml blood volumes after 60 minutes of testing in the centrifugal pump flow systems.

Descriptives

NIH

	N	Mean	Std. Deviation	Std. Error	95% Confidence Interval for Mean		Minimum	Maximum
					Lower Bound	Upper Bound		
60 ml	6	1.3524	.49192	.20082	.8361	1.8686	1.06	2.34
125 ml	8	.6848	.51430	.18183	.2549	1.1148	.11	1.45
250 ml	6	.1398	.05370	.02192	.0834	.1961	.07	.20
500 ml	6	.1002	.03372	.01376	.0648	.1355	.06	.13
Total	26	.5782	.60969	.11957	.3319	.8244	.06	2.34

Table D. 2. Levene's Test for Homogeneity of Variances for the normalized index of hemolysis calculated for the 60 ml, 125 ml, 250 ml and 500 ml blood volumes after 60 minutes of testing in the centrifugal pump flow systems.

Test of Homogeneity of Variances

NIH

Levene Statistic	df1	df2	Sig.
7.588	3	22	.001

Table D. 3 and **Table D. 4** show multiple regression analysis using the power model of the IH (ΔfreeHb/tHb) in 60 ml, 125 ml, 250 ml and 500 ml 30% hematocrit bovine blood

volumes after 60 minutes of testing in the centrifugal pump flow systems. The model summary is shown in **Table D. 3** and the empirical coefficients of the power law model are shown in **Table D. 4**.

Table D. 3. Multiple regression of the change in plasma free hemoglobin concentration from baseline divided by the total hemoglobin concentration after 60 minutes of testing in the centrifugal pump flow systems.

Model Summary

R	R Square	Adjusted R Square	Std. Error of the Estimate
.814	.662	.633	.653

The independent variables are Damage_exposure_time and Shear_stress.

Table D. 4. Coefficients of the power model applied to the Index of Hemolysis after 60 minutes of testing in the centrifugal pump flow systems.

Coefficients

	Unstandardized Coefficients		Standardized Coefficients		
	B	Std. Error	Beta	t	Sig.
Damage_exposure_time	1.055	.359	.514	2.935	.007
Shear_stress	2.614	.537	1.748	3.494	.04
(Constant)	.0000482	.001		3.250	.003

The dependent variable is delta_freeHb_divHb.

APPENDIX E

CHAPTER 6 STATISTICAL ANALYSIS

Table E. 1 and **Table E. 2** show the descriptive statistics and Homogeneity of Variances Test, respectively, for the Index of Hemolysis calculated for the 40% RBC in PBS, 10% RBC and 30% GRBC in PBS, 20% RBC and 20% GRBC in PBS, 10% RBC in 7% Dextran 40 and 20% RBC in 7% Dextran 40 suspensions after 120 minutes of testing in the capillary flow system.

Table E. 1. Descriptive statistics of the Index of Hemolysis calculated for the 40% RBC in PBS, 10% RBC and 30% GRBC in PBS, 20% RBC and 20% GRBC in PBS, 10% RBC in 7% Dextran 40 and 20% RBC in 7% Dextran 40 suspensions after 120 minutes of testing in the capillary flow system.

Descriptives

Hemolysis_Index

	N	Mean	Std. Deviation	Std. Error	95% Confidence Interval for Mean		Minimum	Maximum
					Lower Bound	Upper Bound		
40% RBCs in PBS	12	1.09775	.497771	.143694	.78148	1.41402	.656	2.156
30% GRBCs and 10% RBCs in PBS	6	1.13650	.421060	.171897	.69462	1.57838	.787	1.946
20% GRBCs and 20% RBCs in PBS	6	.88383	.319330	.130366	.54872	1.21895	.358	1.124
10% RBCs in 7% Dextran 40	6	.17800	.070029	.028589	.10451	.25149	.113	.266
20% RBCs in 7% Dextran 40	6	.23750	.090276	.045138	.09385	.38115	.152	.365
Total	36	.80332	.537751	.092223	.61569	.99095	.113	2.156

Table E. 2. Levene's Test for Homogeneity of Variances of the Index of Hemolysis calculated for the 40% RBC in PBS, 10% RBC and 30% GRBC in PBS, 20% RBC and 20% GRBC in PBS, 10% RBC in 7% Dextran 40 and 20% RBC in 7% Dextran 40 suspensions after 120 minutes of testing in the capillary flow system.

Test of Homogeneity of Variances

Hemolysis_Index

Levene Statistic	df1	df2	Sig.
2.798	4	29	.044

Table E. 3 and **Table E. 4** show the descriptive statistics and Homogeneity of Variances Test, respectively, for the MFI calculated for the 40% RBC in PBS, 10% RBC and 30% GRBC in PBS, 20% RBC and 20% GRBC in PBS, 10% RBC in 7% Dextran 40 and 20% RBC in 7% Dextran 40 suspensions after 120 minutes of testing in the capillary flow system.

Table E. 3. Descriptive statistics of the mechanical fragility index calculated for the 40% RBC in PBS, 10% RBC and 30% GRBC in PBS, 20% RBC and 20% GRBC in PBS, 10% RBC in 7% Dextran 40 and 20% RBC in 7% Dextran 40 suspensions after 120 minutes of testing in the capillary flow system.

Descriptives

MFI

	N	Mean	Std. Deviation	Std. Error	95% Confidence Interval for Mean		Minimum	Maximum
					Lower Bound	Upper Bound		
40% RBCs in PBS	12	1.7950	.35367	.10210	1.5703	2.0197	1.22	2.27
30% GRBCs and 10% RBCs in PBS	6	1.5667	.42693	.17429	1.1186	2.0147	1.03	1.97
20% GRBCs and 20% RBCs in PBS	6	1.6783	.22311	.09108	1.4442	1.9125	1.27	1.87
10% RBCs in 7% Dextran 40	6	.1800	.08485	.03464	.0910	.2690	.09	.27
20% RBCs in 7% Dextran 40	4	.3375	.11871	.05935	.1486	.5264	.16	.41
Total	34	1.2776	.73968	.12685	1.0196	1.5357	.09	2.27

Table E. 4. Levene's Test for Homogeneity of Variances for the mechanical fragility index calculated for the 40% RBC in PBS, 10% RBC and 30% GRBC in PBS, 20% RBC and 20% GRBC in PBS, 10% RBC in 7% Dextran 40 and 20% RBC in 7% Dextran 40 suspensions after 120 minutes of testing in the capillary flow system.

Test of Homogeneity of Variances

MFI

Levene Statistic	df1	df2	Sig.
8.236	4	29	.000

APPENDIX F

MICROCHANNEL FABRICATION

The novel microchannel geometries used in the study of trafficking of GRBC and platelet-sized particles described in **Chapter 7** were examined for fabrication from several commercial sources (ibidi LLC, CFD Research Corporation, etc.), but these sources proved to be too costly. Consequently, I investigated using 3D printing technology to fabricate the desired microchannels due to the availability of a 3D printer in Professor Antaki's Laboratory.

F.1 METHODS

Microchannel designs were created in SolidWorks 2013 (Dassault Systèmes SolidWorks Corporation, Waltham, MA). **Figure F.1** shows three iterations of the serpentine channel design. The designs were uploaded to and fabricated in a 3D printer (Perfactory, EnvisionTEC, Gladbeck, Germany).

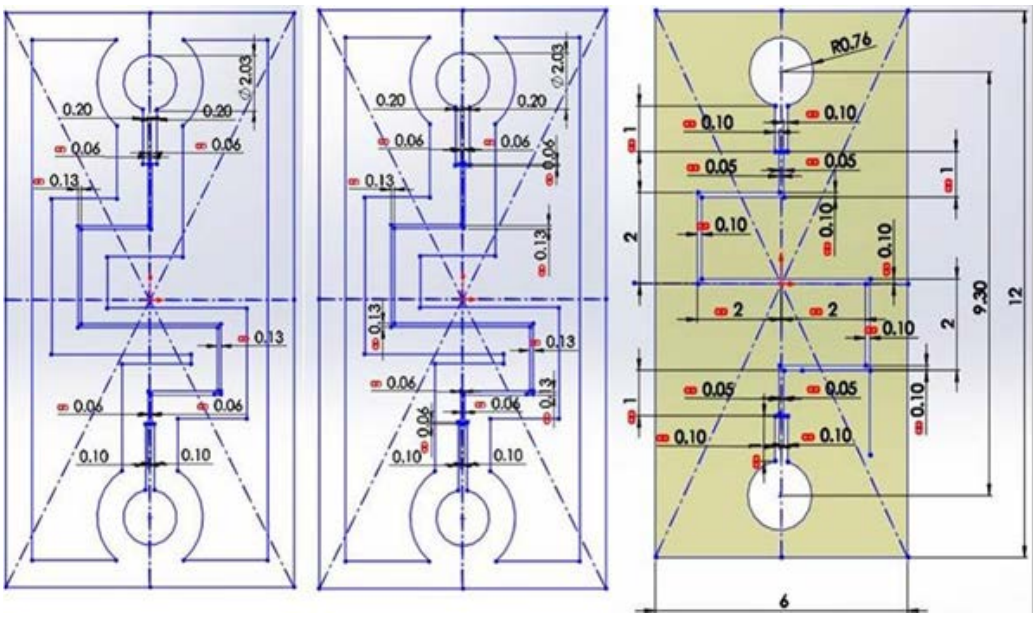

Figure F. 1. Three iterations of the serpentine microchannel design created in SolidWorks. Units are shown in millimeters.

A variety of filtered resins (E-shell 300, E-shell 500, R11), channel printing orientations (horizontal or vertical) and numerous revisions of the microchannel designs were investigated in our many attempts to fabricate the desired channel geometries with a well-defined flow path and smooth walls. A further problem was attaining an effective seal with corona treatment to attach the resin to glass coverslips to form the channels (**Figure F.2**).

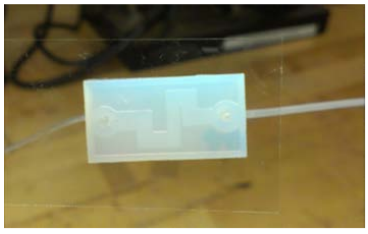

Figure F. 2. Serpentine microchannel fabricated in E-shell 500 and sealed on a glass coverslip.

Unfortunately, I was ultimately unable to make channels with smooth walls or a well-defined flow path in a reproducible manner using the 3D printer (**Figure F.3**). Hence, microchannel fabrication using 3D printing technology was abandoned.

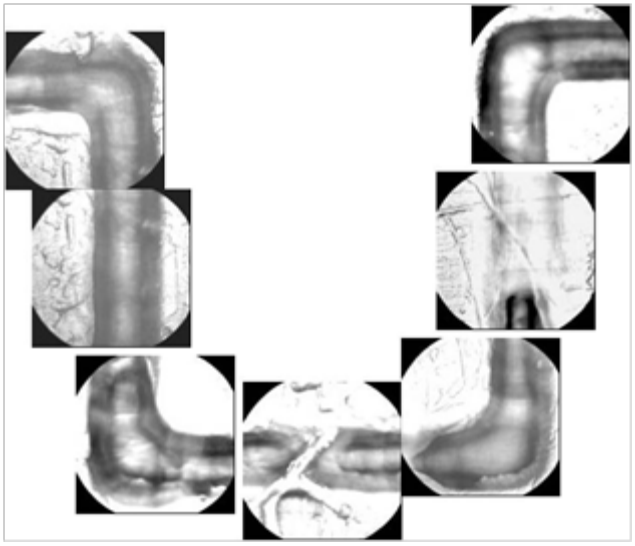

Figure F. 3. Brightfield visualization of a representative serpentine microchannel fabricated in E-shell 500 resin using a 3D printer. 40x magnification. Field of view in each image is 500 μm by 500 μm.

Microchannel fabrication was pursued using PDMS to make the channels. **Figure F.4** shows novel designs of a serpentine microchannel and a microchannel with multiple crevices were made in SolidWorks 2013. A mask was created with these designs and purchased from Photo Sciences, Inc. Once the mask was received, a 4" D Silicon wafer was created in the CMU Nanofabrication Laboratory by Dr. Collin Edington. The wafer was treated with an adhesion promoter (HMDS), spin coated with a photo resist, baked to harden the resist and then exposed to UV light in an aligner.

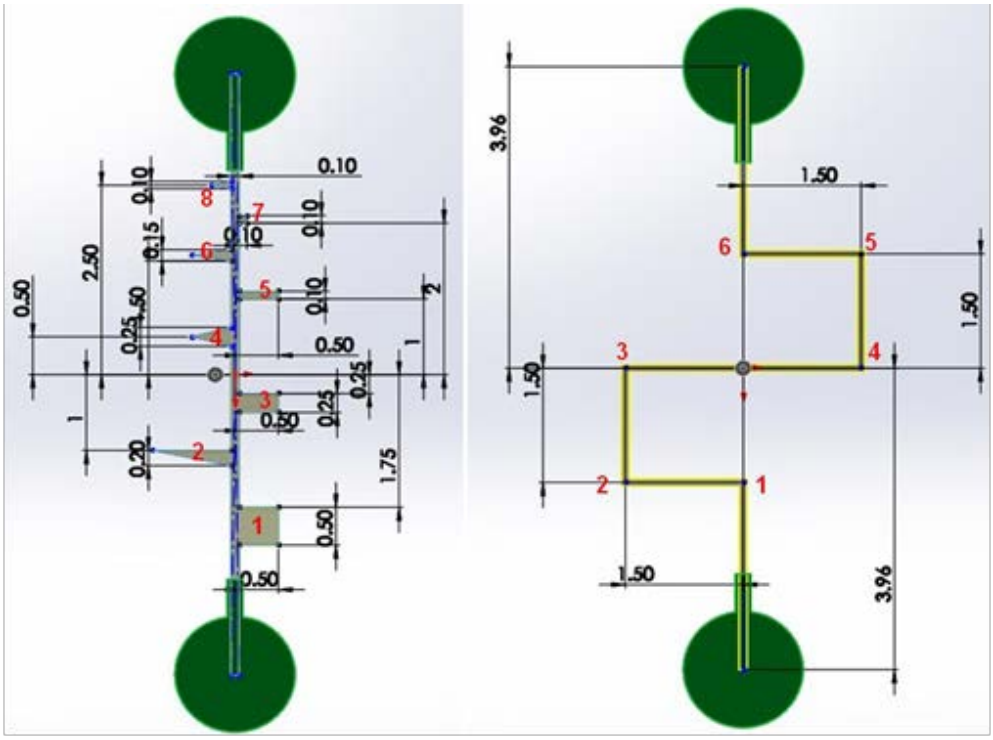

Figure F. 4. Novel designs of a crevice microchannel [left] and serpentine microchannel [right] used to study the trafficking of GRBC and platelet-sized particles under flow conditions that may promote thrombosis in the assisted blood circulation. The height of both channels is 75 µm.

Units are shown in millimeters. The red numbers designate the crevice and bend numbering convention.

Next, the wafer was submerged in developer to dissolve away the resist that was exposed to light, thus leaving the areas that were covered by the dark patterns on the mask. The remaining resist serves as a protective layer during etching of the wafer. Etching was performed in cycles, where the wafer was first exposed to a thin protective layer of material, followed by an etchant. The cycles were very short (8-12 seconds), and repeated back and forth for a few hours. The cyclic passivating/etching allowed for anisotropic etching, which kept the sidewalls of the pattern vertical and protected them from etching inward during the process. After etching, the protective resist layer was removed and the PDMS mold was complete. The PDMS was then treated with chlorosilane vapor that created a non-stick surface to more easily remove the PDMS.

In a laminar flow hood, the individual channels were cut from the wafer using an X-ACTO knife with razor blades treated with tape that removes any surface artifacts or debris and leaves no surface residue. Holes for the inlet and outlet of the channels were punched using a custom fabricated blunt needle and a stereoscope. Individual PDMS channels and coverslips (Fisherfinest™ Premium Cover Glasses, Fisher Scientific Inc.) were treated with no-residue tape before sealing the channels to coverslips using corona treatment. The sealed channels were placed on a glass petri dish and baked overnight in an oven at 60°C. After cooling, tubing (PE-60, Braintree Scientific, Inc.) was treated with no-residue tape and inserted into the inlet (8 cm length) and outlet (11 cm length) of the microchannel to be tested. A 200 µl pipet tip was treated with no-residue tape and carefully inserted in the open end of the inlet tubing. A sterile 21 gauge 1.5” L needle was inserted into the open end of the outlet tubing and the flow path of the microchannel was viewed with the microscope to ensure that the channel was suitable for testing (smooth walls, no debris in channel, etc).

F.2 RESULTS

Representative crevice and serpentine channels after fabrication and prior to sealing on glass coverslips are shown in **Figures F.5-F.26**. The channels were carefully placed on glass coverslips and images were acquired using the setup described in **Section 7.2**. **Figure F. 5** shows the inlet region to a representative crevice channel. The inlet contraction region is shown in **Figure F. 6** and the first crevice in the flow path of the crevice microchannel is shown in **Figure F. 7**.

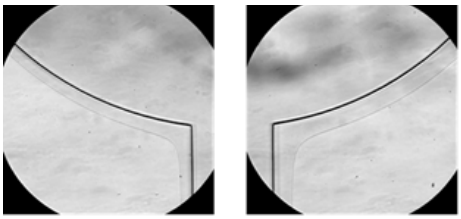

Figure F. 5. Left and right walls of the inlet region to the Crevice microchannels prior to sealing. 40x magnification. Field of view in each image is 500 µm by 500 µm.

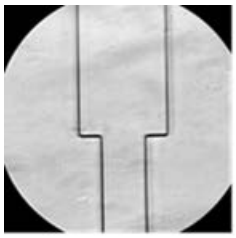

Figure F. 6. Inlet contraction region to the Crevice microchannels prior to sealing. 40x magnification. Field of view is 500 µm by 500 µm.

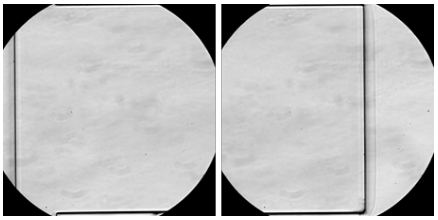

Figure F. 7. First crevice in the flow path of the Crevice microchannels prior to sealing. 40x magnification. Field of view in each image is 500 µm by 500 µm.

Figure F. 8, Figure F. 9 and **Figure F. 10** shows the second, third and fourth crevices in the flow path of the crevice microchannels before sealing. Crevices 5, 6 and 7 prior to sealing are shown in **Figure F. 11, Figure F. 12** and **Figure F. 13**, respectively.

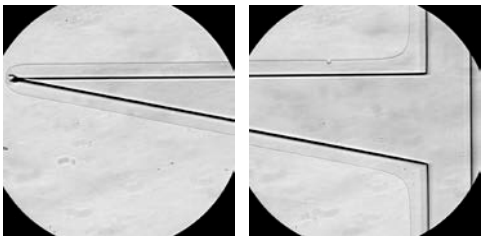

Figure F. 8. Second crevice in the flow path of the Crevice microchannels prior to sealing. 40x magnification. Field of view in each image is 500 µm by 500 µm.

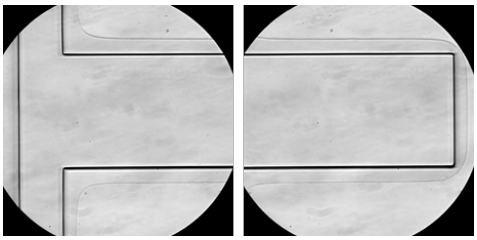

Figure F. 9. Third crevice in the flow path of the Crevice microchannels prior to sealing. 40x magnification. Field of view in each image is 500 µm by 500 µm.

Figure F. 10. Fourth crevice in the flow path of the Crevice microchannels prior to sealing. 40x magnification.

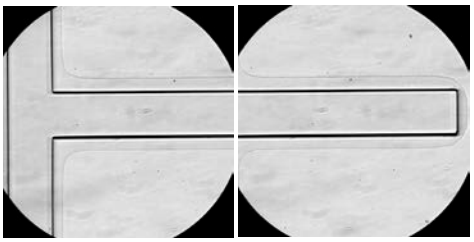

Figure F. 11. Fifth crevice in the flow path of the Crevice microchannels prior to sealing. 40x magnification. Field of view in each image is 500 µm by 500 µm.

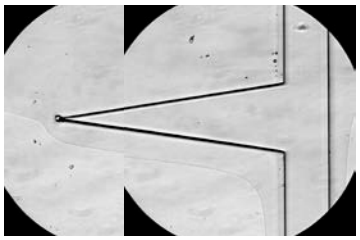

Figure F. 12 Sixth crevice in the flow path of the Crevice microchannels prior to sealing. 40x magnification.

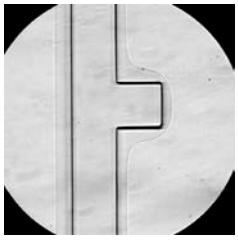

Figure F. 13. Seventh crevice in the flow path of the Crevice microchannels prior to sealing. 40x magnification. Field of view in the image is 500 µm by 500 µm.

Figure F. 14 shows Crevice 8 of the representative crevice microchannel prior to sealing. A backward step in the flow path of the crevice microchannels before sealing is shown in **Figure F. 15**. **Figure F. 16** shows the left and right walls of the outlet region of the crevice microchannels prior to sealing.

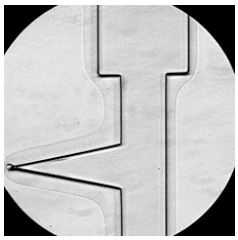

Figure F. 14. Eighth crevice in the flow path of the Crevice microchannels prior to sealing. 40x magnification. Field of view in the image is 500 µm by 500 µm.

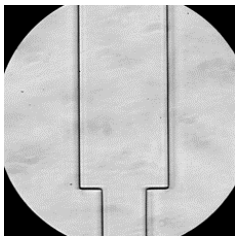

Figure F. 15. Backward step in the flow path of the Crevice microchannels prior to sealing. 40x magnification. Field of view in the image is 500 µm by 500 µm.

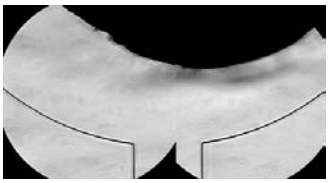

Figure F. 16. Left and right walls of the outlet region of the Crevice microchannels prior to sealing. 40x magnification.

Figure F. 17 shows the inlet region to a representative serpentine channel prior to sealing. The inlet contraction region is shown in **Figure F. 18** and the first bend in the flow path of the serpentine microchannel before sealing is shown in **Figure F. 19**.

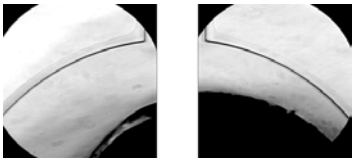

Figure F. 17. Left and right walls of the inlet region to the serpentine microchannels prior to sealing. 40x magnification. Field of view in each image is 500 µm by 500 µm.

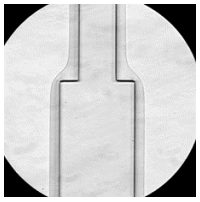

Figure F. 18. Inlet contraction region to the serpentine microchannels prior to sealing. 40x magnification. Field of view is 500 µm by 500 µm.

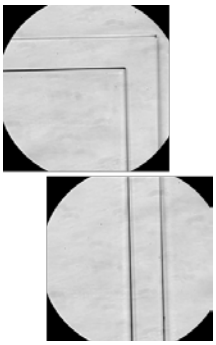

Figure F. 19. First bend in the flow path of the serpentine microchannels prior to sealing. 40x magnification. Field of view in each image is 500 µm by 500 µm.

Figure F. 20, Figure F. 21 and **Figure F. 22** shows the second, third and fourth bends in the flow path of the serpentine microchannels before sealing. Bends 5 and 6 prior to sealing are shown in **Figure F. 23** and **Figure F. 24**, respectively.

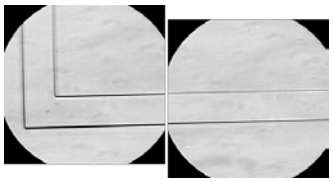

Figure F. 20. Second bend in the flow path of the serpentine microchannels prior to sealing. 40x magnification. Field of view in each image is 500 µm by 500 µm.

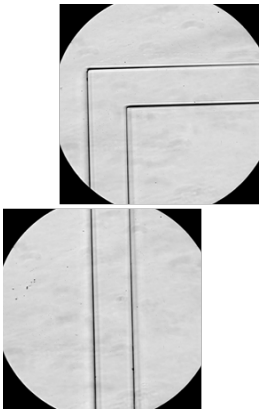

Figure F. 21. Third bend in the flow path of the serpentine microchannels prior to sealing. 40x magnification. Field of view in each image is 500 µm by 500 µm.

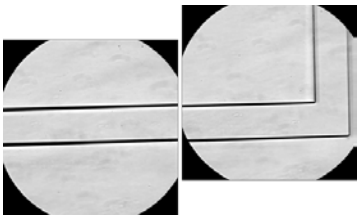

Figure F. 22. Fourth bend in the flow path of the serpentine microchannels prior to sealing. 40x magnification. Field of view in each image is 500 µm by 500 µm.

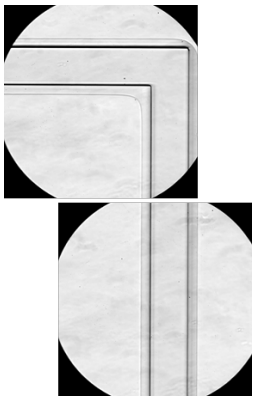

Figure F. 23. Fifth bend in the flow path of the serpentine microchannels prior to sealing. 40x magnification. Field of view in each image is 500 µm by 500 µm.

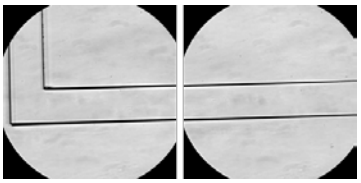

Figure F. 24. Sixth bend in the flow path of the serpentine microchannels prior to sealing. 40x magnification. Field of view in each image is 500 µm by 500 µm.

Figure F. 25 shows a backward step in the flow path of the serpentine microchannels before sealing. **Figure F. 26** shows the left and right walls of the outlet region of the serpentine microchannels prior to sealing.

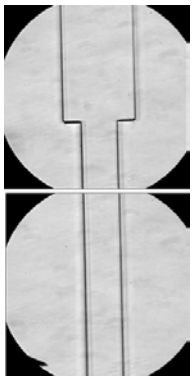

Figure F. 25. Backward step in the flow path of the serpentine microchannels prior to sealing. 40x magnification. Field of view in each image is 500 µm by 500 µm.

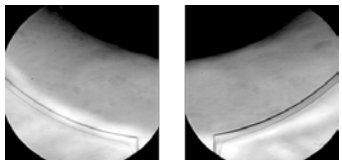

Figure F. 26. Left and right walls of the outlet region to the serpentine microchannels prior to sealing. 40x magnification. Field of view in each image is 500 µm by 500 µm.

Representative crevice and serpentine channels sealed on glass coverslips and filled with 1% BSA in PBS are shown in **Figures F.27-F.45**. The channels were examined under Brightfield visualization using the setup described in **Section 7.2**. **Figure F. 27** shows the inlet and contraction regions of a representative crevice channel. The first, second and third crevices in the flow path of the crevice microchannel are shown in **Figure F. 28, Figure F. 29** and **Figure F. 30**, respectively.

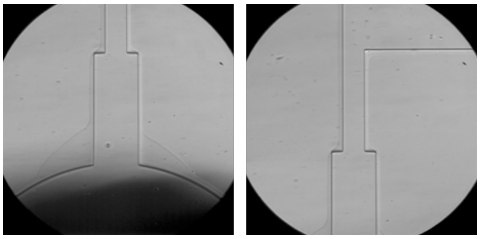

Figure F. 27. Inlet and contraction regions of a representative crevice microchannel filled with 1% bovine serum albumin. 20x magnification. Field of view in each image is 1000 µm by 1000 µm.

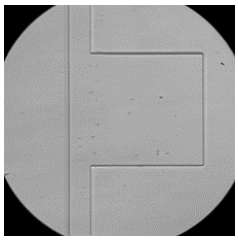

Figure F. 28. First crevice in the flow path of a representative crevice microchannel filled with 1% bovine serum albumin. 20x magnification. Field of view in each image is 1000 µm by 1000 µm.

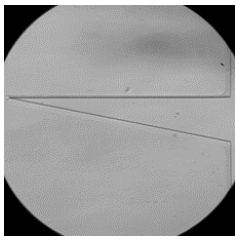

Figure F. 29. Second crevice in the flow path of a representative crevice microchannel filled with 1% bovine serum albumin. 20x magnification. Field of view in each image is 1000 µm by 1000 µm.

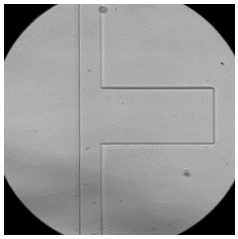

Figure F. 30. Third crevice in the flow path of a representative crevice microchannel filled with 1% bovine serum albumin. 20x magnification. Field of view in each image is 1000 µm by 1000 µm.

The fourth, fifth and sixth crevices in the flow path of a representative crevice microchannel filled with 1% BSA in PBS are shown in **Figure F. 31, Figure F. 32** and **Figure F. 33**, respectively. The seventh and eighth crevices in the flow path of a crevice microchannel filled with 1% BSA in PBS is shown in **Figure F. 34**.

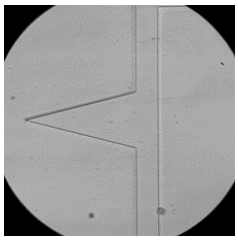

Figure F. 31. Fourth crevice in the flow path of a representative crevice microchannel filled with 1% bovine serum albumin. 20x magnification. Field of view in each image is 1000 µm by 1000 µm.

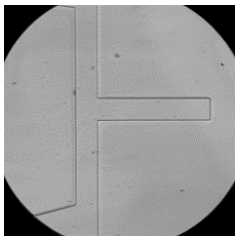

Figure F. 32. Fifth crevice in the flow path of a representative crevice microchannel filled with 1% bovine serum albumin. 20x magnification. Field of view in each image is 1000 µm by 1000 µm.

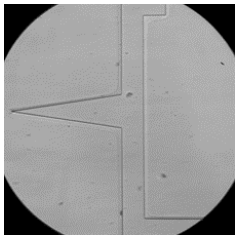

Figure F. 33. Sixth crevice in the flow path of a representative crevice microchannel filled with 1% bovine serum albumin. 20x magnification. Field of view in each image is 1000 µm by 1000 µm.

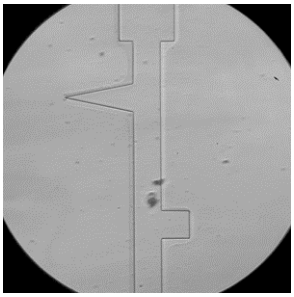

Figure F. 34. Seventh and eighth crevices in the flow path of a representative crevice microchannel filled with 1% bovine serum albumin. 20x magnification. Field of view in each image is 1000 µm by 1000 µm.

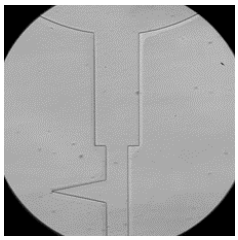

Figure F. 35. Eighth crevice, backward step and outlet regions of a representative crevice microchannel filled with 1% bovine serum albumin. 20x magnification. Field of view in each image is 1000 µm by 1000 µm.

Figure F. 36 and **Figure F. 37** show the inlet and contraction regions of a representative serpentine channel filled with 1% BSA in PBS. The first, second and third bends in the flow path of a representative serpentine microchannel filled with 1% BSA in PBS are shown in **Figure F. 38, Figure F. 39** and **Figure F. 40**, respectively.

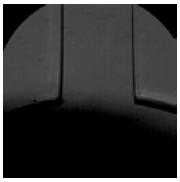

Figure F. 36. Left and right walls of the inlet region of a representative serpentine microchannel filled with 1% bovine serum albumin. 40x magnification. Field of view in each image is 500 µm by 500 µm.

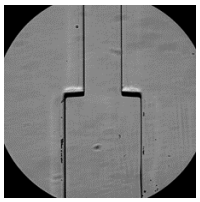

Figure F. 37. Contraction region of a representative serpentine microchannel filled with 1% bovine serum albumin. 40x magnification. Field of view in each image is 500 µm by 500 µm.

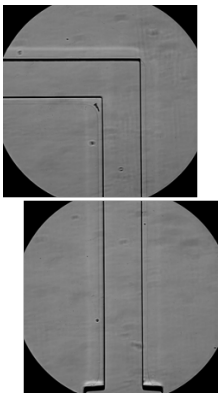

Figure F. 38. First bend in the flow path of a representative serpentine microchannel filled with 1% bovine serum albumin. 40x magnification. Field of view in each image is 500 µm by 500 µm.

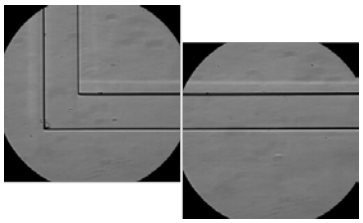

Figure F. 39. Second bend in the flow path of a representative serpentine microchannel filled with 1% bovine serum albumin. 40x magnification. Field of view in each image is 500 µm by 500 µm.

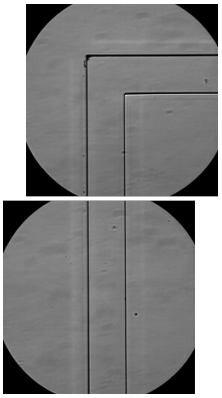

Figure F. 40. Third bend in the flow path of a representative serpentine microchannel filled with 1% bovine serum albumin. 40x magnification. Field of view in each image is 500 µm by 500 µm.

The fourth, fifth and sixth bends in the flow path of a representative serpentine microchannel filled with 1% BSA in PBS are shown in **Figure F. 41, Figure F. 42** and **Figure F. 43**, respectively. A backward step in the flow path of a representative serpentine microchannel

filled with 1% BSA is shown in **Figure F. 44**. **Figure F. 45** shows the left and right walls of the outlet region of a representative serpentine microchannel filled with 1% BSA in PBS.

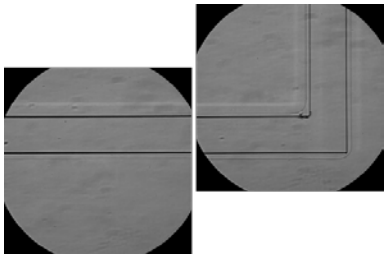

Figure F. 41. Fourth bend in the flow path of a representative serpentine microchannel filled with 1% bovine serum albumin. 40x magnification. Field of view in each image is 500 µm by 500 µm.

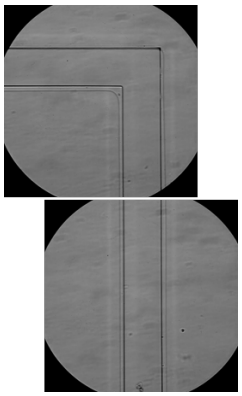

Figure F. 42. Fifth bend in the flow path of a representative serpentine microchannel filled with 1% bovine serum albumin. 40x magnification. Field of view in each image is 500 µm by 500 µm.

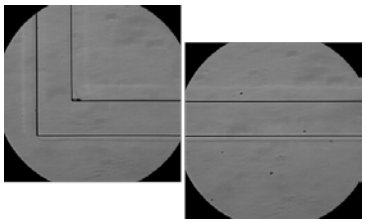

Figure F. 43. Sixth bend in the flow path of a representative serpentine microchannel filled with 1% bovine serum albumin. 40x magnification. Field of view in each image is 500 µm by 500 µm.

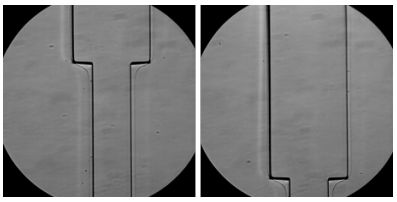

Figure F. 44. Backward step in the flow path of a representative serpentine microchannel filled with 1% bovine serum albumin. 40x magnification. Field of view in each image is 500 µm by 500 µm.

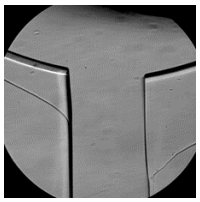

Figure F. 45. Left and right walls of the outlet region of a representative serpentine microchannel filled with 1% bovine serum albumin. 40x magnification. Field of view in each image is 500 µm by 500 µm.

F.3 DISCUSSION

Experiments conducted in **Chapter 7** were performed using a novel multiple crevice microchannel fabricated in PDMS. Multiple crevice microchannels were pretreated with no-residue tape and microscopically examined for any defects. Suitable channels were sealed on glass coverslips using corona treatment and incubated overnight at 60°C to irreversibly seal the channels. All sealed channels were reexamined under Brightfield visualization to ensure that there were no channel defects or artifacts present in the channels prior to testing.

APPENDIX G

TRAFFICKING OF ERYTHROCYTE GHOSTS AND PLATELETS OR PLATELET-SIZED PARTICLES IN BACKWARD STEP, STRAIGHT AND Y-BIFURCATION MICROCHANNEL GEOMETRIES

G.1 INTRODUCTION

In the artificial blood circulation, RBC and platelets are exposed to non-physiological forces and surfaces that may promote hemolysis and thrombosis. Channel geometries previously used to study particle/cell distributions under physiological or supra-physiological shear stresses include straight channels (τ_{wall}~0.15-30 Pa) [214, 221], sudden expansions [159, 227] and rounded and square T-junctions [228, 229]. Platelet margination was first reported by Goldsmith in sudden expansion channels using GRBC and particles [159]. The margination of platelet-sized particles flowing through a 100 μm height straight channel (τ_{wall}~40-200Pa) [230] and a 100 μm:200μm height backward step microchannel (similar to the gap sizes in many circulatory-assist devices) exposed to τ_{wall}~20-100 Pa was recently reported by Zhao *et al.* using suspensions of bovine RBC and fluorescent platelet-sized particles [231].

The objective of this study was to examine the trafficking of GRBC and fluorescently-labeled platelets or PSFP under flow in several microchannel geometries. The microscopic examination of trafficking of GRBC and platelets or PSFP will provide additional insight into the flow conditions and interaction of cells that may lead to the formation of thrombosis in the microcirculation, small gaps similar to those within some circulatory-assist devices and in conditions resulting in flow separation.

G.2 TRAFFICKING OF ERYTHROCYTE GHOSTS AND PLATELETS IN A BACKWARD STEP MICROCHANNEL

G.2.1 Methods

Human O- RBC units were purchased from Valley Biomedical Inc. RBC are sterilely extracted from the bag and washed thrice in PBS. GRBC were prepared according to the protocol described in **Section 6.2**. Fixed, fluorescently-labeled PRP was prepared from human blood obtained from healthy human donors via venipuncture collection in 3.2% sodium citrate vacutainers per Carnegie Mellon University IRB Protocol HS12-504. PRP was prepared by centrifugation of vacutainers at 250xg for 15 minutes at 22°C. PRP was then transferred to a polypropylene tube and incubated with 5 μM final concentration of mepacrine, a granular dye, to stain platelets [71]. After incubation, stained platelets were fixed in 1% paraformaldehyde (USB Corporation, Cleveland, OH) and washed twice in PBS to remove excess dye and paraformaldehyde. Gentamicin (0.25 mg/L, Gentamax 100, Nature Vets) was added to fixed

dyed PRP to prevent bacterial growth. Fixed dyed platelets were used within seven days of preparation. Platelet counts were performed for human PRP before and after the washing procedure using the Countess Automated Cell Counter (Life Technologies, Grand Island, NY). Additional platelet counts were performed for baseline and post-shear samples collected from the microchannel experiments.

GRBC and fixed dyed PRP were prepared (n=4 each). Suspensions of 20% GRBC and ~300,000 fixed dyed platelets/µl in 3.5% Dextran 70 solution (n=4), 30% GRBC and ~300,000 fixed dyed platelets/µl in 3% Dextran 70 solution (n=1), and 40% GRBC and ~300,000 fixed dyed platelets/µl in 1% Dextran 70 solution (n=3) were prepared and the viscosity of all tested suspensions was measured using a Wells-Brookfield Cone/Plate viscometer (DVIII+, Middleboro, MA) at shear rates of 10-500 s^{-1} and a 25°C temperature. The viscosity of all tested suspensions was 4.4 ± 0.5 cP at a 200 s^{-1} shear rate.

Microchannel fabrication was performed by Dr. Chen of the Pekkan Laboratory of Carnegie Mellon University. The channel design is shown in **Figure G. 1**. The channel geometry had a height of 100 µm and width containing a 100 µm:200 µm backward step. The length of each width section was 500 µm. The channels were fabricated in polydimethylsiloxane (PDMS) and sealed on glass coverslips using corona treatment.

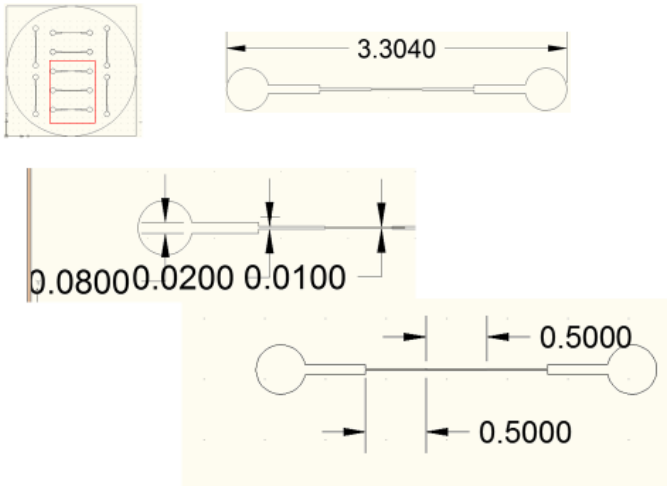

Figure G. 1. Design of a backward step microchannel to study the trafficking of GRBC and fluorescently-dyed platelets under flow conditions that may promote thrombosis in the assisted blood circulation. Units are shown in centimeters.

All microchannels were rinsed twice with sterile filtered PBS and incubated with sterile filtered 1% BSA for 30 minutes prior to testing to passivate all cell-contacting surfaces. Suspensions were driven through the custom fabricated PDMS microchannels at flow rates of 0.25, 0.5 and 1.0 ml/min. The flow system consisted of a syringe pump (PHD2000, Harvard Apparatus), an inlet pressure transducer (R-07356-61, Cole-Parmer Instrument Company), 5 ml syringe, and a microchannel on the stage of a microscope. The microchannel was visualized through an inverted fluorescent microscope (IX70, Olympus Inc., Melville, NY) with a 40X objective (Olympus Inc.). A high speed camera (FastCam SA4, Photron USA Inc., San Diego, CA) attached to the side port of the microscope was used to capture magnified images of GRBC (Brightfield visualization) and platelets (fluorescent visualization) along the span of the microchannel. A personal computer with Photron FASTCAM Viewer software was used to record video of flowing GRBC and platelets in several regions of interest (ROI) in the microchannel (**Figure G. 2**).

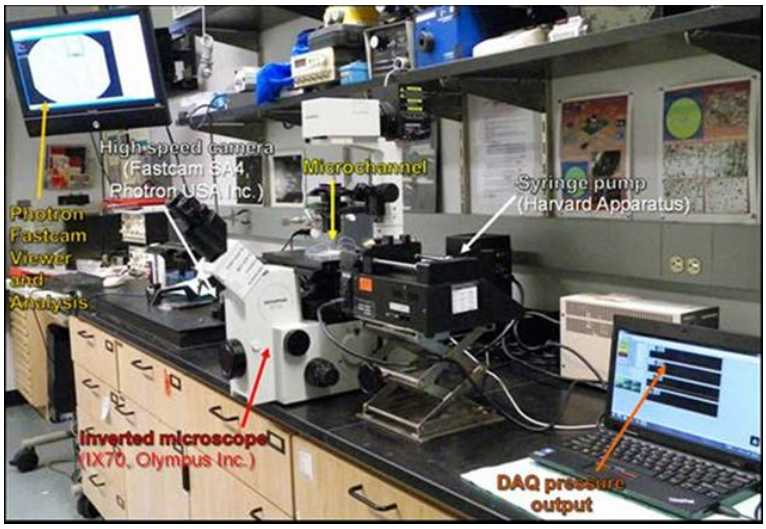

Figure G. 2. Experimental system for the study of trafficking of GRBC and platelets or platelet-sized particles in several microchannel geometries.

G.2.2 Results and Discussion

20% GRBC and ~300,000 fixed, dyed platelets/µl at flow rates of 0 and 0.5 ml/min flowing through the 100µm:200µm sudden expansion are shown in **Figure G. 3**. Fixed, fluorescent platelets were not well visualized using the PDMS sudden expansion microchannels prepared by the Pekkan Laboratory at Carnegie Mellon University. It was found that fixed, dyed platelets adhered to the surface of PDMS and thus concluded that these microchannels were not suitable for additional studies. For continuing microchannel experiments with fixed dyed platelets and GRBC, straight microchannels were purchased from a commercial source (ibidi, LLC).

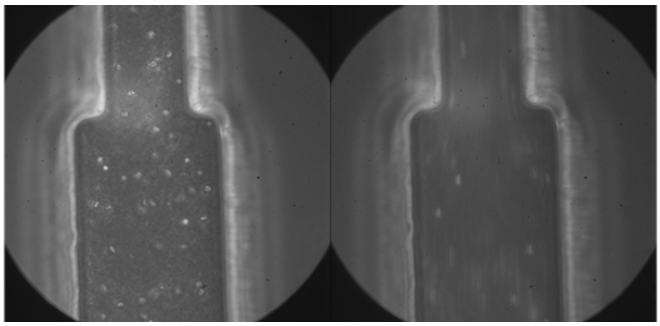

Figure G. 3. 20% hematocrit human GRBC and fluorescent platelets flowing through a 100:200 μm sudden expansion in microchannel at 0 ml/min (left) and 0.5 ml/min (right).

40x magnification. Field of view is 500 μm by 500 μm.

G.3 TRAFFICKING OF ERYTHROCYTE GHOSTS AND PLATELETS IN A STRAIGHT MICROCHANNEL

G.3.1 Methods

GRBC were prepared according to the protocol described in **Section 6.2** and fixed, fluorescently-labeled platelets were prepared according to the protocol described in **Section G.2.1** (n=3 each). Suspensions of 20% GRBC and ~300,000 fixed dyed platelets/μl in 3.5% Dextran 70 solution (n=14), 30% GRBC and ~300,000 fixed dyed platelets/μl in 3% Dextran 70 solution (n=3), and 40% GRBC and ~300,000 fixed dyed platelets/μl in 2.5% Dextran 70 solution (n=9) were prepared and the viscosity of all tested suspensions was measured using a Wells-Brookfield Cone/Plate viscometer (DVIII+, Middleboro, MA) at shear rates of 10-500 s^{-1} and a 25°C temperature. The viscosity of all tested suspensions was 5.0 ± 0.3 cP at a 200 s^{-1} shear rate. The straight microchannels (μ–Slide I 0.1 Luer, ibidi LLC) had a height of 100 μm, width of 5 mm

and length of 50 mm. All microchannels were rinsed twice with sterile filtered PBS and incubated with sterile filtered 1% BSA for 30 minutes prior to testing to passivate all cell-contacting surfaces. The flow system described in **Section G.2.1** was used to examine test suspensions at controlled flow rates of 0.10, 0.25, 0.5 and 1.0 ml/min corresponding to Re ~0.1-0.7 and wall shear stresses of 6-18 Pa in the straight microchannels.

G.3.2 Results and Discussion

Figure G. 4 shows 20% GRBC and ~300,000 fixed, dyed platelets/µl flowing through the straight microchannel near the wall at flow rates of 0.1, 0.25 and 0.5 ml/min. Fixed, fluorescent platelets were not well visualized using the PDMS microchannels or the ibidi straight microchannels. For continuing microchannel experiments, It was chosen to replace platelets with platelet-sized fluorescent particles (Duke Scientific Corporation) and use a Y-bifurcation microchannel from a commercial source (CFD Research Corporation).

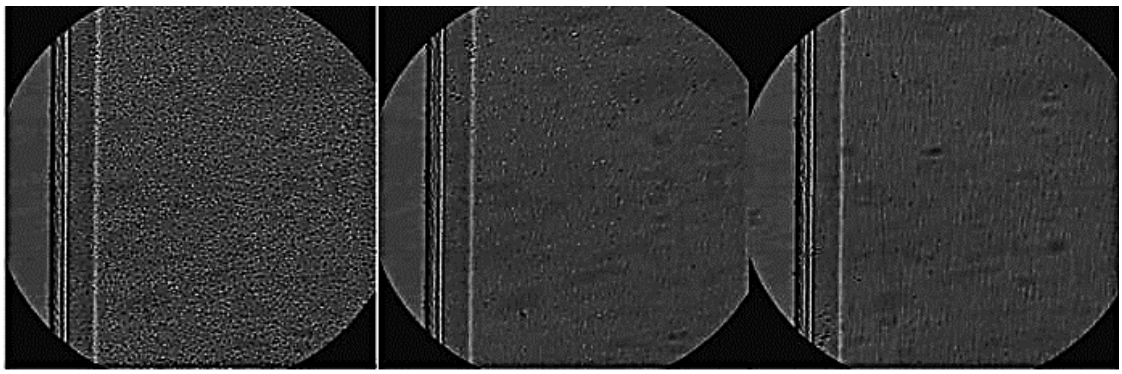

Figure G. 4. 20% hematocrit human GRBC and fluorescent platelets flowing through a 100 µm height straight channel near the wall at 0.1 ml/min (left), 0.25 ml/min (middle) and 0.5 ml/min (right).
40x magnification. Field of view in each image is 500 µm by 500 µm.

G.4 TRAFFICKING OF ERYTHROCYTE GHOSTS AND PLATELET-SIZED PARTICLES IN A Y-BIFURCATION MICROCHANNEL

G.4.1 Methods

GRBC were prepared according to the protocol described in **Section 6.2** (n=4). Platelet-sized fluorescent polystyrene particles (2 μm diameter, #R0200) were purchased from Duke Scientific Corporation. Suspensions of 20% GRBC and ~1,000,000 PSFP/μl in 30% Dextran 40 solution (n=8), 30% GRBC and ~1,000,000 fixed dyed platelets/μl in 25% Dextran 40 solution (n=8) and 40% GRBC and ~1,000,000 fixed dyed platelets/μl in 20% Dextran 40 solution (n=7) were prepared. The viscosity of all tested suspensions was measured using a Wells-Brookfield Cone/Plate viscometer (DVIII+, Middleboro, MA) at shear rates of 10-100 s^{-1} and a 25°C temperature. The viscosity of all tested suspensions was 20 ± 2 cP at a 100 s^{-1} shear rate. All microchannels were rinsed twice with sterile filtered PBS and incubated with sterile filtered 1% BSA for 30 minutes prior to testing to passivate all cell-contacting surfaces. Suspensions were pulled through SynVivo microvascular network channels (Lot# 2-015, 100 μm height, 100 μm width) at withdrawal flow rates of 5, 10, 15, 25, 50 and 100 μl/min corresponding to Re ~5-100 and wall shear stresses -20--500 Pa.

The flow system consisted of a syringe pump (PHD2000, Harvard Apparatus), 200 μl pipet tip (fluid inlet), small cap over the inlet (prevent debris from entering the channel), an outlet pressure transducer (Abbott Laboratories), 5 ml syringe, and a microchannel on the stage of a microscope (**Figure G. 5**). The microchannel was visualized through an inverted fluorescent microscope (IX70, Olympus Inc., Melville, NY) with a 20X, 40X or 100X objective (Olympus

Inc.). A high speed camera (FastCam SA4, Photron USA Inc., San Diego, CA) attached to the side port of the microscope was used to capture magnified images of GRBC (Brightfield visualization) and PSFP (fluorescent visualization) and a personal computer with Photron FASTCAM Viewer software was used to record video of flowing GRBC and PSFP in several ROI in the microchannel.

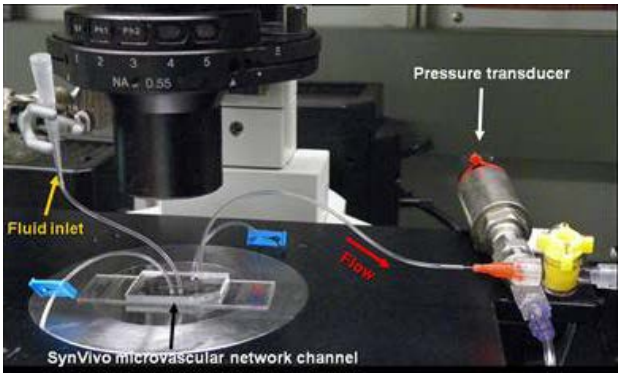

Figure G. 5. Close up view of the flow system used for the study of trafficking of GRBC and PSFP in several microchannel geometries.

G.4.2 Results

Figure G. 6 shows 20% GRBC and ~1,000,000 PSFP/µl, 30% GRBC and ~1,000,000 PSFP/µl and 40% GRBC and ~1,000,000 PSFP/µl flowing through a straight section of the microchannel at flow rates of 5, 25 and 50 µl/min. **Figure G. 7** shows the same suspensions flowing through a Y-bifurcation section of the microchannel at flow rates of 5, 25 and 50 µl/min.

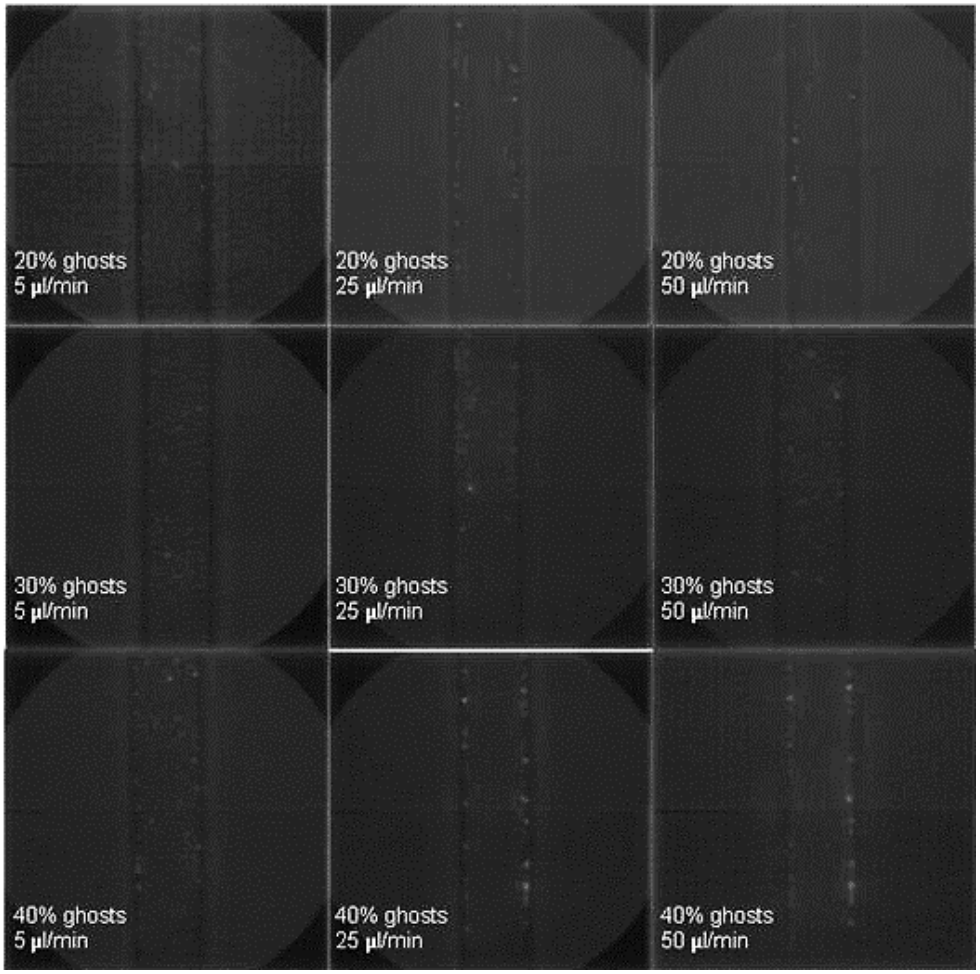

Figure G. 6. 20% GRBC and ~1,000,000 PSFP/µl in 30% Dextran 40 solution [top row], 30% GRBC and ~1,000,000 PSFP/µl in 25% Dextran 40 solution [middle row], and 40% GRBC and ~1,000,000 PSFP/µl in 20% Dextran 40 solution [bottom row] flowing through a straight section of the microchannel at 5 µl/min [left column], 25 µl/min [middle column], and 50 µl/min [right column]. 40x magnification.

Field of view in each image is 500 µm by 500 µm.

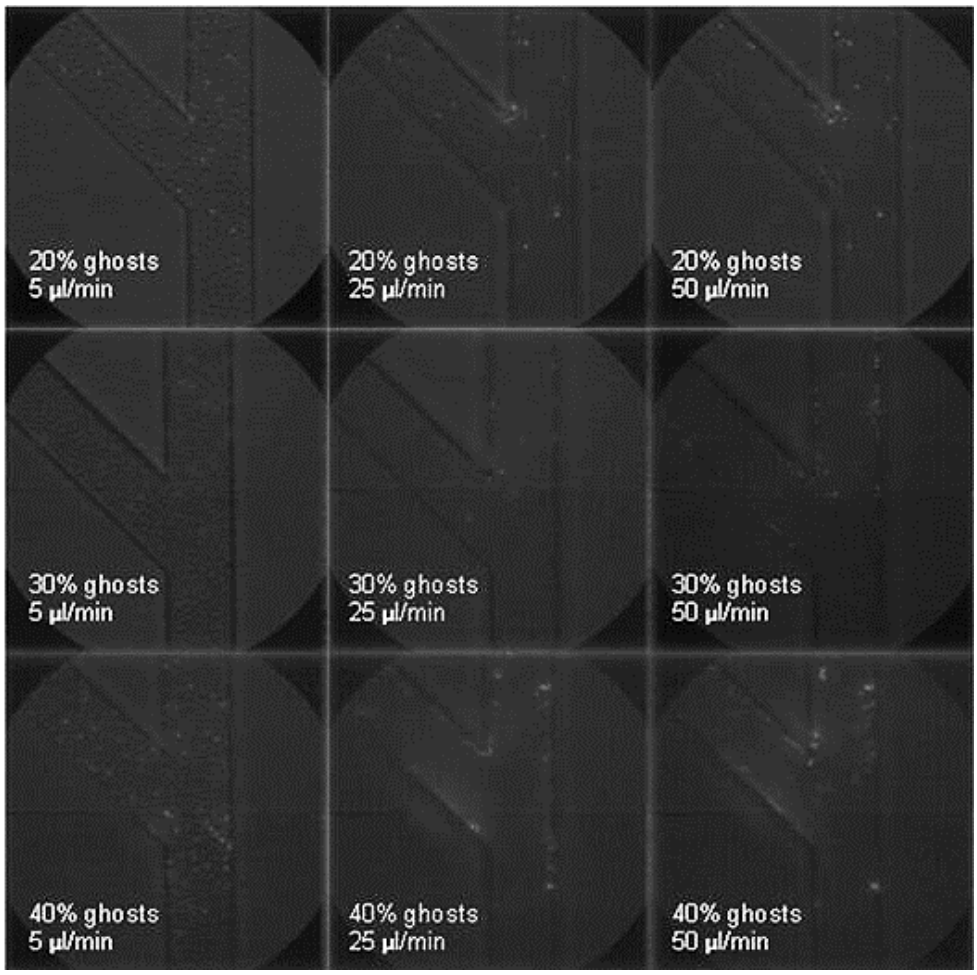

Figure G. 7. 20% GRBC and ~1,000,000 PSFP/µl in 30% Dextran 40 solution [top row], 30% GRBC and ~1,000,000 PSFP/µl in 25% Dextran 40 solution [middle row], and 40% GRBC and ~1,000,000 PSFP/µl in 20% Dextran 40 solution [bottom row] flowing through a Y-bifurcation section of the microchannel at 5 µl/min [left column], 25 µl/min [middle column], and 50 µl/min [right column].

40x magnification. Field of view in each image is 500 µm by 500 µm.

G.5 DISCUSSION

This study showed regions of elevated platelet-sized particle concentrations in straight and Y-bifurcation microchannel geometries over a range of flow conditions relevant to the operation of CAD. Suspensions of 20% and 30% GRBC with the same particle concentration produced similar cell/particle distributions and areas of particle adhesion. This study preceded the study described in **Chapter 7** characterized the trafficking of 20% and 40% GRBC and 1,000,000 PSFP/µl suspensions in novel, custom-fabricated microchannel geometries.

BIBLIOGRAPHY

1. Shen, S.C., T.H. Ham, and E.M. Fleming, *Studies on the Destruction of Red Blood Cells.* New England Journal of Medicine, 1943. **229**(19), 701-713.

2. Kusserow, B.K. and J.F. Clapp, 3rd, *Partial substitution of ventricular function over extended periods by a mechanical pump.* Trans Am Soc Artif Intern Organs, 1961. **7**, 332-342.

3. Brinsfield, D.E., M.A. Hopf, R.B. Geering, and P.M. Galletti, *Hematological changes in long-term perfusion.* J Appl Physiol, 1962. **17**(3), 531-534.

4. Bernstein, E.F., A.R. Castaneda, and R.L. Varco, *Some Biologic Limitations to Prolonged Blood Pumping.* Trans Am Soc Artif Intern Organs, 1965. **11**, 118-121.

5. Blackshear, P.L., Jr., F.D. Dorman, and J.H. Steinbach, *Some Mechanical Effects That Influence Hemolysis.* Trans Am Soc Artif Intern Organs, 1965. **11**, 112-117.

6. Brown, C.H., 3rd, R.F. Lemuth, J.D. Hellums, L.B. Leverett, and C.P. Alfrey, *Response of human platelets to shear stress.* Trans Am Soc Artif Intern Organs, 1975. **21**, 35-39.

7. Johnson, C.A., Jr., S. Vandenberghe, A.R. Daly, J.R. Woolley, S.T. Snyder, J.E. Verkaik, et al., *Biocompatibility assessment of the first generation PediaFlow pediatric ventricular assist device.* Artif Organs, 2011. **35**(1), 9-21.

8. Maul, T.M., E. Kocyildirim, C.A. Johnson, Jr., A.R. Daly, S.E. Olia, J.R. Woolley, et al., *In Vitro and In Vivo Performance Evaluation of the Second Developmental Version of the PediaFlow Pediatric Ventricular Assist Device.* Cardiovasc Eng Technol, 2011. **2**(4), 253-262.

9. Hung, T.C., R.M. Hochmuth, J.H. Joist, and S.P. Sutera, *Shear-induced aggregation and lysis of platelets.* Trans Am Soc Artif Intern Organs, 1976. **22**, 285-291.

10. Karino, T. and H.L. Goldsmith, *Aggregation of human platelets in an annular vortex distal to a tubular expansion.* Microvasc Res, 1979. **17**(3 Pt 1), 217-237.

11. Johnston, G.G., U. Marzec, and E.F. Berstein, *Effects of surface injury and shear stress on platelet aggregation and serotonin release.* Trans Am Soc Artif Intern Organs, 1975. **21**, 413-421.

12. Bernstein, E.F., R.A. Indeglia, M.A. Shea, and R.L. Varco, *Sublethal damage to the red blood cell from pumping.* Circulation, 1967. **35**(4 Suppl), I226-233.

13. Indeglia, R.A., M.A. Shea, R. Forstrom, and E.F. Bernstein, *Influence of mechanical factors on erythrocyte sublethal damage.* Trans Am Soc Artif Intern Organs, 1968. **14**, 264-272.

14. Sandza, J.G., Jr., R.E. Clark, C.S. Weldon, and S.P. Sutera, *Subhemolytic trauma of erythrocytes: recognition and sequestration by the spleen as a function of shear.* Trans Am Soc Artif Intern Organs, 1974. **20 B**, 457-462.

15. Sutera, S.P., *Flow-induced trauma to blood cells.* Circ Res, 1977. **41**(1), 2-8.

16. Smedira, N.G., K.J. Hoercher, B. Lima, M.M. Mountis, R.C. Starling, L. Thuita, et al., *Unplanned Hospital Readmissions After HeartMate II Implantation: Frequency, Risk Factors, and Impact on Resource Use and Survival.* JACC: Heart Failure, 2013. **1**(1), 31-39.

17. Rampling, M.W., *Compositional Properties of Blood*, in *Handbook of Hemorheology and Hemodynamics*, O.K. Baskurt, et al., Editors. 2007, IOS Press: Amsterdam. 34-44.

18. Fung, Y.C., *Blood flow in the capillary bed.* J Biomech, 1969. **2**(4), 353-372.

19. Schmid-Schonbein, G.W., Y.Y. Shih, and S. Chien, *Morphometry of human leukocytes.* Blood, 1980. **56**(5), 866-875.

20. Cokelet, G.R. and H.J. Meiselman, *Rheological comparison of hemoglobin solutions and erythrocyte suspensions.* Science, 1968. **162**(850), 275-277.

21. Viallat, A. and M. Abkarian, *Red blood cell: from its mechanics to its motion in shear flow.* International Journal of Laboratory Hematology, 2014. **36**(3), 237-243.

22. Wintrobe, M.M., *Clinical Hematology*. 6 ed. 1967, Philadelphia: Lea & Febiger.

23. Copley, A.L., *The rheology of blood. A survey.* Journal of Colloid Science, 1952. **7**(3), 323-333.

24. Fåhraeus, R., *Suspension stability of blood.* Physiological Reviews, 1929. **9**, 241.

25. Fåhraeus, R. and T. Lindqvist, *The viscosity of blood in narrow capillary tubes.* Am. J. Physiol, 1931. **96**(3), 562-568.

26. Fåhraeus, R., *Über die Ursachen der verminderten Suspensionsstabilität der Blutkörperchen während der Schwangerschaft.* Biochem Z, 1918. **89**, 355-364.

27. Fåhraeus, R., *The suspension stability of the blood.* Acta Med Scand, 1921. **55**, 1-228.

28. Brundage, J.T., *Blood and plasma viscosity determined by the method of concentric cylinders.* Am J Physiol, 1934. **110**(3), 659-665.

29. Copley, A.L., L.C. Krchma, and M.E. Whitney, *Humoral Rheology : I. Viscosity Studies and Anomalous Flow Properties of Human Blood Systems with Heparin and Other Anticoagulants.* J Gen Physiol, 1942. **26**(1), 49-64.

30. Wells, R.E., Jr. and E.W. Merrill, *Shear rate dependence of the viscosity of whole blood and plasma.* Science, 1961. **133**(3455), 763-764.

31. Cokelet, G.R., E.W. Merrill, E.R. Gilliland, and H. Shin, *The rheology of human blood-measurement near and at zero shear rate.* Trans Soc Rheology, 1963. **7**, 303-317.

32. Thurston, G.B., *Viscoelasticity of human blood.* Biophysical Journal, 1972. **12**(9), 1205-1217.

33. Thurston, G.B., *Frequency and shear rate dependence of viscoelasticity of human blood.* Biorheology, 1973. **10**(3), 375-381.

34. Dintenfass, L., *Thixotrophy of blood and proneness to thrombus formation.* Circulation Research, 1962. **11**, 233-239.

35. Thurston, G.B., *Rheological parameters for the viscosity viscoelasticity and thixotropy of blood.* Biorheology, 1979. **16**(3), 149-162.

36. Stoltz, J.F. and M. Lucius, *Viscoelasticity and thixotropy of human blood.* Biorheology, 1981. **18**(3-6), 453-473.

37. Cokelet, G.R. and H.J. Meiselman, *Macro- and Mico-Rheological Properties of Blood*, in *Handbook of Hemorheology and Hemodynamics*, O.K. Baskurt, et al., Editors. 2007, IOS Press: Amsterdam. 45-71.

38. Chien, S., S. Usami, R.J. Dellenback, and M.I. Gregersen, *Blood viscosity: influence of erythrocyte deformation.* Science, 1967. **157**, 827.

39. Chien, S., S. Usami, R.J. Dellenback, M.I. Gregersen, L.B. Nanninga, and M.M. Guest, *Blood viscosity: influence of erythrocyte aggregation.* Science, 1967. **157**(3790), 829-831.

40. Schmid-Schonbein, H., P. Gaehtgens, and H. Hirsch, *On the shear rate dependence of red cell aggregation in vitro.* J Clin Invest, 1968. **47**(6), 1447-1454.

41. Casson, N. *A flow equation for pigment-oil dispersions of the printing ink type*. in *Conference of University College*. 1957. Swansea: Pergamon Press.

42. Pries, A.R. and T.W. Secomb, *Rheology of the microcirculation.* Clin Hemorheol Microcirc, 2003. **29**(3-4), 143-148.

43. Cokelet, G.R., *Poiseuille Award Lecture. Viscometric, in vitro and in vivo blood viscosity relationships: how are they related?* Biorheology, 1999. **36**(5-6), 343-358.

44. Secomb, T.W. and A.R. Pries, *Basic Principles of Hemodynamics*, in *Handbook of Hemorheology and Hemodynamics*, O.K. Baskurt, et al., Editors. 2007, IOS Press: Amsterdam. 289-306.

45. Brånemark, P.I. and U. Bagge, *Erythrocytes, leukocytes and platelets in the human microcirculation*, in *Symposium on Hemorheology and Diseases*, J.F. Stoltz and P. Drouin, Editors. 1980, P. Doin Editeurs: Paris.

46. Smith, H.P., H.R. Arnold, and G.H. Whipple, *Comparative values of Welcker, carbon monoxide and dye methods for blood volume determinations. Accurate estimation of absolute blood volume.* Am J Physiol, 1921. **56**, 336-360.

47. Dintenfass, L., *Inversion of the Fahraeus-Lindqvist phenomenon in blood flow through capillaries of diminishing radius.* Nature, 1967. **215**(5105), 1099-1100.

48. Barbee, J.H. and G.R. Cokelet, *The Fahraeus effect.* Microvasc Res, 1971. **3**(1), 6-16.

49. Whittaker, S.R. and F.R. Winton, *The apparent viscosity of blood flowing in the isolated hindlimb of the dog, and its variation with corpuscular concentration.* J Physiol, 1933. **78**(4), 339-369.

50. Lipowsky, H.H., S. Usami, and S. Chien, *In vivo measurements of "apparent viscosity" and microvessel hematocrit in the mesentery of the cat.* Microvasc Res, 1980. **19**(3), 297-319.

51. Thurston, G.B., *Viscoelastic properties of blood and blood analogs*, in *Advances in Hemodynamics and Hemorheology*, T.C. Howe, Editor. 1996, JAI Press. 1-30.

52. Skalak, R. and P.I. Branemark, *Deformation of red blood cells in capillaries.* Science, 1969. **164**(3880), 717-719.

53. Braasch, D., *Red Cell Deformability and Capillary Blood Flow*. Physiol Rev, 1971. **51**(4), 679-701.

54. Rheology, I.E.P.o.B., *Guidelines for Measurement of Blood Viscosity and Erythrocyte Deformability.* Clin Hemorheol, 1986. **6**, 439-453.

55. Fung, Y.C., *Biomechanics: Mechanical Properties of Living Tissues* 1993, New York: Springer.

56. Kameneva, M.V. and J.F. Antaki, *Mechanical trauma to blood*, in *Handbook of Hemorheology and Hemodynamics*, O.K. Baskurt, et al., Editors. 2007, IOS Press: Amsterdam. 206-227.

57. Sutera, S.P., R.A. Gardner, C.W. Boylan, G.L. Carroll, K.C. Chang, J.S. Marvel, et al., *Age-related changes in deformability of human erythrocytes.* Blood, 1985. **65**(2), 275-282.

58. Kameneva, M.V., J.F. Antaki, H.S. Borovetz, B.P. Griffith, K.C. Butler, K.K. Yeleswarapu, et al., *Mechanisms of red blood cell trauma in assisted circulation. Rheologic similarities of red blood cell transformations due to natural aging and mechanical stress.* ASAIO J, 1995. **41**(3), M457-460.

59. Nash, G.B. and H.J. Meiselman, *Alteration of red cell membrane viscoelasticity by heat treatment: effect on cell deformability and suspension viscosity.* Biorheology, 1985. **22**(1), 73-84.

60. Stuart, J., *Erythrocyte Deformability*, in *Clinical Blood Rheology*, G. Lowe, Editor. 1988, CRC Press: Boca Raton.

61. Raval, J.S., J.H. Waters, A. Seltsam, E.A. Scharberg, E. Richter, A.R. Daly, et al., *The use of the mechanical fragility test in evaluating sublethal RBC injury during storage.* Vox Sang, 2010. **99**(4), 325-331.

62. Daly, A., J.S. Raval, J.H. Waters, M.H. Yazer, and M.V. Kameneva, *Effect of blood bank storage on the rheological properties of male and female donor red blood cells.* Clin Hemorheol Microcirc, 2014. **56**(4), 337-345.

63. Kameneva, M.V., A. Undar, J.F. Antaki, M.J. Watach, J.H. Calhoon, and H.S. Borovetz, *Decrease in red blood cell deformability caused by hypothermia, hemodilution, and mechanical stress: factors related to cardiopulmonary bypass.* ASAIO J, 1999. **45**(4), 307-310.

64. Kameneva, M.V., P.F. Marad, J.M. Brugger, B.M. Repko, J.H. Wang, J. Moran, et al., *In vitro evaluation of hemolysis and sublethal blood trauma in a novel subcutaneous vascular access system for hemodialysis.* ASAIO J, 2002. **48**(1), 34-38.

65. Trevan, J.W., *The Viscosity of Blood.* Biochem J, 1918. **12**(1-2), 60-71.

66. Couette, M.M., *Etudes sur le frottement des liquides.* Ann Chim Phys, 1890. **21**, 433-510.

67. Taylor, G.I., *Fluid Friction between Rotating Cylinders. II. Distribution of Velocity between Concentric cylinders when Outer One is Rotating and Inner One Is at Rest.*

Proceedings of the Royal Society of London. Series A, Mathematical and Physical Sciences, 1936. **157**(892), 565-578.

68. Wells, R.E., Jr., R. Denton, and E.W. Merrill, *Measurement of viscosity of biologic fluids by cone plate viscometer.* J Lab Clin Med, 1961. **57**, 646-656.

69. Berga, L., J. Dolz, J.L. Vives-Corrons, E. Feliu, and C. Rozman, *Viscometric methods for assessing red cell deformability and fragmentation.* Biorheology Suppl, 1984. **1**, 297-301.

70. Daly, A.R., H. Sobajima, S.E. Olia, S. Takatani, and M.V. Kameneva, *Application of drag-reducing polymer solutions as test fluids for in vitro evaluation of potential blood damage in blood pumps.* ASAIO J, 2010. **56**(1), 6-11.

71. Jamiolkowski, M.A., J.R. Woolley, M.V. Kameneva, J.F. Antaki, and W.R. Wagner, *Real time visualization and characterization of platelet deposition under flow onto clinically relevant opaque surfaces.* J Biomed Mater Res A, 2015. **103**(4), 1303-1311.

72. Chmiel, H., I. Anadere, and E. Walitza, *The determination of blood viscoelasticity in clinical hemorheology.* Biorheology, 1990. **27**(6), 883-894.

73. Roger, V.L., A.S. Go, D.M. Lloyd-Jones, E.J. Benjamin, J.D. Berry, W.B. Borden, et al., *Heart disease and stroke statistics--2012 update: a report from the American Heart Association.* Circulation, 2012. **125**(1), e2-e220.

74. Institute, N.H.L.a.B. *The Heart Transplant Waiting List*. 2014; Available from: http://www.nhlbi.nih.gov/health//dci/Diseases/ht/ht_before.html.

75. Rose, E.A., A.C. Gelijns, A.J. Moskowitz, D.F. Heitjan, L.W. Stevenson, W. Dembitsky, et al., *Long-term use of a left ventricular assist device for end-stage heart failure.* N Engl J Med, 2001. **345**(20), 1435-1443.

76. Long, J.W., A.G. Kfoury, M.S. Slaughter, M. Silver, C. Milano, J. Rogers, et al., *Long-term destination therapy with the HeartMate XVE left ventricular assist device: improved outcomes since the REMATCH study.* Congest Heart Fail, 2005. **11**(3), 133-138.

77. Galletti, P.M., F.J. Martinez, D.E. Brinsfield, and E.C. Peirce, 2nd, *A pediatric perfusion system.* Trans Am Soc Artif Intern Organs, 1963. **9**, 244-250.

78. Galletti, P.M., *Laboratory Experience with 24 Hour Partial Heart-Lung Bypass.* J Surg Res, 1965. **5**, 97-104.

79. Bernstein, E.F., P.L. Blackshear, Jr., and K.H. Keller, *Factors influencing erythrocyte destruction in artificial organs.* Am J Surg, 1967. **114**(1), 126-138.

80. Bernstein, E.F. and L.R. Gleason, *Factors influencing hemolysis with roller pumps.* Surgery, 1967. **61**(3), 432-442.

81. Indeglia, R.A., M.A. Shea, R.L. Varco, and E.F. Bernstein, *Mechanical and biologic considerations in erythrocyte damage.* Surgery, 1967. **62**, 47-55.

82. Kusserow, B.K., B. Machanic, F.M. Collins, Jr., and J.F. Clapp, 3rd, *Changes Observed in Blood Corpuscles after Prolonged Perfusions with Two Types of Blood Pumps.* Trans Am Soc Artif Intern Organs, 1965. **11**, 122-126.

83. Sutera, S.P., P.A. Croce, and M. Mehrjardi, *Hemolysis and subhemolytic alterations of human RBC induced by turbulent shear flow.* Trans Am Soc Artif Intern Organs, 1972. **18**(0), 335-341, 347.

84. Dormandy, J.A., P.N. Matthews, A.J. Dodds, and P.T. Flute, *Effect of operations on red blood cell deformability,* in *Symposium on Hemorheology and Diseases*, J.F. Stoltz and P. Drouin, Editors. 1980, P. Doin Editeurs: Paris. 451-454.

85. Baker, L.C., W.C. Davis, J. Autieri, M.J. Watach, K. Yamazaki, P. Litwak, et al., *Flow cytometric assays to detect platelet activation and aggregation in device-implanted calves.* J Biomed Mater Res, 1998. **41**(2), 312-321.

86. Snyder, T.A., M.J. Watach, K.N. Litwak, and W.R. Wagner, *Platelet activation, aggregation, and life span in calves implanted with axial flow ventricular assist devices.* Ann Thorac Surg, 2002. **73**(6), 1933-1938.

87. Snyder, T.A., K.N. Litwak, H. Tsukui, T. Akimoto, S. Kihara, K. Yamazaki, et al., *Leukocyte-platelet aggregates and monocyte tissue factor expression in bovines implanted with ventricular assist devices.* Artif Organs, 2007. **31**(2), 126-131.

88. Snyder, T.A., H. Tsukui, S. Kihara, T. Akimoto, K.N. Litwak, M.V. Kameneva, et al., *Preclinical biocompatibility assessment of the EVAHEART ventricular assist device: coating comparison and platelet activation.* J Biomed Mater Res A, 2007. **81**(1), 85-92.

89. Woolley, J.R., J.J. Teuteberg, C.A. Bermudez, J.K. Bhama, K.L. Lockard, R.L. Kormos, et al., *Temporal Leukocyte Numbers and Granulocyte Activation in Pulsatile and Rotary Ventricular Assist Device Patients.* Artif Organs, 2013.

90. Hung, T.C., D.B. Butter, R.L. Kormos, Z. Sun, H.S. Borovetz, B.P. Griffith, et al., *Characteristics of blood rheology in patients during Novacor left ventricular assist system support.* ASAIO Transactions, 1989. **35**(3), 611-613.

91. Schima, H., M.R. Muller, D. Papantonis, C. Schlusche, L. Huber, C. Schmidt, et al., *Minimization of hemolysis in centrifugal blood pumps: influence of different geometries.* Int J Artif Organs, 1993. **16**(7), 521-529.

92. Antaki, J.F., C.G. Diao, F.J. Shu, J.C. Wu, R. Zhao, and M.V. Kameneva, *Microhaemodynamics within the blade tip clearance of a centrifugal turbodynamic blood pump.* Proc Inst Mech Eng H, 2008. **222**(4), 573-581.

93. Kim, N.J., C. Diao, K.H. Ahn, S.J. Lee, M.V. Kameneva, and J.F. Antaki, *Parametric study of blade tip clearance, flow rate, and impeller speed on blood damage in rotary blood pump.* Artif Organs, 2009. **33**(6), 468-474.

94. Antaki, J.F., G.W. Burgreen, Z.J. Wu, D. Borzelleca, M.V. Kameneva, J.A. Holmes, et al., *Development Progress of the University of Pittsburgh Streamliner: A Mixed Flow Blood Pump with Magnetic Bearings.* ASAIO J, 2000. **46**, 194.

95. Borovetz, H.S., S. Badylak, J.R. Boston, C. Johnson, R. Kormos, M.V. Kameneva, et al., *Towards the development of a pediatric ventricular assist device.* Cell Transplant, 2006. **15 Suppl 1**, S69-74.

96. Kusserow, B.K. and L.W. Kendall, *In vitro changes in the corpuscular elements of blood flowing in tubular conduits.* Trans Am Soc Artif Intern Organs, 1963. **9**, 262-268.

97. Nevaril, C.G., E.C. Lynch, C.P. Alfrey, Jr., and J.D. Hellums, *Erythrocyte damage and destruction induced by shearing stress.* J Lab Clin Med, 1968. **71**(5), 784-790.

98. Leverett, L.B., J.D. Hellums, C.P. Alfrey, and E.C. Lynch, *Red blood cell damage by shear stress.* Biophys J, 1972. **12**(3), 257-273.

99. Kusserow, B.K. and J.F. Clapp, 3rd, *A small ventricle-type pump for prolonged perfusions: construction and initial studies, including attempts to power a pump biologically with skeletal muscle.* Trans Am Soc Artif Intern Organs, 1964. **10**, 74-78.

100. Kusserow, B.K. and J.F. Clapp, *Red blood cell survival after prolonged perfusion with a blood pump.* Trans Am Soc Artif Intern Organs, 1966. **12**, 121-123.

101. Blackshear, P.L., Jr., F.D. Dorman, J.H. Steinbach, E.J. Maybach, A. Singh, and R.E. Collingham, *Shear, wall interaction and hemolysis.* Trans Am Soc Artif Intern Organs, 1966. **12**, 113-120.

102. Blackshear, P.L., Jr., R.J. Forstrom, F.D. Dorman, and G.O. Voss, *Effect of flow on cells near walls.* Fed Proc, 1971. **30**(5), 1600-1611.

103. Shapiro, S.I. and M.C. Williams, *Hemolysis in simple shear flows.* AIChE Journal, 1970. **16**, 575-580.

104. Sutera, S.P. and M.H. Mehrjardi, *Deformation and fragmentation of human red blood cells in turbulent shear flow.* Biophys J, 1975. **15**(1), 1-10.

105. Sallam, A.M. and N.H.C. Hwang, *Human red blood cell hemoloysis in a turbulent shear flow: Contribution of Reynolds shear stresses.* Biorheology, 1984. **21**, 783-797.

106. Kameneva, M.V., G.W. Burgreen, K. Kono, B. Repko, J.F. Antaki, and M. Umezu, *Effects of turbulent stresses upon mechanical hemolysis: experimental and computational analysis.* ASAIO J, 2004. **50**(5), 418-423.

107. Stewart, J.W. and M.F. Sturridge, *Haemolysis caused by tubing in extracorporeal circulation.* Lancet, 1959. **1**(7068), 340-342.

108. Champion, J.V., P.F. North, W.T. Coakley, and A.R. Williams, *Shear fragility of human erythrocytes.* Biorheology, 1971. **8**, 23-29.

109. Bacher, R.P. and M.C. Williams, *Hemolysis in capillary flow.* J Lab Clin Med, 1970. **76**(3), 485-496.

110. Williams, A.R., D.E. Hughes, and W.L. Nyborg, *Hemolysis near a transversely oscillating wire.* Science, 1970. **169**(3948), 871-873.

111. Rooney, J.A., *Hemolysis near an ultrasonically pulsating gas bubble.* Science, 1970. **169**(3948), 869-871.

112. Giersiepen, M., L.J. Wurzinger, R. Opitz, and H. Reul, *Estimation of shear stress-related blood damage in heart valve prostheses--in vitro comparison of 25 aortic valves.* Int J Artif Organs, 1990. **13**(5), 300-306.

113. Song, X., A.L. Throckmorton, H.G. Wood, J.F. Antaki, and D.B. Olsen, *Computational fluid dynamics prediction of blood damage in a centrifugal pump.* Artificial Organs, 2003. **27**(10), 938-941.

114. Song, X., A.L. Throckmorton, H.G. Wood, J.F. Antaki, and D.B. Olsen, *Quantitative Evaluation of Blood Damage in a Centrifugal VAD by Computational Fluid Dynamics.* Journal of Fluids Engineering, 2004. **126**, 410-418.

115. Schmid-Schönbein, H. and R. Wells, *Fluid drop-like transition of erythrocytes under shear.* Science, 1969. **165**(3890), 288-291.

116. Fischer, T.M., M. Stohr-Lissen, and H. Schmid-Schonbein, *The red cell as a fluid droplet: tank tread-like motion of the human erythrocyte membrane in shear flow.* Science, 1978. **202**(4370), 894-896.

117. Frattini, P.L., C. Wachter, T.C. Hung, R.L. Kormos, B.P. Griffith, and H.S. Borovetz, *Erythrocyte deformability in patients on left ventricular assist systems.* ASAIO Trans, 1989. **35**(3), 733-735.

118. Yokoyama, N., D. Sakota, E. Nagaoka, and S. Takatani, *Alterations in red blood cell volume and hemoglobin concentration, viscoelastic properties, and mechanical fragility caused by continuous flow pumping in calves.* Artif Organs, 2011. **35**(8), 791-799.

119. Baskurt, O.K. and H.J. Meiselman, *Red blood cell mechanical stability test.* Clin Hemorheol Microcirc, 2013. **55**(1), 55-62.

120. Kameneva, M.V., J.F. Antaki, K.C. Butler, M.J. Watach, R.L. Kormos, B.P. Griffith, et al., *A sheep model for the study of hemorheology with assisted circulation. Effect of an axial flow blood pump.* ASAIO J, 1994. **40**(4), 959-963.

121. Kameneva, M.V., M.J. Watach, P. Litwak, J.F. Antaki, K.C. Butler, D.C. Thomas, et al., *Chronic animal health assessment during axial ventricular assistance: importance of hemorheologic parameters.* ASAIO J, 1999. **45**(3), 183-188.

122. Marascalco, P., Ritchie, SP, Snyder, TA, Kameneva, MV, *Development of Standard Tests to Examine Viscoelastic Properties of Blood of Experimental Animals for Pediatric Mechanical Support Device Evaluation.* ASAIO J, 2006. **52**(5), 567-574.

123. La Celle, P.L., *Pathologic erythrocytes in the capillary microcirculation.* Blood Cells, 1975. **1**, 269-284.

124. Kameneva, M.V., K.O. Garrett, M.J. Watach, and H.S. Borovetz, *Red blood cell aging and risk of cardiovascular diseases.* Clin Hemorheol Microcirc, 1998. **18**(1), 67-74.

125. Shen, S.C., W.B. Castle, and E.M. Fleming, *Experimental and Clinical Observations on Increased Mechanical Fragility of Erythrocytes.* Science, 1944. **100**(2600), 387-389.

126. Kameneva, M.V., J.F. Antaki, H. Konishi, J.J. Whalen, J.P. Kerrigan, M.J. Watach, et al., *Effect of perfluorochemical emulsion on blood trauma and hemorheology.* ASAIO J, 1994. **40**(3), M576-579.

127. Baskurt, O.K., M. Uyuklu, S. Ozdem, and H.J. Meiselman, *Measurement of red blood cell aggregation in disposable capillary tubes.* Clin Hemorheol Microcirc, 2011. **47**(4), 295-305.

128. Wintrobe, M.M. and J.W. Landsberg, *A Standardized Technique for the Blood Sedimentation Test.* Am J Med Sci, 1935. **189**, 102-115.

129. Baskurt, O.K. and H.J. Meiselman, *Cellular determinants of low-shear blood viscosity.* Biorheology, 1997. **34**(3), 235-247.

130. Dintenfass, L., *Rheology of blood in cardiovascular diseases.* Bibl Anat, 1967. **9**, 525-531.

131. Baskurt, O.K., A. Temiz, and H.J. Meiselman, *Red blood cell aggregation in experimental sepsis.* J Lab Clin Med, 1997. **130**(2), 183-190.

132. Antaki, J.F., K.C. Butler, R.L. Kormos, A. Kawai, H. Konishi, J.P. Kerrigan, et al., *In vivo evaluation of the Nimbus axial flow ventricular assist system. Criteria and methods.* ASAIO J, 1993. **39**(3), M231-236.

133. Kormos, R.L., H.S. Borovetz, B.P. Griffith, and T.C. Hung, *Rheologic abnormalities in patients with the Jarvik-7 total artificial heart.* ASAIO Trans, 1987. **33**(3), 413-417.

134. Hung, T.C., D.B. Butter, C.L. Yie, R.L. Kormos, H.S. Borovetz, B.P. Griffith, et al., *Effects of long-term Novacor artificial heart support on blood rheology.* ASAIO Trans, 1991. **37**(3), M312-313.

135. Undar, A., W.K. Vaughn, and J.H. Calhoon, *The effects of cardiopulmonary bypass and deep hypothermic circulatory arrest on blood viscoelasticity and cerebral blood flow in a neonatal piglet model.* Perfusion, 2000. **15**(2), 121-128.

136. Virchow, R.L.K., *Thrombosis and Embolie (1846-1856)*. 1997: Science History Pubns. 234.

137. Baumgartner, H.R., *The role of blood flow in platelet adhesion, fibrin deposition, and formation of mural thrombi.* Microvasc Res, 1973. **5**(2), 167-179.

138. Turitto, V.T. and H.R. Baumgartner, *Inhibited platelet adhesion and irreversible thrombus formation under high shear conditions.* Trans Am Soc Artif Intern Organs, 1978. **24**, 719-726.

139. Turitto, V.T., H.J. Weiss, and H.R. Baumgartner, *The effect of shear rate on platelet interaction with subendothelium exposed to citrated human blood.* Microvasc Res, 1980. **19**(3), 352-365.

140. Friedman, L.I. and E.F. Leonard, *Platelet adhesion to artificial surfaces: consequences of flow, exposure time, blood condition, and surface nature.* Fed Proc, 1971. **30**(5), 1641-1648.

141. Grabowski, E.F., L.I. Friedman, and E.F. Leonard, *Effect of shear rate on the diffusion and adhesion of blood platelets to a foreign surface.* Ind Eng Chem Fundam, 1972. **11**, 224-232.

142. Wurzinger, L.J., R. Opitz, P. Blasberg, H. Eschweiler, and H. Schmid-Schonbein, *The role of hydrodynamic factors in platelet activation and thrombotic events: The effects of shear stress of short duration*, in *Fluid Dynamics as a Localizing Factor for Atherosclerosis*, G. Schettler, Editor. 1983, Springer-Verlag Berlin Heidelberg: New York. 91-102.

143. Wurzinger, L.J., P. Blasberg, and H. Schmid-Schönbein, *Towards a concept of thrombosis in accelerated flow: rheology, fluid dynamics, and biochemistry.* Biorheology, 1985. **22**(5), 437-450.

144. Wurzinger, L.J., R. Opitz, M. Wolf, and H. Schmid-Schonbein, *"Shear induced platelet activation"--a critical reappraisal.* Biorheology, 1985. **22**(5), 399-413.

145. Sheriff, J., D. Bluestein, G. Girdhar, and J. Jesty, *High-shear stress sensitizes platelets to subsequent low-shear conditions.* Ann Biomed Eng, 2010. **38**(4), 1442-1450.

146. Born, G.V., *Aggregation of blood platelets by adenosine diphosphate and its reversal.* Nature, 1962. **194**, 927-929.

147. Born, G.V. and M.J. Cross, *The Aggregation of Blood Platelets.* J Physiol, 1963. **168**, 178-195.

148. Goldsmith, H.L., J.C. Marlow, and S.K. Yu, *The effect of oscillatory flow on the release reaction and aggregation of human platelets.* Microvasc Res, 1976. **11**(3), 335-359.

149. Nomura, S., N.N. Tandon, T. Nakamura, J. Cone, S. Fukuhara, and J. Kambayashi, *High-shear-stress-induced activation of platelets and microparticles enhances expression of cell adhesion molecules in THP-1 and endothelial cells.* Atherosclerosis, 2001. **158**(2), 277-287.

150. Hellem, A.J., *The adhesiveness of human blood platelets in vitro.* Scand J Clin Lab Invest, 1960. **12 Suppl**, 1-117.

151. Gaarder, A., J. Jonsen, S. Laland, A. Hellem, and P.A. Owren, *Adenosine diphosphate in red cells as a factor in the adhesiveness of human blood platelets.* Nature, 1961. **192**, 531-532.

152. Born, G.V.R., *Current ideas on the mechanism of platelet aggregation.* Ann NY Acad Sci, 1972. **201**, 4-12.

153. Hellem, A.J. and A.E. Odegaard, *Investigations on Adenosine Diphosphate (ADP) Induced Platelet Adhesiveness in Vitro. I. The ADP-Platelet Reaction in Various Experimental Conditions.* Thromb Diath Haemorrh, 1963. **10**, 61-70.

154. Reimers, R.C., S.P. Sutera, and J.H. Joist, *Potentiation by red blood cells of shear-induced platelet aggregation: relative importance of chemical and physical mechanisms.* Blood, 1984. **64**(6), 1200-1206.

155. Alkhamis, T.M., R.L. Beissinger, and J.R. Chediak, *Red blood cell effect on platelet adhesion and aggregation in low-stress shear flow. Myth or fact?* ASAIO Trans, 1988. **34**(3), 868-873.

156. Wurzinger, L.J., P. Blasberg, E. Jungling, and H. Schmid-Schonbein, *The influence of red blood cell hemolysate (RBCH) on platelet aggregation (PA) and release of serotonin and β-thromboglobulin (β-TG) in heparinized platelet rich plasma (PRP)* Thrombosis and Haemostasis, 1978. **42**, 273.

157. Wurzinger, L.J., P. Blasberg, M. van de Loecht, W. Suwelack, and H. Schmid-Schonbein, *Model experiments on platelet adhesion in stagnation point flow.* Biorheology, 1984. **21**(4), 649-659.

158. Wurzinger, L.J. and H. Schmid-Schonbein, *The Interaction of Fluid-Dynamic, Physicochemical and Cell Biological Reactions in Thrombus Formation.* Ann NY Acad Sci, 1987. **516**, 316-332.

159. Goldsmith, H.L., *Blood flow and thrombosis.* Thromb Diath Haemorrh, 1974. **32**(1), 35-48.

160. Goldsmith, H.L., S.S. Yu, and J. Marlow, *Fluid mechanical stress and the platelet.* Thromb Diath Haemorrh, 1975. **34**(1), 32-41.

161. Blackshear, P.L., Jr., *Artificial heart.* Minn Med, 1968. **51**(3), 363, 365.

162. Schima, H., C. Schlusche, B.V. Jeremejev, I. Schor, G. Geihseder, M.R. Muller, et al., *Influence of centrifugal blood pumps on the elasticity of erythrocytes.* ASAIO Transactions, 1991. **37**(4), 658-661.

163. Naito, K., K. Mizuguchi, and Y. Nose, *The need for standardizing the index of hemolysis.* Artif Organs, 1994. **18**(1), 7-10.

164. Lawson, D.S., R. Ing, I.M. Cheifetz, R. Walczak, D. Craig, S. Schulman, et al., *Hemolytic characteristics of three commercially available centrifugal blood pumps.* Pediatr Crit Care Med, 2005. **6**(5), 573-577.

165. Watanabe, N., D. Sakota, K. Ohuchi, and S. Takatani, *Deformability of red blood cells and its relation to blood trauma in rotary blood pumps.* Artif Organs, 2007. **31**(5), 352-358.

166. Sakota, D., R. Sakamoto, H. Sobajima, N. Yokoyama, S. Waguri, K. Ohuchi, et al., *Mechanical damage of red blood cells by rotary blood pumps: selective destruction of aged red blood cells and subhemolytic trauma.* Artif Organs, 2008. **32**(10), 785-791.

167. Rous, P. and J.R. Turner, *The Preservation of Living Red Blood Cells in Vitro : I. Methods of Preservation.* J Exp Med, 1916. **23**(2), 219-237.

168. Oku, T., H. Harasaki, W. Smith, and Y. Nose, *Hemolysis. A comparative study of four nonpulsatile pumps.* ASAIO Trans, 1988. **34**(3), 500-504.

169. Kameneva, M.V., J.F. Antaki, K.K. Yeleswarapu, M.J. Watach, B.P. Griffith, and H.S. Borovetz, *Plasma protective effect on red blood cells exposed to mechanical stress.* ASAIO J, 1997. **43**(5), M571-575.

170. Kameneva, M.V., M.J. Watach, and H.S. Borovetz, *Gender difference in rheologic properties of blood and risk of cardiovascular diseases.* Clin Hemorheol Microcirc, 1999. **21**(3-4), 357-363.

171. Maruyama, O., K. Yamaguchi, M. Nishida, T. Onoguchi, T. Tsutsui, T. Jikuya, et al., *Hemolytic evaluation using polyurethane microcapsule suspensions in circulatory*

support devices: normalized index of hemolysis comparisons of commercial centrifugal blood pumps. Artif Organs, 2008. **32**(2), 146-156.

172. Pohl, M., O. Samba, M.O. Wendt, and G. Vlastos, *Shear stress related hemolysis and its modelling by mechanical degradation of polymer solutions.* Int J Artif Organs, 1998. **21**(2), 107-113.

173. Pohl, M., M.O. Wendt, B. Koch, and G.A. Vlastos, *Mechanical degradation of polyacrylamide solutions as a model for flow induced blood damage in artificial organs.* Biorheology, 2000. **37**(4), 313-324.

174. Marhefka, J.N., *Study of drag reducing polymers and mechanisms of their intravascular effect*, in *Bioengineering*. 2007, University of Pittsburgh: Pittsburgh.

175. Toms, B.A. *Some observation on the flow of linear polymer solutions through straight tubes at large Reynolds numbers*. in *Proc. 1st Intl. Congr. on Rheology*. 1949. Amsterdam.

176. Virk, P.S. and H. Baher, *The effect of polymer concentration on drag reduction.* Chem Eng Sci, 1970. **25**(7), 1183–1189.

177. Marhefka, J.N., S.S. Velankar, T.M. Chapman, and M.V. Kameneva, *Mechanical degradation of drag reducing polymers in suspensions of blood cells and rigid particles.* Biorheology, 2008. **45**(5), 599-609.

178. Fisher, D.H. and F. Rodriguez, *Degradation of drag reducing polymers.* J. Appl. Polym. Sci. , 1971. **15**, 2975-2985.

179. Kenis, P.R., *Turbulent flow friction reduction effectiveness and hydrodynamic degradation of polysaccharides and synthetic polymers.* J Appl Polym Sci, 1971. **15**, 607-618.

180. Sellin, R.J.H., J.W. Hoyt, and O. Scrivener, *The effect of drag-reducing additives on fluid flows and their industrial applications. Part 1: Basic aspects.* J Hydr Res, 1982. **20**, 29-68.

181. Koller, T., Jr. and A. Hawrylenko, *Contribution to the in vitro testing of pumps for extracorporeal circulation.* J Thorac Cardiovasc Surg, 1967. **54**(1), 22-29.

182. Haradin, A.R., R.I. Weed, and C.F. Reed, *Changes in physical properties of stored erythrocytes relationship to survival in vivo.* Transfusion, 1969. **9**(5), 229-237.

183. van de Watering, L., *Red cell storage and prognosis.* Vox Sang, 2011. **100**(1), 36-45.

184. Gueguen, M., F. Durand, J. Cherpi, A. Feuillu, and B. Genetet, *Filterability and bank blood conservation media.* Scand J Clin Lab Invest Suppl, 1981. **156**, 313-316.

185. Gladwin, M.T. and D.B. Kim-Shapiro, *Storage lesion in banked blood due to hemolysis-dependent disruption of nitric oxide homeostasis.* Curr Opin Hematol, 2009. **16**(6), 515-523.

186. Roback, J.D., B.J. Grossman, T. Harris, and C.D. Hillyer, eds. *Technical Manual*. 17th ed. 2011, AABB: Bethesda.

187. Riquelme, B.D., P.G. Foresto, J.R. Valverde, and J.R. Rasia, *Alterations to complex viscoelasticity of erythrocytes during storage.* Clin Hemorheol Microcirc, 2000. **22**(3), 181-188.

188. Relevy, H., A. Koshkaryev, N. Manny, S. Yedgar, and G. Barshtein, *Blood banking-induced alteration of red blood cell flow properties.* Transfusion, 2008. **48**(1), 136-146.

189. Farges, E., R. Grebe, and M. Baumann, *Viscoelastic and biochemical properties of erythrocytes during storage with SAG-M at +4 degrees C.* Clin Hemorheol Microcirc, 2002. **27**(1), 1-11.

190. Chien, S., R.G. King, R. Skalak, S. Usami, and A.L. Copley, *Viscoelastic properties of human blood and red cell suspensions.* Biorheology, 1975. **12**(6), 341-346.

191. Thurston, G.B. and N.M. Henderson, *Effects of flow geometry on blood viscoelasticity.* Biorheology, 2006. **43**(6), 729-746.

192. Bennett-Guerrero, E., T.H. Veldman, A. Doctor, M.J. Telen, T.L. Ortel, T.S. Reid, et al., *Evolution of adverse changes in stored RBCs.* Proc Natl Acad Sci U S A, 2007. **104**(43), 17063-17068.

193. Henkelman, S., M.J. Dijkstra-Tiekstra, J. de Wildt-Eggen, R. Graaff, G. Rakhorst, and W. van Oeveren, *Is red blood cell rheology preserved during routine blood bank storage?* Transfusion, 2010. **50**(4), 941-948.

194. Edgren, G., M. Kamper-Jorgensen, S. Eloranta, K. Rostgaard, B. Custer, H. Ullum, et al., *Duration of red blood cell storage and survival of transfused patients (CME).* Transfusion, 2010. **50**(6), 1185-1195.

195. Triulzi, D.J. and M.H. Yazer, *Clinical studies of the effect of blood storage on patient outcomes.* Transfus Apher Sci, 2010. **43**(1), 95-106.

196. Mohnle, P., S.A. Snyder-Ramos, Y. Miao, A. Kulier, B.W. Bottiger, J. Levin, et al., *Postoperative red blood cell transfusion and morbid outcome in uncomplicated cardiac surgery patients.* Intensive Care Med, 2011. **37**(1), 97-109.

197. Aubron, C., A. Nichol, D.J. Cooper, and R. Bellomo, *Age of red blood cells and transfusion in critically ill patients.* Ann Intensive Care, 2013. **3**(1), 2.

198. Frank, S.M., B. Abazyan, M. Ono, C.W. Hogue, D.B. Cohen, D.E. Berkowitz, et al., *Decreased erythrocyte deformability after transfusion and the effects of erythrocyte storage duration.* Anesth Analg, 2013. **116**(5), 975-981.

199. ASTM, *Annual Book of ASTM standards*, in *F1841-97 Standard Practice for Assessment of Hemolysis in Continuous Flow Blood Pumps*. 1998, American Society for Testing and Materials. 1288-1292.

200. Mueller, M.R., H. Schima, H. Engelhardt, A. Salat, D.B. Olsen, U. Losert, et al., *In vitro hematological testing of rotary blood pumps: remarks on standardization and data interpretation.* Artif Organs, 1993. **17**(2), 103-110.

201. Fok, F.P. and H. Schubothe, *Studies on various factors influencing mechanical haemolysis of human erythrocytes.* Br J Haematol, 1960. **6**, 355-361.

202. Schubothe, H. and F.P. Fok, *The quantitative estimation of mechanical haemolysis for clinical application.* Br J Haematol, 1960. **6**, 350-354.

203. Fleisch, H. and A. Fleisch, *[The hemoresistometer. An instrument for the determination of the mechanical resistance of the erythrocytes]*. Schweiz Med Wochenschr, 1960. **90**, 186-190.

204. Gu, L., W.A. Smith, and G.P. Chatzimavroudis, *Mechanical fragility calibration of red blood cells.* ASAIO J, 2005. **51**(3), 194-201.

205. Schwoch, G. and H. Passow, *Preparation and properties of human erythrocyte ghosts.* Mol Cell Biochem, 1973. **2**(2), 197-218.

206. Nash, G.B. and H.J. Meiselman, *Red cell and ghost viscoelasticity. Effects of hemoglobin concentration and in vivo aging.* Biophys J, 1983. **43**(1), 63-73.

207. Nash, G.B. and H.J. Meiselman, *Effects of preparative procedures on the volume and content of resealed red cell ghosts.* Biochim Biophys Acta, 1985. **815**(3), 477-485.

208. Bozzo, J., R. Tonda, M.R. Hernandez, M. Alemany, A.M. Galan, A. Ordinas, et al., *Comparison of the effects of human erythrocyte ghosts and intact erythrocytes on platelet interactions with subendothelium in flowing blood.* Biorheology, 2001. **38**(5-6), 429-437.

209. Goldsmith, H.L., O. Lichtarge, M. Tessier-Lavigne, and S. Spain, *Some model experiments in hemodynamics: VI. Two-body collisions between blood cells.* Biorheology, 1981. **18**(3-6), 531-555.

210. Goldsmith, H.L. and T. Karino, *Microrheology and clinical medicine: Unraveling some problems related to thrombosis.* Clinical Hemorheology, 1982. **2**, 143-155.

211. Goldsmith, H.L., *The microrheology of red blood cell suspensions.* J Gen Physiol, 1968. **52**(1), 5Suppl-28s.

212. Goldsmith, H.L. and J.C. Marlow, *The effect of red cells on platelet collisions in blood flow*. Federation Proceedings, 1973. **32**, 414.

213. Turitto, V.T. and H.R. Baumgartner, *Platelet interaction with subendothelium in a perfusion system: physical role of red blood cells.* Microvasc Res, 1975. **9**(3), 335-344.

214. Beck, M.R., Jr. and E.C. Eckstein, *Preliminary report on platelet concentration in capillary tube flows of whole blood.* Biorheology, 1980. **17**(5-6), 455-464.

215. Eckstein, E.C., D.L. Bilsker, C.M. Waters, J.S. Kippenhan, and A.W. Tilles, *Transport of Platelets in Flowing Blood.* Ann NY Acad Sci, 1987. **516**, 442-452.

216. Aarts, P.A., P.A. Bolhuis, K.S. Sakariassen, R.M. Heethaar, and J.J. Sixma, *Red blood cell size is important for adherence of blood platelets to artery subendothelium.* Blood, 1983. **62**(1), 214-217.

217. Aarts, P.A., R.M. Heethaar, and J.J. Sixma, *Red blood cell deformability influences platelets--vessel wall interaction in flowing blood.* Blood, 1984. **64**(6), 1228-1233.

218. Aarts, P.A., S.A. van den Broek, G.W. Prins, G.D. Kuiken, J.J. Sixma, and R.M. Heethaar, *Blood platelets are concentrated near the wall and red blood cells, in the center in flowing blood.* Arteriosclerosis, 1988. **8**(6), 819-824.

219. Goldsmith, H.L., *Red cell motions and wall interactions in tube flow.* Fed Proc, 1971. **30**(5), 1578-1590.

220. Goldsmith, H.L., *The flow of model particles and blood cells and its relation to thrombogenesis*, in *Progress in hemostasis and thrombosis*, T.H. Spaet, Editor. 1972, Grune and Stratton: New York. 97-139.

221. Corattiyl, V. and E.C. Eckstein, *Regional platelet concentration in blood flow through capillary tubes.* Microvasc Res, 1986. **32**(2), 261-270.

222. Aarts, P.A., J.D. Banga, H.C. van Houwelingen, R.M. Heethaar, and J.J. Sixma, *Increased red blood cell deformability due to isoxsuprine administration decreases platelet adherence in a perfusion chamber: a double-blind cross-over study in patients with intermittent claudication.* Blood, 1986. **67**(5), 1474-1481.

223. Aarts, P.A., P. Steendijk, J.J. Sixma, and R.M. Heethaar, *Fluid shear as a possible mechanism for platelet diffusivity in flowing blood.* J Biomech, 1986. **19**(10), 799-805.

224. Baumgartner, H.R., M.B. Stemerman, and T.H. Spaet, *Adhesion of blood platelets to subendothelial surface: distinct from adhesion to collagen.* Experientia, 1971. **27**(3), 283-285.

225. Baumgartner, H.R. and C. Haudenschild, *Adhesion of platelets to subendothelium.* Ann N Y Acad Sci, 1972. **201**, 22-36.

226. Sakariassen, K.S., P.A. Aarts, P.G. de Groot, W.P. Houdijk, and J.J. Sixma, *A perfusion chamber developed to investigate platelet interaction in flowing blood with human vessel wall cells, their extracellular matrix, and purified components.* J Lab Clin Med, 1983. **102**(4), 522-535.

227. Karino, T. and H.L. Goldsmith, *Blood cell flow behavior in a captive annular vortex.* Federation Proceedings, 1974. **33**, 427.

228. Karino, T., H.H. Kwong, and H.L. Goldsmith, *Particle flow behaviour in models of branching vessels: I. Vortices in 90 degrees T-junctions.* Biorheology, 1979. **16**(3), 231-248.

229. Karino, T. and H.L. Goldsmith, *Disturbed flow in models of branching vessels.* Trans Am Soc Artif Intern Organs, 1980. **26**, 500-506.

230. Zhao, R., M.V. Kameneva, and J.F. Antaki, *Investigation of platelet margination phenomena at elevated shear stress.* Biorheology, 2007. **44**(3), 161-177.

231. Zhao, R., J.N. Marhefka, F. Shu, S.J. Hund, M.V. Kameneva, and J.F. Antaki, *Micro-flow visualization of red blood cell-enhanced platelet concentration at sudden expansion.* Ann Biomed Eng, 2008. **36**(7), 1130-1141.

232. Leonard, E.F., *The role of flow in thrombogenesis.* Bull N Y Acad Med, 1972. **48**(2), 273-280.

233. Goldsmith, H.L. and T. Karino, *Platelets in a region of disturbed flow.* Trans Am Soc Artif Intern Organs, 1977. **23**, 632-638.

234. Giersiepen, M., U. Krause, E. Knott, H. Reul, and G. Rau, *Velocity and shear stress distribution downstream of mechanical heart valves in pulsatile flow.* Int J Artif Organs, 1989. **12**(4), 261-269.

235. Hund, S.J., J.F. Antaki, and M. Massoudi, *On the Representation of Turbulent Stresses for Computing Blood Damage.* Int J Eng Sci, 2010. **48**(11), 1325-1331.

236. Herbertson, L.H., S.E. Olia, A. Daly, C.P. Noatch, W.A. Smith, M.V. Kameneva, et al., *Multilaboratory Study of Flow-Induced Hemolysis Using the FDA Benchmark Nozzle Model.* Artif Organs, 2014, n/a-n/a.

237. van Leeuwenhoek, A., *Microscopical observations concerning blood, milk, bones, the brain, spittle and cuticula.* Philosoph Trans Royal Soc London, 1674. **9**, 121-128.

238. Goldsmith, H.L., *Red cells and rouleaux in shear flow.* Science, 1966. **153**(3742), 1406-1407.

239. Goldsmith, H.L., *Deformation of human red cells in tube flow.* Biorheology, 1971. **7**(4), 235-242.

240. Chien, S., S. Usami, R.J. Dellenback, and M.I. Gregersen, *Shear-dependent deformation of erythrocytes in rheology of human blood.* American Journal of Physiology, 1970. **219**(1), 136-142.

241. Chien, S., *Determinants of blood viscosity and red cell deformability.* Scand J Clin Lab Invest Suppl, 1981. **156**, 7-12.

242. Chien, S., *Red cell deformability and its relevance to blood flow.* Annual Review of Physiology, 1987. **49**, 177-192.

243. Sutera, S.P., M. Mehrjardi, and N. Mohandas, *Deformation of erythrocytes under shear.* Blood Cells, 1975. **1**, 369-374.

244. Mitchison, J.M. and M.M. Swann, *The mechanical properties of the cell surface. I. The cell elastimeter.* J Exp Biol, 1954. **31**(3), 443-461.

245. Paulitscke, M. and G.B. Nash, *Micropipette methods for analysing blood cell rheology and their application to clinical research.* Clin Hemorheol, 1993. **13**, 407-434.

246. Hardeman, H.R., P.T. Goedhart, and S. Shin, *Methods in Hemorheology*, in *Handbook of Hemorheology and Hemodynamics*, O.K. Baskurt, et al., Editors. 2007, IOS Press: Amsterdam. 242-266.

247. Glenister, F.K., R.L. Coppel, A.F. Cowman, N. Mohandas, and B.M. Cooke, *Contribution of parasite proteins to altered mechanical properties of malaria-infected red blood cells.* Blood, 2002. **99**(3), 1060-1063.

248. Smith, C.M., 2nd, J.F. Kuettner, D.P. Tukey, S.M. Burris, and J.G. White, *Variable deformability of irreversibly sickled erythrocytes.* Blood, 1981. **58**(1), 71-77.

249. Nash, G.B., C.S. Johnson, and H.J. Meiselman, *Mechanical properties of oxygenated red blood cells in sickle cell (HbSS) disease.* Blood, 1984. **63**(1), 73-82.

250. Itoh, T., S. Chien, and S. Usami, *Effects of hemoglobin concentration on deformability of individual sickle cells after deoxygenation.* Blood, 1995. **85**(8), 2245-2253.

251. Reid, H.L., A.J. Barnes, P.J. Lock, J.A. Dormandy, and T.L. Dormandy, *A simple method for measuring erythrocyte deformability.* Journal of Clinical Pathology, 1976. **29**(9), 855-858.

252. Petit, K.I., W.B. Hunt, S.J. George, and A.J. Barnes, *Is impaired red cell filtration in diabetics due to a small abnormal sub-population of cells?* Clin Hemorheol, 1996. **16**, 479-485.

253. Symeonidis, A., G. Athanassiou, A. Psiroyannis, V. Kyriazopoulou, K. Kapatais-Zoumbos, Y. Missirlis, et al., *Impairment of erythrocyte viscoelasticity is correlated with*

levels of glycosylated haemoglobin in diabetic patients. Clin Lab Haematol, 2001. **23**(2), 103-109.

254. Buchan, P.C., *Evaluation and modification of whole blood filtration in the measurement of erythrocyte deformability in pregnancy and the newborn.* Br J Haematol, 1980. **45**(1), 97-105.

255. Linderkamp, O., B.J. Hammer, and R. Miller, *Filterability of erythrocytes and whole blood in preterm and full-term neonates and adults.* Pediatr Res, 1986. **20**(12), 1269-1273.

256. Buonocore, G., S. Bernie, D. Gioia, G. Garosi, and R. Bracci, *Whole blood filterability in the neonate.* Clin Hemorheol, 1991. **11**, 41-48.

257. Kenny, M.W., M. Meakin, D.J. Worthington, and J. Stuart, *Erythrocyte deformability in sickle-cell crisis.* Br J Haematol, 1981. **49**(1), 103-109.

258. Cabrales, P., *Effects of erythrocyte flexibility on microvascular perfusion and oxygenation during acute anemia.* Am J Physiol Heart Circ Physiol, 2007. **293**(2), H1206-1215.

259. Svenmarker, S., E. Jansson, H. Stenlund, and K.G. Engstrom, *Red blood cell trauma during cardiopulmonary bypass: narrow pore filterability versus free haemoglobin.* Perfusion, 2000. **15**(1), 33-40.

260. Kirschenbaum, L.A., M. Aziz, M.E. Astiz, D.C. Saha, and E.C. Rackow, *Influence of rheologic changes and platelet-neutrophil interactions on cell filtration in sepsis.* Am J Respir Crit Care Med, 2000. **161**(5), 1602-1607.

261. Wegner, G., W. Kucera, W. Toursel, and D. Lerche, *Deformability of human red blood cells stored for different periods at subzero temperatures.* Biomed Biochim Acta, 1987. **46**(7), 599-603.

262. Berezina, T.L., S.B. Zaets, C. Morgan, C.R. Spillert, M. Kamiyama, Z. Spolarics, et al., *Influence of storage on red blood cell rheological properties.* J Surg Res, 2002. **102**(1), 6-12.

263. Hardeman, M.R., P.T. Goedhart, J.G. Dobbe, and K.P. Lettinga, *Laser-assisted Optical Rotational Cell Analyser (LORCA); A new instrument for measurement of various structural hemorheological parameters.* Clin Hemorheol, 1994. **14**, 605-618.

264. Dobbe, J.G.G., *Engineering developments in hemorheology*. 2002, University of Amsterdam, The Netherlands.

265. Shin, S., Y. Ku, M.S. Park, and J.S. Suh, *Slit-flow ektacytometry: laser diffraction in a slit rheometer.* Cytometry B Clin Cytom, 2005. **65**(1), 6-13.

266. Lee, S.S., J.F. Antaki, M.V. Kameneva, J.G. Dobbe, M.R. Hardeman, K.H. Ahn, et al., *Strain hardening of red blood cells by accumulated cyclic supraphysiological stress.* Artif Organs, 2007. **31**(1), 80-86.

267. Dobbe, J.G.G., G.J. Streekstra, M.R. Hardeman, C. Ince, and C.A. Grimbergen, *Measurement of the Distribution of Red Blood Cell Deformability Using an Automated Rheoscope.* Cytometry, 2002. **50**(6), 313-325.

268. Cranston, H.A., C.W. Boylan, G.L. Carroll, S.P. Sutera, J.R. Williamson, I.Y. Gluzman, et al., *Plasmodium falciparum maturation abolishes physiologic red cell deformability.* Science, 1984. **223**(4634), 400-403.

269. Miller, L.H., S. Usami, and S. Chien, *Alteration in the rheologic properties of Plasmodium knowlesi--infected red cells. A possible mechanism for capillary obstruction.* J Clin Invest, 1971. **50**(7), 1451-1455.

270. Hardeman, M.R. and C. Ince, *Clinical potential of in vitro measured red cell deformability, a myth?* Clin Hemorheol Microcirc, 1999. **21**(3-4), 277-284.

271. Shin, S., Y. Ku, N. Babu, and M. Singh, *Erythrocyte deformability and its variation in diabetes mellitus.* Indian J Exp Biol, 2007. **45**(1), 121-128.

272. Hardeman, M.R., P. Goedhart, and D. Breederveld, *Laser diffraction ellipsometry of erythrocytes under controlled shear stress using a rotational viscosimeter.* Clin Chim Acta, 1987. **165**(2-3), 227-234.

273. Thurston, G.B. and N.M. Henderson, *Viscoelasticity of Human Blood*, in *Handbook of Hemorheology and Hemodynamics*, O.K. Baskurt, et al., Editors. 2007, IOS Press: Amsterdam. 72-90.

274. Field, A.P., *Discovering statistics using SPSS : (and sex, drugs and rock 'n' roll).* 2nd ed. ISM introducing statistical methods. 2005, London ; Thousand Oaks, Calif.: Sage Publications. xxxiv, 779 p.